Institut für Wasserbau · Universität Stuttgart

Mitteilungen

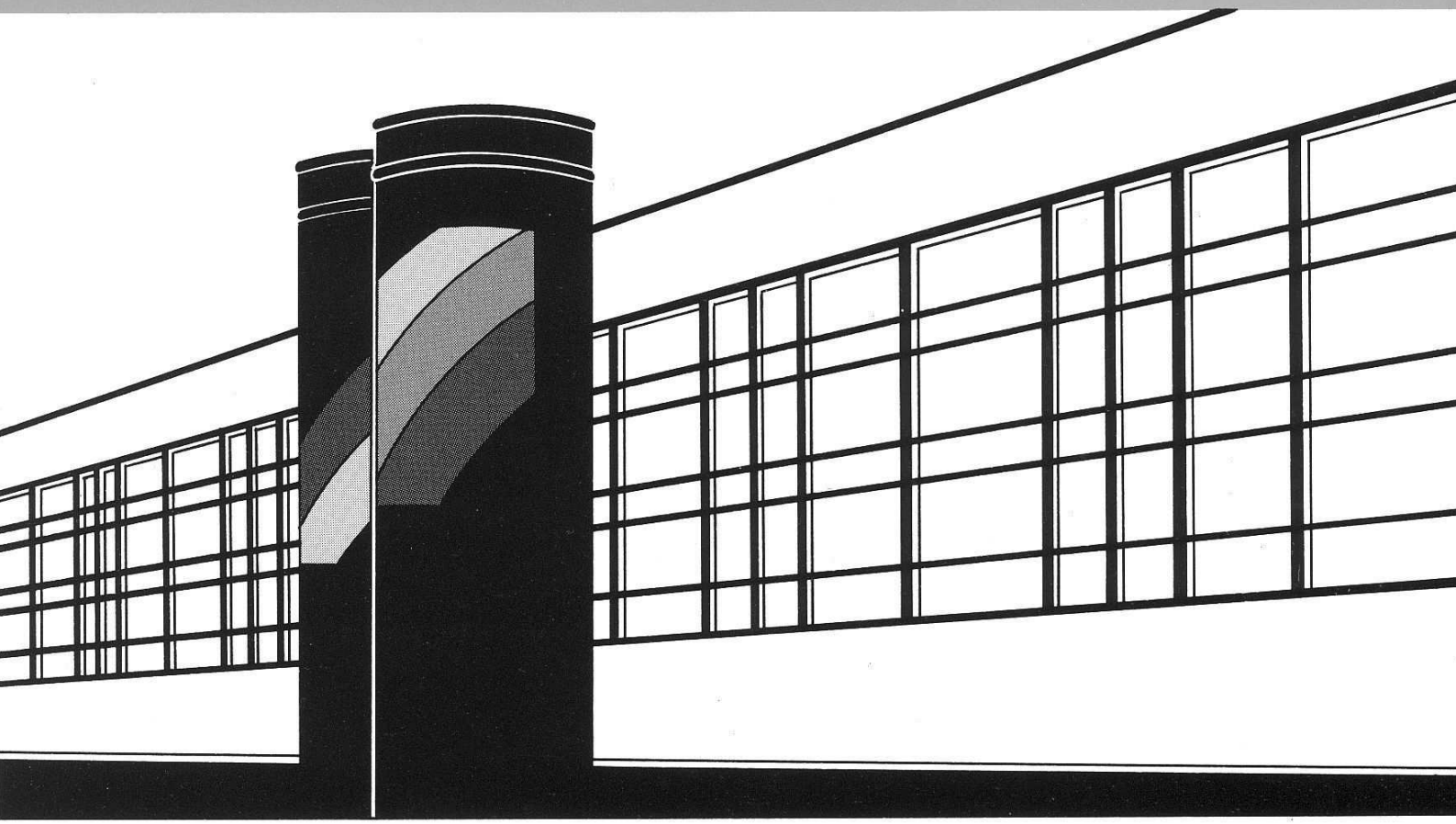

Heft 179

Patrick Laux

Statistical Modeling of Precipitation for Agricultural Planning in the Volta Basin of West Africa

Statistical Modeling of Precipitation for Agricultural Planning in the Volta Basin of West Africa

Von der Fakultät Bau- und Umweltingenieurwissenschaften der Universität Stuttgart zur Erlangung der Würde eines Doktor-Ingenieurs (Dr.-Ing.) genehmigte Abhandlung

Vorgelegt von
Patrick Laux
aus Wadern

Hauptberichter:	Prof. Dr. rer. nat. Dr.-Ing. habil. András Bárdossy
Mitberichter:	Prof. Dr. rer. nat. habil. Jucundus Jacobeit

Tag der mündlichen Prüfung: 16. Januar 2009

Institut für Wasserbau der Universität Stuttgart
2009

Heft 179

Statistical Modeling of Precipitation for Agricultural Planning in the Volta Basin of West Africa

von
Dr.-Ing.
Patrick Laux

Eigenverlag des Instituts für Wasserbau der Universität Stuttgart

D93 Statistical Modeling of Precipitation for Agricultural Planning in the Volta Basin of West Africa

Titelaufnahme der Deutschen Bibliothek

Laux, Patrick:
Statistical Modeling of Precipitation for Agricultural Planning in the Volta Basin of West Africa. / von Patrick Laux. Institut für Wasserbau, Universität Stuttgart. - Stuttgart: Inst. für Wasserbau, 2009

(Mitteilungen / Institut für Wasserbau, Universität Stuttgart: H. 179)
Zugl.: Stuttgart, Univ., Diss., 2009)
ISBN 978-3-933761-83-5

NE: Institut für Wasserbau <Stuttgart>: Mitteilungen

Herausgegeben 2009 vom Eigenverlag des Instituts für Wasserbau
Druck: Document Center S. Kästl, Ostfildern

ABSTRACT

Water availability plays a vital role in the promotion of economic growth and reduction of poverty in the Volta Basin. Due to the increasing population pressure, there is a rapidly increasing demand for water. Climate change additionally impacts water availability and may aggravate water scarcity in the future. Agriculture is the major water consuming sector in the Volta Basin. High rainfall variability of the past often led to shortages in food supply and famines, especially in the Sahel.

In such regions, where rainfall is limited to only few months per year, the exact determination of the rainy seasons' onset is of crucial interest for farming management. Every year, farmers are faced with the question when to start sowing. Do the first rainfalls after the dry season resemble the onset of the rainy season or not? The farmers' seeds and effort will be lost if no significant rainfall follows within the following weeks after sowing. If they do not sow but the first rains were already part of the rainy season, valuable time for agricultural production is lost. Apparently, the benefits of a solution to this problem would be enormous. Therefore, one major goal of this thesis is to find relevant indicators to reliably predict the rainy season's onset. To archive this goal, two different strategies were followed within the context of the doctoral thesis:

- The first strategy tackles the problem using solely the measured rainfall time series. Linear discriminant analysis and linear regression analysis were used to predict the onset of the rainy season.

- The second strategy uses large-scale meteorological reanalysis fields from GCM output. A multi objective fuzzy logic-based classification algorithm is used to link large-scale meteorological conditions with the onset of the rainy season.

Apart from the onset of the rainy season, different rainfall characteristics are analyzed, which are important for agricultural management. These are rainfall occurrence probability, rainfall amount and dry spell probability and are presented as risk maps, suitable for agricultural decision support in the Volta Basin. Drought analysis on regional scale is conducted. The *Effective Drought Index* is used to derive drought duration, drought intensity, and drought interarrival time. A bivariate Copula approach is therefore used to model the regional return periods of droughts using jointly drought duration and drought intensity.

For the investigation of the impact of climate change on these agro-meteorological characteristics, local rainfall information on daily time scale is required. Especially in

regions with weak infrastructure like the Volta Basin, all the applied methodologies are hampered by the fact that only little and incomplete meteorological information is available. Statistical downscaling of coarse resolved global circulation models (GCMs) in companion with stochastic rainfall simulation is applied alternatively to avoid these shortcomings. The performance of two different statistical approaches, a simple weather generator and a more sophisticated combined weather pattern classification and simulation approach are evaluated in the context of that doctoral thesis. For the latter, the performance is depending on various factors like e.g. the choice of the predictor(s), the location and size of the domain etc.

The impact of climate change on rainfall variability in the Volta Basin is elaborated in terms of future rainy season onset dates and weather pattern frequencies using the A1B scenario driven ECHAM5 model output. For the future time slice 2011-2040, a drastic delay in the onset of the rainy season is expected. Wet and droughty weather patterns are expected to increase in the two northernmost regions of the Volta Basin.

Finally, the impact of rainfall variability on crop yield is investigated via multiple linear regression analysis. Rainfall variability has been assessed in terms of the annual rainfall amount, the number of rainy days, the onset, cessation and length of the rainy season and the annual mean of the monthly averaged *Effective Drought Index*. Regression models, which explain up to 80% of the total variance of crop yield, could be established. It is found, that the annual precipitation amount is the dominant factor to estimate crop yield.

KURZFASSUNG

Einleitung:

Die vorliegende Doktorarbeit beschäftigt sich mit der statistischen Modellierung von Niederschlag für landwirtschaftliche Zwecke im Voltabecken in Westafrika und ist eingebunden in das GLOWA Volta Projekt (GVP). Das GVP verfolgt das übergeordnete Ziel der Analyse der physischen und sozioökonomischen Bedingungen des Wasserkreislaufs im Voltabecken und der diesbezüglichen Auswirkungen des globalen Klimawandels. Darauf aufbauend wird ein wissenschaftlich fundiertes System zur Entscheidungshilfe (*Decision Support System* – DSS) im Bereich des Wasserressourcenmanagements entwickelt. Das DSS ist als interdisziplinäres Rahmenwerk zur Überwachung und Simulation des Wasserressourcenflusses geplant. Entscheidungsträgern soll damit die Einschätzung des Einflusses verschiedener Faktoren auf die soziale, ökonomische und biologische Produktivität der Wasserressourcen erleichtert werden. Diese Arbeit liefert in diesem Zusammenhang eine wissenschaftliche Basis in Form von Entscheidungshilfeinstrumenten bezüglich der exakten Terminierung des Regenzeitbeginns für die Landwirtschaft. Für Regionen mit vorherrschend praktiziertem Regenfeldbau und einer zeitlich begrenzter Wasserverfügbarkeit (Regenzeit) ist die Terminierung des Regenzeitbeginns (gleichbedeutend mit dem Aussaatdatum) von zentraler Bedeutung für die landwirtschaftliche Produktion: bleiben nach einer frühen Aussaat die Niederschläge für längere Zeit aus, kann dies zum Totalverlust der Ernte führen; eine späte Aussaat hingegen verkürzt die Wachstumsperiode und führt zu Ertragseinbußen.

Das Projekt ist Teil des übergeordneten GLOWA Programms, das vom Bundesministerium für Bildung und Forschung finanziert wird. Zusätzliche Mittel werden vom Ministerium für Wissenschaft und Forschung des Landes Nordrhein-Westfalen zur Verfügung gestellt.

Die in dieser Doktorarbeit bearbeiteten übergeordneten Fragestellungen sind:

- Entwicklung einer Definition des Regenzeitbeginns im landwirtschaftlichen Sinn (Terminierung des Anpflanzzeitpunktes) für das Voltabecken.
- Vorhersage des Regenzeitbeginns im Voltabecken.
- Einfluss der globalen Klimaänderung auf die Niederschlagsvariabilität im Voltabecken.

Die Innovationen dieser Arbeit lassen sich wie folgt zusammenfassen:

- Entwicklung einer regionalen und Fuzzy-Logik basierten Definition des Regenzeitbeginns, die auf die Terminierung des optimalen Aussaattermins ausgerichtet ist. Darauf aufbauend Anwendung von linearer Diskriminanzanalyse zur Vorhersage des Regenzeitbeginns im Voltabecken mit einer Trefferquote bis zu 80%.
- Identifikation 1) großskaliger Wetterlagen mit dem singulären Ereignis Regenzeitbeginn durch die Verwendung eines Fuzzy Regel basierten Klassifikationsalgorithmus, 2) besonders feuchter und trockener Wetterlagen im Voltabecken und 3) geeigneter Prädiktoren.
- Analyse der mit der globalen Klimaänderung bis 2040 erwarteten Veränderung der Häufigkeiten dieser Wetterlagen auf Basis des Emissionsszenarios A1B und ECHAM5.
- Entwicklung einer auf dem *Effective Drought Index* EDI basierenden Dürredefinition für das Voltabecken. Analyse der Wiederkehrintervalle von Dürren im Voltabecken mittels Copula Ansatz.

Untersuchungsgebiet:

Das in Westafrika gelegene Voltabecken (Abbildung I) umfasst eine Fläche von ca. 414000 km^2, wobei Ghana mit 40% und Burkina Faso mit 42% den größten Anteil an der Gesamtfläche teilen. Weitere an der Gesamtfläche des Voltabeckens beteiligte Länder sind Benin, Togo, Niger, Mali und Elfenbeinküste. Das Voltabecken setzt sich aus mehreren Teileinzugsgebieten zusammen, von denen die der Schwarzen- und Weißen Volta die größten sind. Beide Flüsse münden in den ca. 8500 km^2 großen Volta Stausee, welcher durch den im Südosten Ghanas liegenden Akosombodamm aufgestaut wird. Der Volta Stausee stellt den flächenmäßig größten vom Menschen vollständig geschaffenen Stausee der Erde dar.

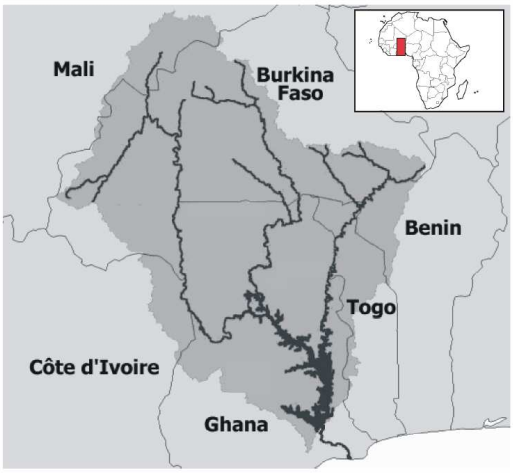

Abbildung I: Volta – Einzugsgebiet (Modifizierte Abb.: MARX et al., 2007).

Das Klima des Volta-Beckens reicht von semi-arid in Norden bis sub-humid im Süden. Die mittlere Jahrestemperatur liegt im Norden zwischen 27° C und 36° C, im Süden zwischen 24° C und 30° C. Die mittleren Jahresniede rschlagssummen reichen von ca. 400 mm im Norden bis 2000 mm im Südosten (HAYWARD & OGUNTOYINBO, 1987). Dabei fallen ca. 80% der Niederschläge zwischen Juli und September. Insgesamt ist ein starker Nord-Süd Gradient in den Isohyeten des Voltabeckens zu erkennen.

Der Verlauf der Regenzeit in West Afrika wird größtenteils durch saisonale Verlagerung der Intertropischen Konvergenzzone (ITCZ) gesteuert. Demnach weisen Stationen im Norden des Untersuchungsgebiets eine unimodale Niederschlags-verteilung auf, im Süden dagegen finden zwei Regenzeiten statt. Die Länge der ersten Regenzeit (*major season*) nimmt dabei von Süden nach Norden hin ab. Das Einsetzen der ersten Regenzeit erfolgt abrupt mit einer sprunghaften Nordwärtsbewegung der ITCZ, die im Mittel mit der 37. Pentade (29.06 – 04.07) beginnt. Dabei springt die ITCZ von einem quasi-stabilen Zustand bei 3 - 6° N zu ei nem weiteren quasi-stabilen Zustand bei 8 – 12° N.

Die Gründe für die Niederschlagsvariabilität lassen sich wie folgt zusammenfassen:
Auf der **interannuellen Skala** ist die Stärke des *African Easterly Jet* AEJ und *Tropical Easterly Jet* TEJ für abnormal trockene und feuchte Bedingungen verantwortlich (JENKINS et al., 2002). Verstärkte Amplituden des AEJ werden begleitet von einem abgeschwächten monsunalen Fluß, wohingegen ein starker TEJ zu feuchten Bedingungen führt. Zusätzlich zum Einfluss der Windfelder in höheren Schichten sind geringere Niederschlagsummen verbunden mit:

- Einer Verstärkung des Azorenhochs und einer Abschwächung des St. Helena Hochs. Dies ist verbunden mit einer Zunahme der *Sea Surface Temperature* SST des äquatorialen und südsubtropischen Atlantik und einer Abschwächung der SST im Nordatlantik und einer südlicheren Lage der ITCZ (LAMBERGEON, 1977), und

- Einer positiven *Sea Level Pressure* SLP Anomalie über dem nordöstlichen Atlantik.

Auf **interdekadischer Skala** stellt die SST im Nord- und Südatlantik die wichtigste Einflussgröße dar, die SST im Pazifik ist eher zweitrangig. Daneben sind Einflüsse durch Landnutzungsänderung und Luftqualität (direkter und indirekter Aerosoleffekt) nachgewiesen worden.

Datengrundlage und Methodischer Überblick:

Die Grundlage für alle verwendeten statistischen Methoden stellen 29 Niederschlagszeitreihen für Ghana und Burkina Faso dar. Diese wurden vom *Institute Nationale de l'Environnement et des Recherches Agricoles (INERA)* in Ouagadougou (Burkina Faso) als auch von den Wetterdiensten in Ouagadougou und Accra (Ghana) zur Verfügung gestellt. Die Zeitreihen wurden vorab auf Plausibilität und Vollständigkeit untersucht und für die Zeit 1961-2000 verwendet. Ferner wurden für die Wetterlagenklassifikation diverse meteorologische Felder verwendet, die von NCEP/NCAR bereitgestellt werden. Zur Abschätzung der Niederschlagsvariabilität in der Periode 2011-2040 werden Ergebnisse des globalen Klimamodells ECHAM5 verwendet, die mittels des A1B Szenario angetrieben werden.

Abbildung II gibt einen schematischen Überblick über die drei übergeordneten Strategien und die dabei zum Einsatz kommenden Methoden:

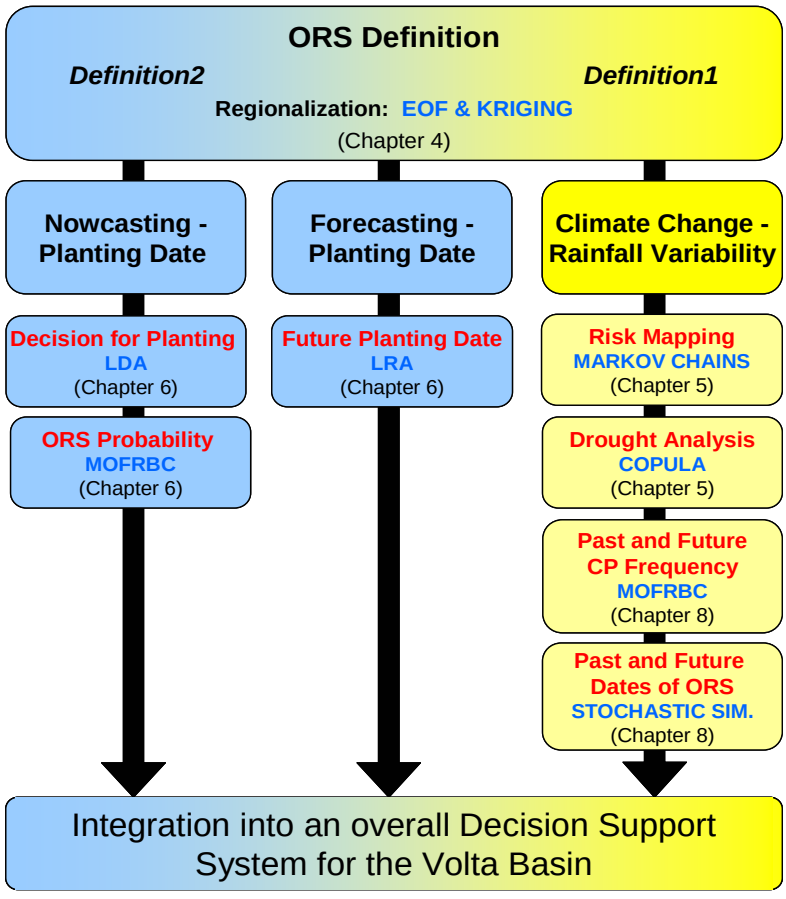

Abbildung II: Schematischer Überblick über die drei verschiedenen Strategien, die in dieser Arbeit verfolgt wurden. Die unterschiedlichen Untersuchungsthemen sind in rot, die verwendeten statistischen Verfahren in blau hervorgehoben.

Die drei übergeordneten Strategien umfassen ein *Nowcasting* und ein *Forecasting* für die Bestimmung des optimalen Anpflanzzeitpunktes sowie die Analyse des Einflusses des Klimawandels auf die Niederschlagsvariabilität. Für das *Now-* und *Forecasting* und teilweise die Erfassung des Klimawandels stellt die Definition des Regenzeitbeginns eine wichtige Voraussetzung dar. Die Regionalisierung der Ergebnisse wurde mittels Hauptkomponentenanalyse und Kriging durchgeführt. Das übergeordnete Ziel dieser Arbeit ist es Entscheidungshilfeinstrumente für den landwirtschaftlichen Sektor zu entwickeln, die mit dem Enden von Phase 3 des GLOWA Volta Projekts in ein übergeordnetes DSS integriert werden sollen. Die drei Strategien werden im Folgenden beschrieben:

i) Eine *Nowcasting Strategie*, welche die Lineare Diskriminanzanalyse (LDA) und einen auf Fuzzy-Logik basierenden Klassifikationsalgorithmus (MOFRBC) zur Problemlösung verwendet. Die LDA wird Tag für Tag benutzt, um zu prüfen, ob die Regenzeit (nach Definition) bereits eingesetzt hat.

   MOFRBC wird zur Identifizierung von Wetterlagen verwendet, die signifikant mit dem Einsetzen der Regenzeit einhergehen. Zur Modellkalibrierung wurden NCEP/NCAR Reanalysen von 1961-1999 verwendet. Die Klassifizierung täglicher von NCEP/NCAR zur Verfügung gestellter GFS Felder in die auf den Regenzeitbeginn hin optimierten Wetterlagen erlaubt eine wahrscheinlichkeitstheoretische Aussage, ob der aktuelle Tag als Regenzeitbeginn angesehen werden kann.

ii) Eine *Forecasting Strategie* basierend auf einer Linearen Regressionsanalyse (LRA). Obwohl die LRA streng genommen nicht zur Vorhersage eingesetzt werden soll, wird sie im Folgenden zur Abschätzung des regionalen Regenzeitbeginns verwendet. Unter der Voraussetzung, dass man den Regenzeitbeginn einer Region kennt, lässt sich der Regenzeitbeginn sukzessive für alle anderen Regionen schätzen.

iii) Es werden die Auswirkungen des Klimawandels auf die Niederschlagsvariabilität im Voltabecken untersucht. Dabei kommen Markov Ketten, ein Copula Ansatz sowie der Wetterlagenklassifikationsansatz in Verbindung mit stochastischer Niederschlagssimulation zum Einsatz.

Eine auf den an der Erdoberfläche gemessenem Niederschlag basierende Definition des Regenzeitbeginns wurde entwickelt. Diese Definition ähnelt dem Ansatz von SARRIA-DODD & JOLLIFFE (2001), welcher wiederum ein modifizierter Ansatz von STERN et al. (1982) darstellt. Nach SARRIA-DODD & JOLLIFFE (2001) müssen folgende Bedingungen für den Regenzeitbeginn gleichzeitig erfüllt sein:

1. Es fallen mindestens 25 mm Niederschlag in 5 aufeinanderfolgenden Tagen;

2. Der erste und mindestens zwei weitere Tage dieser 5-Tage-Periode sind Regentage (Niederschlag ≥ 0.1mm);

3. Es findet keine Trockenperiode > 6 Tagen innerhalb der nächsten 30 Tage statt.

Da ein gleichzeitiges Erfüllen der o. g. Kriterien zu keinem oder zu einem für landwirtschaftliche Zwecke zu späten Regenzeitbeginn (zu kurze Vegetationsperiode) im Untersuchungsgebiet führt, werden die drei Kriterien jeweils durch Zugehörigkeitsfunktionen (Fuzzy-Logik) entschärft (Abbildung III):

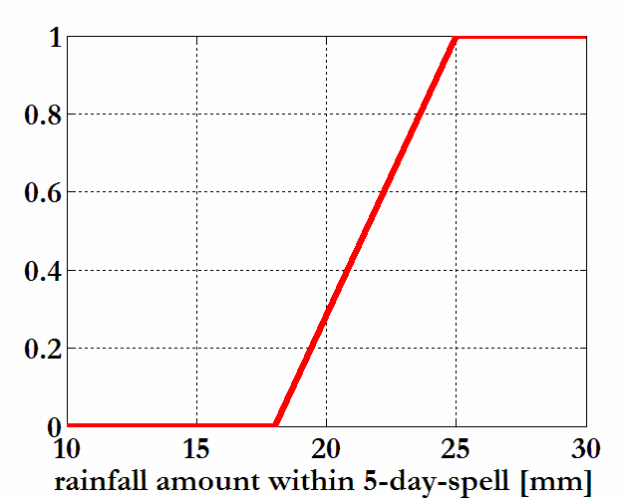

Abbildung III: Dreiecksfunktion zur “Fuzzifizierung” der 1. Bedingung für den Regenzeitbeginn. Für den Fall, dass Niederschlag > 18 mm innerhalb 5 aufeinanderfolgenden Tagen fällt, nimmt die Zugehörigkeitsfunktion Funktionswerte > 0 an und kann potentiell zum Regenzeitbeginn führen.

Die Berücksichtigung aller o. g. Kriterien (nachfolgend als Definition1 bezeichnet) ist lediglich ex-post möglich. Für das *Now- und Forecasting* können nur die ersten beiden Kriterien berücksichtigt werden (Definition2), da eine verlässliche Vorhersage des Niederschlags für die nächsten 30 Tage derzeit noch nicht möglich ist. Unter Verwendung der Niederschlagszeitreihen wird das Produkt der Funktionswerte der zwei bzw. drei Zugehörigkeitsfunktionen berechnet. Übersteigt das Produkt an einem Tag X einen vordefinierten Schwellenwert, dann kann der Tag als Regenzeitbeginn angesehen werden. Die Definition des Regenzeitbeginns und dem damit verbundenen Termin zur Aussaat kann durch die Auswahl des Schwellenwerts als auch durch Modifikation der Zugehörigkeitsfunktionen (z.B. Abbildung III) auf bestimmte Anbaufrüchte und Regionen optimiert werden.

Ausgewählte Ergebnisse:

Abbildung IV zeigt die räumliche Verteilung des langjährigen Mittelwertes (1961-2000) sowie der Standardabweichung des Regenzeitbeginns im Voltabecken unter Verwendung eines Schwellenwertes von 0.4 für Definition1. Diese Karten stellen wertvolle Informationen für das landwirtschaftliche Management im Voltabecken dar. Zusätzlich zum Regenzeitbeginn wurden Karten für das Ende, die Länge der Regenzeit, schwellenwertabhängige Regenwahrscheinlichkeiten und Risikokarten für das Auftreten von Dürreperioden > 6 Tage innerhalb der nächsten 30 Tage (3. Definitionskriterium) erstellt.

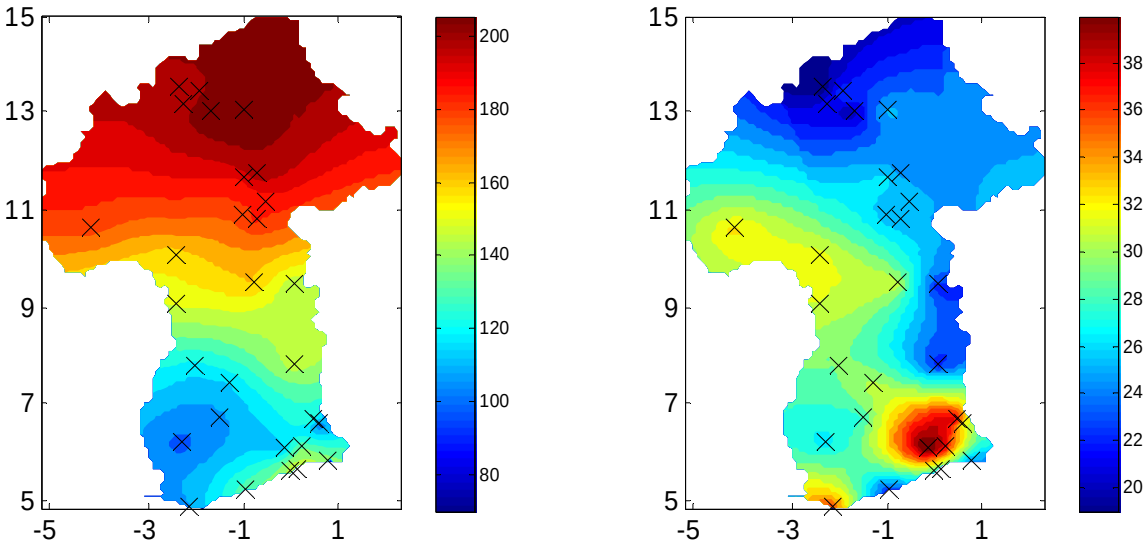

Abbildung IV: Interpolierter Mittelwert (links) und Standardabweichung (rechts) des Regenzeitbeginns [Julianischer Tag] unter Berücksichtigung der drei o. g. Kriterien für den Regenzeitbeginn (Definition1).

Zusätzlich wurde das Voltabecken zuvor mittels Hauptkomponentenanalyse in 5 Regionen unterteilt, die ein ähnliches Niederschlagsverhalten zeigen (Abbildung V):

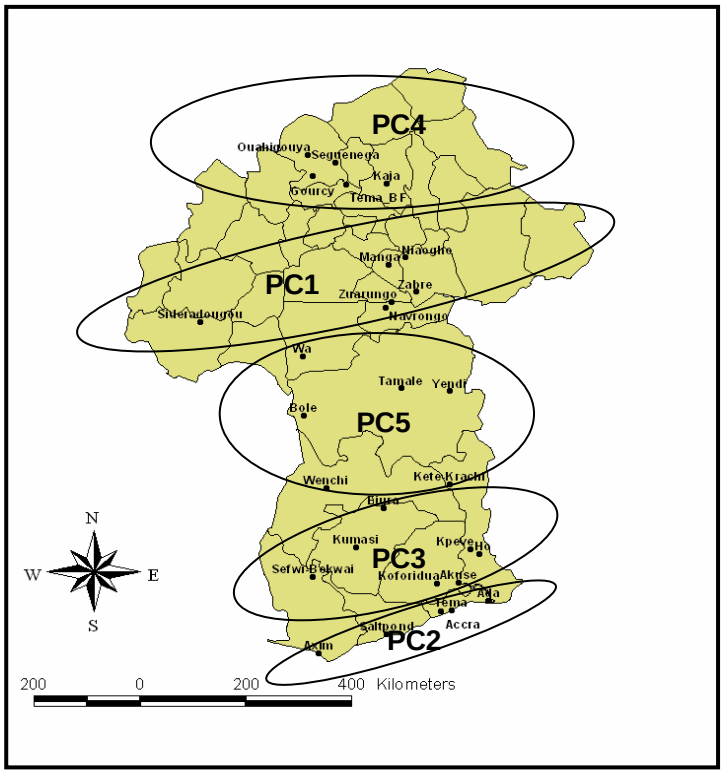

Abbildung V: Unterteilung des Voltabeckens in 5 Regionen mit unterschiedlichem Niederschlagsverhalten. Die Gruppierung wurde auf das saisonale Verhalten des Niederschlags fokussiert, weniger wichtig für die Klassifizierung waren die Niederschlagssummen.

Es ließen sich teilweise große regionale Unterschiede im Regenzeitbeginn beobachten. Tabelle I gibt eine Zusammenfassung der regionalen Unterschiede im Regenzeitbeginn unter Berücksichtigung von Definition1 und Definition2, berechnet für den Zeitraum 1961-2001:

Definition1	Mean onset [Julian day]	Standard dev. [days]	Trend [days/year]	Signif. [%]
PC1	140	19	0.71	99
PC2	96	22	0.45	88
PC3	75	16	0.44	96
PC4	168	16	0.22	70
PC5	101	22	0.42	99
Definition2	**Mean onset [Julian day]**	**Standard dev. [days]**	**Trend [days/year]**	**Signif. [%]**
PC1	147	24	0.32	80
PC2	102	24	0.01	20
PC3	71	19	0.31	80
PC4	172	19	-0.10	62
PC5	102	23	0.30	79

Tabelle I: Mittelwert, Standardabweichung, Trend und Signifikanzniveau des regionalen Regenzeitbeginns unter Verwendung von Definition1 und Definition2; (LAUX et al., 2008).

Die wichtigsten Ergebnisse für die in Abbildung II beschrieben drei unterschiedlichen Strategien lassen sich wie folgt zusammenfassen:

i) ***Nowcasting*:** Die LDA eignet sich als Methode zur Überprüfung auf Tagesbasis, ob die Regenzeit bereits eingesetzt hat. Ausgehend von einer Apriori-Wahrscheinlichkeit von 7% für die Klasse Regenzeitbeginn, konnte eine Trefferquote von bis zu 80% nach erfolgter Reklassifizierung unter Verwendung der ermittelten Diskriminanzfunktionen erreicht werden. Die Trefferquoten sind regional sehr unterschiedlich und schwanken zwischen 56% (PC2) bis 80% (PC4).

   Unter Verwendung eines auf Fuzzy-Logik basierenden Wetterlagen-klassifikationsalgorithmus konnten Wetterlagen signifikant mit dem Regenzeitbeginn in Verbindung gebracht werden. Für die Küstenregion (PC2) wurde in diesem Zusammenhang eine starke positive Anomalie der Oberflächentemperatur mit dem Zentrum über 10° S und 20° W detektiert. Für die zentrale Region (PC5) eignete sich besonders die horizontale Komponente des Feuchteflusses in 500hPa. Bei der entsprechenden Wetterlage dominieren eine große positive Anomalie mit dem Zentrum über Ägypten sowie eine relativ starke positive Anomalie östlich des Voltabeckens. Dieses Muster kann mit dem Auftreten von Böhenlinien (sog. *squall lines*) in Verbindung gebracht werden, welche aus Osten bis Nordosten kommend über das Voltabecken ziehen und im Zentrum für den größten Teil des Niederschlags verantwortlich sind.

ii) ***Forecasting*:** Unter der Voraussetzung der Kenntnis des Regenzeitbeginns einer Region (PC3) kann der Regenzeitbeginn aller weiteren Regionen sukzessive geschätzt werden. Dazu wird ein linearer Regressionsansatz verwendet. Der Varianzerklärungsanteil ist als schwach bis mittelstark zu beurteilen.

iii) ***Auswirkungen Klimaänderung*:** Trendanalysen zeigen eine Verspätung des Regenzeitbeginns aller 5 Regionen von 1961-2001. Dabei sind im zentralen Voltabecken (PC3, PC5 und PC1) nach Anwendung beider Definitionen die stärksten und signifikantesten Trends zu erkennen. Die Küstenregion (PC2) und der nördliche Teil des Beckens (PC4) zeigen jeweils schwächere Trends. PC1 weist den größten Trend auf. Für Definition1 (Definition2) kann eine signifikante Verzögerung im Regenzeitbeginn von 28 Tagen (13 Tagen) beobachtet werden.

Die regionalen Häufigkeitsverteilungen des Regenzeitbeginns zwischen Vergangenheit (1961-2000) und der Periode 2001-2040 wurden verglichen. Unter der Annahme des gemäßigten Szenarios A1B (ECHAM5) wird sich der Regenzeitbeginn weiterhin

verspäten, speziell für die zentralen Regionen PC3, PC5 und PC1. Abbildung VI zeigt die Häufigkeitsverteilung des Regenzeitbeginns beider Zeitscheiben für Region PC5.

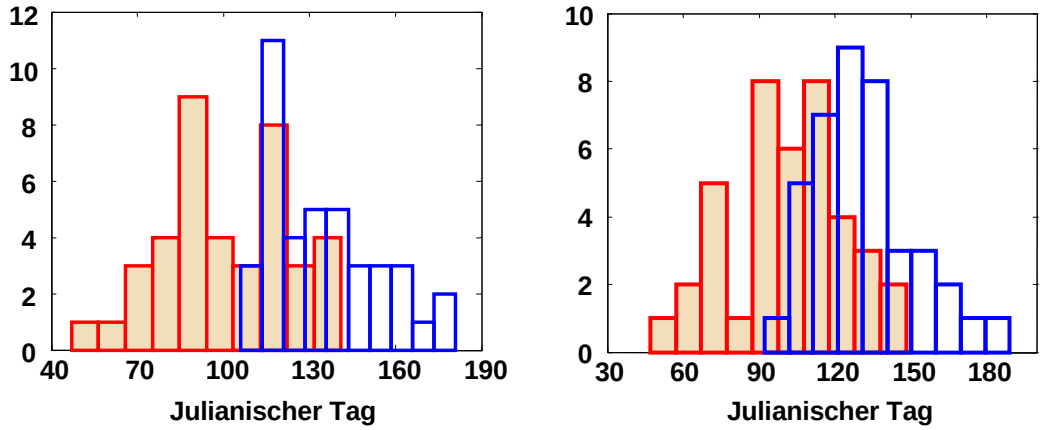

Abbildung VI: Häufigkeitsverteilung des Regenzeitbeginns innerhalb PC5 [Julianischer Tag] der Zeitscheibe 1961-2000 (rot) und der Zeitscheibe 2001-2040 (blau) unter Verwendung von Definition1 (links) und Definition2 (rechts).

Auch für die Analyse der Klimaänderung wurde eine Wetterlagenklassifikation durchgeführt. Die Klassifikation der Wetterlagen basiert auf Fuzzy-Regeln, die zuvor auf die Tagesniederschlagssummen hin optimiert wurden. Als Prädiktorvariable eignete sich besonders der ostwärts gerichtete Feuchtefluß in 500hPa. Die ermittelten Regeln (Anomalieverteilung einer Wetterlage) wurden im nächsten Schritt zur Klassifikation zukünftiger Wetterlagen verwendet. Besonders feuchte als auch trockene Wetterlagen der vergangenen Klimanormalperiode (Referenzperiode) 1961-1990 wurden identifiziert. Die Auftrittshäufigkeiten der Zeitscheibe 2011-2040 wurden mit denen der Referenzperiode in Beziehung gebracht (Abbildung VII). Für die zukünftige Zeitscheibe 2011-2040 lassen sich für PC5 (zentrales Voltabecken) teilweise drastische Zu- und Abnahmen trockener (CP1, CP2, CP3, CP4, CP11) und feuchte (CP7) Wetterlagen erkennen.

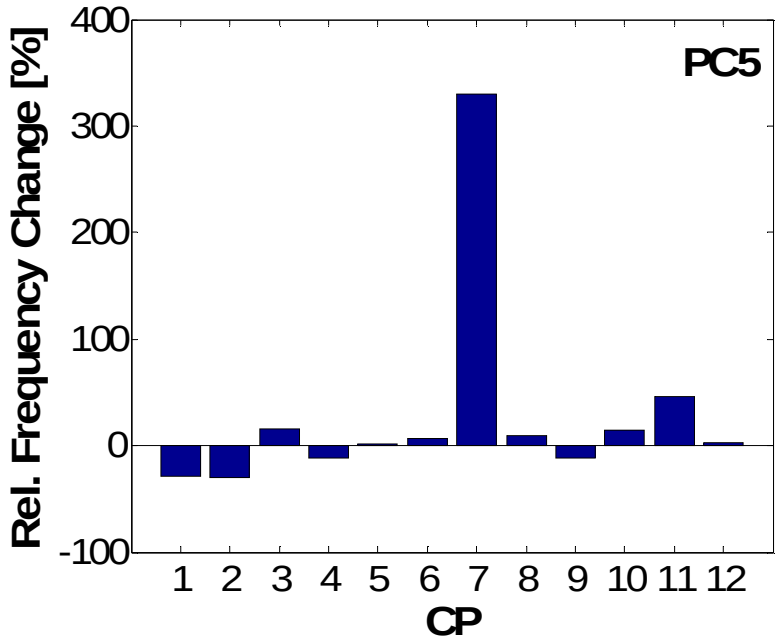

Abbildung VII: Änderung der Auftrittshäufigkeiten von Wetterlagen in der Region PC5 der zukünftigen Periode 2011-2040 relativ zur Klimanormalperiode 1961-1990. Die Prädiktorvariable der zugrundeliegenden Wetterlagenklassifikation ist der ostwärts gerichtete Feuchtefluß in 500hPa.

TABLE OF CONTENTS

LIST OF FIGURES

Number **Page**

LIST OF TABLES

Number **Page**

ACKNOWLEDGEMENTS

Though the following dissertation is an individual work, I could never have reached the heights and explore the depths without the support and guidance of a lot of people:

First, I would like to express my gratitude to Dr. Harald Kunstmann (IMK-IFU) for proposing the interesting topic, his continuous support and guidance throughout this work.

I am very grateful to Prof. András Bárdossy (University of Stuttgart) for his excellent supervision, valuable suggestions and support.

My sincere gratitude goes to Prof. Jucundus Jacobeit (University of Augsburg) for his kind agreement to act as secondary referee and for his valuable suggestions.

This work is part of the research project GLOWA-Volta founded by the German Ministry of Education and Research (BMBF). Many thanks to all co-workers and partners of the GLOWA-Volta project for the good cooperation. The collaboration with the Meteorological Services Department in Ghana is greatly acknowledged.

Special thanks to all my colleagues and friends at the institute for the good working atmosphere, the funny coffee and lunch breaks and the spare time activities. Special thanks to Dr. Andreas Marx (IMK-IFU) and Daniel Naumann (University of Treves) for proofreading the manuscript and the English correction.

I am extremely grateful to my family for their encouragement and their financial support throughout my previous path of life.

Most of all, I would like to thank my partner Selina Utzig for her understanding, her loyalty and commitment. Thank you for taking care of our little son Marlon especially during my overtimes.

LIST OF ABBREVIATIONS

AEJ	African Easterly Jet
ARA	Annual Rainfall Amount
ARMA	Autoregressive Moving Average
ANN	Artificial Neural Networks
ANOVA	Analysis of Variance
CDC	Climate Diagnostics Centre
CIRES	Cooperative Institute for Research in Environmental Sciences
CONV	Lower Convergence Zone
CP	Circulation Pattern/Weather Pattern
CPA	Circulation Pattern Analysis
CRS	Cessation of the Rainy Season
CRU	Climatic Research Unit
DDS	Dynamical Downscaling
DIV	Upper Divergence Zone
DOY	Day of Year
DOF	Degree of Fulfillment
DSS	Decision Support System
ECHAM	European Centre Hamburg (global climate model)
EDI	Effective Drought Index
ENSO	El Nino Southern Oscillation
EOF(s)	Empirical Orthogonal Function(s)
GCM(s)	Global Circulation Model(s)
GFS	Global Forecast System
GLOWA	Globaler Wandel des Wasserkreislaufes (Global Change in the Hydrological Circle)
GPCP	Global Precipitation Climatology Project
GPH	Geopotential Height
GVP	GLOWA Volta Project
INERA	Institute Nationale de l'Environnement et des Recherches Agricoles
IPCC	Intergovernmental Panel on Climate Change

ITCZ	Intertropical Convergence Zone
ITF	Intertropical Front at the surface
KLIWA	Klimaveränderung und Konsequenzen für die Wasser-wirtschaft
LDA	Linear Discriminant Analysis
LRA	Linear Regression Analysis
LRS	Length of the rainy season
MEI	Multivariate ENSO Index
MF_U	Easterly Moisture Flux
MF_V	Northerly Moisture Flux
MF_UV	Resulting Moisture Flux
MOFRBC	Multi Objective Fuzzy Rule Based Classification
MPI	Max Planck Institute
MSE	Mean of squares due to error
MSR	Mean of squares due to regression
NaN	Not a Number
NAO	North Atlantic Oscillation
NCAR	National Center for Atmospheric Research
NCEP	National Centers for Environmental Prediction
NRD	Number of rainy days
NRD_X	Number of rainy days x days before
NOAA	National Oceanic and Atmospheric Administration
ORS	Onset of the Rainy Season
PCA	Principal Component Analysis
PC(s)	Principal Component(s)
pET	potential Evapotranspiration
RA_X	Rainfall Amount x days before
RCM	Regional Climate Model
SA	Simulated Annealing
SARI	Savannah Agricultural Research Institute (Ghana)
SDS	Statistical Downscaling
SH	Specific Humidity
SL(s)	Squall Line(s)
SLP	Sea Level Pressure
SLPA	Sea Level Pressure Anomaly

SOI	Southern Oscillation Index
SPI	Standardized Precipitation Index
SRES	Special Report on Emissions Scenarios
SST	Sea Surface Temperature
SSTo	Sum of squares due to total
SSE	Sum of squares due to error
SSR	Sum of squares due to regression
T_{SKIN}	Skin Temperature
TEJ	Tropical Easterly Jet
TNA	Tropical North Atlantic
TSA	Tropical South Atlantic
U	Eastward wind speed
V	Northward wind speed
VIF	Variance-Inflation factor
WAM	West African Monsoon
WC	Walker Cell
WG	Weather Generator

Chapter 1

1. Introduction

"All models are wrong, but some are useful" - George Edward Pelham Box

(One of the most influential statisticians of the 20th century)

1.1 Motivation

The Volta Basin, which is located in a semi-arid to sub-humid environment of West Africa within latitudes 5° 30' N and 14° 30' N and longitudes 2°00' E and 5°30' W, is covering an area of about 414000 km^2. The main parts of the basin are situated in Burkina Faso (43%) and Ghana (42%). Minor parts are distributed among Togo, Côte d´Ivoire, Mali and Benin (Figure 1). The construction of the Akosombo dam in 1965 eventually leads to the existence of the Lake Volta, which is the largest artificial lake all over the world in terms of surface area. It covers approximately 4% of Ghana's total area.

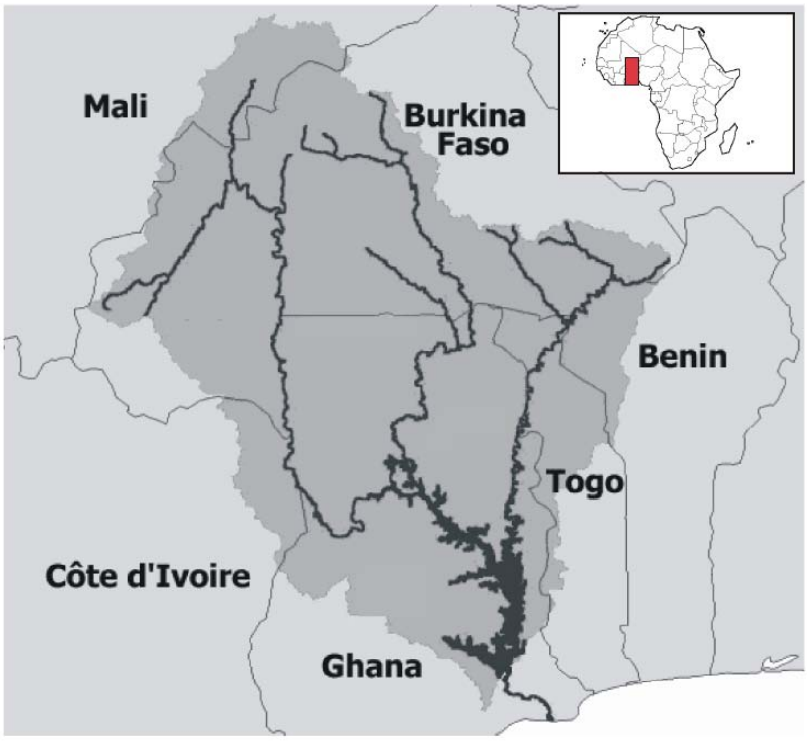

Figure 1: The Volta Basin (modified after: MARX et al., 2007).

However, the livelihood of the population remains dependent on rainfed agriculture, especially in the semi-arid north of the Volta Basin. In the past, West Africa has experienced a long history of rainfall fluctuations of varying lengths and intensities. The worst reported droughts have taken place in the 1910s, which affected East and West Africa alike. They were followed by increasing rainfall amounts, but reversal trends where observed again from 1950 onwards culminating in the mid 1980s and early 1990s. As a result, severe and long-lasting droughts occurred affecting the whole Sahel. More than 30 million people were in urgent need of food aid and about 250000 people died of starvation. Since the 1990s West Africa has recorded a series of wet years frequently accompanied by floods which were often interpreted as the end of the Sahelian drought (NICHOLSON et al., 2000).

In 2007, shortages in rainfall led to crop failure of the cocoa in West Africa, resulting in a drastic increase of the cocoas' world market price. A few months later, during the months of August and early September 2007, heavy rainfall led to severe flooding in several West African countries resulting in the loss of lives, displacement of vulnerable persons and the destruction of key infrastructure, food stocks and livestock throughout the region. More than 600.000 people have been affected by the floods in Ghana, Nigeria, Burkina Faso, Togo, Mali, The Gambia, Niger, Senegal, Côte d'Ivoire, Liberia, Mauritania, Sierra Leone and Benin. The floods coincide with the most critical time of the year, the lean season, when West African families - mostly in the Sahel region - face food insecurity. Thus, the destruction of crop and food stocks has aggravated the vulnerability of poor families and needs to be addressed promptly through emergency and recovery interventions[1].

Figure 2: Destroyed maize field (left) and flooded rice farm (right) in Ghana 2007.

For the future, continuing rainfall fluctuations with abnormally wet and dry years are expected. Especially in areas, where rainfall is the most limiting factor for agriculture, farming management is of major concern to ensure food supply for the rapidly growing

[1] http://ochaonline.un.org/

population. Every year farmers face the crucial question with regard to the best date for sowing: Do the first rainfalls after the dry season resemble the onset of the rainy season or not? The farmers' seeds and efforts will be lost if no significant rainfall follows within the next one or two weeks after seeding. If they do not sow, but the first rains were already part of the rainy season, valuable time for agricultural production is lost. Apparently, the benefits of a solution to this problem would be enormous. The main challenge of the research topic ONSET OF THE RAINY SEASON (ORS), which is part of the GLOWA Volta atmosphere cluster, is to find the relevant indicators to reliably predict the rainy seasons' onset and include these data into a Decision Support System (DSS).

The overall objective of the GVP is the analysis of the physical and socio-economic determinants of the hydrological cycle in the face of global climate change. Based on this, the project aims at the establishment of a scientifically sound DSS for water resource management accessible by a wide range of stakeholders. The envisaged time frame is nine years. The GVP is part of the larger GLOWA Program, which is financed by the Federal Ministry of Education and Research. Additional funding comes from the Ministry of Science and Research of North Rhine – Westphalia[2]. The tools developed in the context of the GVP are intended to serve two goals:

i. to advance the scientific understanding of the complex linkages between atmosphere, land use, human settlement & economic activities and the hydrologic cycle; and

ii. to support economically- and ecologically sound water management decision-making in the Volta Basin[3].

1.2 Objectives of the Thesis

According to the above outlined problems in this drought prone region and the classification of the topic ONSET OF THE RAINY SEASON (ORS) in the overall context of the GVP, the following research questions are addressed:

- What is an agricultural meaningful definition of the rainy seasons' onset with special regard to applicability for West African farmers?
- Is it possible to predict reliably the onset of the rainy season for the current season?
- What are the impacts of global climate change on rainfall variability in the Volta Basin?

[2] http://www.glowa.org/

[3] http://www.glowa-volta.de/

1.3 Innovation of the Doctoral Thesis

Innovative work of this thesis includes:

- Development of a regional and fuzzy logic-based definition of the onset of the rainy season for the Volta Basin. Basing on this, the application of the linear discriminant analysis for the prediction of the rainy season in the Volta Basin with a hit ratio up to 80%.

- Identification of 1) large scale weather patterns to the single event ORS using a multi objective fuzzy rule based classification method, 2) wet and droughty weather patterns in the Volta Basin and 3) suitable predictor variables.

- Analysis of the expected frequency change of these weather patterns until 2040 due to global climate change basing on the emission scenario A1B and ECHAM5.

- Development of a drought definition basing on the *Effective Drought Index* EDI. Analysis of return periods of drought by means of a Copula approach.

Chapter 2

2. Climatology of the Volta Basin

This chapter deals with the large scale climatology of West Africa with a special focus on regional aspects within the Volta Basin. In general, the climate can be described as semi-arid to sub-humid. In the semi-arid climate, the potential evaporation (pET) exceeds precipitation within 6-9 months. In contrast, a climate is defined as sub-humid whether in 6-9 months precipitation exceeds the pET (HAYWARD & OGUNTOYINBO, 1987). Under all climatologic aspects, rainfall is the dominant factor for the rainfed agriculture in West Africa. In West Africa, life is revolving around the occurrence or non-occurrence of rainfall (SIVAKUMAR, 1992A). West Africa has experienced an increasing scientific attention since the occurrence of the severe droughts in the mid 1980s. Since then, these years were generally followed by a number of wet years with higher-than-average rainfall amounts. But rainfall will continue fluctuating, averagely wet and dry years will alternate. Consequently, there are a lot of studies dealing with rainfall variability in West Africa. Some basic information of the West African climatology with special focus to rainfall is given: The large scale dynamics controlling weather in West Africa are discussed in Chapter 2.1, followed by a short introduction of the meteorological measures of temperature in Chapter 2.2, rainfall in Chapter 2.3, and evaporation in Chapter 2.4. The agro-ecological zones are described in Chapter 2.5 and past trend of the most prominent hydro-meteorological are exposed in Chapter 2.6.

2.1 Large Scale Dynamics

The general climate characteristics, like e.g. the annual cycle of temperature and rainfall, are primarily controlled by the large scale dynamics of the atmosphere. The global circulation system is formed as a consequence of the latitudinal dependence of solar insolation. It transports the thermal energy polewards, and is thus reducing the resulting equator-to-pole temperature contrast. The basic structure of the atmospheric circulation remains fairly constant, but it is seasonally modulated by the altitude of the sun showing weak year-to-year variability. In equatorial areas, Hadley circulation and Walker circulation are elements of the global circulation system mainly influencing West African climate dynamics. The Hadley cell is a circulation pattern that dominates the tropical atmosphere, with rising motion near the equator, poleward flow of about 10-15 kilometers above the surface, descending motion in the subtropics, and equatorward flow near the surface. This circulation is intimately related to the trade winds, tropical rain belts, subtropical deserts as well as the jet streams. The Walker cell is arranged in zonal

direction. As the easterly trades move at low levels across the Pacific Ocean, the air rises in the Western Pacific and then descends again in the Eastern Pacific. This large scale zonal circulation results in rising air over the Western Pacific and descending air over the Eastern Pacific and is called a Walker Cell.

The Intertropical Convercenge Zone (ITCZ)[4] is posing a boundary zone between the two Hadley-type cell circulations of the two hemispheres and it is influencing most flow characteristics in West Africa. It separates humid maritime air masses from dry continental air masses from the Sahara, the Harmattan. The mean West African boreal summer circulation has yet been described by various authors (e.g. HASTENRATH, 2000; MCGREGOR & NIEUWOLT, 1998, KAMARA, 1986). Following an annual cycle, the ITCZ moves northwards up to 25° - 30° N in boreal summer. The wet south-westerly flow moves into the inner continent as a function of pressure and thermal gradients that settle between the relatively cool ocean and the heated desert.

During the rainy season from May to approximately November, a thermally induced low pressure cell is prevailing over the Sahara with its axis located between 18° N and 22° N and a subtropical anticyclone intensifies and extends equator-wards. As a function of the pressure gradients between these two cells an unstable wet and cold south-westerly flow (south-west monsoon) penetrates deep into the inner continent and reaches latitudes of 20° N - 22° N in August. During the dry season the prevailing flow is the Harmattan. Regions in the southern part of West Africa therefore experience two rainy seasons, whereas regions in the north only show one.

In upper levels, monsoonal winds and Harmattan are overlain by the the African Easterly Jet (AEJ) at approximately 600 - 700hPa and the Tropical Easterly Jet (TEJ) at 200hPa, both also related to the ITCZ. Strength and location affect the climatic conditions in West Africa. Figure 3 is illustrating schematically the dominant factors affecting West African climate.

[*4] The general term for the convergence of the northeasterly and southeasterly trade winds in the tropics is the Intertropical Convergence Zone (ITCZ), but some literature refers to it as the Inter-Tropical Discontinuity (ITD). ITD is a more specific term indicating the discrimination of two differing air masses, e.g. for West Africa cold moist air masses and warm dry air masses.

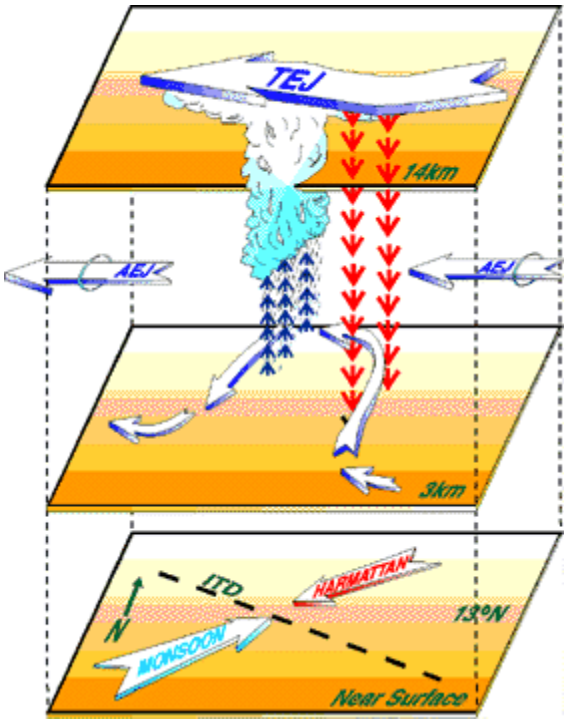

Figure 3: Schematic overview of the most prominent elements determining climate in West Africa at different levels. Instabilities of the AEJ are responsible for the formation of African Easterly Waves (AEWs) (http://www.giss.nasa.gov/research/briefs/druyan_01/).

2.2 Temperature

The mean annual temperature values in the Volta Basin are ranging between 27° and 36° C in the northern part (OGUNTUNDE, 2004), and between 24° C in August and 30° C in March for the South (HAYWARD & OGUNTOYINBO, 1987). The daily range amounts 8 - 14° C in the North and solely 3 - 5° C in the South. The lowest temperatures usually occur in January and are invariably associated with the presence of the Harmattan[5].

2.3 Rainfall

2.3.1 Rainfall Mechanisms

Rainfall is traditionally classified into Convectional, Cyclonic/Frontal and Convergence rainfall according to the processes in the vertical displacement of air and subsequent adiabatic cooling and condensation. In the tropics and especially in tropical West Africa, there is no evidence of cyclonic/frontal activities. With special reference to the Volta Basin these rainfall types are known: monsoonal rainfall and convective rainfall, which may be further distinguished into local convective and squall line rainfall. The different types exhibit specific rainfall amounts, intensities and occurrence frequencies. Almost every cloud development in tropical latitudes is triggered by large scale convergence.

[5] http://www.meteo.gov.gh/climatology.html/

This is because a rather uniform land surface exists and inhomogeneities in the lower surface cannot be counted on to supply the initial perturbation for cloud growth as in continental regions. The three main types are described in the following:

- Monsoonal rainfall: Most of the flow characteristics in West Africa are linked with the Intertropical Discontinuity (ITD), which separates humid maritime air masses from dry, continental air masses from the Sahara. The monsoon of western sub-Saharan Africa is the result of the seasonal shifts of the Intertropical Convergence Zone and the great seasonal temperature differences between the Sahara and the equatorial Atlantic Ocean. The dry, northeasterly trade winds, and their more extreme form, the Harmattan, are interrupted by the northern shift in the ITCZ and resultant southerly, rain-bearing winds during the summer. The semi-arid Sahel and Sudan depend on this pattern for most of their precipitation.

Convective rainfall is always associated with a heating of the land surface and uplifting of air. In combination with an unstable atmosphere cumulus or cumulonimbus towers may be developed that result either in local rainstorms or squall line formations. These clouds may even develop from intense heat induced through slashing and burning or natural bush fires in forest zones or savannah regions. Both, features of local convective rainstorms and linear systems (squall lines), especially with regard to rainfall amount and intensities are described subsequently:

- Local convective rainstorms: Local convective rainstorms are resulting from intense heating of land surfaces such as grasslands, urban areas, rocky mountain terrain and forest clearings. A typical local rainfall is affecting an area of 20 - 50 km^2 with a lifetime of 1 - 2 hours and thus highly variable in space and time. They exhibit the most prominent surface disturbance and together with other small scale disturbances they account for the “patchiness” character of tropical rainfall (KAMARA, 1986). Intense rainfalls with high rainfall rates are the result of the local rainstorms.

- Linear Rainstorms (Squall Lines): According to EAKER (1945), referred to in LEROUX, (2001), squall lines (SLs) are “tropical Africa’s most spectacular phenomena”. Squall lines are organized, long lived mesoscale convective systems propagating from east to west. Southern Chad, the region to the west of the Jos Plateau in Nigeria and Central Ghana are areas with the most frequent squall line activity (OMOTOSHO, 1984). A strong vertical wind shear in the lower troposphere, conditional instability and an atmospheric layering characterized by warm, dry air at middle levels overlying colder, humid air at lower levels are necessary climatological background conditions for their genesis (ROWELL & MILFORD, 1993). The low-level vertical wind shear is related to the African Easterly Jet (AEJ) at 600-700hPa which is generated due to the near surface

meridional temperature gradient between the dry, hot desert air and the humid, cooler air originating from the Gulf of Guinea. They belong to the most important rain-bearing weather systems in tropical West Africa with variable contribution to the annual rainfall amounts depending on the location. Their contribution of squall line systems to the annual rainfall amounts ranges from between 16 and 32% at the Guinea Coast (ACHEAMPONG, 1982; OMOTOSHO, 1985) to around 50% in the Soudanian zone (ELDRIDGE, 1957; OMOTOSHO, 1985) and to eventually 80% in the Sahelian zone. Consequently, interannual rainfall variation is likely to be linked with the interannual variability in the occurrence and intensity of squall lines (FINK & REINER, 2003). Typical rain rates in the convective region of West African SLs are 30 mm h-1, peak values up to 110 mm h^{-1} and durations of about 30 minutes whereas the stratiform part offers a characteristic intensity of 4 mm h^{-1} and a mean duration of 2 - 3 h. Detailed knowledge about the theory of squall lines can be found in ROWELL & MILFORD (1993). Their dynamics are well described in ROUX & TESTUT (1984), and their spatio-temporal variability and relationship to the African Easterly Waves (AEWs) is investigated by FINK & REINER (2003).

2.3.2 Rainy Season

According to SULTAN & JANICOT (2000, 2003A), and SULTAN et al. (2003A), the West African Monsoon onset dynamics follows two distinct phases, the pre-onset and the onset phase. The pre-onset occurs in late spring when the ITCZ establishes itself at 5° (~ May 14th), whereas the actual onset occurs when the ITCZ shifts abruptly northwards (~ June 24th). Afterwards, the ITCZ moves from 5° to 10° N, where it stays for the whole August. Figure 4 is illustrating the Time-Latitude-Rainfall Diagraph for the Volta Basin, which confirms their results. Following the movement of the ITCZ, the monsoon is of bimodal character in the Guinea region and of single mode in the Sahel zone. In these zones, the rainy season's onset seldom occurs abruptly and is often preceded by short isolated showers with intermittent dry spells of various lengths, which are often misinterpreted as the start of the rainy season.

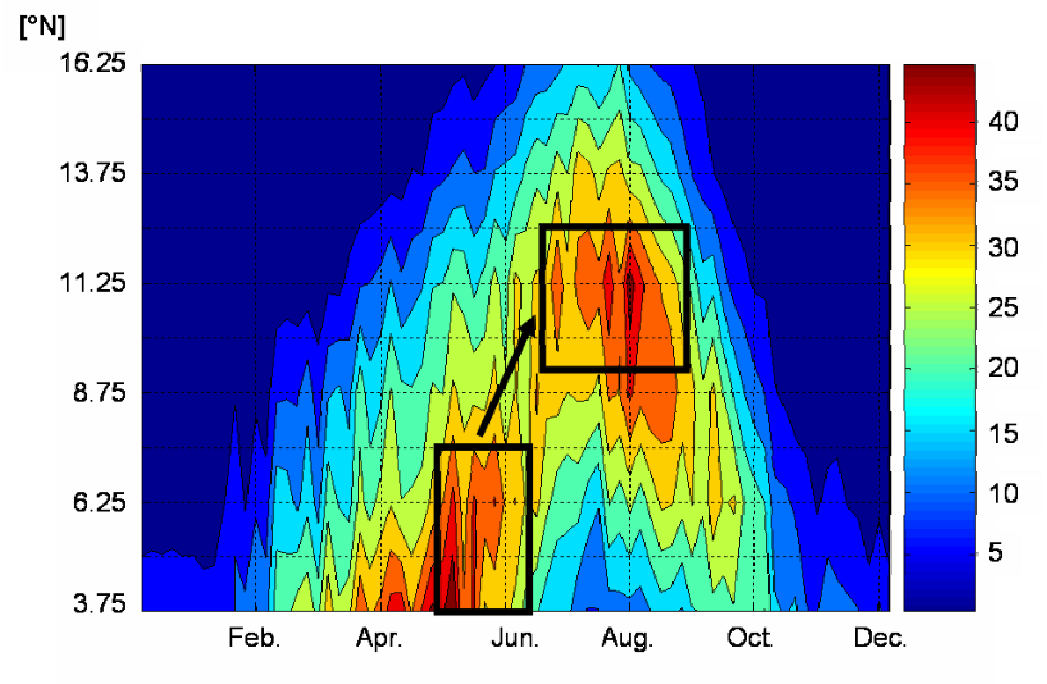

Figure 4: Time-Latitude-Rainfall Diagraph (data source: GPCP 1979-2003, pentadly resolution). At the beginning of June the major rainfall belt with rainfall > 25 mm/5 days (indicated by the black boxes) jumps abruptly northward from ~ 5°N to ~ 11°N.

2.3.3 Rainfall Variability

A high spatial and temporal rainfall variability, evident over the timescales (from intra-seasonal, annual to decadal), can be assigned to the Volta Basin. Figure 5 is illustrating the spatial distribution of the long term mean annual rainfall amount of the Volta Basin. The annual rainfall amount is ranging from 500 mm in the North to ~ 2000 mm in the Southwest. A north south gradient exist with almost parallel latitudinal isohyets, except of a region at the Ghanaian East coast with reduced rainfall amounts, called the “Dahomey-Gap”. In comparison to the West coast region, the rainfall amounts are reduced to about 50% there. The spatial distribution of the rainfall variability is in agreement with the map of the mean annual rainfall isohyets from 1951-1989 (L'HOTE, 1992).

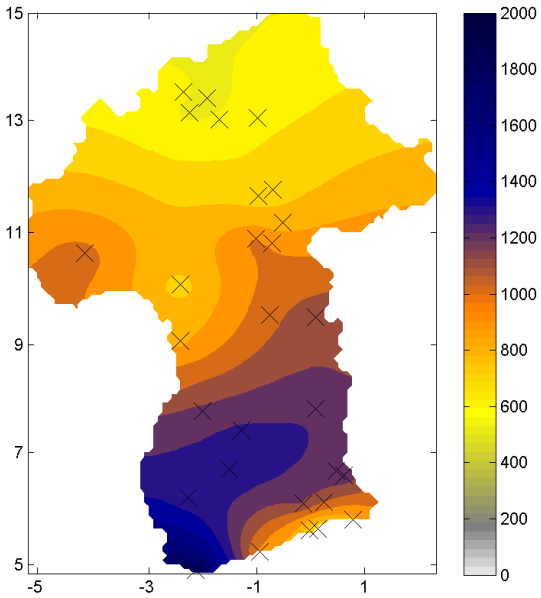

Figure 5: Spatial interpolation of annual rainfall amount [mm] using external drift kriging and the distance to sea. Observation data from 1961-1999 of 29 weather stations (represented by crosses) were used for the interpolation.

While the climate in the humid areas is relatively stable, variability increases towards the sub-humid and semi-arid zones. In the northern Sahel, the standard deviation of the mean annual precipitation is more than 50% (e.g. Nicholson, 2001). Since the beginning of the 1970s, all climatic zones in tropical West Africa, from the arid Sahelian to the humid Guinea Coast climate, have experienced a decade-long period of below-normal annual rainfall amounts (WAGNER & DA SILVA, 1994; NICHOLSON et al., 2000). In this context, LE BARBÉ & LEBEL (1997) noted a decrease in the number of rainy events over the central Sahelian country of Niger in the two dry decades from 1970 to 1989. SHINODA et al. (1999) pointed out that the frequency of heavy rainfall events was especially reduced in years with below-normal rainfall. Despite considerable debate still exist about the current climatic situation i.e. for the Sahel, it seems clear that rainfall has been gradually recovered since the mid 1990s (NICHOLSON, 2005).

The intra-annual rainfall variability is analyzed based on the measured rainfall data from 1961-1999. For this reason, the available rainfall stations are grouped to regions with similar rainfall characteristics. Further information about the regionalization methodology is given in Chapter 4.2.

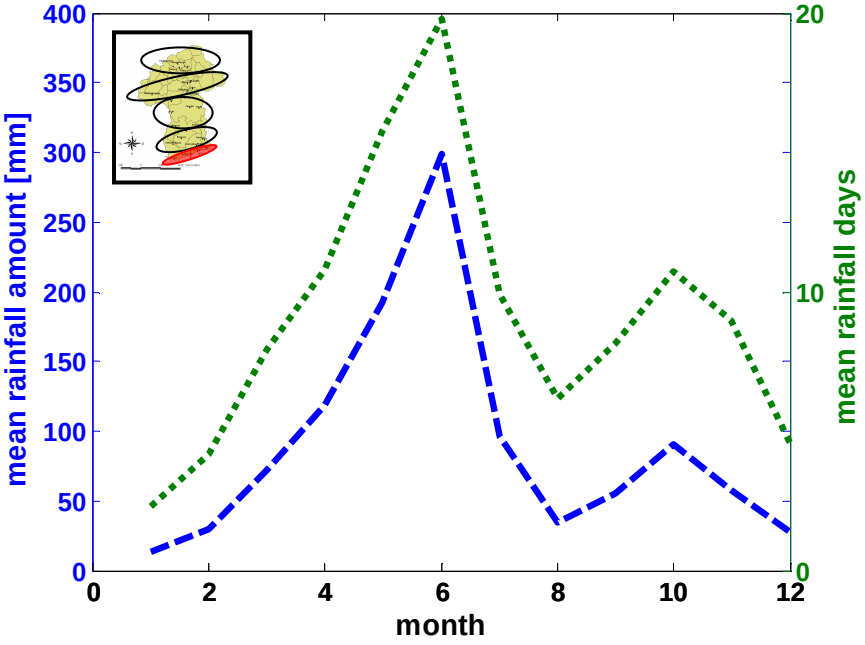
mean rainfall amount [mm]
mean rainfall days
month
0
50
100
150
200
250
300
350
400
0
5
10
15
20
0
2
4
6
8
10
12

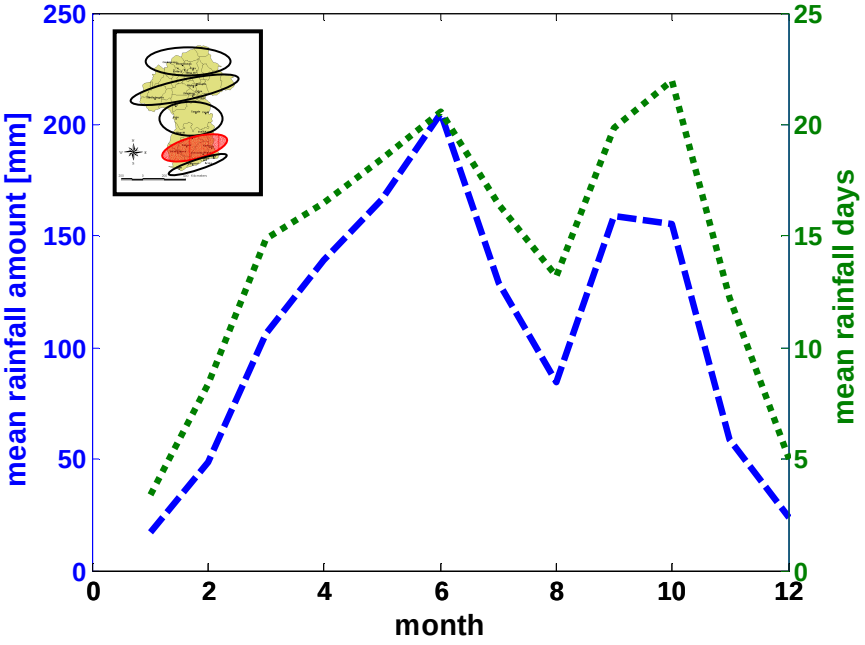
mean rainfall amount [mm]
mean rainfall days
month
0
50
100
150
200
250
0
5
10
15
20
25
0
2
4
6
8
10
12

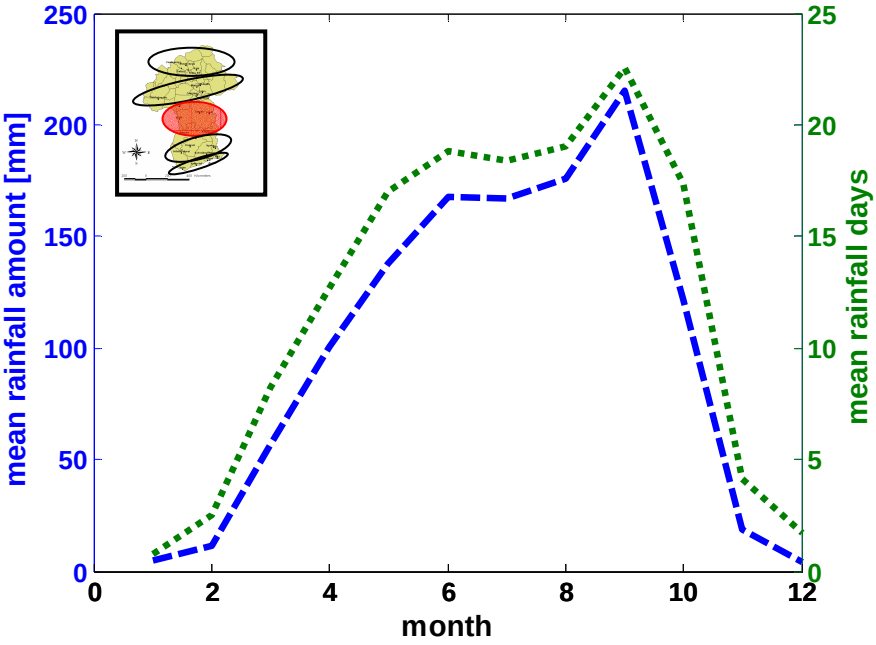
mean rainfall amount [mm]
mean rainfall days
month
0
50
100
150
200
250
5
10
15
20
25
2
4
6
8
10
12

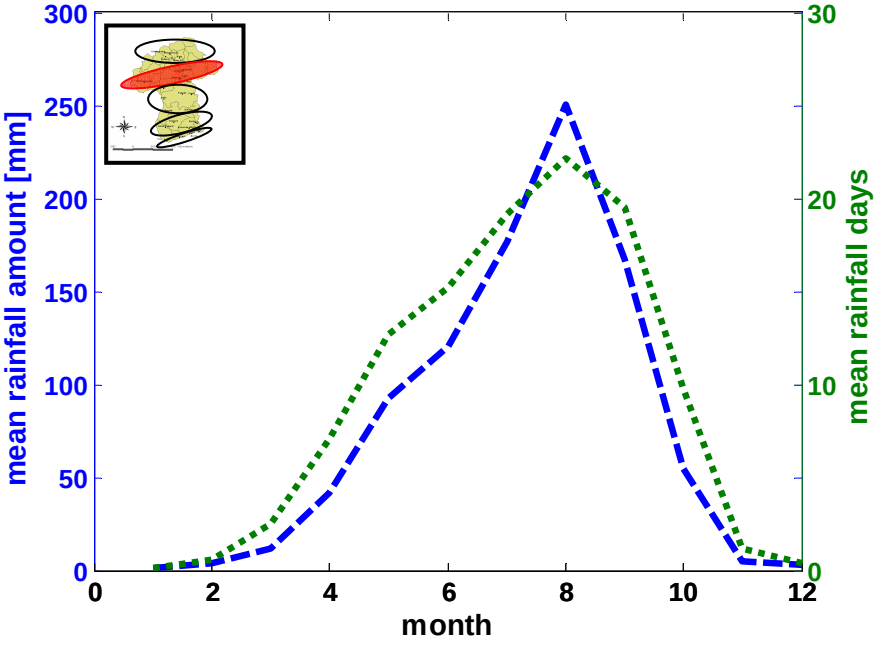
mean rainfall amount [mm]
mean rainfall days
month
0
50
100
150
200
250
300
10
20
30
2
4
6
8
10
12

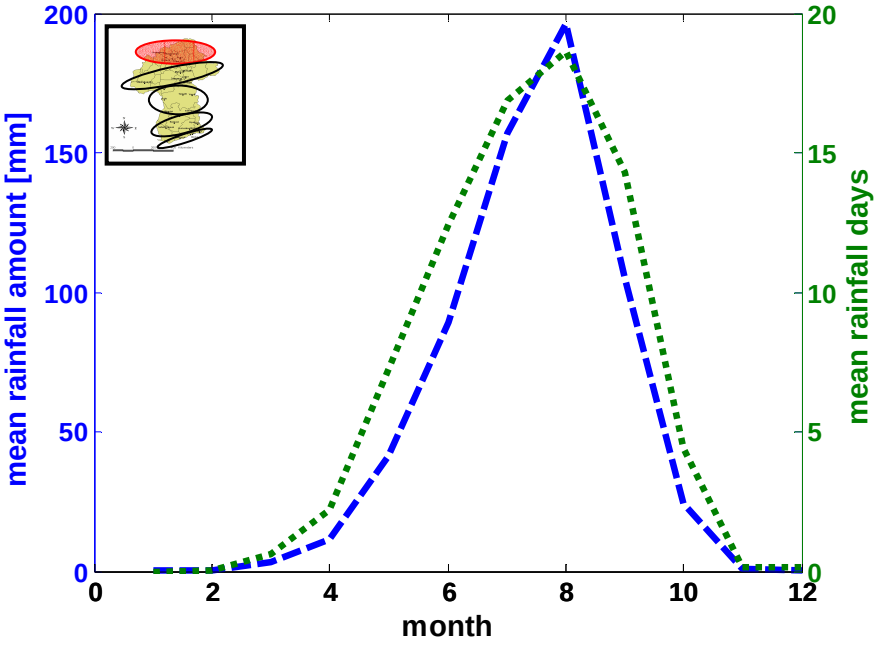

Figure 6: Regional intra-annual rainfall statistics over the past (1961-2000). The locations of the respective regions within the Volta Basin are highlighted in red.

Figure 6 is illustrating the regional intra-annual rainfall statistics for 5 regions within the Volta Basin. The rainfall amount is highly correlated (Pearson correlation coefficient > 0.95) with the number of rainy days (day with recorded rainfall). Following strictly the movement of the ITCZ, the three southernmost regions show a bimodale, the two northernmost regions an unimodale rainfall distribution.

Rainfall variability is dominated by the strength of the West African Monsoon system, but what drives the monsoon? A brief review of the potential reasons for rainfall variability at interannual and decadal scale is given in the following:

- At interannual scale, the strength of AEJ and TEJ plays a major role for abnormally drought and wet conditions (JENKINS et al., 2002). Intensified magnitudes of the AEJ are accompanied by a weakened monsoonal flow and therefore dry conditions, whereas a stronger TEJ is associated with wet conditions.

Additionally to this influence of the upper-layer wind fields, minor total rainfall amounts are associated with:

- An enhancement of the Azores anticyclone and a weakening of the St. Helena anticyclone linked with an increase of the sea surface temperature (SST) of the equatorial and south subtropical Atlantic Ocean, a decrease of the SST in the

Northern Atlantic Ocean and a more southward position of the ITCZ (LAMBERGEON, 1977), and

- A positive Sea Level Pressure Anomalies (SLPA) over the northeast Atlantic.

Several climatologists seem to agree that the extent of climate change on West African rainfall variability remains uncertain at decadal time scale. Concerning the principle drivers, however, there is a broad consensus in literature. The primary driver of rainfall variability in this region is the SST of the Atlantic (north and south), and to minor extend, the SST of the Pacific Ocean. Changes in land use and possibly dust production (or aerosol in general) act as a secondary feedback mechanisms (e.g. IPCC, 2001). A brief review is given below:

- **SST:** GIANNINI et al. (2003) separated the signal of rainfall variability induced to land-use change and SST forcing performing numerical ensemble simulations spanning the period 1930-2000. In the ensemble mean, any agreement with observed climate variability can only come from the observed SSTs imposed as the common oceanic boundary condition, because atmospheric CO_2 concentrations are held constant in time and vegetation cover is prescribed to vary seasonally but not on interannual time scales. Due to the fact that the historical climatic progression can be reproduced using SST as the only external forcing, they concluded that the rainfall change in Sahel during the past century was not a direct consequence of regional anthropogenic influence.

- **Land use change:** The influence of land use on climate, and especially precipitation, has been conducted by several studies. CHARNEY et al. (1975) stated that a reduction of the vegetation in combination with an increase of the albedo is increasing the aridity in the Sahel. LOS et al. (2006) found evidence for a positive feedback between vegetation and rainfall at the monthly time scale, and for a vegetation memory operating at the annual time scale. They concluded that the vegetation-rainfall interactions increase the interannual variation in Sahelian precipitation; accounting for as much as 30% of the variability in annual precipitation in some hot spot regions between 15° and 20° N. LI et al. (2007) performed numerical simulations of idealized deforestation and overgrazing for the Niger and the Lake Chad Basin using both a terrestrial ecosystem model and an aquatic transport model. They found out that tropical forests, although they are occupying just little portion (<5%) of the total basins area, have a disproportional large impact on the water balance of the basins. A total deforestation is increasing the simulated runoff ratio from 0.15 to 0.44, and the annual streamflow by 35-65%. The complete removal of grassland and savannah is increasing the annual streamflow by 33-91%. They found strong evidence that the hydrological response to progressive land use change is non-

linear and exhibits a threshold effect. KUNSTMANN & JUNG (2007) investigated the effect of soil moisture and land use change in the Volta Basin performing numerical mesoscale meteorological modeling in three different resolutions. Scale dependent positive as well as negative soil moisture – precipitation feedback mechanisms were found. In order to investigate the effect of land use change to total rainfall amounts, they substituted successively the land use from cropland woodland mosaic into shrub land and finally into grassland. They found out that the sensitivity of precipitation with respect to the land use change was very heterogeneous.

- **Aerosol:** PROSPERO & NEES (1977) found evidence for an enhanced dust traverse over the Atlantic during dry years in the Sahel. ROTSTAYN & LOHMANN (2001) investigated the indirect effect of aerosols on climate and detected a cooling effect at high latitudes in the Northern Hemisphere through aerosol. The result is a shift of the ITCZ. They suggested that the southward shift of the ITCZ might partly explain the droughts in the Sahel region in Africa in the 1970s and 1990s. They concluded that varying aerosol-related forcing (both direct and indirect) can substantially alter low-latitude circulation and rainfall.

2.4 Evaporation

Mean annual evaporation rate is less than 1500 mm in the South, but exceeds 2500 mm in the North. The evapotranspiration accounts for approximately 80% of the rainfall amount during the wet season (OGUNTUNDE, 2004). The daily rates of the actual evaporation are ranging from 10 mm/d in the rainy season to 2 mm/d in the dry season (e.g. MARTIN, 2005).

2.5 Agro-Ecological Zones

Vegetation and land use is strongly impacted by climate and climate variability in West Africa. According to the prevailing climate in the Volta Basin and anthropogenic interventions (e.g. deforestation), 7 agro-ecological zones can be identified (Figure 7).

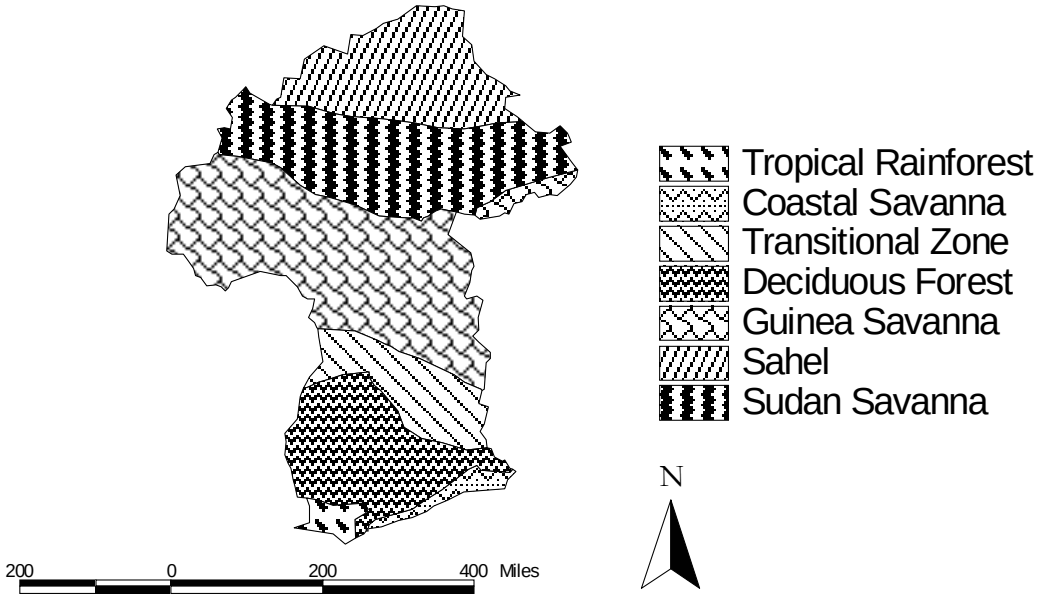

Figure 7: Agro-ecological zones of Ghana and Burkina Faso (Datasource: DVD - Volta Basin Starter Kit, 2006).

2.6 Trend Analysis of Past Climate

Looking at historical climatological time series may help to judge the question whether climate change has already consigned its footprints in West Africa. There, the impact of climate change on rainfall is of major interest for policy makers, since its economy strongly depends on rainfed agriculture and hydropower generation. In this section results of a linear trend analysis for rainfall, runoff and temperature on monthly and annual scale are presented using historical time series of exclusive observation sites within the Volta Basin. The trends have been tested for significance, using the Mann-Kendall trend test and the trend stability has been analyzed using a reverse arrangement test. For the complete analysis the reader is referred to NEUMANN et al., 2007. Here, only a brief summary is given. Strongly differing signals have been revealed:

- Predominantly positive and very stable temperature trends have been detected within the Volta Basin. Figure 8 is showing the spatial interpolation of the observed trend of the annual maximum temperature values. The general conclusion of an increasing temperature can be drawn.

- For precipitation, positive as well as negative trends across the Volta Basin were detected. For the annual maximum, amount (see Figure 8, right) and standard deviations, all of the significant trends are negative. Due to the limited number of significant cases, however, a general trend towards decreasing precipitation in the Volta Basin cannot be ascertained. On monthly time scale, the observed trends are positive and negative, but just few are significant.

- The discharge time series showed a trend towards a reduction of discharge in the dry season and an accretion in the rainy season. However, the observed decrease in river discharge in the dry season cannot be directly linked to a decrease in precipitation; it is more likely due to anthropogenic influences like building dams and the intensification of landuse in terms of irrigation.

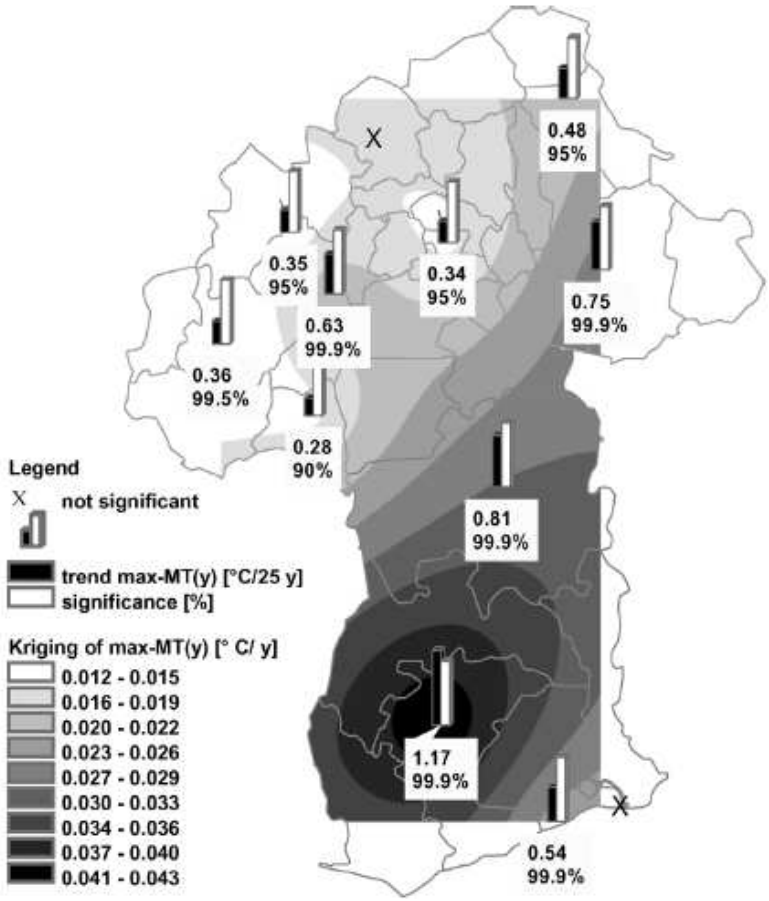

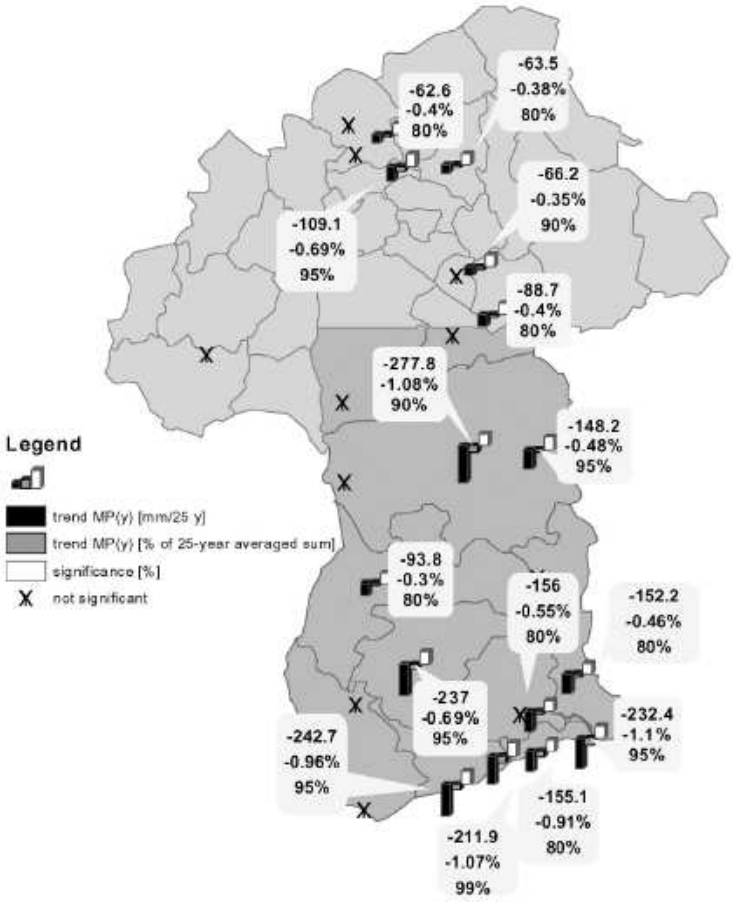

Figure 8: Spatial interpolation of the observed trends of the annual maximum temperature (top), and of the annual rainfall amounts (bottom).The black bars are indicating the linear trend in [℃ / 25 years] and [mm / 25 years], and the white bars are indicating the level of significance [%]. The interpolation has been carried out using ordinary kriging algorithm (NEUMANN et al., 2007).

Chapter 3

3. Statistical Methodologies and Data

According to the addressed research questions and agricultural needs, which are discussed briefly in Chapter 1, the following Figure 9 gives a schematic overview of the different strategies followed within this thesis. The principle goal of the thesis is to afford decision support for the agricultural sector in the Volta Basin and thus contributing to an overall Decision Support System, which should be finalized with the end of Phase 3 of the GVP.

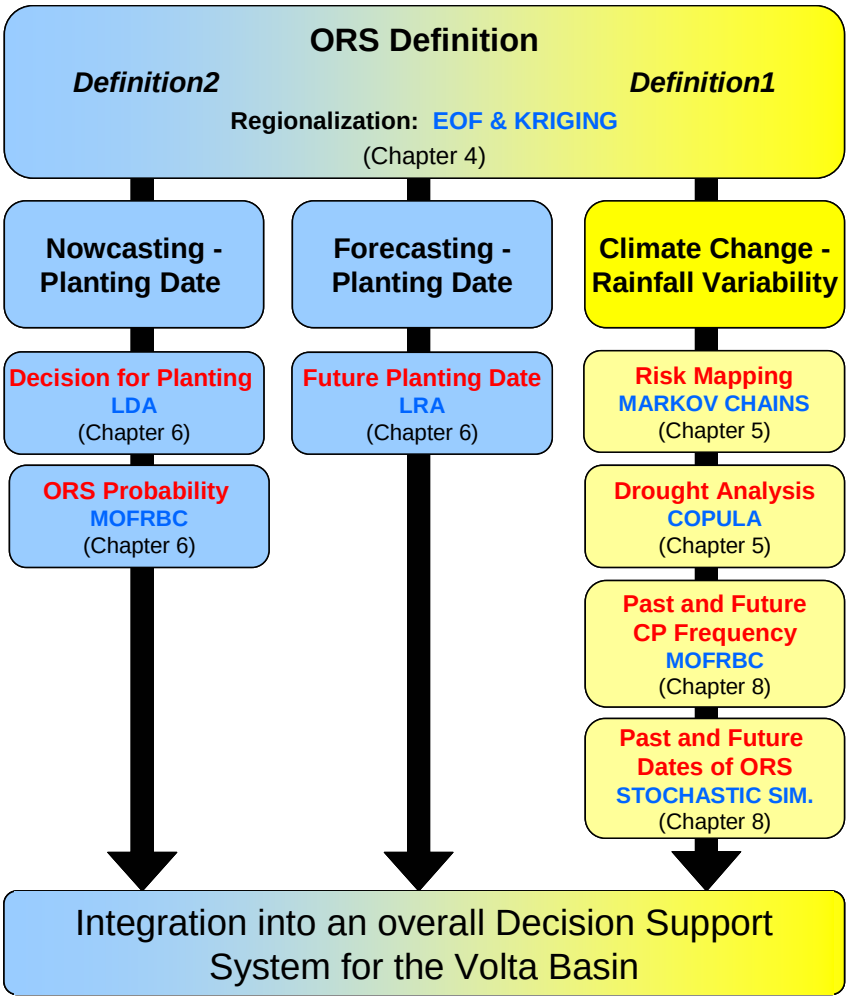

Figure 9: Schematic overview of the three general strategies followed within this thesis. The different research topics are highlighted in red, and the used statistical methodologies in blue colour.

Three different general strategies are followed to archive this goal. Both, for the now- and forecasting, the Definition of the ORS and regionalization are elementary prerequisites. Regionalization has been archived by means of Empirical Orthogonal Function and Kriging interpolation (Chapter 4). The three strategies are described subsequently:

1) A *nowcasting strategy* using Linear Discriminant Analysis (subsequently referred to LDA) and Multi-Objective Fuzzy Rule Based Classification (MOFRBC). LDA is used to judge day-by-day if the rainy season has already begun relying solely on daily rainfall amounts. The more sophisticated MOFRBC has been used to find connections between large-scale atmospheric patterns (referred to CPs) and the ORS.

2) A *forecasting strategy* using Linear Regression Analysis (LRA) to estimate the regional ORS, although the LRA is known as not to be an appropriate method for forecasting. With the knowledge of the date of the ORS within a region, the dates for the other regions can be estimated successively.

3) The *impact of climate change* on rainfall variability. First, Markov chains have been used to create risk maps for agriculture in terms of e.g. heavy rainfall events, regionalized via Kriging interpolation. Risk assessment in terms of regional drought return periods has been performed using the *Effective Drought Index* EDI and a Copula approach. The occurrence frequency of past and future, wet and dry weather patterns has been determined by means of MOFRBC. A comparison of past and future dates using two different stochastic simulation approaches is given.

In the following subsections, the most important methodologies used in this thesis are introduced. For the applied inference statistics the reader is referred to Appendix 8.

3.1 Empirical Orthogonal Function

Empirical Orthogonal Function (EOF), in literature often misleadingly[6] referred to as Principal Component Analysis (PCA), is a multivariate statistical technique, which can be used to derive the dominant patterns of variability from meteorological fields. It was described for the first time by PEARSON in 1902 and HOTELLING in 1935, and introduced into meteorology by Lorenz in 1956. EOF is possibly the most widely used methodology in atmospheric sciences (WILKS, 2006). The main goal of the EOF is to reduce the number of input variables (observation sites or grid points) to a number of uncorrelated EOFs. The results of the EOF analysis are EOFs with similar seasonality and long-term variability characteristics (CAHALAN et al., 1996), which are representing orthogonal

[6] In EOF, the spatial eigenvectors are normalized (unit length). Apart from the PCA, the loadings cannot be regarded as correlation coefficients between the EOFs and the input variables.

stochastic variables owning many advantages over the use of the original variables. Due to their orthogonality (mutually uncorrelated EOFs) they can be analyzed be means of several statistical methods that require independent data. In practice, EOF is often used prior to high computationally demanding operations in order to reduce the number of dimensions and hence calculation time. In this thesis, EOF is applied for regionalization (Chapter 4.2.1) and for detecting the main variability patterns in meteorological fields (Chapter 9.1.3). A short mathematical description of the EOF methodology is given in the following:

The matrix X contains measurements of a variable (like e.g. precipitation) at the locations x_1, x_2,…, x_p taken at times t_1, t_2,…, t_n. Each column (1,…, p) in X represents a time series for a given location[7]:

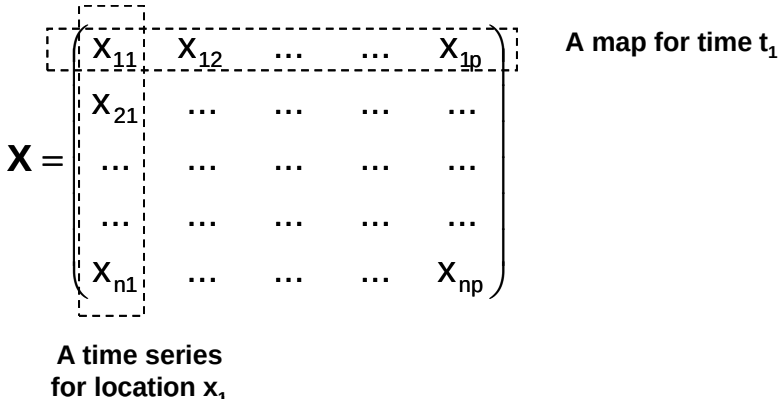

The EOFs have been calculated as a linear combination of the anomalies (Wilks, 2006), so that each column has a mean value 0. Additionally, each grid point has been weighted by the square root of the cosine of the latitude in order to capture the influence of the grid cells sizes, represented by the grid points. The covariance matrix R is calculated as follows:

$$R = \frac{1}{n-1} X^T X , \tag{3.1}$$

where T denotes the transposed of the matrix and n the number of time steps. By that, the eigenvalue problem can be solved:

$$RC = C\Lambda . \tag{3.2}$$

Λ is the diagonal matrix containing the eigenvalues λ_i of R. The column vectors c_i of C are the eigenvectors of R corresponding to the eigenvalues λ_i. Both, Λ and C are of size p x p. EOF_1 is the eigenvector associated with the biggest eigenvalue, the one

[7] This way of ordering data into a matrix is referred to S-modal analysis.

associated with the second biggest eigenvalue is EOF_2, etc. Dividing each eigenvalue λ_i by the sum of all other eigenvalues (trace of Λ), one gets the fraction of the total variance in R explained by each EOF. Plotting the obtained EOFs as a map is representing a standing oscillation. To see how the EOFs are evolving in time, the expansion coefficients $\vec{a}_j$ can be calculated:

$$\vec{a}_j = X\vec{c}_j \,. \tag{3.3}$$

The n components of the vector $\vec{a}_j$ are the projections of the maps in X on the EOF_j. Unlike the EOFs are uncorrelated in space, the expansion coefficients are uncorrelated in time. Finally, one can reconstruct the data using the EOFs and the expansion coefficients:

$$X = \sum_{j=1}^{p} \vec{a}_j (EOF_j) \,. \tag{3.4}$$

Commonly only few EOFs are used to reconstruct the data by truncating the sum at some j=N < p. The conception behind is that the first N eigenvectors are capturing the dynamics of the system, and additionally ones are enlarging mainly the fraction of random noise in comparison to the total variance fraction. The question after an adequate truncation of the EOF decomposition of field X is depending on the scope of the research questions. Potential criterions for N are the cumulative amount of variance, or a threshold for the minimum portion of the last EOF mode of 1% or 5% (e.g. KAISER, 1958).

3.2 Linear Discriminant Analysis

Linear Discriminant Analysis LDA is a statistical tool to detect the variables that allows discrimination between two or more groups and for assigning cases to different groups with a better-than-chance accuracy. Within this thesis, LDA has been used to judge day by day whether the onset of the rainy season has already begun. Therefore, the 4 classes *dry season*, *transition*, *ORS* and *wet season* are predefined following Table 2. The results for different regions in the Volta Basin are presented in Chapter 6.1. Here, only a brief mathematical description of the LDA is given:

Two prerequisites have to be noted: the number of groups must not exceed the number of variables describing the data set and the groups must have the same covariance structure. Given a sample $X = (x_1, x_2, \ldots, x_p)$ of n observations on a vector of p variables from g populations ζ1,…, ζg, the linear discriminant functions are of the form:

$$Y_{1,\ldots,nu} = \sum_{k=1}^{p} \upsilon_k X_k \ , \tag{3.5}$$

with X_k being the variables describing the data set. The discrimination coefficients υ_k have to be determined such that the discrimination between the groups is best. Determination of the coefficients of the discriminating function is quite simple. In principle, the discriminating functions are formed such that the separation (= distance) between the groups B is maximized, the distance within the groups W is minimized, and, hence, the ratio (= discriminant criteria) of B and W is maximized. B, W, and the overall weighted mean $\bar{\mu}$ are computed as follows:

$$B = \sum_{j=1}^{g} \pi_j (\mu_j - \bar{\mu})(\mu_j - \bar{\mu}) , \tag{3.6}$$

$$W = \sum_{j=1}^{g} \pi_j \Sigma_j , \tag{3.7}$$

where π_j is the prior probability of an observation belonging to a certain group, Σ_j is the population covariance, and μ_j is the population mean. The number of discrimination functions required is the minimum of (g - 1), where g is the number of categories in the grouping variable, or p, the number of discriminating (independent) variables. Similar to multiple regression analysis, not all the candidate predictors contribute to a significant improvement of the discriminant model and there is no established method for assessing which predictors are useful when the assumption of equal variance is dropped (MASON, 1998). Typically, stepwise multiple regression analysis is a first step to detect the best predictor subset for the discriminant model (WARD & FOLLAND, 1991).

3.3 Multi Objective Fuzzy Rule Based Classification and Rainfall Modelling

Multi Objective Fuzzy Rule - Based Classification (subsequently referred to MOFRBC) combined with stochastic modeling is widely established in literature and has been proofed suitable for downscaling temperature and rainfall in regions across the whole world (see Appendix 1). MOFRBC can also be applied as stand alone approach for weather pattern classification. For rainfall simulation, a MOFRBC in combination with stochastic modeling is applied.

3.3.1 Multi Objective Fuzzy Rule Based Classification (MOFRBC)

It is an objective method to classify the state of a variable using logical and probabilistic instead of binary statements. For this reason, triangular fuzzy numbers are used. Figure

10 displays the membership function of a triangular fuzzy number $(a,b,c)_T$, which is defined as:

$$\mu(g) = \begin{cases} 0 \quad \text{if} \quad g < a \\ \dfrac{g-a}{b-a} \quad \text{if} \quad a \le g < b \\ \dfrac{g-c}{b-c} \quad \text{if} \quad b \le g < c \\ 0 \quad \text{if} \quad g > c \end{cases}$$

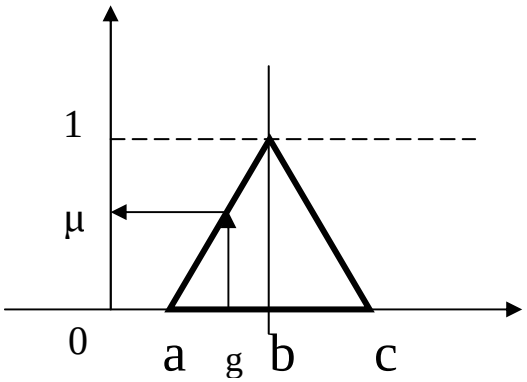

Figure 10: Membership function of triangular fuzzy numbers $(a,b,c)_T$.

In this thesis, two different conceptual ways are followed:

- MOFRBC conditioned on the onset of the rainy season (ORS). The goal is to identify weather patterns, which are significantly linked with the ORS. Under the assumption that the daily weather pattern is classified, a probabilistic statement about the occurrence of the ORS can be drawn. The results of this approach are presented in Chapter 6.3).

- MOFRBC conditioned on daily precipitation time series. This classical way has been followed to identify weather patterns, responsible for wet and dry conditions for the past and future climate (Chapter 8.1.3). In combination with stochastic simulation of time series, MOFRBC has been applied to calculate future dates of the ORS.

For both ways, slightly different subsets are used and introduced in Chapter 3.3.3. The methodology is fully described in BÁRDOSSY et al. (1995). Here only a brief description is given:

First, the 2.5° x 2.5° NCEP/NCAR reanalysis fields are transformed to standardized anomalies by subtracting the long term mean and dividing the difference by the long term standard deviation:

$$g(i,t) = \frac{h(i,t) - h(i,t')}{\sigma(i,t')}, \tag{3.8}$$

with h (i,t) being the observed variable at grid point i and time t; h (i,t') is the mean of variable at grid point i over annual cycle, and σ (i,t') is the standard deviation of variable at grid point i over the annual cycle. The daily anomalies g (i,t) are then classified into the

categories: i) high $(0.2, 1.0, \infty)_T$, ii), medium high $(0, 0.6, 1.4)_T$, iii) medium low $(-1.4, -0.6, 0)_T$, 4), iv) low $(-\infty, -1, -0.2)$ and v) indifferent for the circulation patterns using triangular fuzzy membership functions (subscript T). A triangular fuzzy membership function is schematically presented in Figure 10.

Usually most of the grid-points belong to class number 5, since only characteristic ones are assigned to other classes. For a given time t and location i, the membership corresponding to rule k is defined as:

$$\mu_{(i,k)} = \mu_{v(i)}^{(k)}(g(i,t)), \tag{3.9}$$

Thus, a weather pattern or circulation pattern[8] CP_k is fully characterized by an index vector $v(k) = \{v(1)^{(k)} \ldots v(n)^{(k)}\}$, which defines the location of the five anomaly classes in the target area. After that, classification of daily fields is carried out by calculating the degree of fulfillment (DOF) for each rule based on the membership values μ:

$$DOF(k,t) = \prod_{l=1}^{4} \left(\frac{1}{N(v(i)^k = l)} \sum_{v(i)^{(k)}=l} \mu(i,k)^{Pl} \right)^{\frac{1}{Pl}}, \tag{3.10}$$

with N being the number of grid points classified as class I, and Pl the Parameter, which is modifying the influence of selected classes towards the DOF. Finally, the rule k, where DOF (k,t) is maximal, is selected as CP for the day t and the result is a vector with one objective circulation pattern per selected day.

Two types of objective functions for optimization procedure due to regional precipitation and the onset of the rainy season in the Volta Basin were defined. The first one deals with the probability of the occurrence of each class on a given day:

$$O_1 = \sum_{i=1}^{S} \sqrt{\frac{1}{T} \sum_{i=1}^{T} (p(CP(t))_i - \overline{p}_i)^2}, \tag{3.11}$$

where S is the number of stations or regions with rainfall observations, T is the number of days in the time series and $p(CP(t))_i$ is the CP-conditional probability of the class occurrence at station/region i. A second objective function was introduced basing on the conditional precipitation amounts z(CP):

$$O_2 = \sum_{i=1}^{S} \frac{1}{T} \sum_{t=1}^{T} \left| \log \left(\frac{z(CP(t))_i}{\overline{z}_i} \right) \right|. \tag{3.12}$$

[8] Circulation patterns and weather patterns are used interchangeably within this doctoral thesis. The abbreviation used in this thesis is CP.

To focus the onset of the rainy season, a third objective function was introduced to assign higher weights to higher class values:

$$O_2' = \sum_{i=1}^{S} \frac{1}{T} \sum_{t=1}^{T} \left| \left(\frac{z(CP(t))_i}{\overline{z}_i} \right)^{1.5} \right|, \tag{3.13}$$

where $\overline{z}_i$ is the overall average of the class values at station or region i. High values of O_2 and O_2' indicate that the conditional class amount of a CP differs clearly from the average value.

Optimization of O_1, O_2 and O_2' was performed using Simulated Annealing (SA) (e.g. PRESS et al., 1988; SALAMON et al., 2000) and the sum of O_1 and O_2 as overall objective function O for stochastic rainfall simulation purposes. For optimization concerning the ORS, the overall objective function consists of the sum of O_1 and O_2'. The optimization starts with an arbitrary set of fuzzy rules, which classifies the daily anomalies of the reanalysis field into a CP time series, determines p(CP) and z(CP) by frequency analysis and calculates the overall objective function O. Then a rule is randomly selected and one of the five categories v is randomly assigned to a randomly chosen gridpoint. A new classification is performed and O is calculated again. If O exceeds the corresponding value of the old classification, then the change is accepted. If not, then the change is accepted with a probability that decreases exponentially with decreasing annealing temperature. More details on the optimization are given in BÁRDOSSY et al. (2002).

3.3.2 Performance of the Classification

Various measures for judging the quality of the classification scheme are used:

- The normalized conditional rainfall probability n_p. It is defined as the conditional probability of precipitation at a station/region i given the condition that the reanalysis field at a day is classified into a given CP divided by the average precipitation probability, p_i, at this station/region. A strong deviation of n_p from 1 indicates that the conditional rainfall probability of the CP is much higher or lower than the average:

$$n_p = \frac{p_i(CP)}{\overline{p}_i}. \tag{3.14}$$

- The normalized conditional rainfall amount, n_z, defined as the conditional average precipitation amount on a wet day for a given CP $z_i(CP)$ at station/region i divided by the average precipitation amount, z_i , of a wet day at that station/region. A

strong deviation of n_z from 1 indicates that the conditional rainfall amount of the CP is much higher or lower than the average:

$$n_z = \frac{z_i(CP)}{\overline{z}_i}. \tag{3.15}$$

- The product of n_z and n_p, named the wetness index I_{wet}, is a joint measure of whether the CP combines a higher/lower than average conditional rainfall probability with a higher/lower than average conditional rainfall amount.

- Applying MOFRBC to using the onset of the rainy season as predictand, an additional parameter which is consisting of the ratio of conditional probability at the onset of the rainy season (days classified as '100') and the conditional occurrence probabilities for all classes has been calculated:

$$O_{p(ONSET)} = \frac{p_{i(ONSET)}(CP)}{p_i(CP)}. \tag{3.16}$$

After application of the classification, the CP with the largest value for $O_{p(ONSET)}$ has been detected considering all the analyzed predictors at different levels in the 5 regions.

Next, 500 bootstraps holding the same occurrence probabilities as the original CP time series has been randomly generated and the $O_{p(ONSET)}$ has been calculated for each realization. If $O_{p(ONSET)}$ of none realization is exceeding the respective value of the original time series, which has to be located simultaneously outside the 3s (3 standard deviations) interval of the bootstraps, the CP is seen to be significant for the ORS.

3.3.3 Setup for MOFRBC

This study has been carried out within the sector from 40°W 10°S to 30°E 60°N (domain D1), and additionally within 30°W 20°S to 10°E 0°N additionally for the SST (domain D2), (see therefore Figure 11).

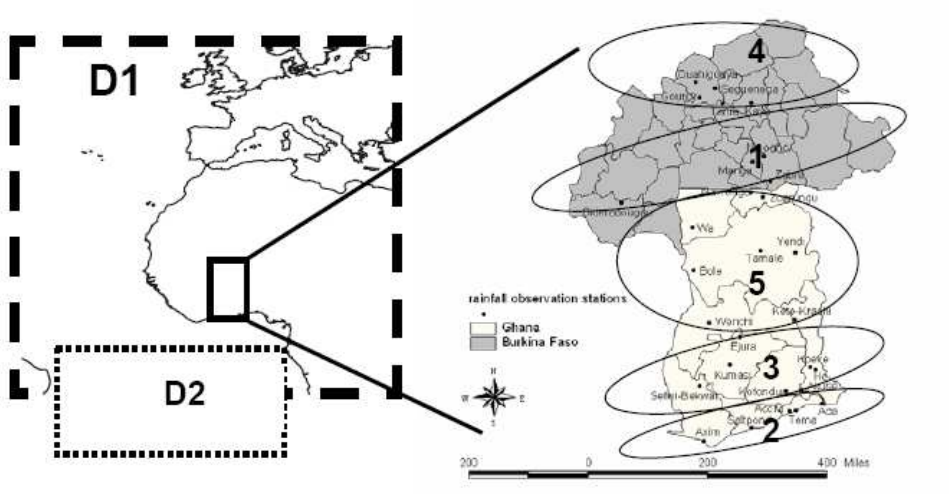

Figure 11: Domains for weather pattern analysis (left) and spatial distribution of areas with similar rainfall characteristics within the Volta Basin, represented by five ellipses (right); (LAUX et al., 2007).

Table 1 lists the potential predictor variables for the weather pattern analysis conditioned to the onset of the rainy season, carried out for different levels, domains and locations using 9 predefined CPs.

Predictor	Level [hPa]	D	Location	Predefined CPs
GPH	500, 850	1	PC 1- PC 5	9
SLP	Surface	1	PC 1- PC 5	9
T_{SKIN}	Surface	1, 2	PC 1- PC 5	9
MF_U	300, 500, 600, 850	1	PC 1- PC 5	9
MF_V	300, 500, 600, 850	1	PC 1- PC 5	9
MF_UV	500, 850	1	PC 1- PC 5	9
U	150, 300, 500, 600, 850	1	PC 1- PC 5	9
V	150, 300, 500, 600, 850	1	PC 1- PC 5	9

Table 1: List of potential predictor variables used for weather pattern analysis conditioned to the onset of the rainy season. (GHP = Geopotential height; SLP = Sea level pressure; T_{SKIN} = Skin temperature; MF_U = eastward component of moisture flux; MF_V = northward component of moisture flux; MF_UV = northeastward component of moisture flux; U = eastward wind speed; V = northward wind speed).

Eventually, the daily anomaly fields of these predictor variables are conditioned to a weight vector which has been built up regarding to the rainy season's onset dates. Two more classes have been introduced to enhance the number of cases. The weights of the different classes have been set in that way that the Onset of the Rainy Season is

weighted disproportionably high. The weather patterns should not be linked to dates prior to the ORS, therefore these dates are assigned to zero, and days during the wet season are weighted by "2". Table 2 is presenting the pre-classification schemes with respect to the date of the ORS and the assignment of the respective weights. All other days of year were assigned to "-9" and thus excluded form the calculations.

Class	Considered time period	Weight
Dry Season	40 to 3 days before the calculated ORS	0
ORS	2 days before to 2 days after the calculated ORS	100
Wet Season	3 to 40 days after the calculated ORS	2

Table 2: Classification table to build up a class vector for each day during the time period 1st March until 31th of October.

For the analysis conditioned to daily precipitation time series of different sites, various experiments using different numbers of predefined CPs have been performed for the most promising predictors (Table 3):

Predictor	Level [hPa]	D	Location	Predefined CPs
GPH	500, 850	1	Sites of PC1-PC5	9
SLP	Surface	1	Sites of PC1-PC5	5, 7, 9, 11, 13
TSKIN	Surface	1, 2	Sites of PC1-PC5	5, 7, 9, 11, 13
MF_U	300, 500, 600, 850	1	Sites of PC1-PC5	5, 7, 9, 11, 13
MF_V	300, 500, 600, 850	1	Sites of PC1-PC5	9
MF_UV	500, 850	1	Sites of PC1-PC5	9
U	150, 300, 500, 600, 850	1	Sites of PC1-PC5	9
V	150, 300, 500, 600, 850	1	Sites of PC1-PC5	9

Table 3: List of potential predictor variables used for weather pattern analysis conditioned to daily precipitation time series.

3.3.4 Weather Pattern Conditional Rainfall Simulation

In the case of above introduced MOFRBC conditioned on daily precipitation, stochastic rainfall simulation can be applied in order to model daily precipitation time series conditioned on the prevailing weather patterns. Due to the spatial and temporal intermittency of daily rainfall series, i.e. the clustering of wet and dry days as well as the clustering of wet and dry areas in the target region, a multi site approach based on random variables with mixed distributions is required to describe daily precipitation. In the subsequently presented time-space model suggested by STEHLÍK & BÁRDOSSY (2002), clustering is assumed to be the consequence of the persistence of atmospheric circulation patterns. Consequently, it is an input variable for the model. Precipitation is linked to the individual CP through the conditional occurrence probability of a wet day:

$$p(CP(t)) = (p(CP(t),u_1),...,p(CP(t),u_M)\,, \tag{3.17}$$

and the conditional average amount:

$$z(CP(t)) = (z(CP(t),u_1),...,z(CP(t),u_M)\,, \tag{3.18}$$

which are derived from a set of observed precipitation time series at locations u = (u_1, …, u_M) via frequency analysis. For a given CP, the probability distribution Z(t,u) of daily precipitation amounts

$$z = z(t,u_1),...,z(t,u_M) \tag{3.19}$$

at various locations is multivariate skewed. STEHLÍK & BÁRDOSSY (2002) relate Z(t,u) to the positive branch of a multivariate normal process N(t,u) by introducing a transformation, which has to be repeated for each CP:

$$Z(t,u) = \begin{cases} 0 & \text{if} \quad N(t,u) \le 0 \\ N^{\beta}(t,u) & \text{if} \quad N(t,u) > 0 \end{cases}. \tag{3.20}$$

Further details of that transformation process can be found in STEHLÍK & BÁRDOSSY (2002). Since rainfall time series are usually too short to evaluate p(CP(u,t)) for each day of the year, the evaluation is done for each month of the year and CP. After transforming Z into the multivariate normal process, the negative values of N are declared as dry days at locations u_i to reflect the intermittency of rainfall. The stochastic rainfall model describes how the deviation from the conditional daily average normal process on a given Julian day of the year evolves from the corresponding deviation at the previous day:

$$\begin{aligned} &N(t+1,u) - E(N(t+1^*,u) \mid CP_i) = r(t^*+1) \cdot (N(t,u) - \\ &E(N(t^* u) \mid CP_i)) + C_{CP_i}(t^*+1) \cdot \Psi(t^*,u) \end{aligned} \tag{3.21}$$

where E denotes the expectation value conditioned to the Julian day t* and the CP_i r, which is assumed to be spatially constant (due to large scale features causing precipitation. Assumption might not hold for shorter time steps), is a function of the annual cycle and denotes the 1 day lag autocorrelation function. r is independent from the circulation pattern and is calculated using Fourier analysis:

$$r(t^*) = \frac{A_0}{2} + \sum_{k=1}^{K} (A_k \cos(k\omega t^*) + B_k \sin(k\omega t^*))\,. \tag{3.22}$$

C is related to the spatial covariance matrix and the 1 day lag spatial covariance matrix of the multivariate normal process and is depending on the annual cycle and the CP. The spatial covariance function cov is estimated from the rainfall stations and is depending on the month of the year and the existing CP:

$$\mathrm{cov}(Z(x), Z(y)) = c_0 \exp\left(\frac{-d(x,y)}{\lambda}\right). \tag{3.23}$$

Ψ denotes a random vector of independent normally distributed random numbers (zero mean and standard deviation 1).

The more simple and unconditional LARS-WG has also been used for rainfall simulation and the performance of both methodologies has been elaborated. The LARS-WG is described in the following:

3.3.5 The Stochastic Weather Generator LARS-WG

The weather generator LARS-WG can be used to generate daily rainfall data at a single site under both current and future climate conditions (e.g. SEMENOV et al, 1998; SEMENOV & BROOKS, 1999). A schematically overview is presented in Figure 12.

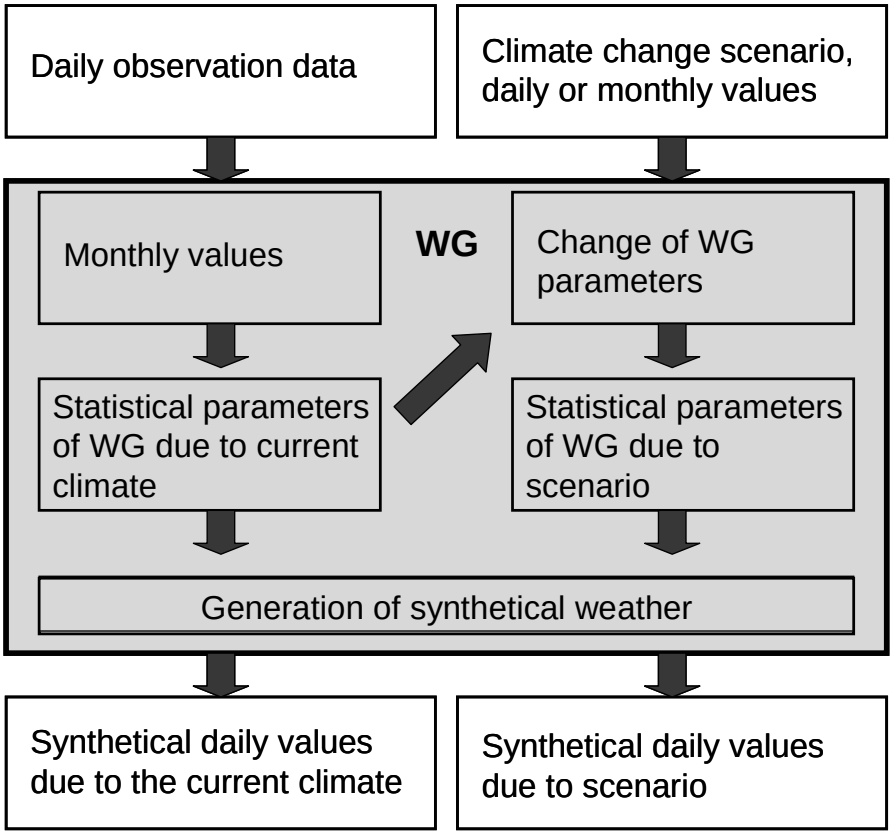

Figure 12: Schematical overview of the generation of synthetical daily time-series using LARS-WG (modified after MATULLA & HAAS, 2003).

LARS-WG has been tested for a wide range of climates and is found to perform well (e.g. SEMENOV et al., 1998). Stochastic weather generators were originally developed for two main purposes:

- To provide a means of simulating synthetic weather time-series with statistical characteristics corresponding to the observed statistics at a site, which were long enough to be used in an assessment of risk in hydrological or agricultural applications

- To provide a means of extending the simulation of weather time-series to unobserved locations, through the interpolation of the weather generator parameters obtained from running the models at neighboring sites.

It cannot be treated as a predictive tool for weather forecasting. It rather provides a tool to generate time-series of synthetic weather, which is statistically identical to the observations. Time series of precipitation, maximum and minimum temperature and solar radiation can be generated. Precipitation is considered as the primary variable and the other three variables of a given day are conditioned on whether the day is dry or wet (SEMENOV & BARROW, 1997). The simulation of precipitation occurrence is based on the semi-empirical distributions of the lengths of continuous sequences of wet and dry days (series). This approach is different from the Markov chain approach, frequently used in weather generators (e.g. WGEN). The main shortcoming of the Markov chain model is the reduced memory of very rare events, like e.g. very long lasting dry or wet spells. Especially for agro-meteorological impact studies, where dry or wet spells significantly affect crop yield, or in areas with a well-defined rainy/dry season, the Markov chain model is less suited than the series approach. The simulation of precipitation occurrence is modelled as alternate wet and dry series, where a wet day is defined to be a day with precipitation > 0 mm. The length of each series is chosen randomly from the wet or dry semi-empirical distribution of the month in which the series starts. In determining the distributions, observed series are also allocated to the month in which they start. For a wet day, the precipitation value is generated from the semi-empirical precipitation distribution for the particular month independent of the length of the wet series or the amount of precipitation on previous days. The semi-empirical distribution:

$$Emp = \{a_0, a_i; h_i, i = 1,...,10\}, \tag{3.24}$$

is a histogram with 10 intervals, $[a_{i-1}, a_i]$, where $a_{i-1} < a_i$, h_i denotes the number of events from the observations in the ith interval. Random variables from the empirical distribution are chosen by first selecting one of the intervals (using the proportion of events in each interval as the selection probability), and later selecting a value within that interval from the uniform distribution.

To incorporate climate change in the generation of artificial time series, the simplest way is to perturb an observed daily time series by monthly changes from the grid box in which the observation station is located. Therefore, the relative change in wet and dry series lengths between baseline period and scenario has been calculated. For the technical execution, a short recipe is given in the following. Note, that the calculations have to be performed for each month separately:

- Calculate the mid-point value for each histogram bin and multiply each value by the number of events in this bin to obtain an average number of days in this category

- Calculate the total number of wet (and dry) days. In order to calculate the mean value for the distribution, the sum of the wet (and dry) days has to be divided by the total number of events

- In order to calculate the relative change in the length of wet (and dry) series the average length of the series in the future time period has to be divided by the average length of the series in the baseline time period, i.e. length 2001-2040/length1961-2000.

In combination with random numbers, these ratios are eventually used to generate artificial precipitation time series.

Leaving the path of *nowcasting*, Linear Regression Analysis is used as a *forecasting* methodology in the context of that doctoral thesis. A brief description is given below:

3.4 Linear Regression Analysis (LRA)

In general, LRA is used for a wide variety of applications in Earth Sciences. In climatology, it is often applied for statistical downscaling or to calculate trends in climatological time series. In this doctoral thesis, LRA is applied to estimate the future dates of the ORS (Chapter 6.2) relying on the onset dates of different regions. In addition to that, it is applied in order to derive trends of past and future rainy season's onset dates (Chapter 8.1.1, Chapter 8.2.2), following the approach of KLIWA (2002) and MAIDMENT (1992). Since most of the observed trends seem to be linear[9] and in order to compare different regions, all trends in this analysis are assumed to be linear. A short mathematical description is given below following the approach of KLIWA (2002) and MAIDMENT (1992):

[9] The term 'linear' is referred to the relation of the response to the explanatory variables, which is assumed to be a linear function of some parameters. It is often erroneously thought that the reason the technique is called "linear regression" is that the graph is a line.

$$x(t) = a + bt\,. \tag{3.25}$$

The coefficients a and b are acquired with the method of least squares. The intercept a and the slope b are calculated as follows:

$$a = \bar{x} - b\bar{t} \tag{3.26}$$

$$b = \frac{s_{x,t}}{s_t^{\,2}}, \tag{3.27}$$

with $\bar{x}$ being the mean value of the measurand **x**, $\bar{t}$ being the mean value of time with time steps $t_i = i \cdot \Delta t$, $s_{x,t}$ the covariance between measurand x and time t, and $s_t^{\,2}$ being the variance of time t. $s_{x,t}$ and $s_t^{\,2}$ are determined as:

$$s_{x,t} = \frac{1}{n-1}\sum_{i=1}^{n}(x_i - \bar{x})(t_i - \bar{t})\,, \tag{3.28}$$

$$s_t^{\,2} = \frac{1}{n-1}\sum_{i=1}^{n}(t_i - \bar{t})^2\,, \tag{3.29}$$

where n is number of time steps.

The following statistical methodologies have been applied following the third route (see Figure 9), dealing with climate change and rainfall variability. These methodologies consist of Markov Chains for risk mapping, a Copula approach for drought analysis, MOFRBC (Chapter 3.3) for frequency analysis of past and future CPs, and stochastic rainfall simulation (Chapter 3.3.4, Chapter 3.3.5).

3.5 Markov Chains

Generalized linear models are used by numerous studies for modeling rainfall. Often, two models are considered separately one for rainfall occurrence and another one for rainfall amounts. The former is often modeled using a binomial distribution and the latter by a gamma distribution (e. g. STERN & COE, 1982). DUNN & WHITE (2005) proposed an integrated approach using the power-variance exponential dispersion models.
In this work, Markov chains has been used to create agricultural risk maps considering e.g. rainfall probability using two different threshold values, 0.1 mm to define a rainy day and 20 mm to consider heavy rainfall events with potential erosive impact. In this context, the unconditional probabilities are of major interest (SARI, 2006). The probabilities for dry spell occurrences have also been calculated, especially to support the definition of the

ORS in the predictive mode (see therefore Chapter 4.1.3). The results are presented in Chapter 5.1, 5.2 and 5.3.

Two models are used, a Markov model for rainfall occurrence and a gamma distribution for modelling the rainfall amounts. Besides the unconditional probability (zero-order Markov chain), the simplest solution for modelling rainfall occurrence is a two-state (occurrence of precipitation or not) first-order (precipitation probability depends solely on the previous day's precipitation occurrence) Markov model which can be defined by two transition probabilities:

$$P_{01} = P \{\text{rainfall on day } t \mid \text{no rainfall on day } t-1\},$$

and: (3.30)

$$P_{11} = P \{\text{rainfall on day } t \mid \text{rainfall on day } t-1\}.$$

The two complementary transition probabilities are $P_{00} = 1 - P_{01}$ and $P_{10} = 1 - P_{11}$. Generally, high-order Markov chain models are also used to model sequences of rainy or dry spells (CHIN, 1977). For a two-state Markov model, the number increases exponentially with the order of the process, in general, 2^k for k^{th} order. As described by STERN et al. (1981), the observed proportions, P, are transformed using the logit transformation:

$$f = \log\left(\frac{P}{1-P}\right). \tag{3.31}$$

This allows f to vary from -∞ (*P*=0) to +∞ (*P*=1). Former studies showed that Fourier series are particularly suited to fit both unimodal and bimodal seasonal patterns, with the advantage that the fitted probabilities at the start and the end of the year are equal (GARBUTT et al., 1981). The fitted probabilities are given by:

$$y = \frac{e^f}{(1+e^f)}, \tag{3.32}$$

where f is the sum of the Fourier series:

$$f = a_0 + \sum_{j=1}^{n}(a_j \cos jt + b_j \sin jt), \tag{3.33}$$

where t = π (date – 183)/183 and n is the number of harmonics. Here, the number of harmonics has been set to 4. The distribution of daily rainfall amounts is highly skewed. The gamma distribution is regarded to be most appropriate to model daily rainfall

amounts (BUISHAND, 1977). Since the mean rain per year often varies through the year, it is useful to consider models which reflect this temporal dependence (STERN & COE, 1982). Gamma distributions were fitted to rainfall amounts of rainy days and days with rainfall below a certain threshold are excluded. The gamma distribution is given by:

$$f(x) = \left(\frac{k}{\mu}\right)^{k} \frac{(x-c)^{k-1} e^{-k(x-c)/\mu}}{\Gamma(k)} . \qquad (3.34)$$

$\Gamma(k)$ is the gamma function with the shape parameter k and mean μ. Since these two parameters may vary temporally and spatially, their monthly values were estimated for each site. The rainfall amounts x, are shifted by the threshold value, c. In this study, rainfall thresholds from 0.5 mm to 2.0 mm with an increment of 0.5 mm were used and compared. A threshold of 1 mm seems to supply reasonable results.

3.6 Drought Analysis

Drought conditions affect agriculture, fire risk, recreation, energy production, water quality, air quality, and species preservation. The impacts differ in type and intensity across the world. Contrary to popular belief, drought is not an anomaly but it is part of the natural variability in the Earth system. Drought mitigation involves making risk assessments of drought based on evaluating the hazard and vulnerability. Within the thesis, a quantitative drought definition (Chapter 3.6.1) has been established basing on the *Effective Drought Index* EDI. Important drought characteristics as e.g. onset, cessation, duration D, intensity S and interarrival time τ of droughts are derived to assess regional drought risks. In Chapter 3.6.2, a bivariate approach for drought modelling using a Clayton Copula has been established.

3.6.1 Drought Definition

Definitions of drought vary from region to region and may depend upon the dominating perception, and the task for which it is defined. A drought should generally be defined relative to some long-term average condition (e.g. rainfall and balance between rainfall and evapotranspiration). These are common elements of a drought definition. PALMER (1965) defined a drought as an interval of time, generally of the order of months or years in duration, during which the actual moisture supply at a given place rather consistently falls short of the climatically expected or climatically appropriate moisture supply. MCMAHON & DIAZ ARENAS (1982) state that a drought is a period of abnormally dry weather sufficiently prolonged for the lack of precipitation to cause a serious hydrological imbalance and carries connotations of a moisture deficiency with respect to man's usage of water. According to BERAN & RODIER (1985), the principle characteristic of a drought is a decrease of water availability in a particular period and over a particular area.

Since these definitions are normally vague and do not provide quantitative answers to "when", "how long" or "how severe" a drought is, they are often referred to conceptual definitions[10]. Figure 13 is illustrating various conceptual drought definitions, depending on their duration. The sequence of impacts associated with meteorological, agricultural, and hydrological drought further emphasizes their differences. When droughts begin, the agricultural sector is usually the first to be affected because of its heavy dependence on the stored soil water. Soil water can be rapidly depleted during extended dry periods. People, who rely on surface water (i.e. reservoirs and lakes) and groundwater, are usually the last to be affected. A short-term drought that persists for 3 to 6 months may have little impact on these sectors, depending on the characteristics of the hydrologic system and water use requirements. A deficit of precipitation has different impacts on different components of hydrological cycle (river flow, groundwater) and components of biosphere (ecosystems, humans). For example, soil moisture conditions respond to precipitation anomalies on a relatively short scale. Groundwater, river flow and reservoir storage reflect the longer-term precipitation anomalies. These anomalies allow different drought types to be defined conceptually and to be described in terms of various drought indices.

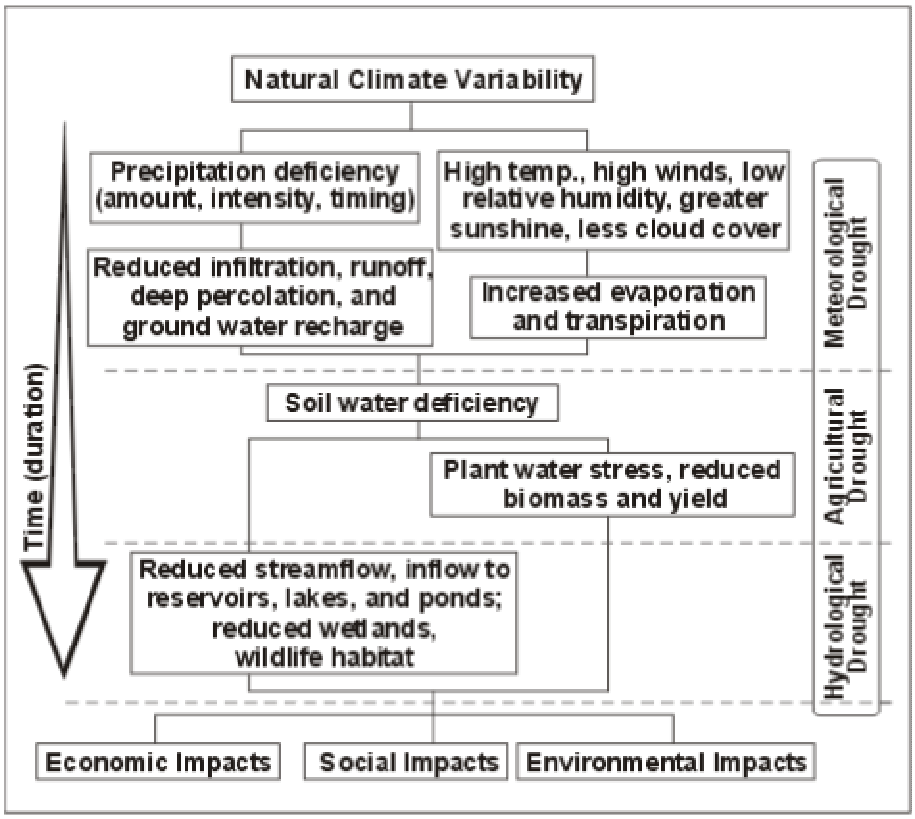

Figure 13: Sequence of impacts of different drought types (Source: National Drought Mitigation Centre, http://enso.unl.edu/ndmc/enigma/def2.htm).

[10] http://drought.unl.edu/

Operational definitions identify the beginning, end, spatial extent and severity of a drought. They are often region specific and are based on scientific reasoning, which follows the analysis of certain amounts of hydro-meteorological information. They are beneficial in developing drought policies, monitoring systems, mitigation strategies and preparedness plans. Operational definitions are formulated in terms of drought indices. MORID et al. (2006) recommended the *Effective Drought Index* EDI and the *Standardized Precipitation Index* SPI for operational drought monitoring.

In this doctoral thesis, a drought is defined as a period with negative effective EDI values (precipitation deficiency) and therefore related to a meteorological drought. Drought duration and drought intensity have been derived using the effective drought index EDI. The first step is the calculation of daily effective precipitation (EP), which is defined as a function of precipitation of the current day and precipitation of the previous days - with lower weights. The duration of the preceding period, over which the EP amount is calculated, may vary but for simplicity may be set to 365 days.

$$EP_j = \sum_{n=1}^{i}[(\sum_{m=1}^{n} P_m)/n], \tag{3.35}$$

where j is the index of a current day and i is duration over which the sum is calculated and P_m is the precipitation m-1 days before the current day. For example, if i equals to 3, then daily equals $(P_1 + (P_1 + P_2)/2 + (P_1 + P_2 + P_3)/3)$. The next step includes the calculation of the mean EP for each day of the year - $MEPj$. This is followed by the calculation of daily deviations of EP from MEP (DEP), standard deviations ST(EP) for each calendar day, and the standardized value of daily deviations SEP, which allows drought intensity at two or more locations to be compared with each other regardless of climatic differences between them.

$$SEP = DEP/ST(EP). \tag{3.36}$$

Drought duration may now be defined similarly to the standardized precipitation index SPI - as a period where SEP is consistently negative. After the calculation of daily DEP values, it is possible to compute the precipitation needed for a return to normal conditions (PRN). PRN is the amount of precipitation, which is necessary to recover the accumulated deficit. Daily PRN values, however, should take into account the actual duration over which DEP values have been calculated:

$$PRN_j = \frac{DEP_j}{\sum_{N=1}^{j}(1/N)}, \tag{3.37}$$

where j is actual duration. Finally, the EDI is calculated as the standardized value of PRN:

$$EDI_j = \frac{PRN_j}{ST(PRN_j)}, \tag{3.38}$$

where ST(PRN) is the standard deviation of each day's PRN.

Basing on the EDI, quantitative drought characteristics as onset, cessation, duration D, intensity S and interarrival time τ (time between the onsets of two consecutive droughts) have been calculated. According to Figure 14, a meteorological drought is defined as a period of time in which the calculated EDI is negative.

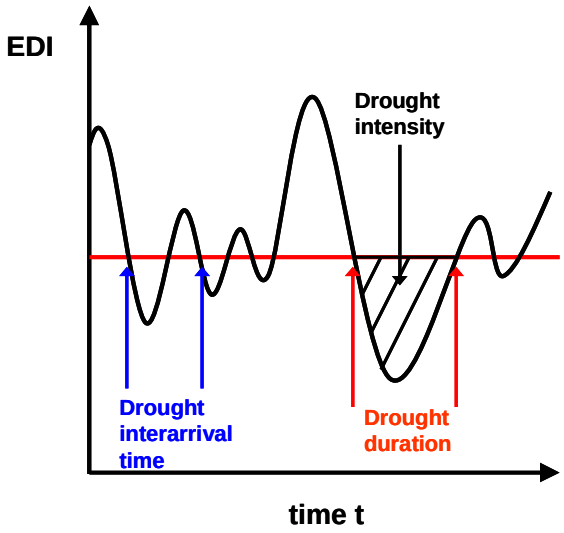

Figure 14: Schematic illustration of calculation of drought specific parameters basing on the Effective Drought Index (EDI).

A change of sign from positive values to negative values is defining the onset, and vice versa the cessation of a drought. The integral of the absolute values of the EDI between onset and cessation of a drought is a measure for the drought intensity. Before applying this definition on the EDI time series, moving-average-filter of different window sizes has been applied to avoid a very short but heavy shower event to be misinterpreted as a flood (EDI > 0) and thus as the end of a drought. A moving average filter of 10 days is found to be work in a reasonable way, which means that it is able to exclude most of

these short intermittent events, but simultaneously keeping the original structure of the EDI time series.

3.6.2 Drought Modelling

Droughts are generally regarded as stochastic processes. Therefore, stochastic modelling is a suited approach to assess their characteristics (SHIAU et al., 2007). Many research papers are dealing with univariate analysis of droughts (e.g. CANCELLIERE & SALAS, 2004; DRACUP et al., 1980A; DRACUP et al., 1980B; MATHIER et al., 1992). However, univariate analysis cannot account for the correlation of drought duration and drought intensity (SHIAU et al., 2007). For this reason, a bivariate distribution which jointly describes these two aspects is adopted. For the bi- or multivariate analysis of two or more variables with unknown or different distribution, Copulas can be applied. Drought indices are well suited to assess joint drought properties quantitatively. Copulas have been mentioned first in literature by SKLAR (1959) and are nowadays widely used for financial or insurance applications. The basic idea of this approach is to separate the dependence and the marginal distributions in a multivariate distribution. Sklar's Theorem states that if H is a joint distribution function of d random variables with $F_1,...,F_d$ marginal distribution functions, then there exist a Copula C such as:

$$H(x_1,...,x_d) = C(F_1(x_1),...,F_d(x_d)). \tag{3.39}$$

Conversely, if C is a Copula and $F_1,...,F_d$ are distribution functions, H is a joint distribution function with marginal distribution functions $F_1,...,F_d$. In other words, a Copula describes how the marginals are tied together. Another practical aspect of Copulas is that they are not restricted to any distinct distribution of the random variables, compared e.g. to the Pearson correlation coefficient r_{bp}, which is restricted to the (multivariate) normal distribution. Other dependence measures like the Spearman rank correlation coefficient ρ_s or Kendall's Tau τ_k are just expressing the "average dependence" in form of one single value. The Clayton Copula has already been proofed suitable to construct the bivariate distribution of drought duration and drought intensity (SHIAU et al., 2007). For this reason, it was chosen for this study. The Clayton Copula and its density function (Equation 6.2) are of the form:

$$C(u,v) = (u^{-\Theta} + v^{-\Theta} - 1)^{-1/\Theta}, \quad \Theta \geq 0 \tag{3.40}$$

$$c(u,v) = (\Theta + 1)(u^{-\Theta} + v^{-\Theta} - 1)^{-(1/\Theta)-2}(uv)^{-\Theta-1}. \tag{3.41}$$

The parameter Θ is a measure of the degree of association between u and v. There is no loss of generality working on unit square (u,v) instead of the original variable space (d,s), because they can be transformed back again, using:

$$u = F_D(d) \Leftrightarrow d = F_D^{[-1]}(u), \tag{3.42}$$

$$v = F_S(s) \Leftrightarrow s = F_S^{[-1]}(v). \tag{3.43}$$

The Clayton Copula parameter Θ has been estimated using maximum likelihood algorithm. Therefore, the log-likelihood function has been calculated as:

$$\log L(\Theta) = \sum_{i=1}^{n} \log c(u_i, v_i, \Theta). \tag{3.44}$$

The maximum likelihood estimate of Θ is the value $\hat{\Theta}$ such that

$$\log L(\hat{\Theta}) = \max\{\log L(\Theta)\}. \tag{3.45}$$

$\hat{\Theta}$ has been estimated for different rainfall regions in the Volta Basin separately (see therefore Chapter 5.4, Table 7).Their drought distributions can therefore be expressed as:

$$F_{D,S}(d,s) = C(F_D(d), F_S(s)) = [(F_D(d)^{-\hat{\Theta}} + F_S(s)^{-\hat{\Theta}} - 1)]^{-1/\hat{\Theta}}. \tag{3.46}$$

3.6.3 Return Periods

The return period is a simple but efficient criterion for risk analysis (SALVADORI, 2004). It is usually defined as the average time elapsing between two successive realizations of an event. The analysis of return periods is often applied for the univariate cases. They can e.g. be defined separately using drought duration (index D) or drought intensity (index s):

$$\tau_D = \frac{\overline{L}}{1 - F_D(d)}, \tag{3.47}$$

$$\tau_S = \frac{\overline{L}}{1 - F_S(s)}, \tag{3.48}$$

where $\overline{L}$ denotes the mean interarrival time of droughts (see therefore Figure 14) and F denotes the cumulative density functions (cdf) of drought duration and drought intensity. Since natural events are often characterized by the joint behaviour of several non-independent random variables, this may lead to an over- or underestimation of the risk of the event. Consequently, the event should be defined in terms of two or more variables (SALVADORI et al., 2007). Instead of considering particular joint distribution F_{XY} with well specified marginals F_X and F_Y, bivariate return periods using Copula approach have been calculated. Two cases of bivariate drought periods can be defined by either drought duration **and** drought severity exceeding a specific value respectively ($\wedge$ - case) or by drought duration **or** drought severity exceeding a specific value ($\vee$ case). Both cases can be calculated by:

$$\tau_{DS\_\vee} = \frac{\overline{L}}{1 - C(F_D(d), F_S(s))}, \tag{3.49}$$

$$\tau_{DS\_\wedge} = \frac{\overline{L}}{1 - F_D(d) - F_S(s) + C(F_D(d), F_S(s))}. \tag{3.50}$$

This methodology offers considerable advantages compared to the above mentioned approaches, because i) it will consider the joint distributions for all marginals, and ii) it is even possible to derive the analytical expressions of the isolines of the return periods (SALVADORI et al., 2007).

3.7 Data

3.7.1 Synoptic Observation Data

For the statistical analyses performed, time series of Burkina Faso and Ghana have been applied. The meteorological data were obtained from the *Institute Nationale de l'Environnement et des Recherches Agricoles (INERA)* at Ouagadougou (Burkina Faso), the Meteorological Service of Burkina Faso in Ouagadougou, and the *Meteorological Service Department* in Accra (Ghana). Especially rainfall data have been used for a wide variety of calculations in this work. Therefore, they have been checked for continuity and plausibility by calculating monthly and annual totals and cross-checking them with neighbouring stations. Due to large data gaps in most of the observation time series, only a limited number of the meteorological observation stations available could be used. Figure 15 shows the spatial distribution of the used synoptic meteorological stations that offered daily data with an acceptable number of missing values from 1961 to 2001. The stations were classified due to their available variables. Figure 16 displays the availability of precipitation data for each station and year. Data as of 2000 have not been considered for the analysis, because ~ 38% of the precipitation data are assigned to *Not a Number*

(NaN) in 2000. Therefore, all the analyses using precipitation data are performed within the time period 1961-1999.

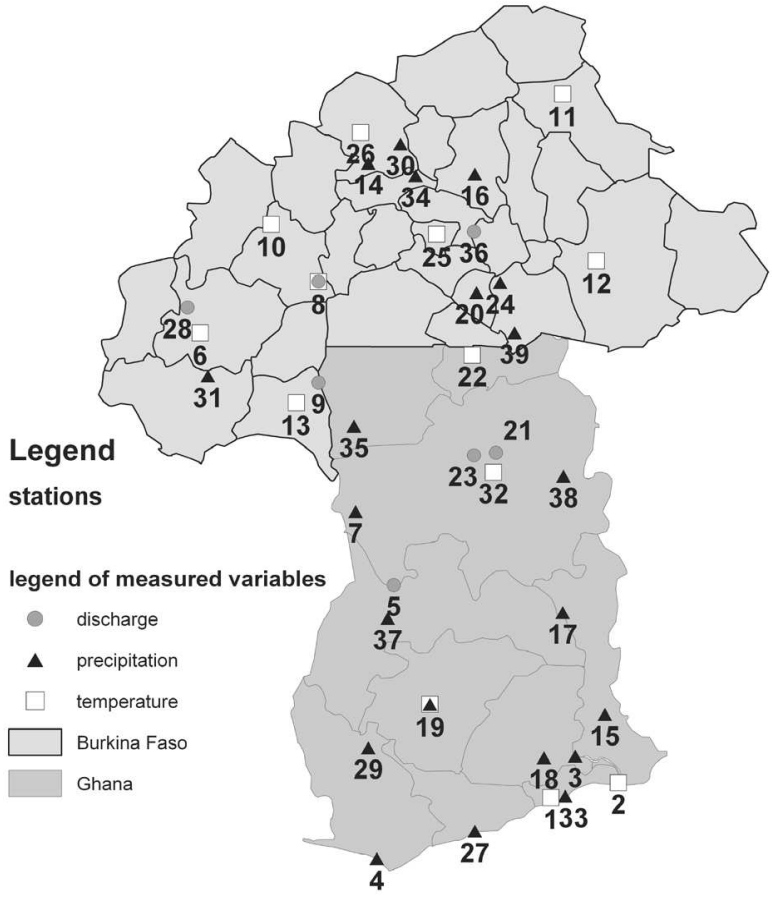

Figure 15: Spatial distribution of observation sites, categorized in discharge, precipitation and temperature. (1 Accra, 2 Ada, 3 Akuse, 4 Axim, 5 Bamboi, 6 Bobo-Dioulasso, 7 Bole, 8 Boromo, 9 Dapola, 10 Dedougou, 11 Dori, 12 Fada-N'Gourma, 13 Gaoua, 14 Gourcy, 15 Ho, 16 Kaya, 17 Kete-Krachi, 18 Koforidua, 19 Kumasi, 20 Manga 10, 21 Nabogo, 22 Navrongo, 23 Nawuni, 24 Niaogho, 25 Ouagadougou, 26 Ouahigouya, 27 Saltpond, 28 Samandeni, 29 Sefwi-Bekwai, 30 Seguenega, 31 Sideradougou, 32 Tamale, 33 Tema (GH), 34 Tema (BF), 35 Wa, 36 Wayen, 37 Wenchi, 38 Yendi, 39 Zabre).

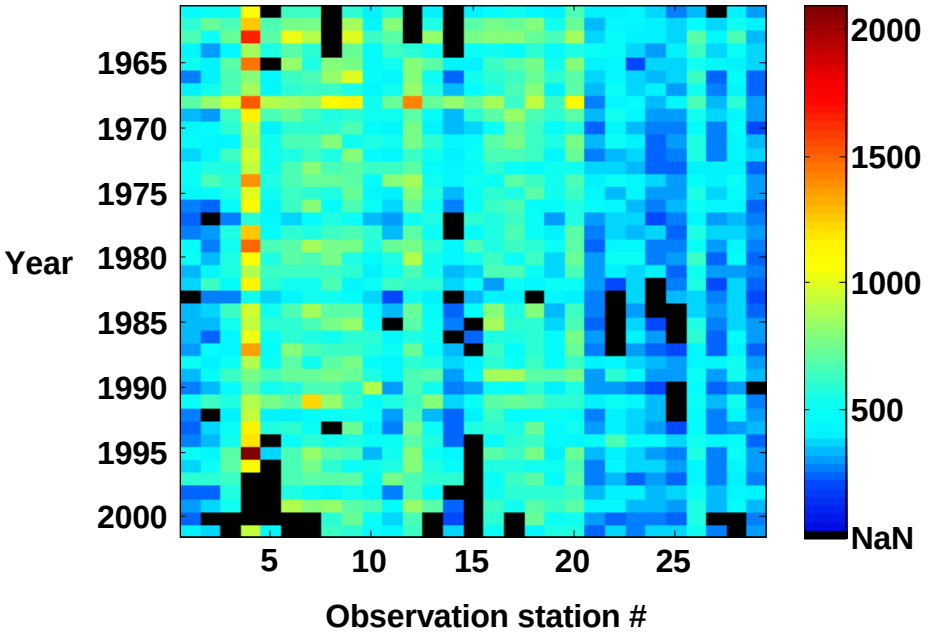

Figure 16: Annual rainfall amount of the 29 observation stations within the Volta Basin. Years with many missing values are displayed as NaN (Not a Number). 6.2% of all data are assigned as NaNs. (Observation station #:1 Accra, 2 Ada, 3 Akuse, 4 Axim, 5 Bole, 6 Ho, 7 Kete-Krachi, 8 Koforidua, 9 Kumasi, 10 Navrongo, 11 Saltpond, 12 Sefwi-Bekwai, 13 Tamale, 14 Tema, 15 Wa,16 Wenchi, 17 Yendi, 18 Kpeve, 19 Zuarungo, 20 Ejura, 21 Kaya, 22 Manga, 23 Niaogho, 24 Ouahigouya, 25 Seguenega, 26 Sideradougou, 27 Tema, 28 Zabre, 29 Gourcy).

3.7.2 NCEP/NCAR Reanalysis Data

The NCEP/NCAR reanalyses (KALNAY et al., 1996) offer the opportunity to investigate the long-term variability of the tropospheric and stratospheric climate as well as the connection between both on a global scale. For this purpose, these data are extensively used world-wide. NCEP/NCAR reanalysis data are produced in a joint effort between the National Center for Environmental Prediction (NCEP) and the National Centers of Atmospheric Research (NCAR). The data has also been applied to investigate the monsoonal system over West Africa (e.g. FONTAINE et al., 2002 & DROBINSKI et al., 2005). They were also chosen as the principle dataset for different atmospheric parameters in this thesis. However, some critical aspects due to the data set should be mentioned. POCCARD et al., 2000 found four inhomogeneities in the NCEP/NCAR rainfall time series over tropical Africa. The main abrupt shift occurred in 1967, where more than 50% of all grid points were concerned. In the observed CRU and CRC data sets, the same shift has been detected, but limited to rather small areas of tropical North Africa. On continental scale, CRC and NCEP/NCAR mean seasonal rainfall patterns are almost the same, however, some regional patterns are not well reproduced, and NCEP/NCAR generally underestimates the rainfall amounts during the rainy season. POHLMAN & GREATBATCH (2006) compared the NCEP/NCAR and ERA40 reanalysis data and also

found discontinuities in both for various surface variables (e.g. SLP and the 2 m temperature) over the African continent in the late 1960s.

For the shortcomings of the data, both studies are blaming the poor synoptic data basis prior to the late 1960s. The data have been retrieved from the NOAA-CIRES Climate Diagnostics Center (CDC) webpage[11] with a temporal resolution of 6 hours and a spatial resolution of 2.5°. The fields, which are known for impacting the West African Monsoon WAM dynamics and energetics, are considered. Table 4 is presenting the utilized reanalysis fields and their classification, respectively: The data are classified in four classes due to their relative influence of (1) the observational data and thus reliability, and (2) the model on the gridded fields. *Class A* indicates the most reliable class of variables: the analysis variable is strongly influenced by the observed data. *Class B* is the next most reliable class of variables. Although some observational data directly affect the value of the variable, the model also has a very strong influence on the output values. *Class C* is representing the least reliable class of variables, where no observations directly affect the output and it is derived solely from the model computations, forced by the model's data assimilation process. Class D fields are fields containing static values. The roughness length and land-sea mask are examples for class D.

Variable	Abbreviation	Level	Class
Sea level pressure	SLP	Surface	A
Skin temperature	SST	Surface	B
Eastward component of wind	U	300hPa, 500hPa, 700hPa	A
Northward component of wind	V	300hPa, 500hPa, 700hPa	A
Specific humidity	SH	500hPa, 850hPa, 1000hPa	B
Geopotential height	GHP	500hPa, 850hPa	A

Table 4: Utilized reanalysis fields and their quality classification. Over land and sea ice, the skin temperature is a prognostic variable. Over open water, the skin temperature is fixed at its initial value (from the Reynolds SST data). The Reynolds SST analyses were done weekly and the reconstructed SST done monthly. The analyses were linearly interpolated to daily values.

Three additional fields, in the following referred as the moisture flux have been calculated using specific humidity (SH) and the eastward and northward component of wind in 500, 600 and 850hPa level:

$$MF\_UV(lv) = SH(lv) \cdot \sqrt{(U(lv)^2 + V(lv)^2)}\,, \tag{3.55}$$

$$MF\_U(lv) = SH(lv) \cdot U(lv)\,, \tag{3.56}$$

[11] http://www.cdc.noaa.gov/cdc/reanalysis/reanalysis.shtml/

$$MF\_V(lv) = SH(lv) \cdot V(lv), \tag{3.57}$$

where lv denotes the atmospheric level in hPa.

3.7.3 ECHAM5/MPI-OM & A1B Scenario

Climate change and its impacts in past, present and future are of mayor interest. In order to understand the future climate system, researchers are falling back on GCMs, driven by different scenarios. Within this thesis, various datasets from the ECHAM5/MPI-OM global climate model (ROECKNER et al., 2006A&B) has been retrieved from the World Data Centre for Climate, Hamburg. ECHAM5 is the 5th generation of the ECHAM general circulation model. Depending on the configuration the model resolves the atmosphere up to 10hPa for tropospheric studies. ECHAM5 output fields from 2011-2040, driven by the SRES-A1B scenario, has been used as input data set for the weather pattern analysis. In order to derive the future eastward component of moisture flux in 300hPa and 500hPa, the eastward wind speed u as well as the specific moisture q has been used. The weather pattern classification has been carried out for the time period 2011–2040, as well as for the period 1961-1990 using the ECHAM5-20C control experiment and NCEP/NCAR reanalysis data. For the generation of future rainfall time series using LARS-WG, daily precipitation fields from the ECHAM5 output have been used.

The IPCC Special Report on Emissions Scenarios (SRES) (NAKICENOVIC et al., 2000) details 4 storylines, narratives of qualitative (e.g., political, social, cultural and educational conditions) emissions drivers. The SRES emissions scenarios are the quantitative interpretations of these qualitative storylines. Six international modelling teams were involved in quantifying the SRES storylines, which resulted in the formulation of 40 alternative SRES scenarios, of which no single scenario is treated as equal probable than others belonging to the same scenario family. Since the A1B scenario is representing an intermediate type of greenhouse gas emissions growth and the business-as-usual development path, it will be used in the following and described in more detail:

The A1 storyline and scenario family describes a future world of very rapid economic growth, global population that peaks in mid-century and declines thereafter, and the rapid introduction of new and more efficient technologies. Major underlying themes are convergence among regions, capacity-building, and increased cultural and social interactions, with a substantial reduction in regional differences in per capita income. The A1 scenario family develops into three groups that describe alternative directions of technological change in the energy system. The three A1 groups are distinguished by their technological emphasis: fossil intensive (A1FI), non-fossil energy sources (A1T), or a balance across all sources (A1B), where balanced is defined as not relying too heavily

on one particular energy source, on the assumption that similar improvement rates apply to all energy supply and end use technologies.

3.7.4 Additional Data Sets

Diverse data sets, as e.g. the DaSilva SST and the Kaplan SLP reconstructions have been used within this work. Because of the inhomogeneous distribution of observations in space and time over the oceans, which are mainly concentrated along the main shipping routes, several authors (e.g., DA SILVA et al., 1994; KAPLAN et al., 1998; KAPLAN et al., 2000) have tried to reconstruct the past ocean surface climate by filling the observation gaps using sophisticated interpolation methods. The results are available as complete reconstructed data sets at the climate explorer website[12]. Furthermore, the grid based GPCP dataset has been used in order to investigate the dependence of rainfall amount with time and latitude.

The crop yield data for Burkina Faso have been obtained from the Direction des Statistiques Agricoles (DSA) in Ouagadougou[13]. The Ministry of Food and Agriculture (MOFA) in Accra have delivered the data for the Ghanaian part of the Volta Basin.

3.8 Interpolation of ECHAM5/MPI-OM Output to Regular Grid

Both, for the CPA as well as for the rainfall simulation of future time periods, scenario data are required. Because of the mismatch of the spatial resolution of the NCEP/NCAR Reanalysis data and the ECHAM5 scenario fields used for CPA, in a first step a transformation has to be performed. Thereby, the ECHAM5 data has been transformed on regular grid using nearest neighbour interpolation. The nearest neighbor algorithm simply selects the value of the nearest point, and does not consider the values of other neighboring points at all. Figure 17 is illustrating schematically the transformation from the ECHAM5 scenario fields, which is provided in T63 spectral resolution (indicated by the squares), to regular 2.5° grid (indicated by the stars) in the sector 5°S5°W-5°N5°E. The arrows are directed to their nearest regular grid point.

[12] http://climexp.knmi.nl/

[13] http://agristat.bf.tripod.com/

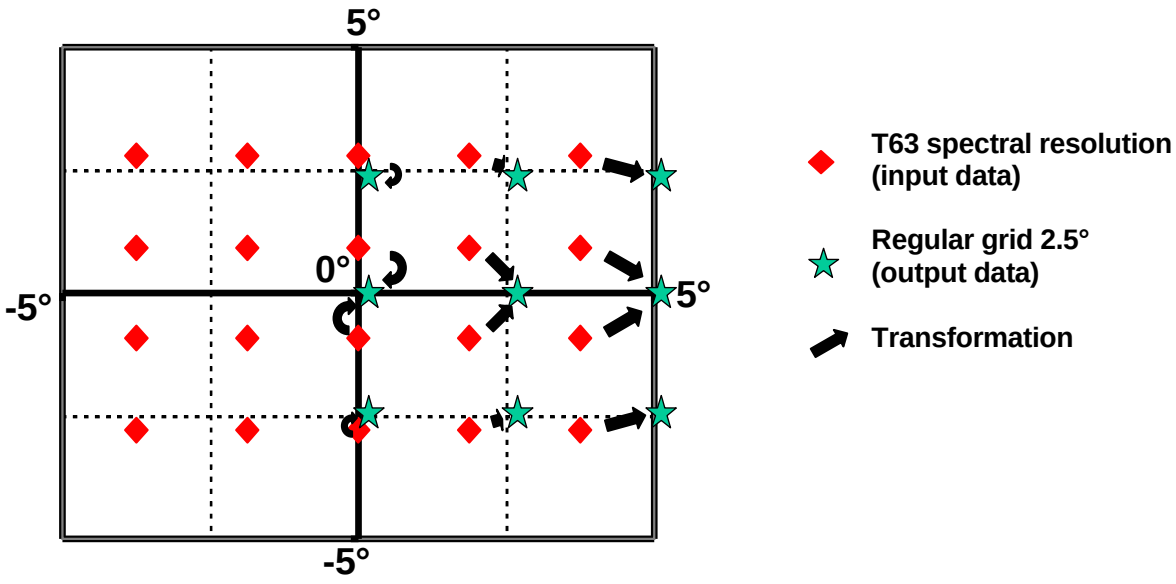

Figure 17: Schematical illustration of grid transformation from T63 spectral resolution to a regular grid (2.5°x 2.5°).

Figure 18 is presenting an exemplarily result of the above mentioned interpolation methodology, used for eastward component of moisture flux in 500hPa. It can be shown that the basis structure is adhered after application of the interpolation:

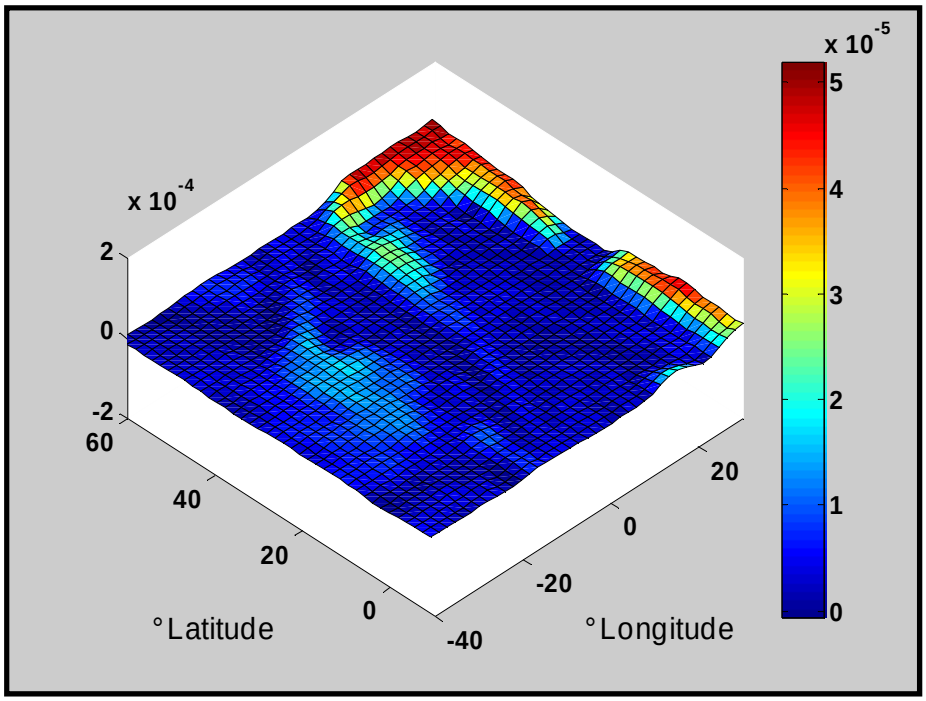

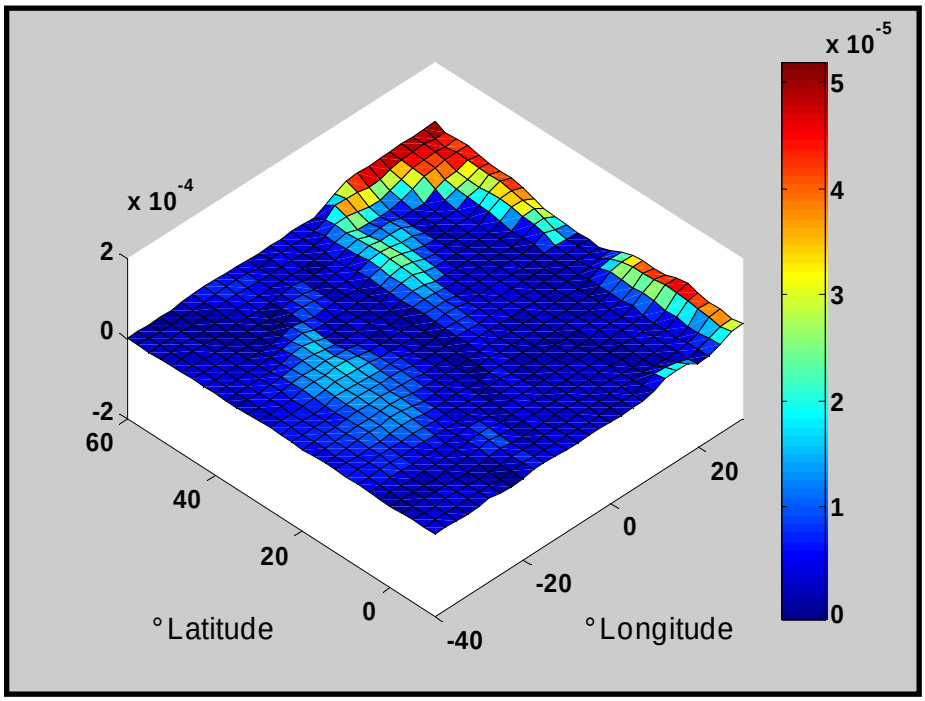

Figure 18: Transformation of Moisture Flux in 500 hPa from T63 spectral resolution (top) to regular grid with a spatial resolution of 2.5° x 2.5° (bottom) using nearest neighbor interpolation strategy.

Chapter 4

4. Definition of Onset and Cessation of the Rainy Season

Onset and cessation dates of the rainy season are important for planning farming activities such as plowing, planting, weeding and harvesting (e.g. SIVAKUMAR, 1988). Various approaches to define the ORS and CRS are currently in use. The onset of the rainy season is of prime importance; therefore the principle effort is given to its determination. Several questionings among West African farmers lead to this result. The cessation plays rather a subordinate role.

4.1 Definition of the Rainy Seasons' Onset and Cessation

4.1.1 Literature Review

Following HESS et al. (1995), "the period of agronomical useful rainfall must be defined in order to consider the social and economic value of the annual rains". In this context, the reliable determination of the onset and cessation of the rainy season are of crucial importance for sustainable food production. According to STEWARD (1991), the onset is the most important variable for agriculture to which all the other seasonal variables are related. Optimally, the start of the sowing time is coinciding with the onset of the rains. Due to the very high spatial and temporal variability of precipitation amounts and a non-uniform distribution of the rains during the rainy season, local farmers have problems to decide when to start with the sowing preparations. Therefore, the farmers have developed a range of strategies to cope with rainfall variability depending on site conditions. According to GRAEF F. & HAIGIS J. (2001), these strategies include:

i) exchange of information on rainfall by seasonal workers,

ii) time-dependent measures, such as dry seeding, re-sowing, and the use of differently maturing crop varieties,

iii) coping with spatial rainfall variability through the cultivation of large and widely dispersed field areas,

iv) measures for sustaining soil fertility.

In a global perspective, various definitions of the onset of the rainy season are in use. The principal research areas are West Africa, India, and Australia, especially areas,

where water availability is scarce and limited to the rainy season. Two main categories of definitions can be distinguished: those relying on parameters measured on the surface and those using atmospheric dynamics:

The first group consists of a huge number of methods, mostly applied for agro-climatological purposes on the local scale. If the ultimate goal is the prediction of the onset and not just its monitoring, it should be defined on regional scale (CAMBERLIN & DIOP, 2003). For the Australian monsoon, there are wind-only (e.g. HOLLAND, 1986) and rain-only definitions (e.g. NICHOLLS, 1984) and a mixture of them (e.g. TROUP, 1961; HENDON & LIEBMANN, 1990a).

The second group of definitions is represented by authors like. DAVIDSON et al. (1983), who analysed the appearance of certain large-scale circulation patterns in combination with the start of the rains. For West African regions, also a large number of definitions are known. ATI et al. (2002) give a good overview of various approaches. Some authors employed a rainfall-evaporation model (e.g. BENOIT, 1977), others use surface pressure, temperature, and relative humidity (e.g. BEER et al., 1977; OMOTOSHO, 1990 & 1992). Most scientists, however, refer to precipitation itself in order to determine the onset and cessation of the rainy season (e.g. WALTER, 1968; ILESANMI, 1972; ATI et al., 2002). The advantage of this approach is that precipitation totals are readily available and it exhibits the most direct relationship rather than some other related factors. Methods using air temperature have not been used widely in West Africa, because of its uniform distribution and the small intra-seasonal variations. In fact, precipitation and not temperature is seen as the most critical factor in tropical agriculture (STERN et al., 1982). For rainfall-alone definitions, two further sub-categories can be found in literature, a definition based on a certain threshold value (e.g. STERN et al., 1982) and a relative definition using a proportion relative to the total amount (ILESANMI, 1972). Table 5 adapted from HESS et al. (1995), summarizes the most frequent applied definitions for the onset, cessation and false starts in West Africa using rainfall-evaporation and/or rainfall-alone approach:

Author	Onset Criteria	Cessation criteria	False Start Criteria
BENOIT (1977)	Rainfall > of at least 0.5 pET over any period (presumably one or few days)	None given	≥ 5 dry days immediately following
KOWAL & KASSAM (1978)	Rainfall ≥ 25 mm within 10 days	The last 10 day period with ≥12.5 mm of rain provided that rainfall in the preceding 10 days exceeded PET	Rainfall < 0.5 PET in the next 10 days
STERN et al. (1982)	Rainfall ≥ 20 mm in 2 days	No rain in 15 days	10 dry days in the following 30 days
SIVAKUMAR (1988)	Rainfall ≥ 20 mm in 3 days	No rain in 20 days	7 dry days in the next 30 (presumably days)

Table 5: Definitions for the onset, cessation and false start of rains using rainfall pET = potential evapotranspiration.

4.1.2 Preliminary Theoretical Considerations for the Development of an Agricultural Meaningful Definition of the ORS

- Real measured data, instead of approaches using more uncertain modeled data, like e.g. the occurrence of wind shears in different levels, as used e.g. in OMOTOSHO et al. (1992), on an agricultural meaningful spatial and temporal scale are required.

- The implementation of additional information (e.g. evapotranspiration, air temperature) throughout the whole year would require additional data, which are not readily available. Moreover, rainfall offers the most direct relationship to the rainy season's onset and other proposed variables just show poor interannual variability. Additional agricultural meaningful aspects should be considered. Since each plant has its individual environmental needs, the following simplifications (generalizations) were made:

  - Adequate soil moisture content, especially at the beginning of the growth period, is demanded to ensure survival of the seedlings.

  - One single heavy event should be excluded to avoid misinterpreted as the onset of the rainy season. A few days of rainfall within a certain period is increasing the probability to be part of the rainy season.

  - Dry stress may harm the seedling irreparably especially during the most sensitive phase of the vegetation period, namely the establishing period (first 2-3 weeks). The definition should be valid across the whole Volta Basin and

should be of flexible usability for different research questions, which are basically demanding different spatial scales.

4.1.3 Fuzzy Logic Approach of Rainy Seasons' Onset

Due to the aforementioned preliminary theoretical considerations a threshold based rainfall-alone definition basing on daily precipitation data constitute the best solution concerning data availability in the target area. The definition, as presented in this section, is similar to the definition of SARRIA-DODD & JOLLIFFE (2001). They modified the approach of STERN et al. (1982) for application in Burkina Faso. The onset is considered to be the first date in the year, for which the following three constraints are valid simultaneously:

i) A total of at least 25 mm of rainfall are observed within a 5-day period;

ii) The starting day and at least two other days in this 5-day period are wet (at least 0.1 mm of rainfall recorded);

iii) No dry period of 7 or more consecutive days is occurring in the following 30 days. This constraint is marking the false start criterion.

Due to the sternness of the three above mentioned constraints, which have to be fulfilled simultaneously and the required validity for the whole Volta Basin, a fuzzy logic modification has been established to facilitate modeling. Each definition constraint is attached to a fuzzy membership function (Figure 19) using triangular (subscript T) fuzzy numbers. Concerning e.g. the first constraint dealing with the total amount of rainfall within a 5-day period the triangular fuzzy numbers are $(18, 25, +\infty)_T$. This means that the membership grade of rainfall totals minor than 18 mm is attached to zero and totals larger than 25 mm to unity. Between 18 and 25 mm the membership grade is linearly interpolated.

Then, the onset date is defined as the first day of the year where the product $\gamma = \gamma_1 \cdot \gamma_2 \cdot \gamma_3$ exceeds a defined threshold value (hereinafter referred as Definition1). For predicting the onset of the ongoing season, however, this definition approach is not useful, as it would require a weather forecast of the following month due to the γ_3 constraint. For this reason, a second definition was applied, with only the fuzzy logic approach of γ_1 and γ_2 being used (hereinafter referred to Definition2). When comparing Definition 1 with Definition 2, the threshold for Definition 2 should be adapted to the reduced number of arguments. Therefore, a threshold $\text{thresh}_{\text{Def2}} = \text{thresh}_{\text{Def1}}^{\,2/3}$ is recommended.

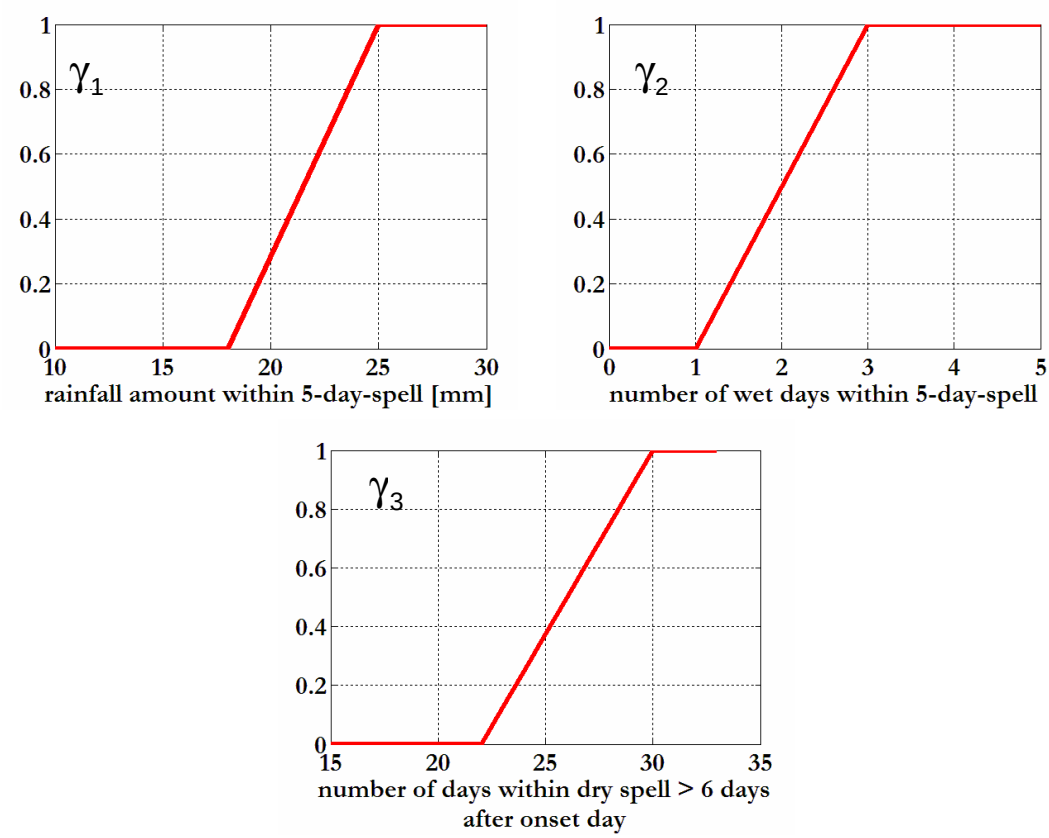

Figure 19: Membership functions representing the three definition constraints. The first day, where the product of all membership grades exceeds a defined threshold value is regarded as the rainy season's onset; (LAUX et al., 2008).

If the calculated onset date is matching the beginning of a period with high rainy day frequency within the year, the date can be regarded as reasonable. In this context sensitivity analysis to clarify the influence of γ has been performed, separately for each region. Figure 20 is depicting the mean onset dates and the standard deviations with varying γ value. An abrupt shift of the mean onset dates as well as standard deviations using $\gamma \geq 0.55$ can be observed, which would decrease the growing time too much.

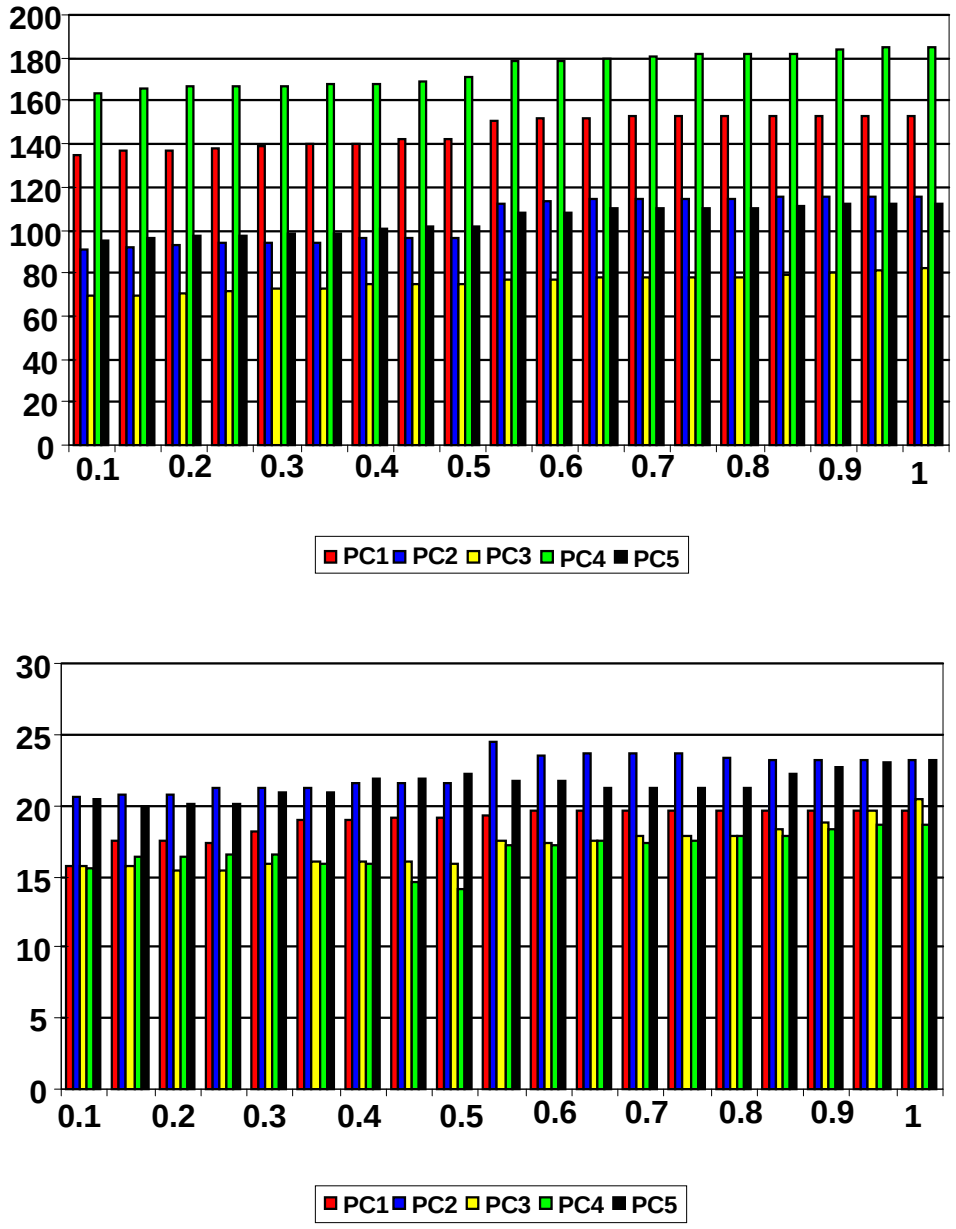

Figure 20: Mean value (top) and standard deviation of the onset dates of PC1-PC5 with varying γ value from 0.1 to 1.0 in an increment of 0.05 using Def.1 (LAUX et al., 2008).

In turn, planting too early should also be avoided. Therefore, a threshold value of 0.4 is proposed, which is delivering reasonable onset dates for all the regions within the Volta Basin. Definition1 is only applicable for ex-post determination of the onset, because of the latter definition constraint, which represents the false start criterion. A false start occurs if the ex-post determination of the onset date using Definition1 overrules the onset dates determined by Definition2 (the first day of the year where the product $\gamma = \gamma_1 \cdot \gamma_2$ exceeds a defined threshold value). Just one false start per year is counted. Figure 21 (top) is showing the number of years with a false start occurrence. For the

southernmost regions PC2 and PC3 and the centred region PC5, the number of false starts is enhanced in February, March and April, whereas false starts are limited to May and June for the northernmost regions PC1 and PC4. Basing on the false start counts, the false start probabilities are derived (Figure 21, bottom).

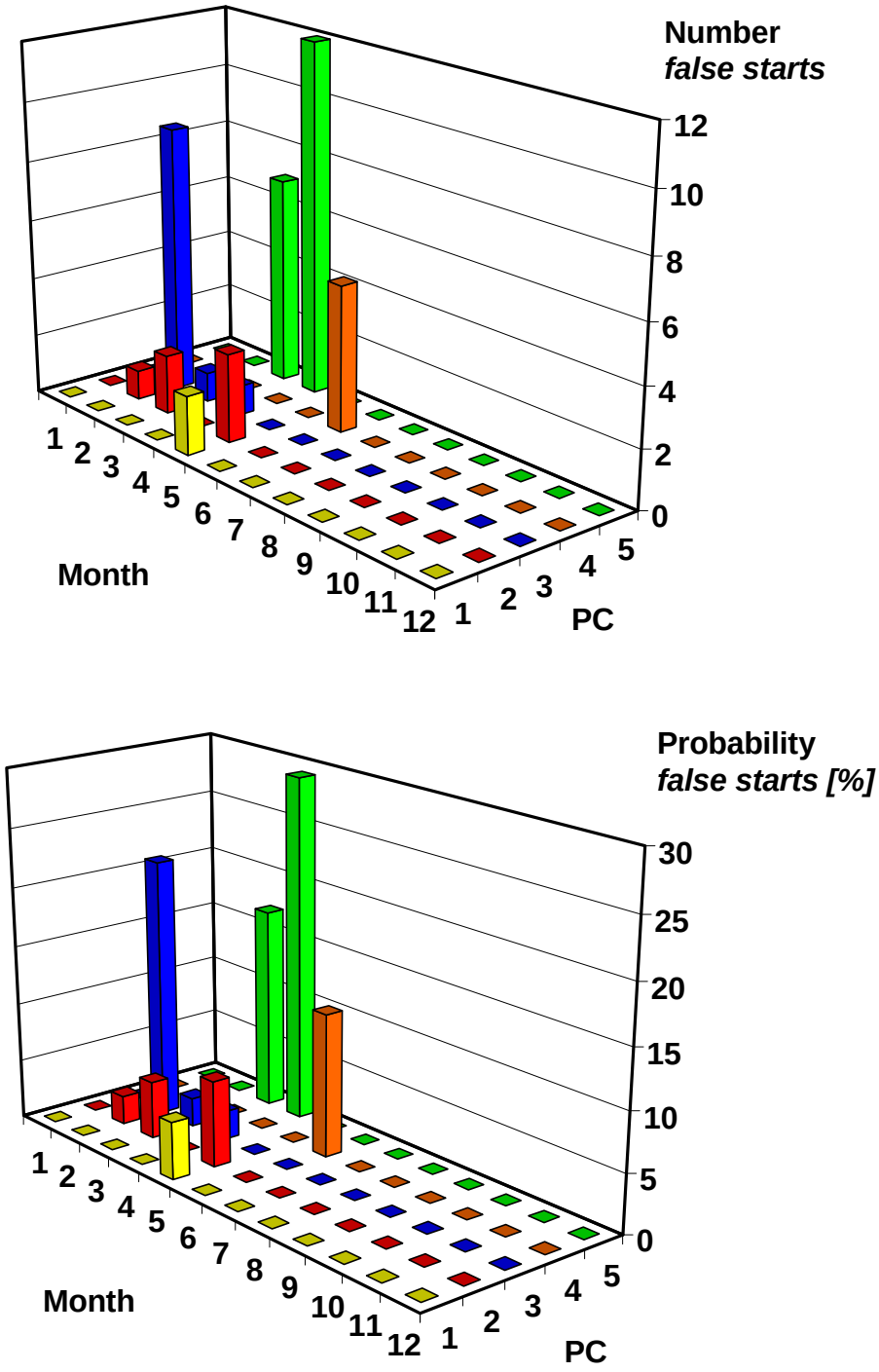

Figure 21: Number of false starts (top) and false start probability [%] (bottom) for each region and month (1961-2001).

Both ORS definitions can be applied operationally. Depending on the research question or the needs, two different strategies are conceivable. Especially for agricultural needs, the calculation of the onset date on site scale is required mostly. Then, regionalization is performed ex post using e.g. external drift kriging algorithm, which is presented in Chapter 4.2.2. Otherwise, regionalization can be performed a prior to reduce the effect of high spatial and temporal rainfall variability. In this case, an approach following Chapter 4.2.1 is recommended.

4.1.4 Fuzzy-Logic Approach of the Rainy Season's Cessation

The cessation of the rainy season is of lower importance compared to the ORS. However, different approaches exist in order to estimate the time for harvesting. The withdrawal of some monsoon systems is often more abrupt, and hence better organized than the onset (e.g. ODEKUNLE, 2004; SEGELE & LAMB, 2005). This can be confirmed looking at the 1st standard deviation of the cumulated mean DOY values (Figure 23, right). A very abrupt end can be observed. For sake of simplicity, the cessation has been simply defined as the last date, where the product of the first two membership functions $\gamma = \gamma_1 \cdot \gamma_2$ (see therefore Figure 19) is exceeding the threshold of 0.4. Considering the standard deviations, which are drastically reduced compared with those of the onset dates, the more abrupt character of the withdrawal can be confirmed for the West African monsoon system.

4.2 Regionalization of Daily Rainfall Time Series

A lot of different methodologies for regionalization are currently in use ranging from Principal component Analysis (PCA) (e.g. MALLANTS, 1990; COMRIE, 1998), Cluster Analysis (e.g. UVO & BERNDTSSON, 1996) to geostatistical techniques, e.g. Kriging (e.g. PIOTROWSKI et al., 1996). Within this section, two potential useful strategies are introduced, and their results are presented in the following.

4.2.1 Regionalization Using PCA

Regionalization is the structuring or segmentation of areas according to its spatially and/or temporally varying properties. In climatology it has been widely applied for many different research questions. Due to the spatially complex precipitation climatology within the Volta Basin with its relatively strong seasonal and interannual variability of amount and occurrence, it is convenient to divide the basin into a manageable number of quasi-homogeneous sub-areas. Within this subsection, regionalization from the site to the regional scale is achieved by means of varimax rotated PCA based on the variance-covariance matrix to generate robust and physically interpretable components (RICHMANN, 1993), subsequently referred to principal components (PCs) (COMRIE & GLENN, 1998).

Figure 22 is illustrating schematically the regionalization strategy followed in this doctoral thesis. The usage of the covariance matrix instead of the correlation matrix allows one to compare relatively wet stations with relatively dry stations in the research area. Thus, stations with the same seasonal timing of monthly rainfall were correlated and grouped together, presumably because of the same atmospheric controls, and the results are linear independent PCs with similar seasonality and long-term variability characteristics (CAHALAN et al., 1996). PCA is used to study the covariances or correlations of variables in order to reduce their number by extracting only a few components, which account for the maximum variation of the original variables. The PCs are an independent set of linear combinations of the variables that redefine the existing variable space. The eigenvalues denote the variability, which is explained by the respective factor in the principal component space. In order to reduce the components to the most important ones, only eigenvalues greater than unity were selected, thus satisfying Kaiser's criterion (KAISER, 1958).

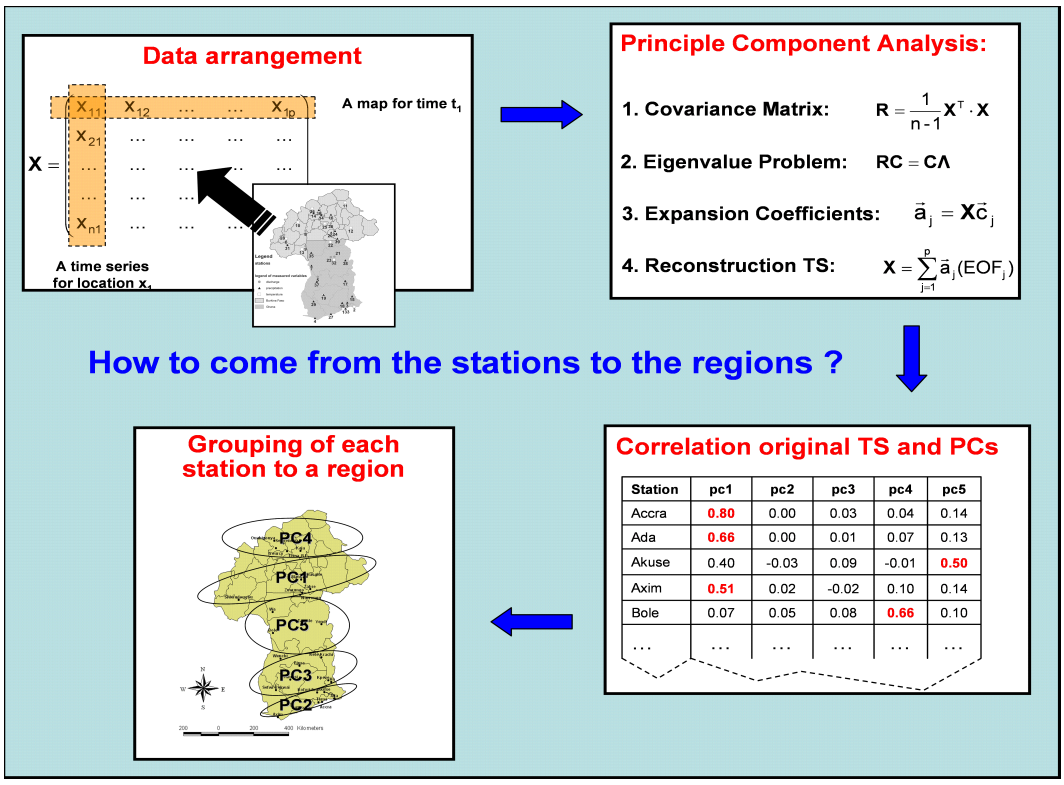

Figure 22: Schematic representation of the applied PCA based regionalization strategy.

The results were five different principal components (PCs) with high within and low between similarities, which explained about 62% of the total daily precipitation variance. To obtain the spatial distribution of the synthetic variables, the Pearson correlation coefficients between the scores of the PCs and the observation stations have been calculated (Appendix 2). Then, each station has been allocated to the region with the highest absolute value of the correlation coefficient. Figure 11 (right) is presenting the

membership of each station to the obtained regions, indicated by ellipses. The nomenclature of the regions is ordered by the fraction of the explained variance, starting with PC1 owning the highest fraction. Finally, artificial time series of the regions have been calculated by averaging the daily rainfall values of all the stations within the respective regions.

Figure 23 illustrates the smoothed long-term mean (averaging period from 1961 to 2001) rainfall per Julian day for the five regions represented by the five principal components. Low slopes of the curves (left side) reflect mean periods of drier spells, whereas high slopes characterize rainy spells. For the regions PC 2 (~ from Julian day 180 - 270) and PC3 (~ from Julian day 230 - 260), a mean dry spell can be observed, followed by a second little rainy season which is much stronger for PC3 than for PC2. The respective figures on the right hand side denote the 1st deviation that highlights the annual distribution of precipitation. As far as the problem of determining the commencement of the rainy season is concerned, these graphs help to detect small rainy spells around the real mean onset date, which were in the past often misinterpreted as the real onset of the rainy season by Ghanaian and Burkinabé farmers. Almost all the regions show rainy spells of gradually different magnitude before the real onset. This knowledge may help to narrow the time frame of the real onset and, hence, to avoid planting too early.

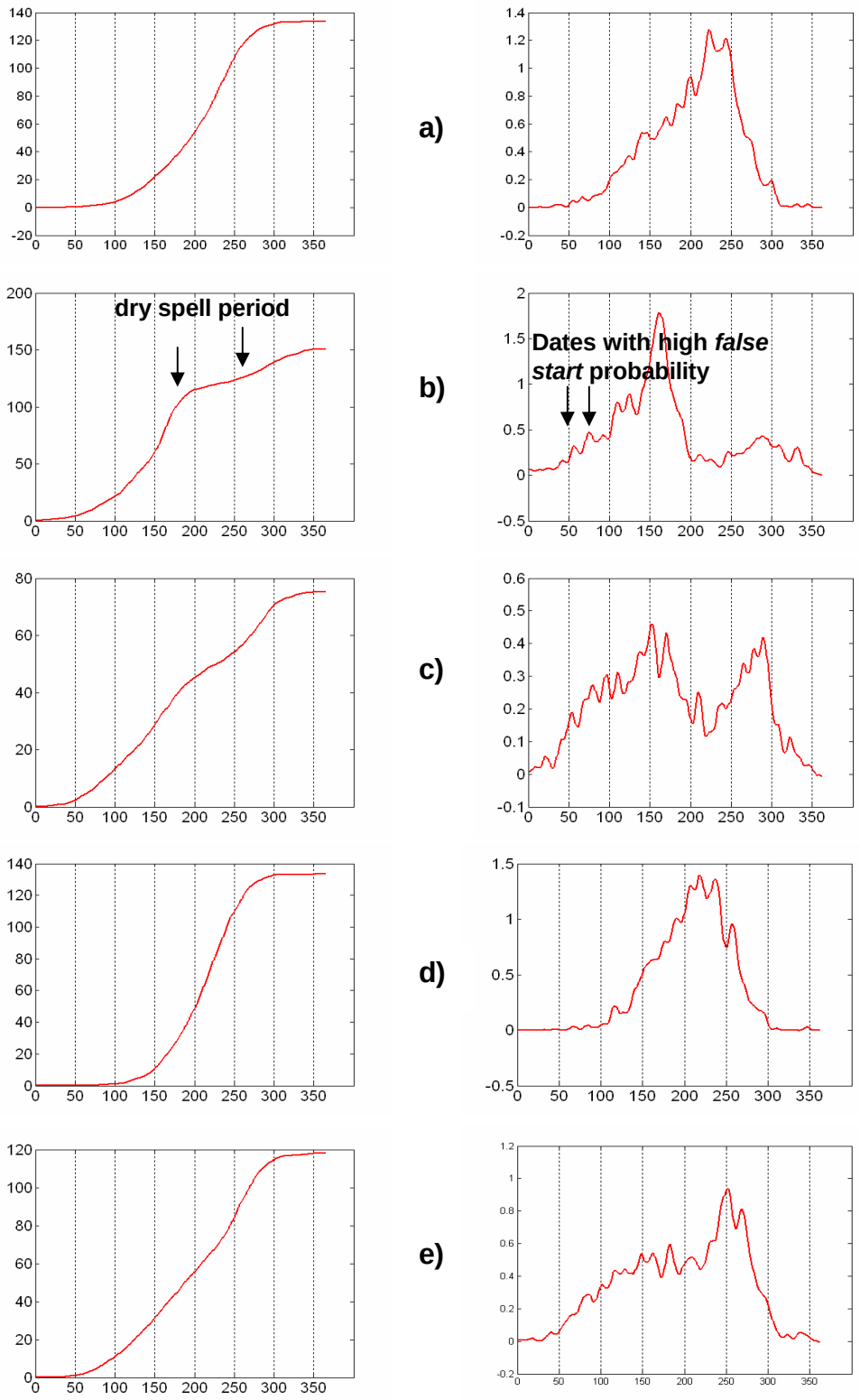

Figure 23: Mean precipitation characteristics of the five regions, represented by the five principal components: a) PC1, b) PC2, c) PC3, d) PC4, and e) PC5. Left: cumulated mean values of rainfall [mm] of all observation sites grouped into a certain region after smoothing. Right: 1st derivation of the cumulated mean rainfall amount [mm/d], (averaging period: 1961-2001); (LAUX et al., 2008).

The mean values of all observation sites allocated to one region were eventually used as input for Definition1 and Definition2 in order to derive past onset dates.

4.2.2 Regionalization Using Kriging

The mean onset dates [DOY] as well as the standard deviations of all the single rainfall stations have been calculated using both definitions. Then, the results are spatially interpolated using external kriging algorithm including distance to sea as additional information. The results are illustrated in Figure 24 and Figure 25. Both definitions are leading to similar mean onset patterns. To avoid systematic differences between the definitions, the threshold values were adopted (see therefore Chapter 4.1.3). The figures resemble the patterns of the annual rainfall amount (see therefore Figure 16). Generally, a progressive onset from the south to the north of the Volta Basin can be found. For both cases, the south easterly coastal region is marking the only exception. There, the onset of the rainy season occurs later than more northerly. This phenomenon is referred to the so called Togo-Gap. Despite of the limited data availability of 29 stations for the whole Volta Basin, relatively smooth maps were obtained for the mean values. High standard deviations can be found in the southern and central part of the basin. For the Sahel, the standard deviations are generally reduced. The withdrawal of the rainy season is ranging between DOY270 in the north and DOY330 in the southwest and shows lower standard deviation than the ORS.

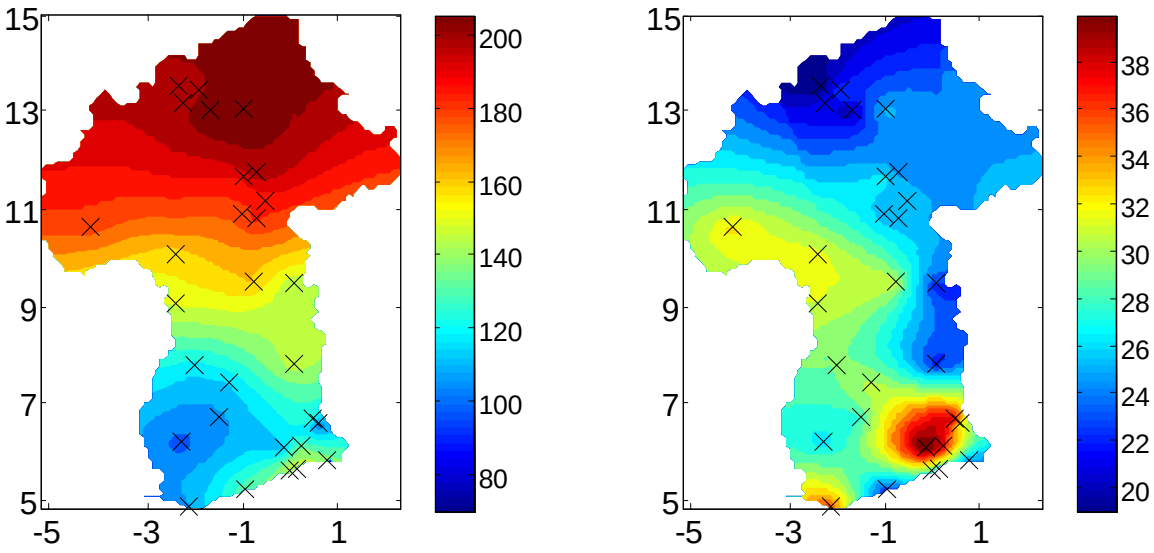

Figure 24: Mean onset date [DOY] (left) and standard deviation [DOY] (right) of 29 synoptic observation stations using Definition1. External drift kriging including distance to sea information was applied for spatial interpolation.

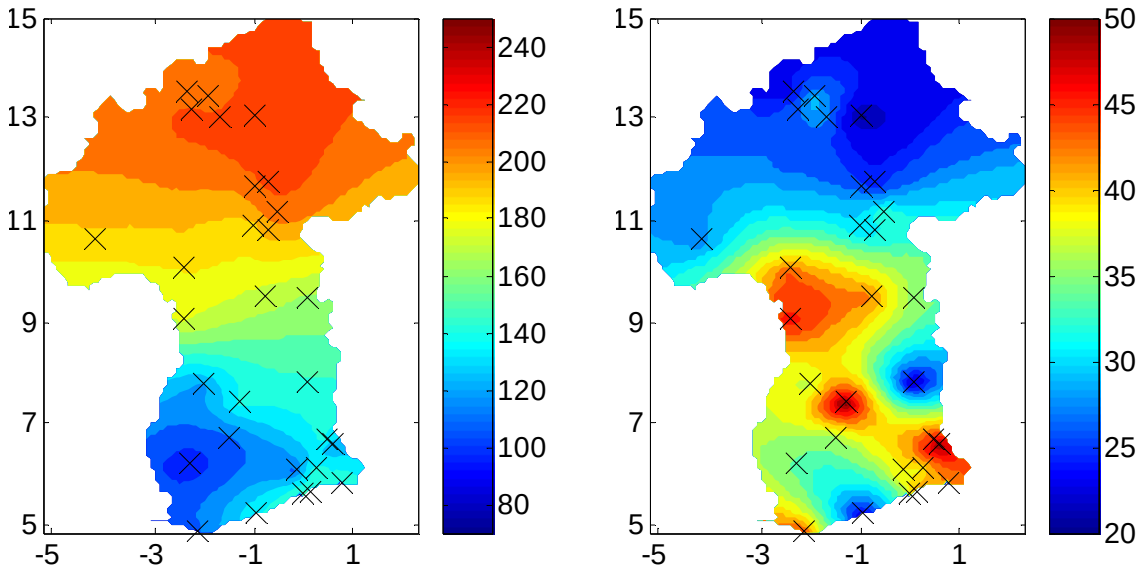

Figure 25: Mean onset date (left) and standard deviation (right) of 29 synoptic observation stations using Definition2. External drift kriging including distance to sea information was applied for spatial interpolation.

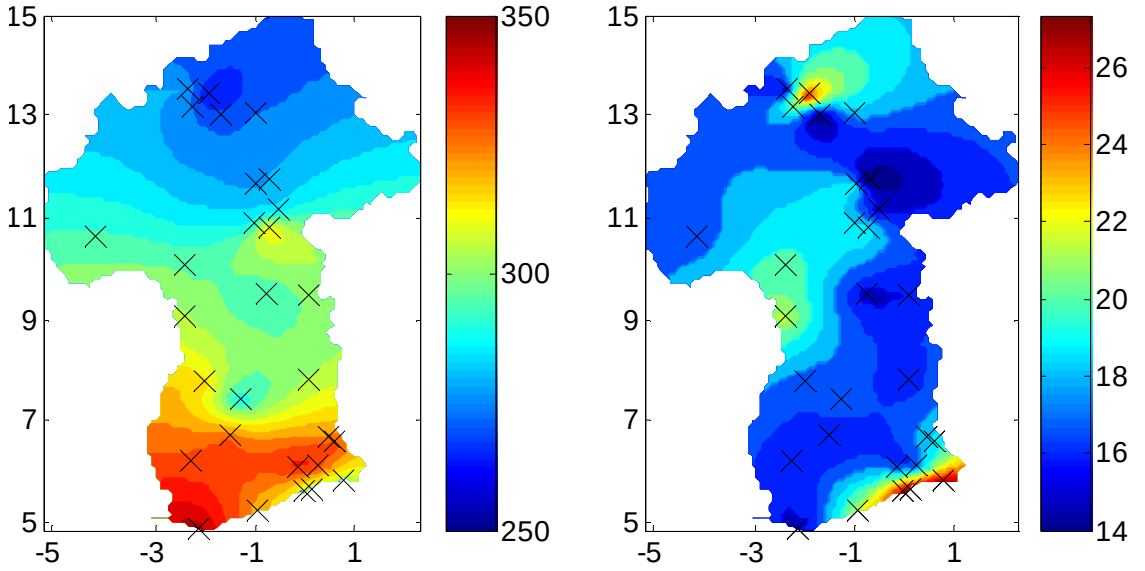

Figure 26: Mean rainy season cessation (left) and standard deviation (right) of 29 synoptical observation stations. External drift kriging including distance to sea information was applied for spatial interpolation.

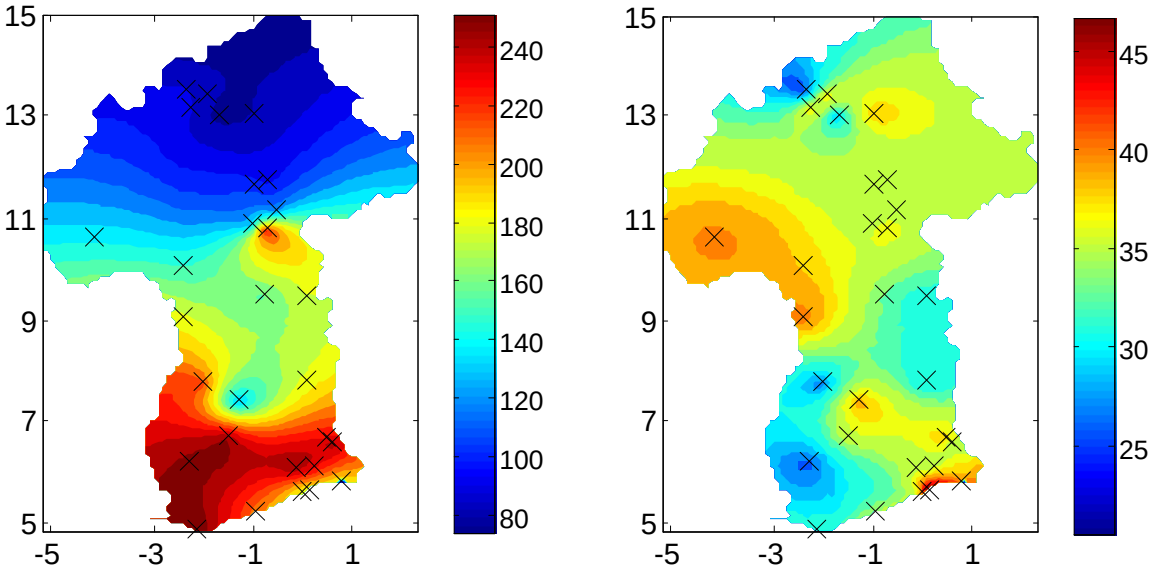

Figure 27: Mean rainy season length (left) and standard deviation (right) of 29 synoptic observation stations using Definition1. External drift kriging including distance to sea information was applied for spatial interpolation.

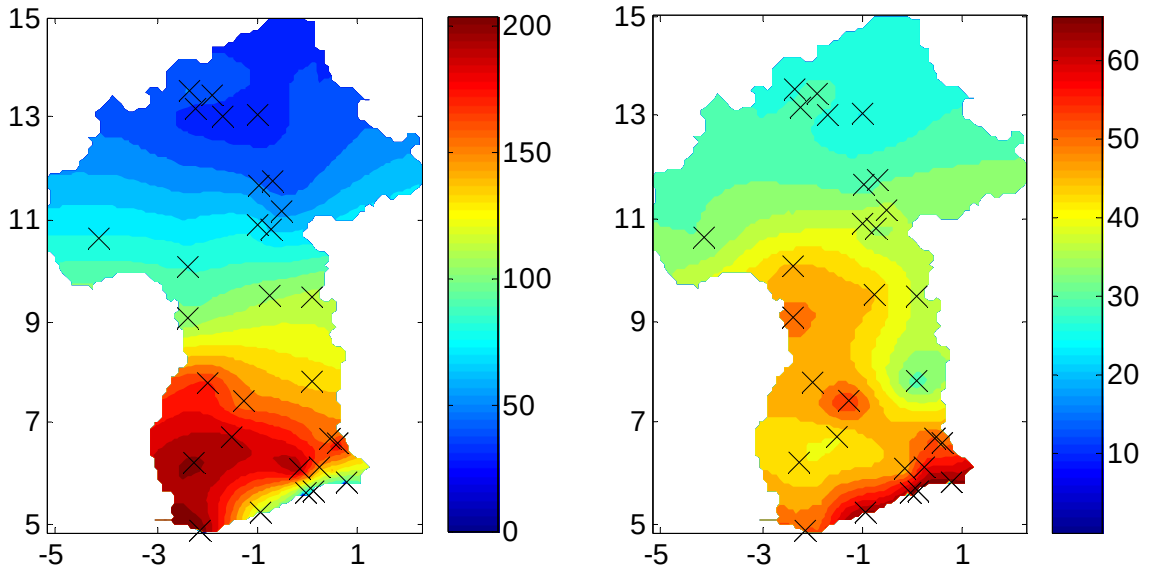

Figure 28: Mean rainy season length (left) and standard deviation (right) of 29 synoptic observation stations using Definition2. External drift kriging including distance to sea information was applied for spatial interpolation.

4.3 Summary of Chapter 4

- Two different definitions for the onset, one for the cessation of the rainy season taking different agricultural requirements into account have been developed and

applied for 29 observation sites and 5 regions across the Volta Basin. The focus is lying on the ORS, which is defined to comply with the planting date. Introducing fuzzy-logic based membership functions is allowing a very flexible approach, which can be easily adapted to the requirements of diverse crops and the regional climatic conditions.

- Both onset definitions can be applied successfully on site-scale and regional scale, the obtained patterns represent the patterns of the annual rainfall amounts and the agro-ecological zones of the Volta Basin. Although the maps of the mean onset dates are very smooth, regional differences are retained.
- The maps of the standard deviation are patchier than those of the mean values. Areas with higher standard deviation constitute higher uncertainties for farmers in matching the “optimal” planting date.
- Reasonable values of the mean cessation dates are derived. The standard deviations of the cessation dates are comparatively low. This indicates a more abrupt withdrawal of the rainy season than the onset.

Chapter 5

5. Precipitation Features for Agricultural Planning

5.1 Rainfall Occurrence Probability

A theoretical description of the following calculations is given in Chapter 3.5. First, the temporal distribution of rainfall is investigated by analysis of its overall probability. The probability of rainfall depends on the conditions of previous days (conditional probabilities). Before analysing the conditional probabilities, it is reasonable to determine the overall chance of rainfall (unconditional probability). These simple calculations can provide very valuable information for farming management (SARI, 2006). By way of example, Figure 29 presents the observed and fitted rainfall probabilities (zero-order Markov model) at Accra based on rainfall data (1961-1999) with a threshold of 1 mm for a rainy day. The probability increases rapidly around DOY 100 (April 08th or 09th), reaching a maximum of more than 50% during the first (major) rainy season from DOY 160 to 170 (June 08th – 18th), remaining relatively constant at 25% from DOY 200 to 270 (July 18th – September 26th) during the second (minor) rainy season in this region, and decreasing again towards the end of the year. Generally, the overall chance of rain during the major season is approximately twice the rainfall probability during the minor rainy season. During the months January, February, November, and December, the probability of getting rain is less than 10%.

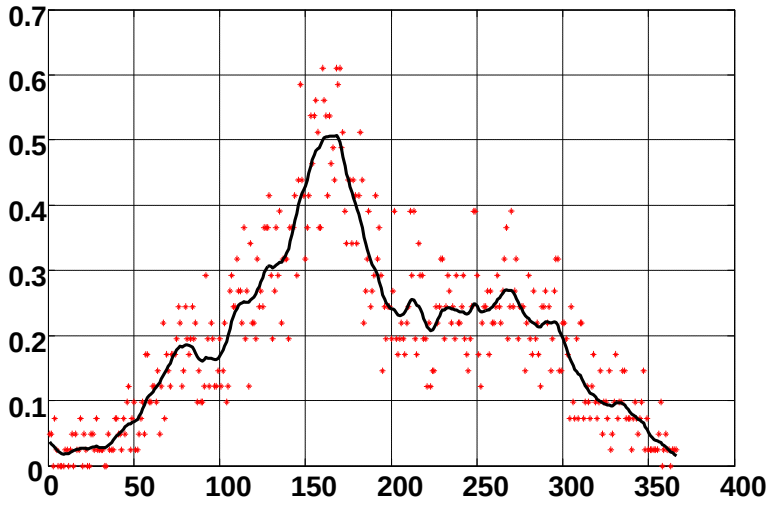

Figure 29: Overall rainfall probability (zero-order Markov model) for each day of the year at Accra, based on rainfall data (1961-1999) with a threshold of 1 mm for a rainy day, observed (*) and fitted (-) using Fourier series with four harmonics.

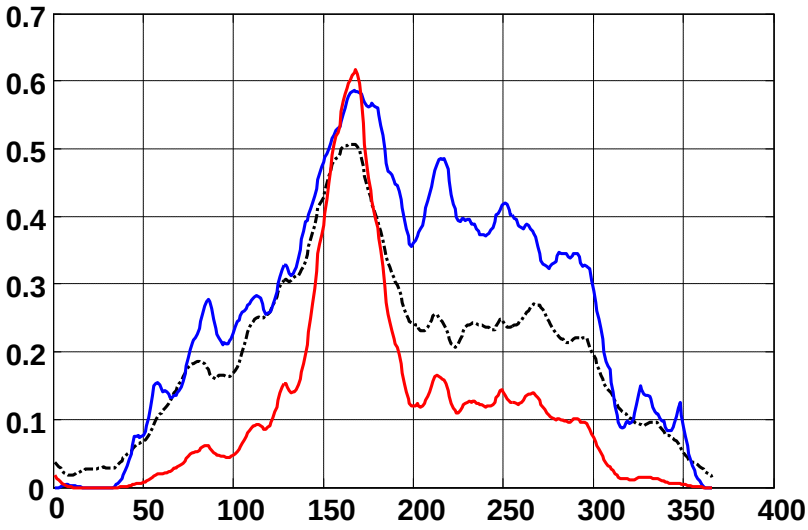

Figure 30: 1st order Markov chain of Accra, the black line is the fitted line of the overall chance of rain. The red line stands for the probability of rain if it is followed by a dry day (fitted line); the blue line stands for the probability of rain if it is followed by a wet day (fitted line).

Figure 30 shows the 1st order Markov chain dealing with rainfall probability depending on whether the previous day was wet or dry. Comparing the conditional probabilities with the overall chance of rainfall (black line), it is found that the probability of rain following a rainy day generally is higher. For the time around the minor season (~ DOY 200 - DOY 300), the probability is about 3 times higher. In the period around the normal onset of the rainy season in Accra (~ DOY 85), a peak occurs, with the probability being more than twice as high as that of rain following a dry day. The overall chance of rainfall at a location predominantly ranges between the curves of rain following a rainy day and rain following a dry day. Small deviation can be observed for the periods DOY 355-45, DOY 150-170 and DOY 320-330. The reason for this is possible the fitting algorithm.

Figure 31 and Figure 32 display the spatial and monthly distribution of occurrence probabilities of rainfall in the Volta Basin for the rainy season. Threshold values of 20 mm/day are used to characterize erosive rainfall with a potentially high risk of soil loss and 5 mm/day to characterize humid periods. The probability of having a humid period in June reaches almost 50% for the coastal area and around 30% for the eastern region. During July, the maximum probability shifts to the central area of Ghana, with low probabilities at the western border of Ghana. In August, high probabilities focus on Burkina Faso, whereas a 0% probability occurs in the southern and western areas of Ghana. In September, the maximum probabilities shift southwards again and are centered in the Volta Basin. In October, the maximum probability is encountered in eastern and western regions of Ghana, while a 0% probability is observed for the whole

of Burkina Faso. Using the threshold of 20 mm/day, the monthly resolved patterns are almost identical, they only vary in magnitude.

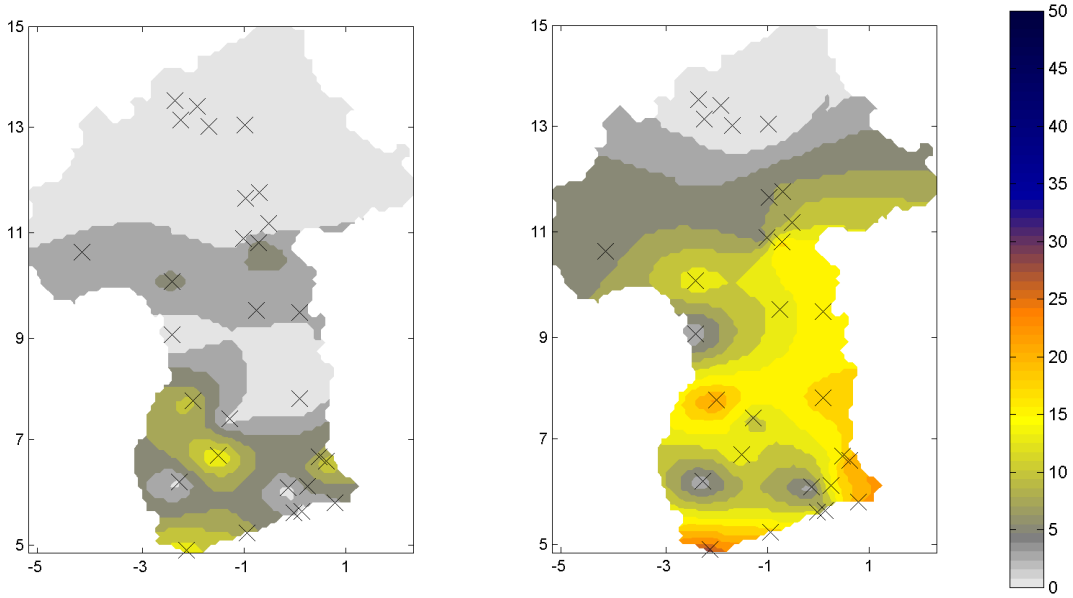

a) b)

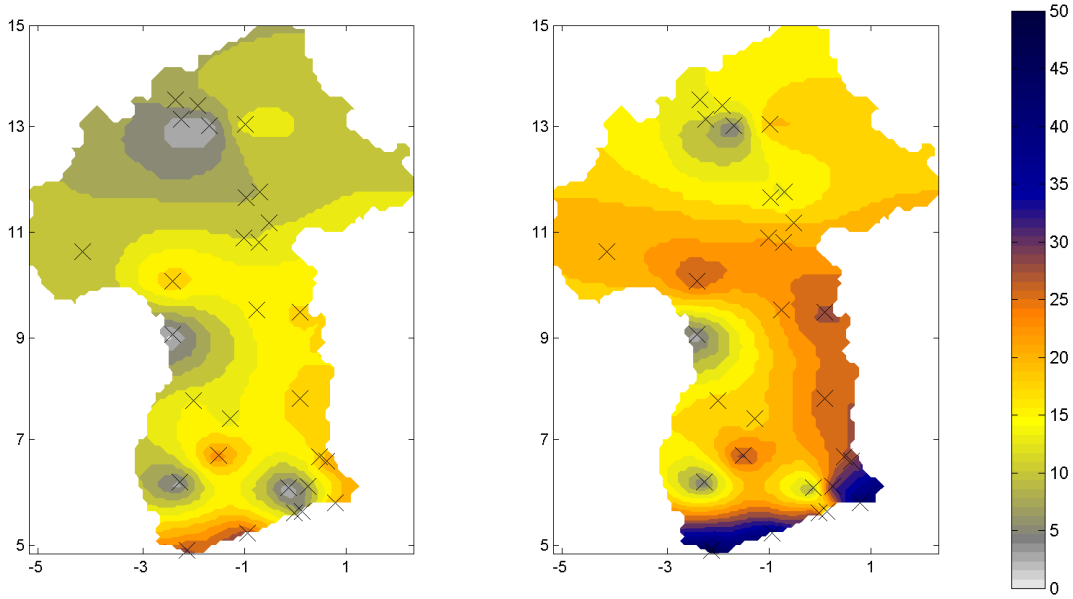

c) d)

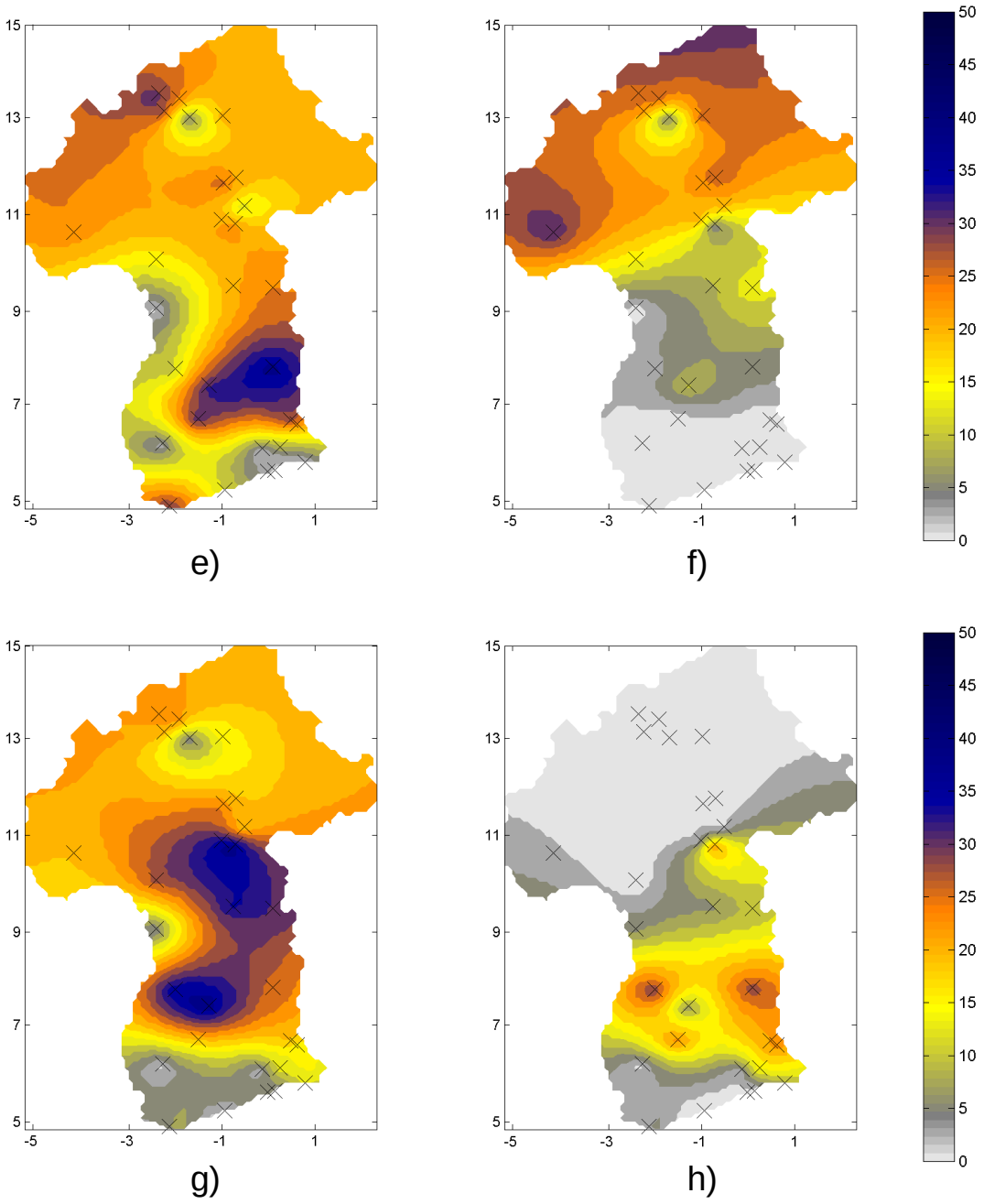

Figure 31: Spatial distribution of rainfall occurrence probabilities [%] exceeding 5 mm/day in the Volta Basin for the month of a) March, b) April, c) May, d) June, e) July, f) August, g) September, and h) October. External drift kriging including distance to sea information was applied for spatial interpolation.

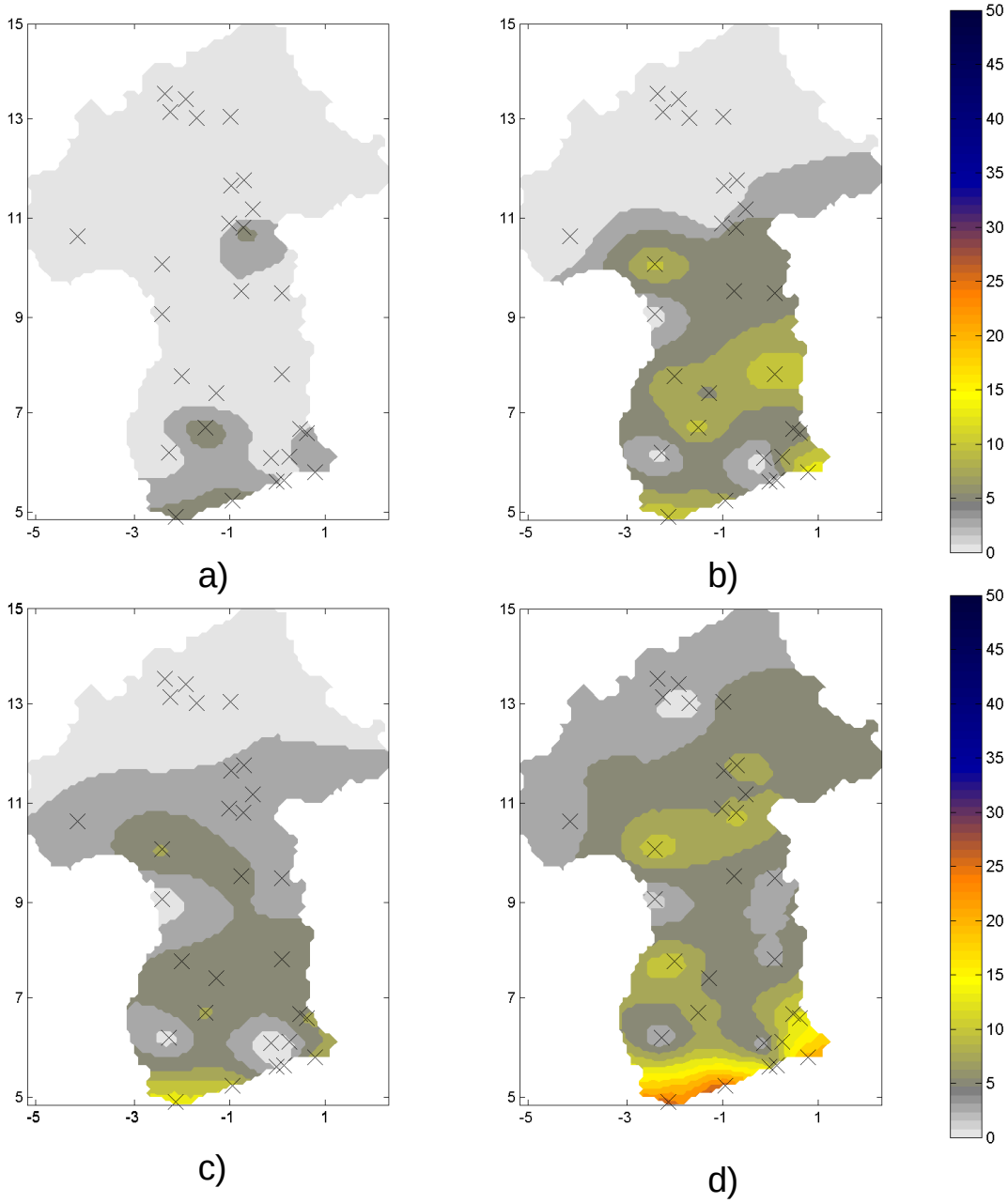
15
13
11
9
7
5
-5
-3
-1
1
50
45
40
35
30
25
20
15
10
5
0
a)
b)
c)
d)

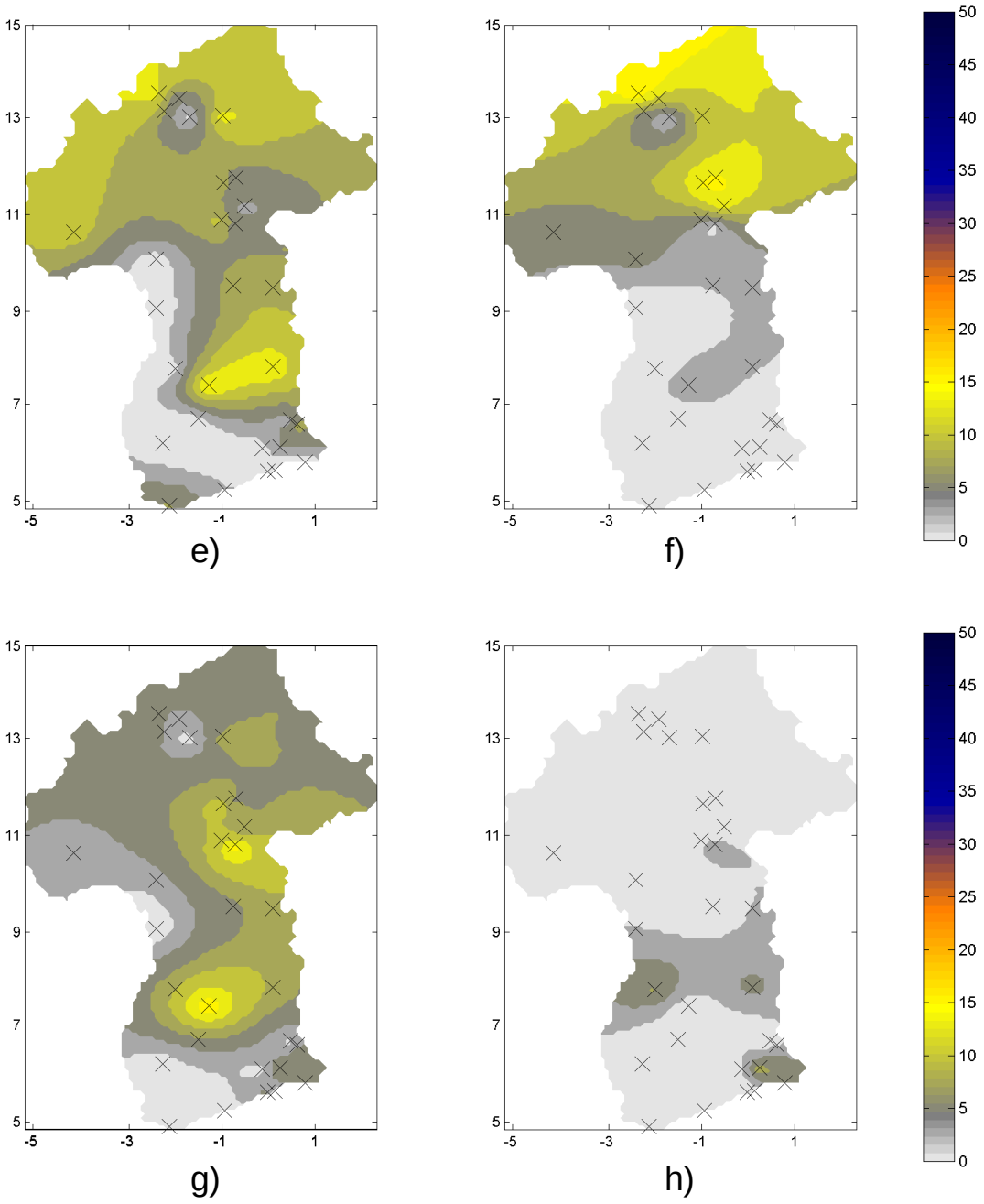

Figure 32: Spatial distribution of rainfall occurrence probabilities [%] exceeding 20 mm/day in the Volta Basin for the month of a) March, b) April, c) May, d) June, e) July, f) August, g) September, and h) October. External drift kriging including distance to sea information was applied for spatial interpolation.

The daily rainfall amount can be described adequately using the gamma distribution (e.g. STERN & COE, 1982). Figure 30 exemplarily depicts the observed and modelled mean rains per rainy day at Accra. The blue line shows the mean daily evaporation rate. For simplicity, it is assumed to be 5 mm/day (e.g. KASEI & AFUAKWA, 1991). The maximum value of the fitted line is slightly higher than 8 mm and reached around June

8th, followed by a period with less than 1 mm per day from DOY 195 to 260 and slightly larger than 2 mm/day up to DOY 300, and again smaller values to the end of year.

5.2 Rainfall Amount

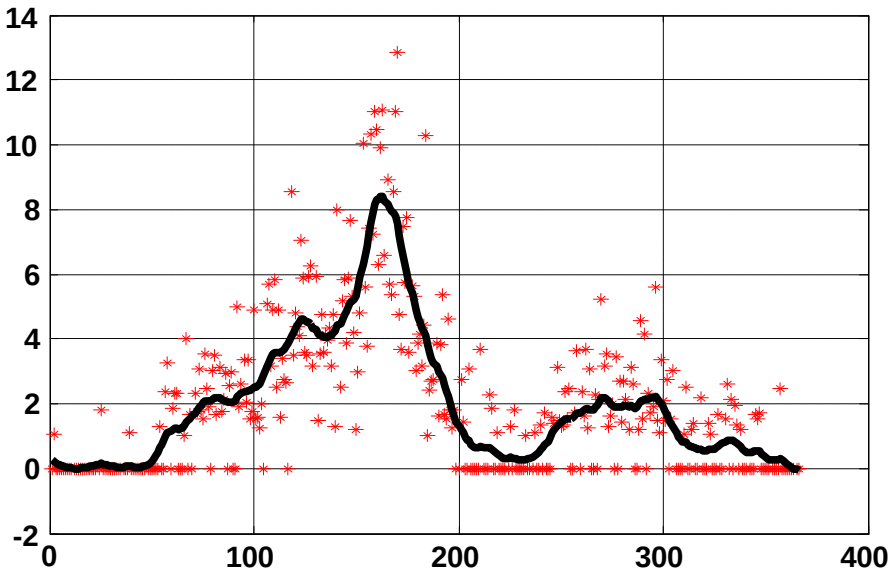

Figure 33: Observed (*) and fitted (-) mean rainfall amount per day at Accra, based on rainfall data (1961-1999) with a threshold of 1 mm for a rainy day, using Fourier series with four harmonics.

Beside of the rainfall probabilities exceeding a threshold value, it is also important to know how the rainfall amounts are distributed during the year. Figure 33 illustrates exemplarily the mean rainfall amount for each DOY in Accra, averaged over the period from 1961-1999. There, the fitted rainfall amounts are exceeding 8 mm during the major rainy season (~DOY 160-175). During the minor rainy season, rainfall amounts around 2 mm can be observed.

Figure 34 is illustrating the spatial distribution of the mean μ and shape parameter k of the gamma distribution. Both parameters show a large spatial variability, which must be taken into account for modelling the rainfall amounts. Generally, μ and k are arranged zonal, following roughly the rainfall distribution within the Volta Basin.

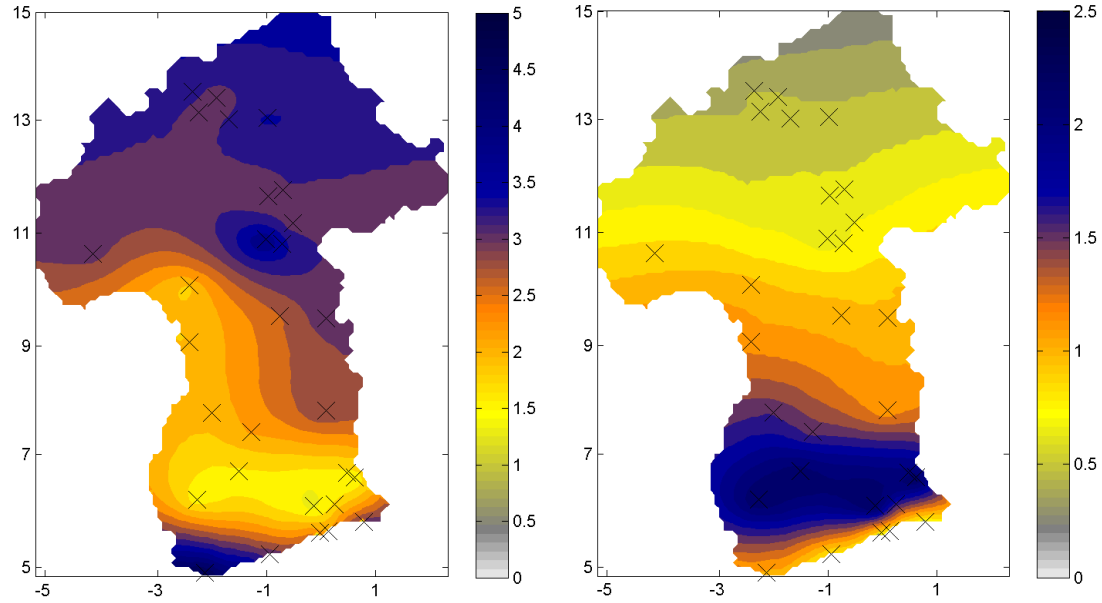

Figure 34: Spatial distribution of the mean μ (left) and the shape parameter k (right) of the gamma distribution, interpolated using external drift kriging with distance to sea information.

5.3 Dry Spell Probability

Beside the onset of the rainy season, the occurrence of dry spells is the most important measure for agriculture in West Africa (SIVAKUMAR, 1992B). Figure 35 exhibits the proportion of a dry spell of > 6 consecutive days at Bole, based on rainfall data (1961-1999) with a threshold of 1 mm for a rainy day. The probability decreases below 10% around DOY 160 (June 08th). Later, the probability of dry spells increases to more than 60% (around August 12th), decreases again to less than 40% (September 25th), and finally increases again rapidly.

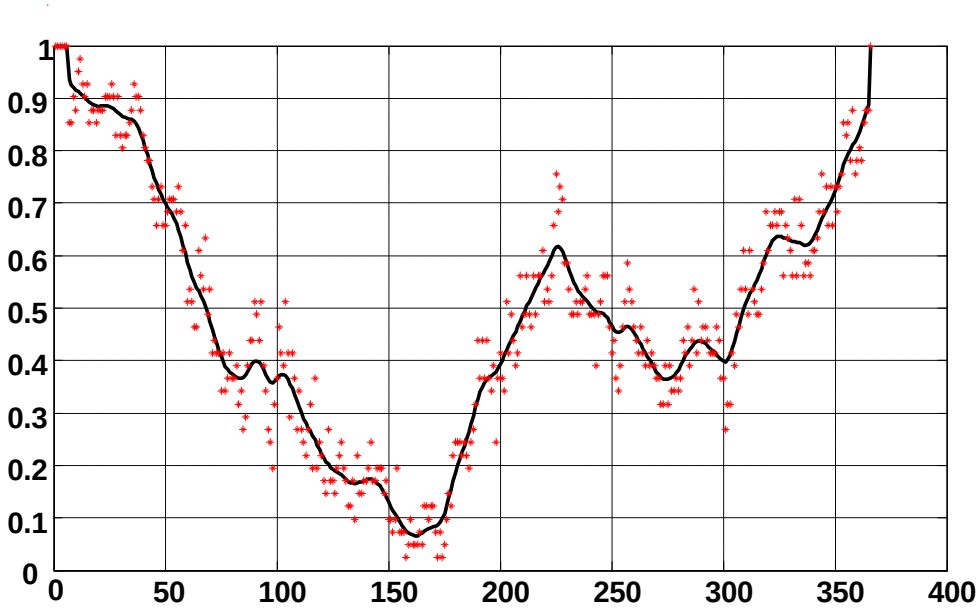

Figure 35: Observed (*) and fitted (-) proportion of a dry spell of 7 or more days at Bole for each day of the year, based on rainfall data (1961-1999) with a threshold of 1 mm for a rainy day.

Assuming e.g. a probability threshold of P=0.2, which is not allowed to be exceeded at planting time, the time window for planting is restricted approximately from DOY 120 to DOY 180. These probabilities have been calculated for all stations across the Volta Basin. Figure 36 (left) illustrates the spatial distribution of the dates with the minimal dry spell occurrence probabilities. With exception of the stations Bole and Ejura, the pattern approximately reflects a north-south distribution following the movement of the ITCZ. The respective probabilities of these dates are presented in Figure 36 (right). The minimum dry spell probabilities hold a regional maximum in northwest Ghana and southwest Burkina Faso (~30%). In these regions, dry spells occur more likely within the following 30 days, so that there is an enhanced risk of crop failure. When modelling rainfall probabilities or the probabilities of dry spells, conditional probabilities should be considered to allow conclusions to be drawn with respect to their persistence in time. The transition probabilities help to estimate the reasonable order of the Markov chains.

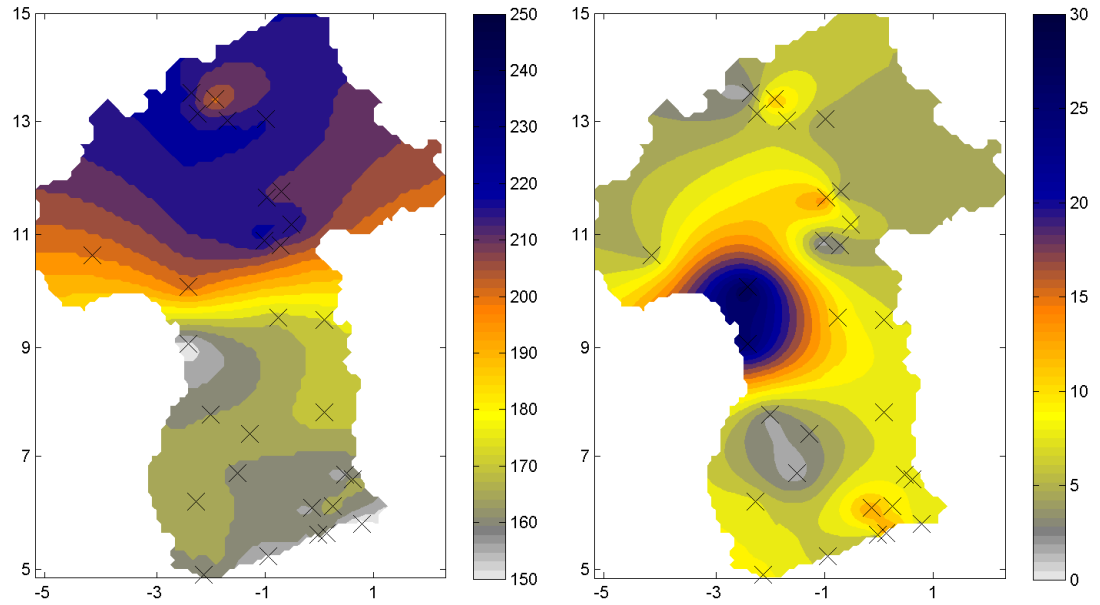

Figure 36: Date [DOY] with the minimum dry spell occurrence probability for the following 30 days, representing the optimal planting date (left), and probability of the dry spell occurrence [%] within the following 30 days (right). External drift kriging including distance to sea information was applied for spatial interpolation.

5.4 Droughts in the Volta Basin

Drought is a normal and recurrent climatic phenomenon affecting sustainably economy, environment and social life. Drought is marking - beside of flood - one of the two prevailing extremes of rainfall variability and is the most significant threat to rain-fed agriculture (USMAN et al., 2005; SALVADORI et al., 2007). Maybe, droughts are the most complex natural hazard, because it develops slowly, is difficult to detect and has many facets in any single region (MORID et al., 2007). Especially for the Volta Basin, in which the economy is strongly depending on rainfed agriculture, droughts are creating a huge risk. Even though it is not possible to avoid droughts, drought preparedness can be developed and their impacts can be managed (SMAKHTIN & HUGHES, 2004). The enhanced risk connected with droughts in turn, discourages investment by farmer, governments and development agencies (SHAPIRO et al., 2007). Therefore, future drought prediction with sufficient lead time is one major challenge. It is also related to the timing (i.e., principal season of occurrence, delays in the start of the rainy season, occurrence of rains in relation to principal crop growth stages) and the effectiveness (i.e., rainfall intensity, number of rainfall events) of the rains[14]. In the past, severe and persistent droughts in the Sahel culminating in the 1970s and 1980s raised the question in the physical sciences community about their reasons. Several studies have been

[14] http://www.drought.unl.edu/whatis/concept.htm/

conducted to answer the question whether to blame the impact of human activity on the local environment or global climate variability. To answer that question, an improved appraisal of the variable nature of rainfall is of prime importance (TRAORÉ et al., 2007). However, Sudano-Sahelian West Africa is one of the climatic most sensitive and complex regions all over the world (ZENG, 2003) due to the superposition of different competing variability modes of rainfall. Rainfall variability ranges from the location and astronomic forcing, determining the seasonality of climate via oceanic-atmospheric large-scale forcing, which condition regional circulation and affect the season's potential, to synoptic and sub-synoptic features, controlling weather patterns and the realization of the season (LISTER & PALUTIKOV, 2001).

Detailed knowledge of the connection between rainfall variability and the driving forces on different scales will probably help to establish an early warning system for this region. Sahelian rainfall could be linked to sea surface temperature in the Pacific (HULME et al., 1992). Other studies found significant correlations between Atlantic SST, in form of SST based indices, and rainfall in parts of the Volta Basin (e.g. NEUMANN et al., 2007; LAUX et al., 2007; OPOKU-ANKOMAH & CORDREY, 1994). ADIKU & STONE (1995) used April Southern Oscillation Index (SOI) phase to predict seasonal rainfall (April to July) for some sites located along the southern coast of Ghana. However, the lead time is too short for effective agricultural planning. In another study, ADIKU (2003) proofed October-November-December El Nino Southern Oscillation (ENSO) index to be suited for seasonal rainfall prediction of Southern Ghana. However, realistic and reasonable seasonal prediction requires a comprehensive understanding of the past long-term rainfall variability (especially the classification of phases with drought and wet conditions in terms of duration and severity).

In the following section, past droughts were identified and classified to different severity classes using suited drought parameters. Finally, suitable functions for stochastic modelling are established and return intervals of droughts are estimated. In this work a drought is defined as a time period, in which one or more consecutive days with 10-day-moving-averaged EDI values less than zero, occur. The Effective Drought Index using a 10-day-moving-average filter has been calculated for five different rainfall regions within the Volta Basin in West Africa from 1962-2001, which are illustrated for the regions PC1-PC5 (Figure 37). The year 1961 has been used for calibration of the EDI.

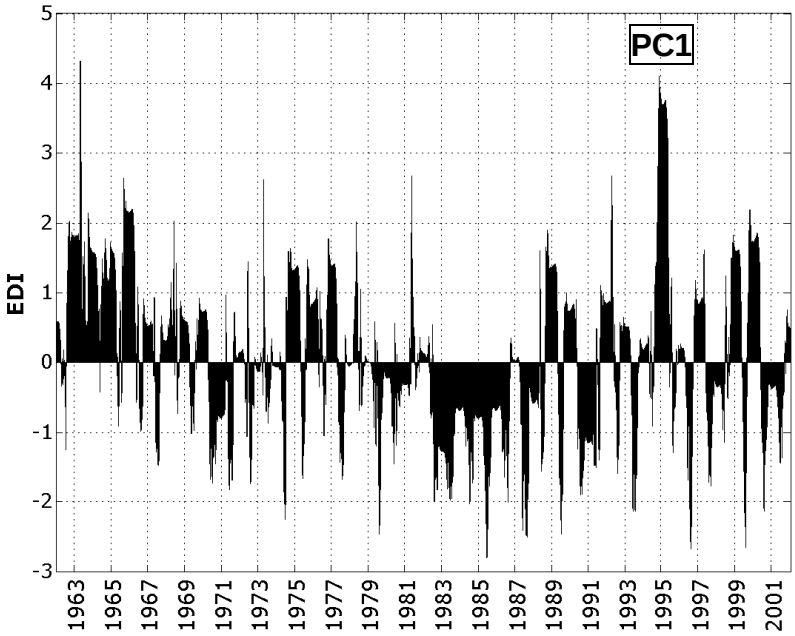
PC1
EDI
5
4
3
2
1
0
-1
-2
-3
1963
1965
1967
1969
1971
1973
1975
1977
1979
1981
1983
1985
1987
1989
1991
1993
1995
1997
1999
2001

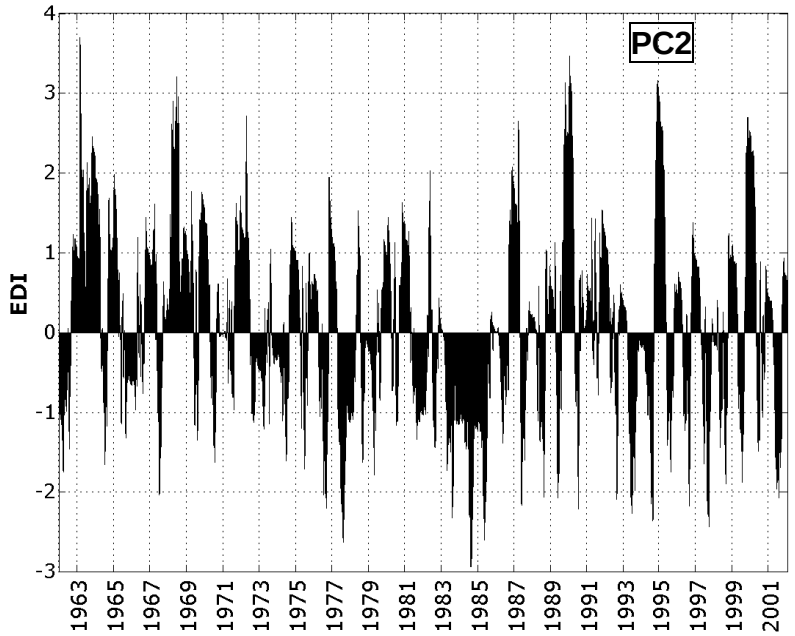
PC2
EDI
4
3
2
1
0
-1
-2
-3
1963
1965
1967
1969
1971
1973
1975
1977
1979
1981
1983
1985
1987
1989
1991
1993
1995
1997
1999
2001

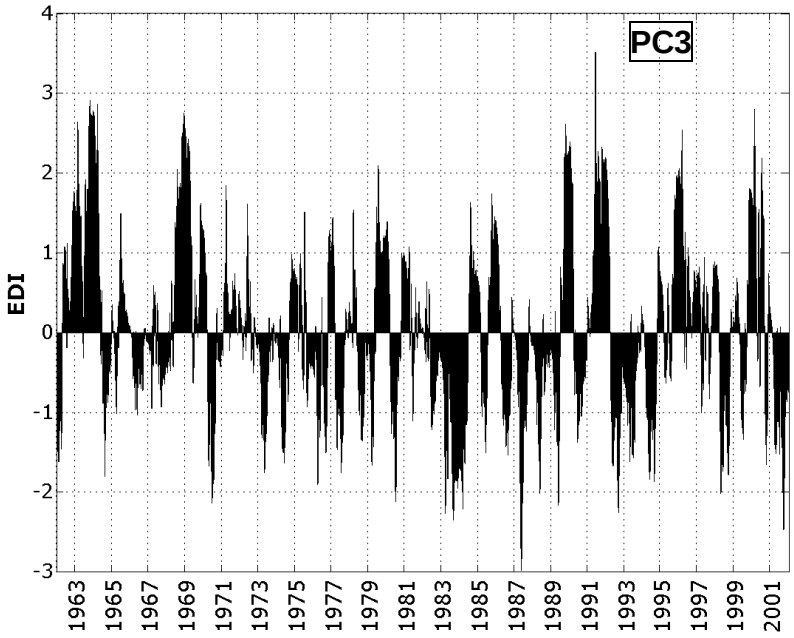
PC3
EDI
4
3
2
1
0
-1
-2
-3
1963
1965
1967
1969
1971
1973
1975
1977
1979
1981
1983
1985
1987
1989
1991
1993
1995
1997
1999
2001

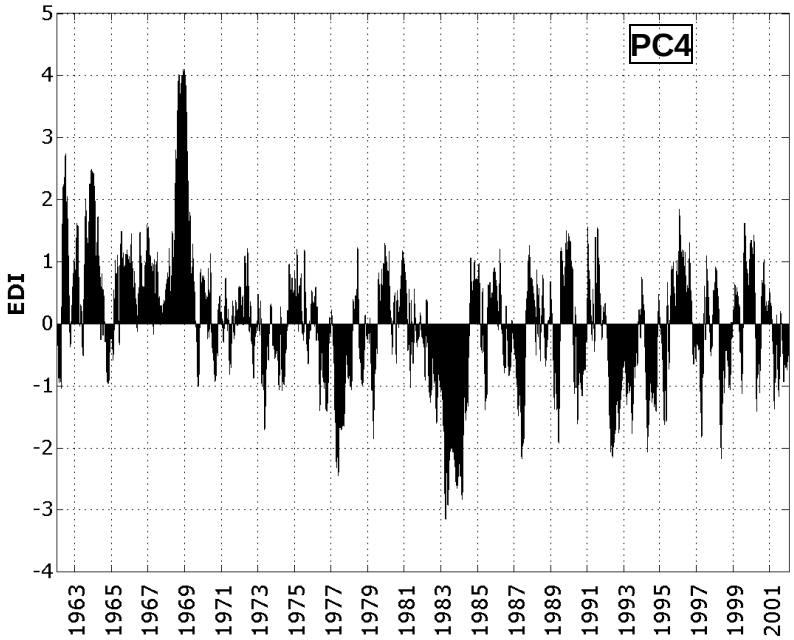
PC4
EDI
5
4
3
2
1
0
-1
-2
-3
-4
1963
1965
1967
1969
1971
1973
1975
1977
1979
1981
1983
1985
1987
1989
1991
1993
1995
1997
1999
2001

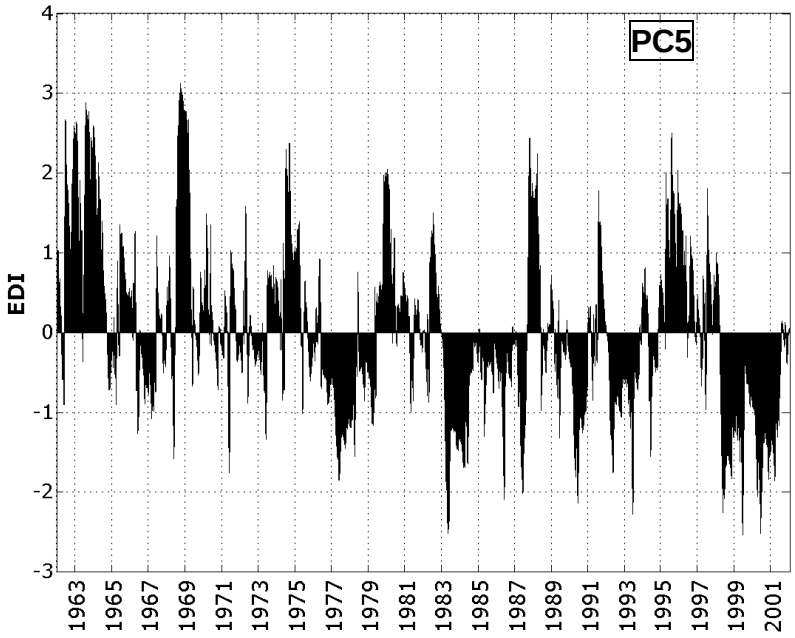

Figure 37: Effective drought index (EDI) for the 5 rainfall regions using a 10-day-moving-average filter. The location of the rainfall regions within the research area can be found in Figure 51.

One can observe wet 1960s, dry 1970s, severe droughts in the 1980s and wetter 1990s. These results are in good agreement with many other studies dealing with droughts in West Africa (e.g. LAMB & PEPPLER, 1992; JANICOT et al., 1996). However, fluctuations in magnitude and duration of droughts can be found between the different rainfall regions. In comparison to all the other regions, the coastal region PC2 shows a long lasting drought period starting in 1998.

The moving average filter has been applied, because heavy isolated showers, which often occur during squall lines in many areas of the Volta Basin, cause breaks in the droughts and affect the statistical values of the drought properties. For many agricultural purposes, however, these short interruptions are not meaningful. Therefore, the definition of a drought should always be adapted to the research area and the special application. After that, important drought properties like drought duration, drought intensity and interarrival time of droughts can be derived. Figure 38 is clarifying the influence of the window size of different drought properties of the northernmost region PC4.

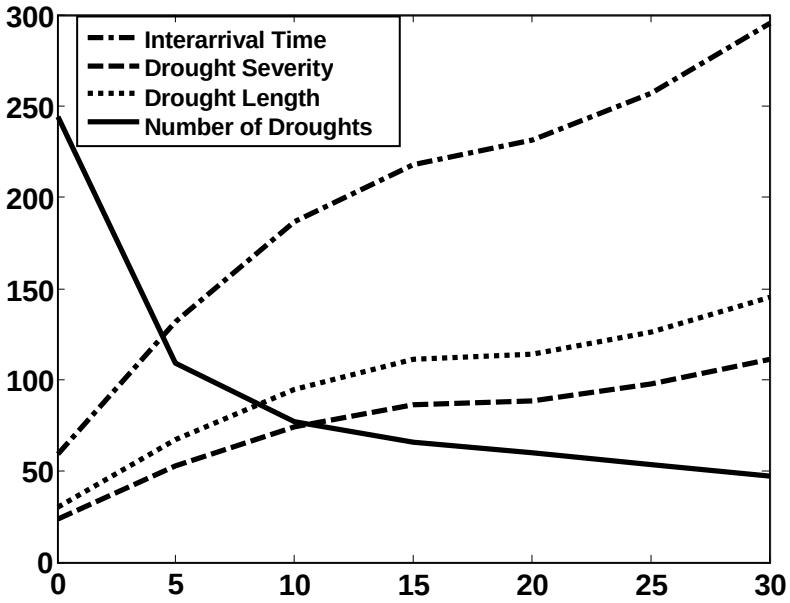

Figure 38: Influence of the moving-average-filter with window size of 5, 10, 15, 20, 25, 30 days and without moving-average-filter (window size = 0) on different mean drought parameters in region PC4 (for the location of region PC4 see Figure 51).

The number of drought events decreases drastically from 244 events without using a filter to 47 applying a 30-day-moving average filter. Applying a 10-day-moving-average filter is reducing slightly the drought events of the severity classes *severe* and *extreme* according to Table 6 and enhancing the *moderate* class (Figure 39).

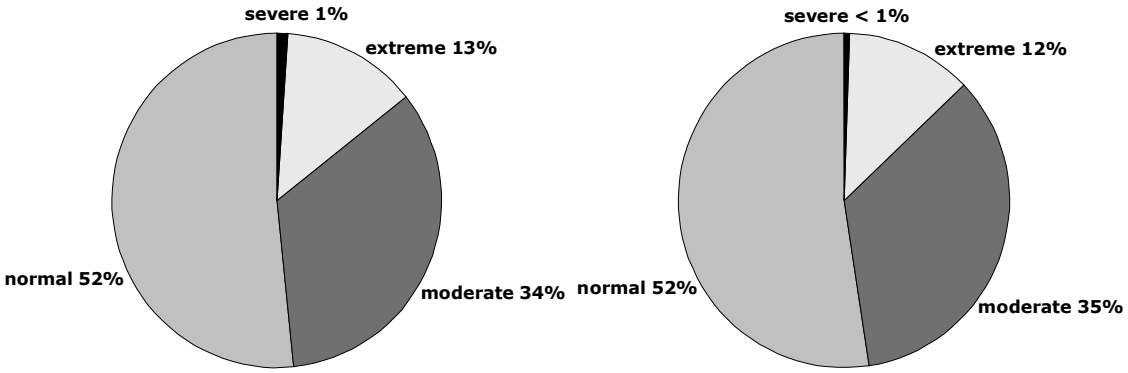

Figure 39: Frequency distribution of the occurrence of the four defined classes (see for rainfall region PC4). The pie chart on the left shows the distribution of the daily-calculated EDI, the right one shows the distribution using a 10-day-moving-average filter.

Class	EDI Intervall		
Normal	0	≥ EDI >	-1
Moderate	-1	≥ EDI >	-2
Extreme	-2	≥ EDI >	-3
Severe	-3	≥ EDI >	- ∞

Table 6: Classification of drought intensity using the Effective Drought Index (EDI).

The mean values of these drought characteristics of the 5 different regions using 10-day-moving-average filter are listed in Table 7:

Rainfall Region	Mean Drought Duration	Mean Drought Intensity	Mean Interarrival Time	$\hat{\Theta}$
PC1	94.79	74.60	186.94	7.50
PC2	86.02	70.90	170.16	5.78
PC3	116.39	84.16	204.23	7.29
PC4	77.62	56.21	143.65	5.51
PC5	72.42	57.50	147.77	10.11

Table 7: Mean drought duration, mean drought intensity, mean interarrival time and $\hat{\Theta}$ of the five different rainfall regions within the Volta Basin using 10-day-moving-window filter for the EDI values. The location of the rainfall regions within the research area can be found in Figure 51.

PC3 is holding the highest mean drought duration (116.4 days) and mean drought intensity values (84.2), calculated as the integral of the $|EDI|$ values from the onset to the cessation of a drought event. The mean interarrival times are ranging from about 144 days (PC4) to about 204 days (PC3). The drought characteristics of PC3 show that this region has the longest and severest droughts across the whole Volta Basin. For all the rainfall regions, the most severe drought events occurred within the rainfall regions PC3 and PC5, starting at 20.02.1998 and 31.03.1982 respectively. The bulk of the drought events is holding drought durations less than 100 days and drought intensities less than 100 [cum. EDI values]. Strong dependencies between drought duration and drought intensity have been found, which are varying slightly between the five rainfall regions (Table 8):

Rainfall Region	n	rbp	ρs	Tk
PC1	77	0.98	0.94	0.83
PC2	84	0.96	0.95	0.84
PC3	71	0.95	0.96	0.84
PC4	99	0.96	0.97	0.85
PC5	96	0.96	0.99	0.92

Table 8: Sample size and measures of dependence between drought duration and drought intensity (rbp = Pearson correlation coefficient, ρs = Spearman rank correlation coefficient, τk = Kendall's Tau) using 10-day-moving-average algorithm for the EDI values. The location of the rainfall regions within the research area can be found in Figure 51.

Small variations between the Pearson correlation coefficient and the Spearman rank correlation coefficient indicate a linear dependency between drought duration and drought intensity, which is very strong. Since the dependency structure between the two variables is linear, Pearson correlation coefficient is also an appropriate measure. In the case of non-linear dependence, a rank correlation coefficient would be more appropriate. These coefficients measure the degree to which large or small values of a variable associate with large or small value of another variable. Even though the distributions of both variables are matching a gamma distribution (Figure 40), a Copula approach has been chosen in order to model their dependence structure. The Clayton Copula has already been successfully applied to model the dependence between drought duration and drought intensity (SHIAU et al., 2007). Alternatively, a bivariate gamma model would also be appropriate in this case. The parameters of the gamma distributions have been estimated using the maximum likelihood method (HAHN & SHAPIRO, 1994).

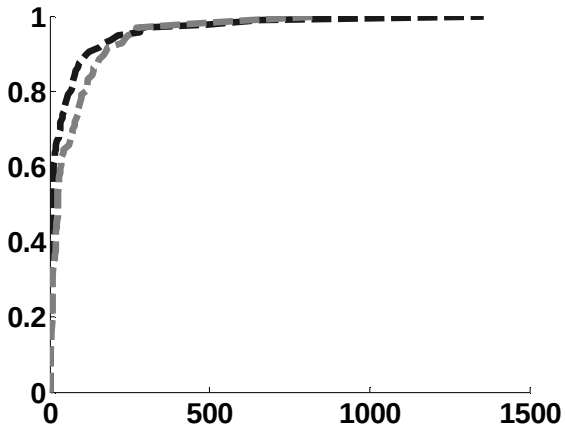

Figure 40: Cumulative density function of drought intensity (black dashed line) and drought duration (gray dashed line) for rainfall region PC3 (for the location of the rainfall regions see Figure 51).

Figure 41 illustrates exemplarily the bivariate Clayton-Copula density ratio for PC2.

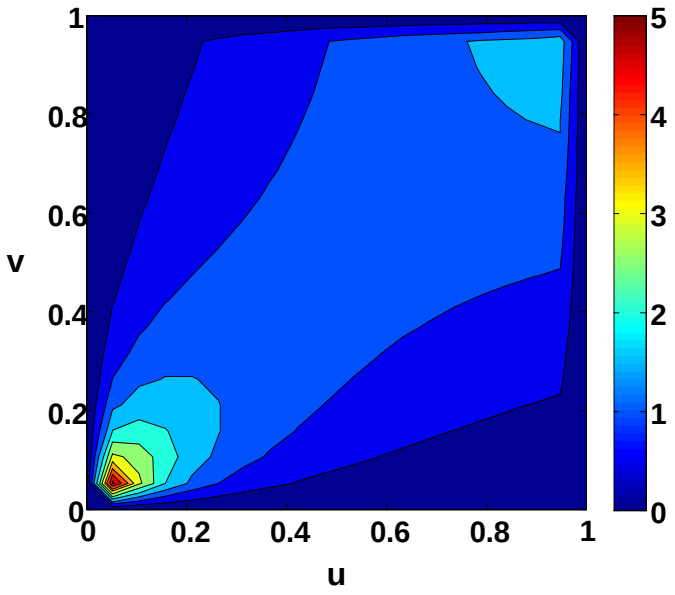

Figure 41: Contour plot of the bivariate Clayton Copula density ratio for Θ=7.29, corresponding to rainfall region PC2 (for the location of the rainfall regions, see Figure 51).

The Copula parameter $\hat{\Theta}$ has been estimated using the Equations 3.44 and 3.45 for each rainfall region separately (Table 7). The relatively tight parameter range is indicating similar shapes of the 5 different Copulas. Figure 42 is illustrating the isolines of bivariate drought duration and drought intensity return periods T_{DS} for the $\wedge$- case (see therefore equation 3.50) for region PC2 (left) and region PC4 (right) using 10-day-moving-averaged EDI values.

Within both regions, 1 larger than one-in-1000-year drought occurred, respectively. This event took place in the early 1980s. For region PC2, 3 larger than one-in-100-year droughts and 1 larger than one-in-10-year droughts occurred, whereas in region PC4 no larger than one-in-100-year drought, but 4 one-in-10-year droughts happened. The $\vee$-case (see therefore equation 3.49), as illustrated in Figure 43, has to be interpreted in a different way: either drought duration or drought intensity can cause one event of a distinct return period; whereas the other parameter is equal or larger than zero. For region PC2, for instance, 1 larger than one-in-1000-year drought occurred due to drought intensity exceeding the values of the τ = 1000 isoline. Within region PC4, just 1 larger than one-in-1000-year and 1 larger than one-in-10-year droughts took place.

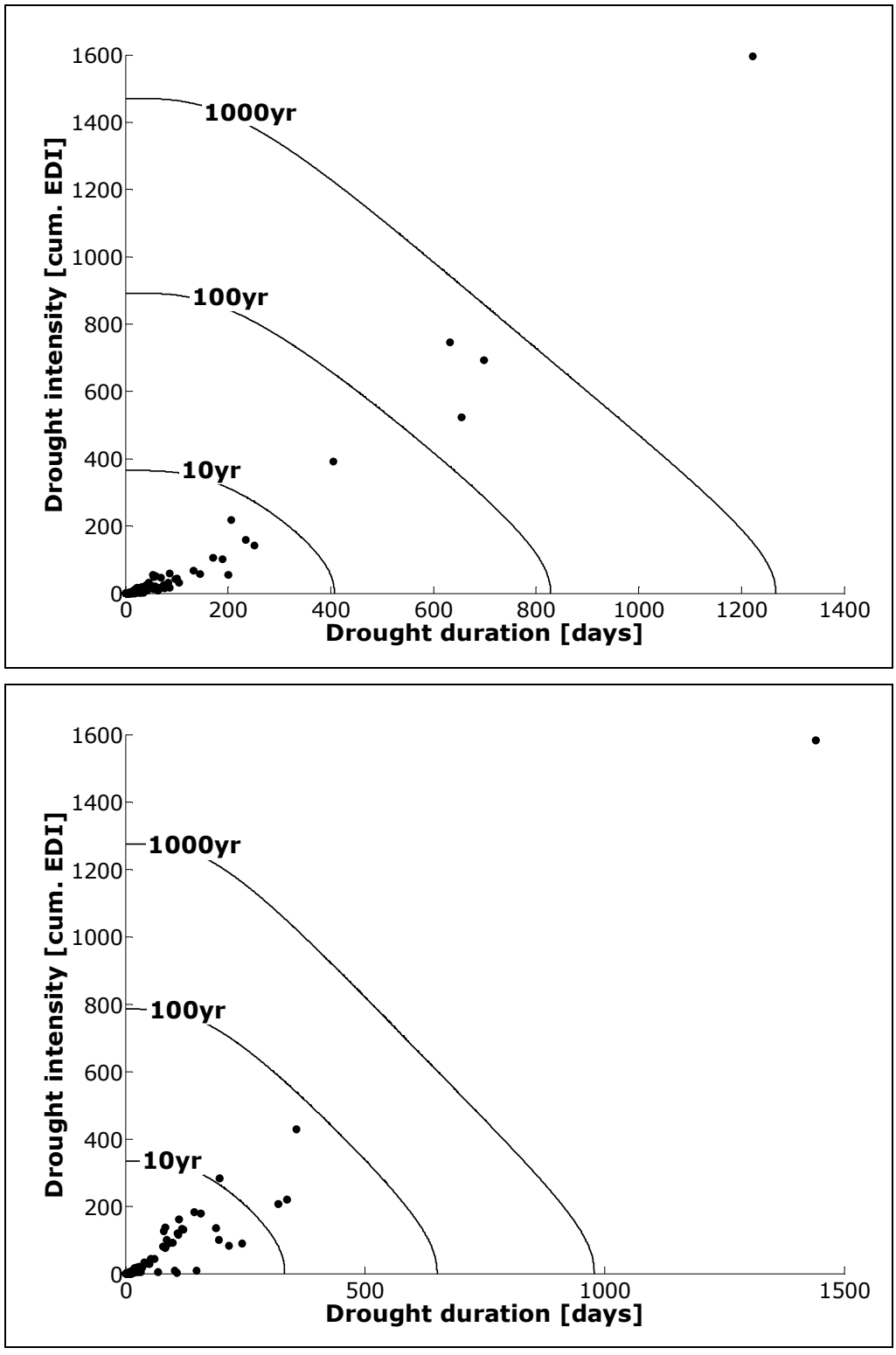

Figure 42: Isolines of bivariate drought duration and drought intensity return periods T_{DS} for the $\wedge$- case for region PC2 (top) and region PC4 (bottom) using 10-day-moving-averaged EDI values. The location of the rainfall regions within the research area can be found in Figure 51. Each dot is representing a drought event.

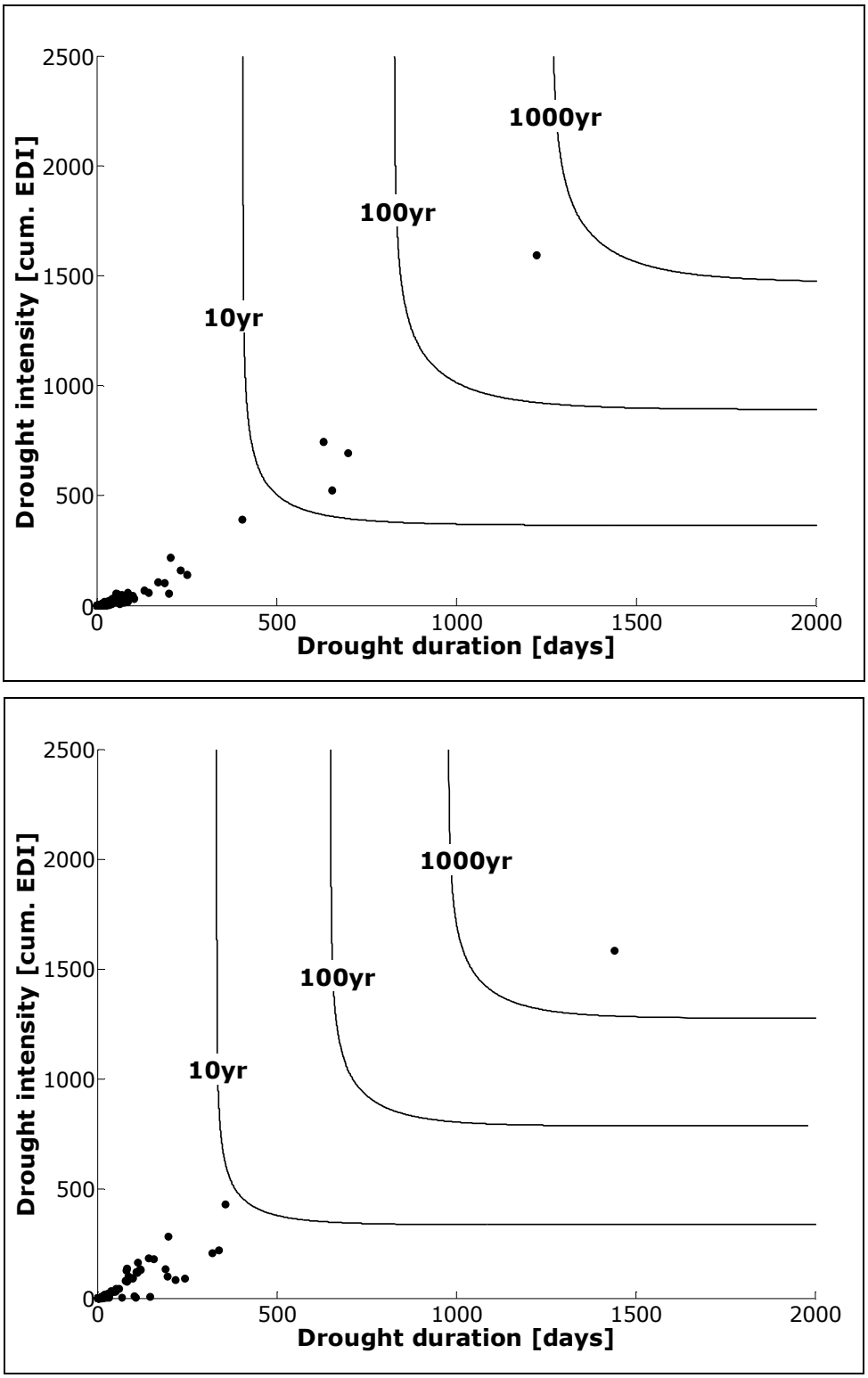

Figure 43: Isolines of bivariate drought duration and drought intensity return periods T_{DS} for the $\vee$- case for region PC2 (top) and region PC4 (bottom) using 10-day-moving-averaged EDI values. The location of the rainfall regions within the research area can be found in Figure 51. Each dot is representing a drought event.

A Copula approach has been chosen to model the dependence between drought duration and drought intensity. Further research in this field is intended and other parameters related to droughts may be easily included. Therefore, a more sophisticated Copula approach is justified here instead of using a bivariate gamma distribution model, because of its more general form and expandability to additional drought variables. Potential input variables, e.g. different climate indices presented in Chapter 5.6, should be able to capture the variability of rainfall and thus contribution to drought or wet conditions within the Volta Basin. The Clayton Copula has proofed suitable for various hydrologic needs (e.g. SHIAU et al., 2007). However, the question which Copula model fits best to the empirical data remains still unanswered and is lying beyond the scope of that work. Remembering the severe floods in September 2007, an operational drought or flood monitoring system for the Volta Basin is required, which currently does not exist. The EDI is useful for this purpose.

5.5 Regional Features of the Rainy Seasons' Onset

For agricultural planning, it is also important to know the exceedance probabilities of the ORS dates. Therefore, the ORS dates have been calculated for the 5 different regions following Definition1 (see therefore Chapter 4). The cumulative distribution function (cdf) of each region has been derived. Figure 44 is illustrating exemplarily the cdf of the ORS dates for region PC1. The exceedance probability of a certain ORS date can directly be taken from the graph. The cumulative density functions for the other regions can be found in Appendix 3.

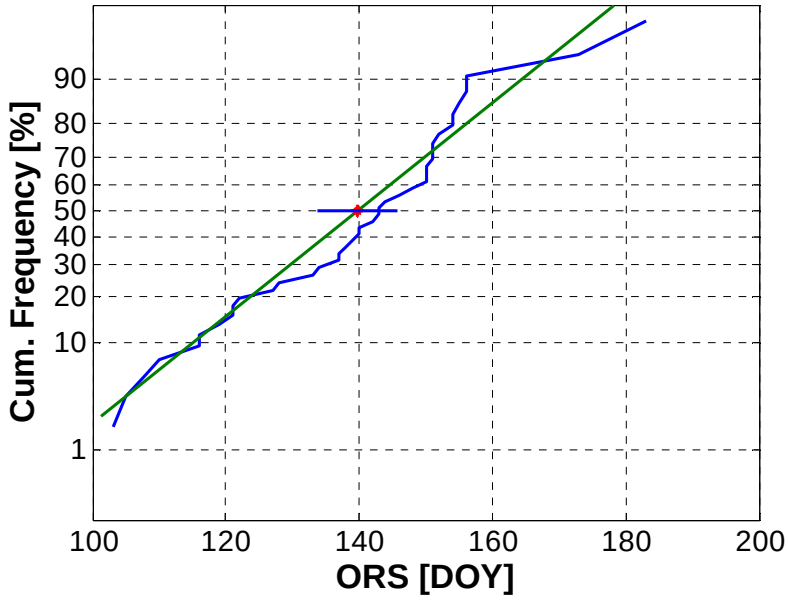

Figure 44: Cumulative distribution functions of the ORS dates (blue line) for PC1 (1961-2001). The red asterisk (blue horizontal line) indicates the mean (two standard error bar), the green line indicates normal distribution of the data.

Basing on the quartiles of the ORS time series, a classification into EARLY (P < 25%), NORMAL (25% ≤ P ≤ 75%) and LATE (P > 75%) ORS has been performed and the ORS dates of the 25% and 75% quartiles as well as the return periods (reciprocal of the respective occurrence probability P) of each quartile have been calculated. Table 9 is summarizing the regional boundary ORS dates [DOY] and the regional return probability of each class:

	EARLY	**NORMAL**	**LATE**
PC1	P < 125.75 **(4.1)**	125.75 ≤ P ≤ 151 **(1.86)**	P > 151 **(4.1)**
PC2	P < 76.75 **(4.1)**	76.75 ≤ P ≤ 113 **(1.86)**	P > 113 **(4.1)**
PC3	P < 61 **(5.13)**	61 ≤ P ≤ 88 **(1.71)**	P > 88 **(5.13)**
PC4	P < 158.75 **(4.1)**	158.75 ≤ P ≤ 179.25 **(1.95)**	P > 179.25 **(4.1)**
PC5	P < 85.75 **(4.1)**	85.75 ≤ P ≤ 117 **(1.86)**	P > 117 **(4.1)**

Table 9: Boundary ORS dates [DOY] for the three different probability classes and return periods for the different classes in brackets.

5.6 Towards Seasonal Prediction of Rainfall

Rainfall variability and its relationship to global climate, expressed in terms of climate indices are investigated for the time period 1961-2001. The goal of these investigations is the identification of factors suitable for rainfall prediction with sufficient lead time before the cropping season commences. While the role of the tropical SST is well known to be linked to West African rainfall (e.g. HULME et al., 1992), the role of the El Nino Southern Oscillation (ENSO) is still discussed controversial in literature. Contrary to studies, suggesting that ENSO plays merely a little role in West African rainfall regions (NICHOLSON, 1986; STOCKENIUS, 1981), other authors like e.g. PALMER et al. (1992) proved the existence of large correlations between West African rainfall and SST in the eastern equatorial Pacific at interannual time scale. More recently, MALHI & WRIGHT (2004) detected ENSO as the primary driver of interannual temperature and precipitation fluctuations across the tropical areas. However, the relation between ENSO and tropical African precipitation appeared less significant. ADIKU (2003) suggests that October-November-December SST in the Nino 3 Pacific region, which is popularly referred to ENSO, may offer a possibility for seasonal rainfall forecasting with sufficient lead time. In another study the found strong influence of ENSO on seasonal rainfall at 3 out of 6 stations located in the southern part of Ghana (ADIKU et al., 2007). While the middle belt of Ghana revealed weak influences, the northern part showed strong ENSO relations again.

NEUMANN et al. (2007) investigated the influence of various teleconnections on rainfall amount at station Tamale, located in the centre of the Volta Basin. This study revealed weak lagged and not lagged correlations between monthly precipitation and the North Atlantic Oscillation (NAO), Southern Oscillation Index (SOI), Tropical Atlantic

Index (TSA) and Tropical Northern Atlantic Index (TNA). Here, beside rainfall amount, the rainfall variability has been extended to the number of wet days and dry spell frequency. A dry spell is defined as a period of 6 consecutive days where no rainfall is recorded (daily rainfall = 0mm). A rainy day is defined as a day with recorded rainfall ≥ 1 mm. The climate indices of interest are the North Atlantic Oscillation (NAO), the Southern Oscillation Index (SOI), the Tropical Northern Atlantic Index (TNA), the Tropical Southern Atlantic Index (TSA), and the Multivariate ENSO Index (MEI), all available from the NOAA Climate Prediction Centre. Table 10 presents a short explanation of the different climate indices used in this study. As the monthly values of climate indices as well as rainfall features may be considered to be normally distributed, linear Pearson correlation coefficient can be regarded as an appropriate dependence measure between them. Time series of the monthly climate indices and rainfall features have been correlated without a shift in time, and with precipitation features shifted by one to three months. They referred to lag1, lag2, and lag3 correlations.

The number of significant correlation coefficients has been counted to assess the influence of the climate index on rainfall features on all available sites.

NAO (North Atlantic Oscillation)	Normalized pressure difference between a station on the Azores and one on Iceland.
SOI (Southern Oscillation Index)	Normalized pressure difference between Tahiti and Darwin.
TNA (Tropical Northern Atlantic Index)	Anomaly of the average of the monthly SST from 5.5°N to 23.5°N and 15°W to 57.5°W. GISST and NOAA OI 1x1 km data sets were used to create this index.
TSA (Tropical Southern Atlantic Index)	Anomaly of the average of the monthly SST from 0° to 20°S and 10°E to 30°W. GISST and NOAA OI 1x1 km data sets were used to create this index.
MEI (Multivariate ENSO Index)	El Niño/Southern Oscillation (ENSO) is the most prominent coupled ocean-atmosphere phenomenon to cause global climate variability on interannual time scales. MEI is used for monitoring ENSO based on the six main variables observed over the tropical Pacific: sea-level pressure (P), zonal (U) and meridional (V) components of the surface wind, sea surface temperature (S), surface air temperature (A), and total cloudiness fraction of the sky (C).

Table 10: Explanation of the most prominent climate indices.

The number of significant ($\alpha = 0.05$) Pearson correlation coefficients between monthly dry spell frequency, wet day frequencies, precipitation amount and various climate indices have been calculated in order to detect the main large-scale forcing of rainfall variability during the rainy season (March to October) (Figure 45 - Figure 47). The absolute amount of the significant Pearson correlation coefficients is approximately 0.38.

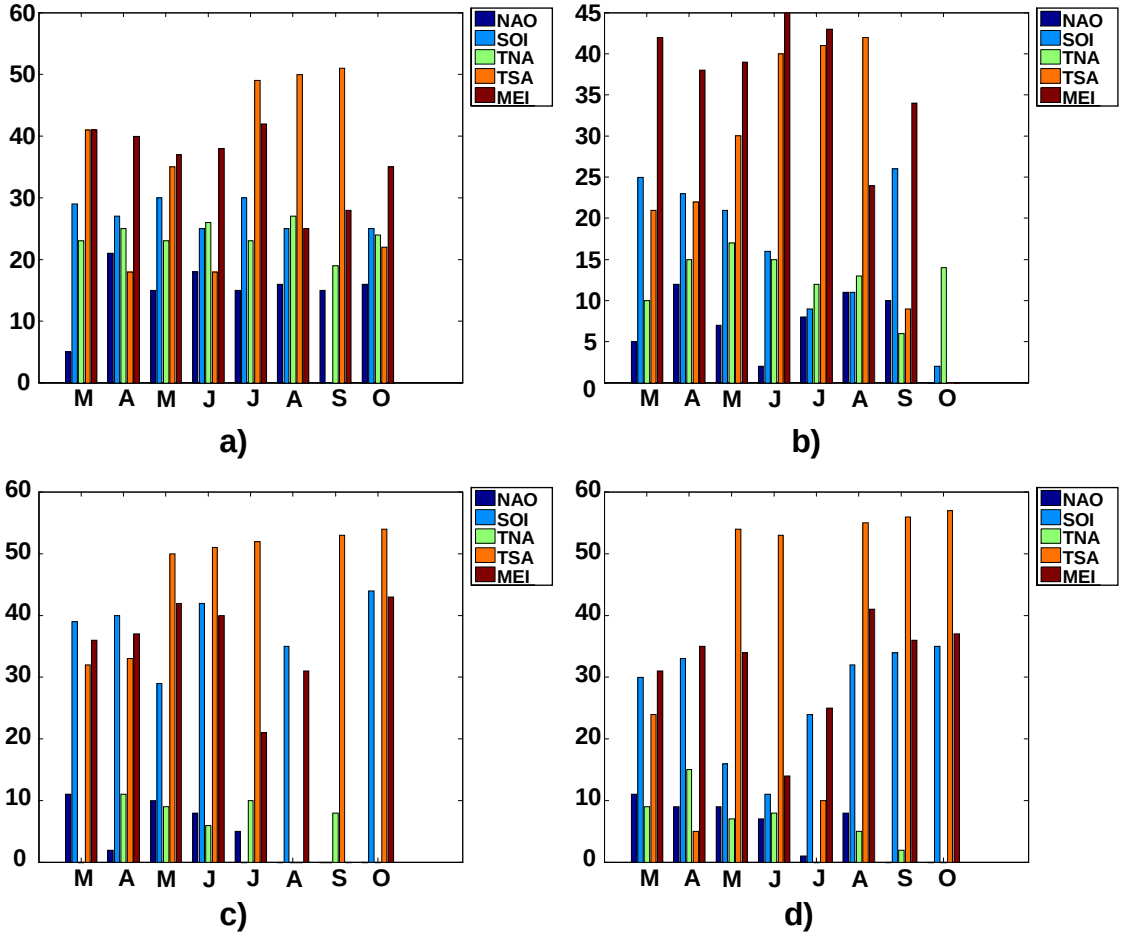

Figure 45: Number of significant a) not lagged, b) 1-month lagged, c) 2-month lagged, and d) 3-month lagged Pearson correlation coefficients between the number of dry spells and the respective climate indices within the rainy season (data source: daily rainfall of 29 rainfall stations within the period 1961-2001).

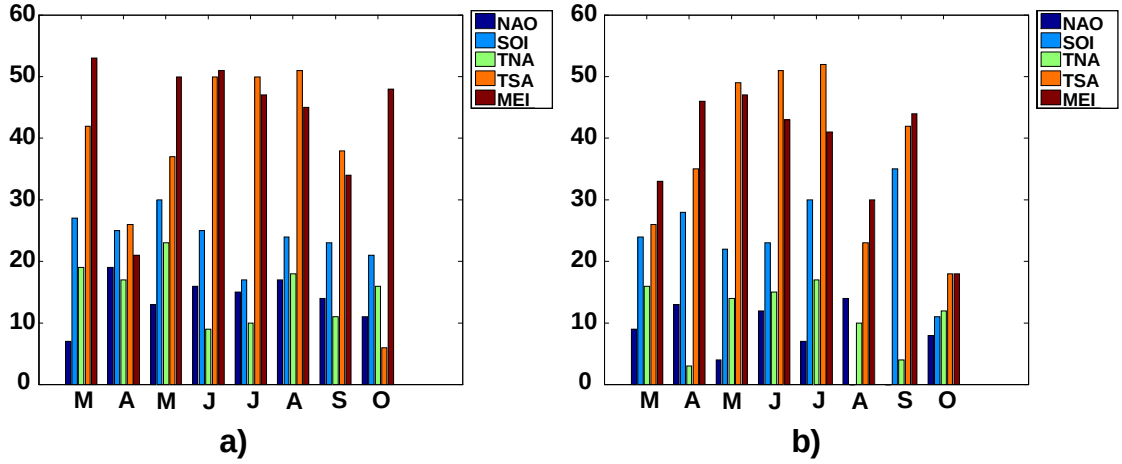

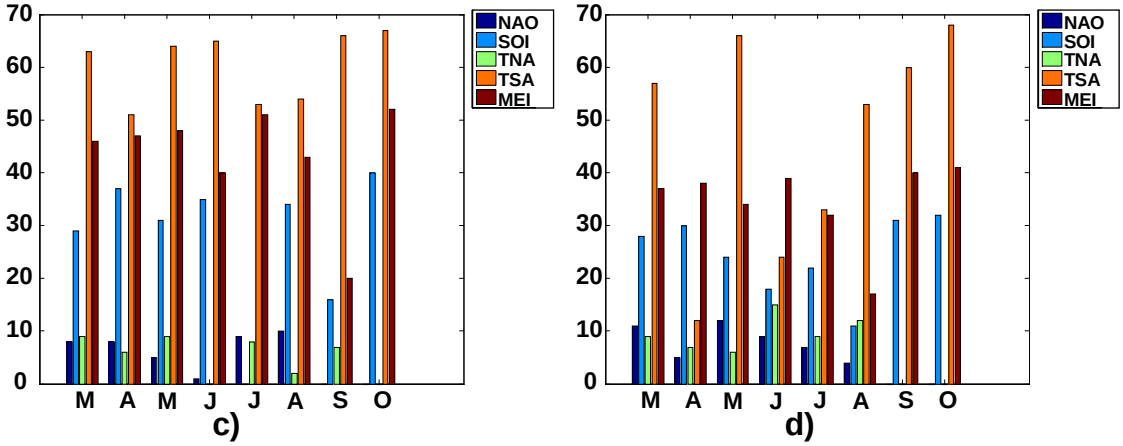

Figure 46: Number of significant a) not lagged, b) 1-month lagged, c) 2-month lagged, and d) 3-month lagged Pearson correlation coefficients between the number of rainy days and the respective climate indices within the rainy season (data source: daily rainfall of 29 rainfall stations within the period 1961-2001).

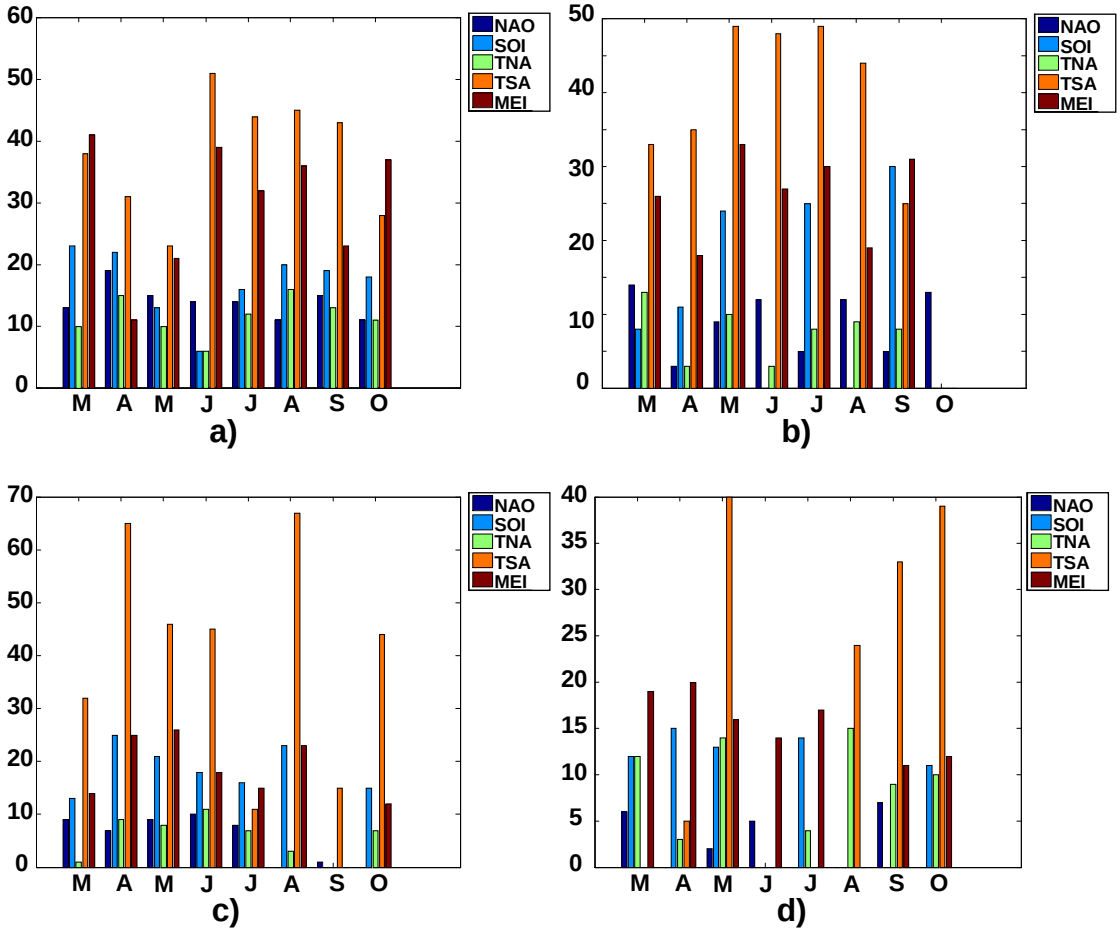

Figure 47: Number of significant a) not lagged, b) 1-month lagged, c) 2-month lagged, and d) 3-month lagged Pearson correlation coefficients between the monthly rainfall amount and the

respective climate indices within the rainy season (data source: daily rainfall of 29 rainfall stations within the period 1961-2001).

This analysis has been carried out for the not lagged as well as the lagged situations, separately each observation station and month. It can be summarized that the TSA followed by the MEI is the most important index, except for the number of rainy days for the not lagged case and the number of dry spells with a time lag of 1 month. There, the MEI shows more significant correlations. Generally, TSA and MEI are holding ~ 60 % of all significant correlation coefficients. In order to clarify whether a spatial dependence between different regions in the Volta Basin and the climate indices exist or not, the most dominant climate index (= climate index holding the highest number of significant correlation coefficients) on the respective rainfall parameter has been illustrated for each observation site. Again, the results are presented for the number of dry spells (Figure 48 a), the number of rainy days (Figure 48 b) and the monthly rainfall totals (Figure 48 c). For the not lagged situation, a relatively clear dominance of the TSA within the southern part and MEI within the northern part of the Volta Basin can be observed.

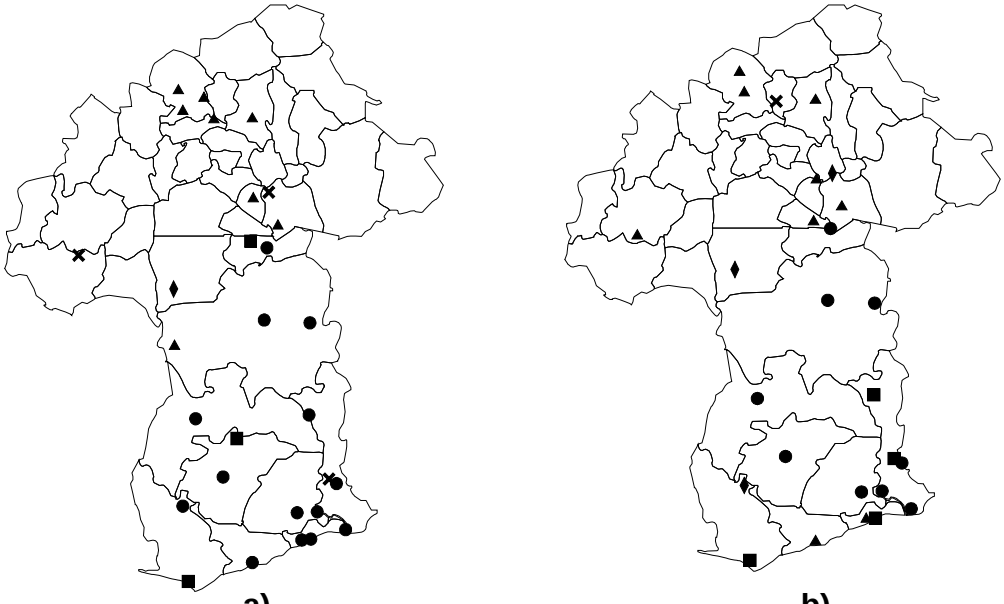

a) **b)**

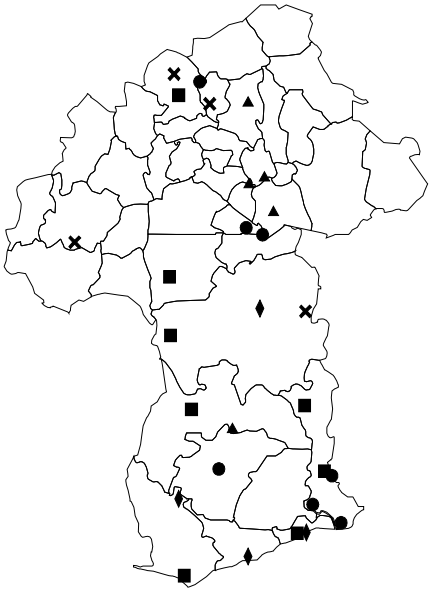

c)

Figure 48: Most important large-scale influence determined by the Pearson product-moment correlation coefficient (time lag = 0 months) between a) monthly rainfall amounts, b) monthly number of rainy days, and c) monthly number of dry spells and climate indices (see Table 9). Data source: 29 daily rainfall time series from 1961 to 2001. (Legend: ♦ = NAO; x = SOI; ■ = TNA; ● = TSA; ▲ = MEI).

Considering the dominating climate indices for the lagged situation, no significant changes have been found (not shown). Considering the distribution of stations within the Volta Basin - 20 stations are located in Ghana and only 9 in Burkina Faso - is then clarifying the higher influence of the TSA expressed by the absolute number of significant correlation coefficients.

5.7 Summary of Chapter 5

- Markov chains are a useful tool to derive important rainfall features for agricultural needs. Even simple calculations like e.g. the overall probability of rainfall (zero order Markov chain) deliver important information for farming management. Probability maps for the occurrence of heavy rainfall events have been derived. Considering higher order Markov chains, the transition probabilities can also provide very useful information.

- The rainfall amounts can be modelled using a gamma distribution model. The distribution of both parameters of the gamma distribution is regionally variable and has to be taken into account for modelling.

- Modelling the dry spell occurrence probability provides very important information with respect to the planting dates. Since the establishing period is of crucial importance for the survival of the seedlings, the probabilities of the occurrence of

a dry spell of more than 6 consecutive days within the following 30 days has been calculated for each DOY. Maps of these regional probabilities as well as the DOY, where the probability is minimized are presented. Since the definition for the ORS in the predictive mode is not able to consider this crucial information, this information provides important a priori information for the decision of the plant time.

- Drought characteristics like drought duration, drought intensity and interarrival time have been calculated using the *Effective Drought Index* EDI. The EDI time series deliver wet 1960s, dry1970s, severe droughts in the 1980s and wetter 1990s. Strong linear dependencies between drought duration and drought intensity have been found, which are varying slightly between the five rainfall regions. Droughts can be modelled adequately considering both the drought duration and the drought intensity using a Copula approach. PC3 is holding the highest mean drought duration and mean drought intensity, calculated as the integral of the $|EDI|$ values from the onset to the cessation of a drought event. The mean interarrival times are ranging from about 144 days (PC4) to 204 days (PC3). The drought characteristics of PC3 show that this region has the longest and severest droughts across the whole Volta Basin. For all the rainfall regions, the most severe drought events occurred within the rainfall regions PC3 and PC5, starting at 20.02.1998 and 31.03.1982 respectively. The bulk of the drought events is holding drought durations less than 100 days and drought intensities less than 100 [cum. EDI values]. A joint distribution function has been established using a Copula approach, which can be regarded as the pure expression of dependence without the influence of a marginal distribution. Basing on the Copula, the regional return periods of droughts have been derived. Modelling drought is a first step towards drought prediction.

Chapter 6

6. Prediction of the Onset of the Rainy Season: towards a Decision Support System

Due to a very high spatial and temporal variability of precipitation amounts, a non-uniform distribution of the rains during the rainy season and a high variability in the onset dates, farmers have problems to decide when to start with the sowing preparations. In the Volta Basin, the onset seldom occurs abruptly and is often preceded by short isolated showers with intermittent dry spells of various lengths, which are often misinterpreted as the start of the rains (*false starts*). Prolonged dry spells of two or more weeks after sowing are disastrous for plants, because they dry out top soil layers and prevent germination, which may lead to total crop failure or yield reduction. The survival of the seedlings is the key point for agriculturists (SULTAN & JANICOT, 2003A).

Therefore, it is important to know, whether:

- the rains are continuous and sufficient to ensure enough soil moisture during planting time; and
- this level will be maintained or even increased during the growing period to avoid crop failure (WALTER, 1967).

Socio-economic researchers found out that farmers are operating in multiple cognitive frameworks to make their decision about the sowing time. Traditional decision criteria, e.g. the observation of the behavior of some insects or birds or flowering of certain trees, seem to fail more frequently and the demand for a scientific decision aid increases among local farmers. Figure 49 is illustrating the traditional decision criteria for farmers due to a study carried out in Burkina Faso (RONCOLI et al., 2002).

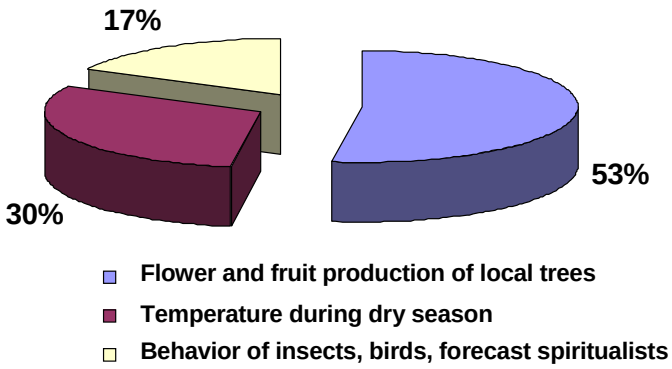

Figure 49: Traditional decision criteria from farmers in Burkina Faso regarding the onset of the rainy season (Datasource: RONCOLI et al., 2002).

Information exchange by seasonal workers, coming from different regions within the Volta Basin to assist local farmers at the sowing, plays an important role. They are reporting from the timing of the rainy seasons' onset within the regions they are coming from. Assuming a relatively constant progression of the rainy belts, they can estimate the start of the rains. Concerning the high spatial and temporal rainfall variability, farmers have developed a range of adaptation strategies in the past. These strategies include time-dependent measures, such as dry seeding, re-sowing, and the use of differently maturing crop varieties, coping with spatial rainfall variability through the cultivation of large and widely dispersed field areas, and measures for sustaining soil fertility (GRAEF & HAIGIS, 2001). According to the aforementioned relevance of determining the rainy seasons' onset and the problems farmers are faced with, it is essential that:

- The start of the rains is predicted on-line on a basis of reliable scientific methods, especially for the ongoing or forthcoming season.
- As the occurrence of rainfall in the Volta Basin is mostly related to small-scale or local processes (convection), the spatial distribution of rainfall is chaotic. Therefore, the prediction of the ORS based on daily rainfall data is strongly recommended to carry out on regional scale.
- Easy accessible information is used for prediction.
- Valuable a-priori knowledge from the farmers is included.

Basing on these points, three different approaches have been developed to support farmers with their decision: First, LDA is applied to judge day by day if the current season has already begun (Chapter 6.1). Therefore, linear discriminant models have been established using accessible and suitable prediction parameters to allow for a

classification of the dry season, transition phase, onset of the rainy season and rainy season using current rainfall data. Second, LRA is used to estimate future onset dates (Chapter 6.2). Linear regression models were generated to estimate the onset of the rainy season for certain regions using the onset dates of regions, where the onset has already begun. This approach provides an example for a scientific application including farmers' a-priori knowledge. Both methodologies are easily applicable and might be used simultaneously to encourage the decision about the planting date. Third, a more sophisticated methodology is presented in Chapter 6.3, which is linking large-scale meteorological fields to the ORS. The methodology does not deliver the decision whether or not to start sowing like the LDA does, nor does it provide exact sowing dates in advance like the LRA does. Probabilistic statements about the commencement of the rainy season can be derived. The presented methodologies are intended to be implemented into a Decision Support System (DSS). Details about the prior applied regionalization strategy as well as the applied onset definition are presented in Chapter 4.

6.1 Prediction of the ORS based on LDA

A mathematical description of the linear discriminant analysis is given in Chapter 3.2. LDA has been carried out to allocate each day to one of the four classes: i) *Dry Season*, ii) *Transition*, iii) *Onset of the Rainy Season*, and, iv) *Wet Season*.

The *transition* class has been introduced in order to check if there is rather an abrupt or a gradual onset according to the discriminant model and the onset definition. A poor hit ratio for this *transition* class and reclassification of these days to the *dry seasons*' class has been expected to guarantee a good discrimination between the *onset* class and the *dry season* class. A similar approach was applied by SARRIA-DODD & JOLLIFFE (2001) to derive a linear discriminant function that distinguishes between *real* and *false starts* of the ORS, applied for Burkina Faso and Mali.

Generally, LDA is a tool for discriminating between two or more groups and to assign cases to different groups with better than chance accuracy. Two pre-requisites have to be noted: the number of groups must not exceed the number of variables describing the data set and the groups must have the same covariance structure. A detailed mathematical description is given in Chapter 3.4.

The overall goal is to find predictor variables for all regions, which are reliable in representing the onset dates. These potential predictor variables are simple rainfall indices that describe the *rainfall amount (RAx)* and *number of rainy days (NRDx)* 30, 25, 15, 10, and 5 days before the potential onsets and γ values, respectively. In this case, three discriminant functions (not shown) are required. Similar to multiple regression analysis, not all the candidate predictors contribute to a significant improvement of the discriminant model. So, there is no established method for

assessing which predictors are useful when the assumption of equal variance is dropped (MASON, 1998). Typically, stepwise multiple regression analysis is a screening method to choose the variables for the discriminant model (WARD & FOLLAND, 1991). According to these results (not shown here), four parameters are selected, which are most suitable for all regions: NRD25, RA5, and both the $\gamma 1$ and $\gamma 2$ values. Starting from the calculated onset date, 40-10 days before this date were taken as *dry season* class, 9-1 day before as *transition*, the date itself and another 2 days as *onset,* and 15-30 days afterwards as *wet season*. Owing to the lack of an adequate measure of model performance, like the R^2 statistic for the regression analysis, validation is a very important component of model construction. Jack-knife validation has been used in order not to reduce the number of observations for the training of the model. Table 11 - Table 15 present the confusion matrices of the classification using the four above-mentioned variables and optimal γ value for Definition2.

γ = ***0.5***		**Class membership after application of linear discriminant analysis [%]**			
		dry season	**transition**	**Onset**	**wet season**
Predetermined Class Membership [%]	**dry season**	**75.07**	16.28	2.23	6.42
	transition	54.58	**22.74**	5.19	17.49
	onset	12.08	8.07	**63.24**	16.61
	wet season	16.02	12.17	11.96	**59.85**

Table 11: Confusion matrix for PC1 to assess the performance of the discrimination using the most suited variables and γ threshold with the main focus on the onset class (LAUX et al., 2008).

γ = ***0.45***		**Class membership after application of linear discriminant analysis [%]**			
		dry season	**transition**	**onset**	**wet season**
Predetermined Class Membership [%]	**dry season**	**76.02**	15.44	2.50	6.04
	transition	53.39	**22.03**	7.42	17.16
	Onset	15.31	10.52	**55.98**	18.19
	wet season	18.61	12.10	10.61	**58.68**

Table 12: Confusion matrix for PC2 to assess the performance of the discrimination using the most suited variables and γ threshold with the main focus on the onset class (LAUX et al., 2008).

γ = *0.5*		Class membership after application of linear discriminant analysis [%]			
		dry season	**transition**	**onset**	**wet season**
Predetermined Class Membership [%]	**dry season**	**83.37**	14.68	1.24	0.71
	transition	50.72	**38.10**	3.47	7.71
	Onset	8.09	11.30	**70.91**	9.70
	wet season	5.38	6.95	8.43	**79.24**

Table 13: Confusion matrix for PC3 to assess the performance of the discrimination using the most suited variables and γ threshold with the main focus on the onset class (LAUX et al., 2008).

γ = *0.4*		Class membership after application of linear discriminant analysis [%]			
		dry season	**transition**	**onset**	**wet season**
Predetermined Class Membership [%]	**dry season**	**80.32**	15.86	1.38	2.44
	transition	52.99	**27.97**	4.01	15.03
	Onset	7.20	5.80	**79.44**	7.56
	wet season	13.94	11.50	10.57	**63.99**

Table 14: Confusion matrix for PC4 to assess the performance of the discrimination using the most suited variables and γ threshold with the main focus on the onset class (LAUX et al., 2008).

γ = *0.25*		Class membership after application of linear discriminant analysis [%]			
		dry season	**transition**	**onset**	**wet season**
Predetermined Class Membership [%]	**dry season**	**80.68**	13.56	1.44	4.32
	transition	49.95	**30.98**	2.15	16.92
	Onset	9.99	8.76	**68.34**	12.91
	wet season	7.61	10.77	12.70	**68.92**

Table 15: Confusion matrix for PC5 to assess the performance of the discrimination using the most suited variables and γ threshold with the main focus on the onset class (LAUX et al., 2008).

The percentage of cases on the diagonal depicts the percentage of correct classification (hit ratio). The number of hits should be compared with the number expected by chance: The prior probabilities for the four classes are: 52, 15, 7, and 27%.

It can be summarized that for most regions (except for the region corresponding to PC2), the hit ratio for the *onset* class ranges between 60% and 80% with an a priori

probability of 7%. Additionally, the classes of *dry season and wet season* show satisfactory results. The fact that the *transition* class cannot be discriminated well indicates that the definition for the onset operates successfully. Most of the cases of this class have been reassigned to the *dry seasons*' class.

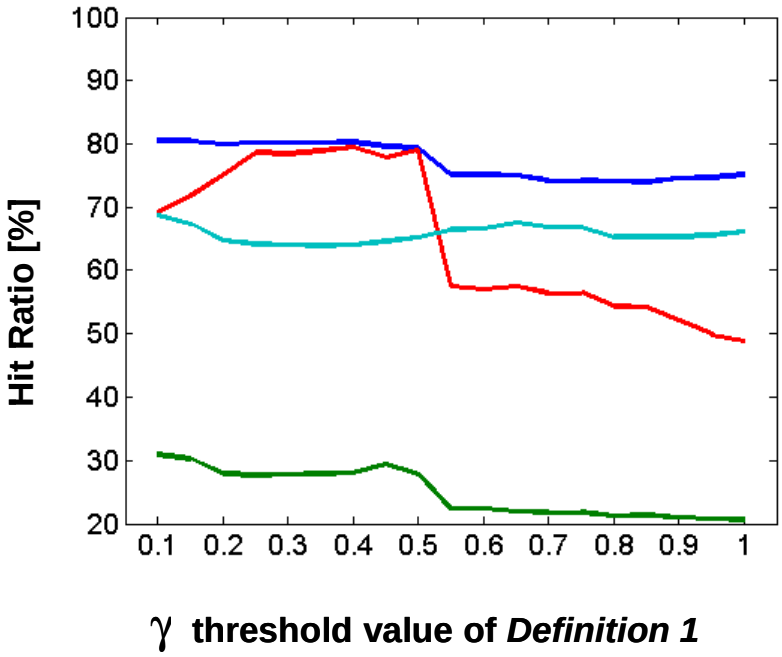

Figure 50: Hit ratio [%] of the Dry Season (blue), Transition (green), Onset of the Rainy Season (red) and Wet Season (cyan) for the region PC4 in dependence of the γ threshold of Definition1.

6.2 Prediction of the ORS based on LRA

Assuming PC3 to be the first rainy season's onset region of the year and knowing the date, linear regression models can be generated to predict successively the onset dates for PC2, PC5, PC1, and PC4. The arrows in Figure 51 represent the direction of regression modelling.

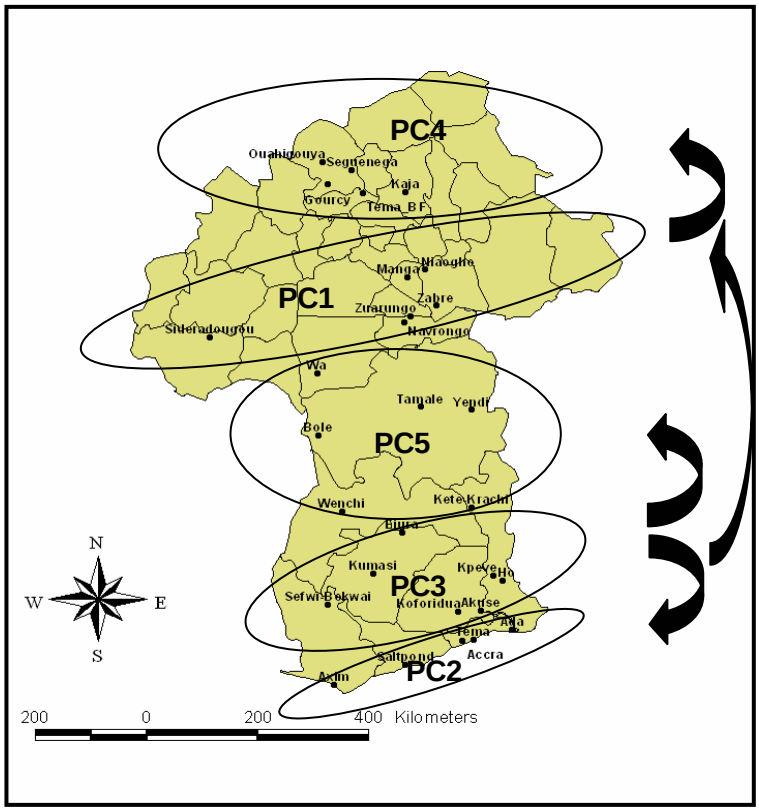

Figure 51: Spatial location of the five different regions (ellipses) corresponding to the principal components. The arrows represent the direction for predicting the rainy season's onset of one region using the current onset date of another region; (LAUX et al., 2008).

In order to enhance the performance of the regression models, the best γ threshold combination of two regions has to be found. For this purpose, the linear correlation coefficient between the onset dates of two regions has been computed by displacing the respective γ threshold against the other. Figure 52 displays the correlation coefficients and significance levels [%] between the onset dates of two regions using varying γ values ranging from 0.1 to 1 with an increment of 0.05. Hot spots regions (= regions showing the highest mutual correlation coefficients) can be recognized easily. The mutual correlation coefficients and significance levels for the other models can be found in Appendix 4.

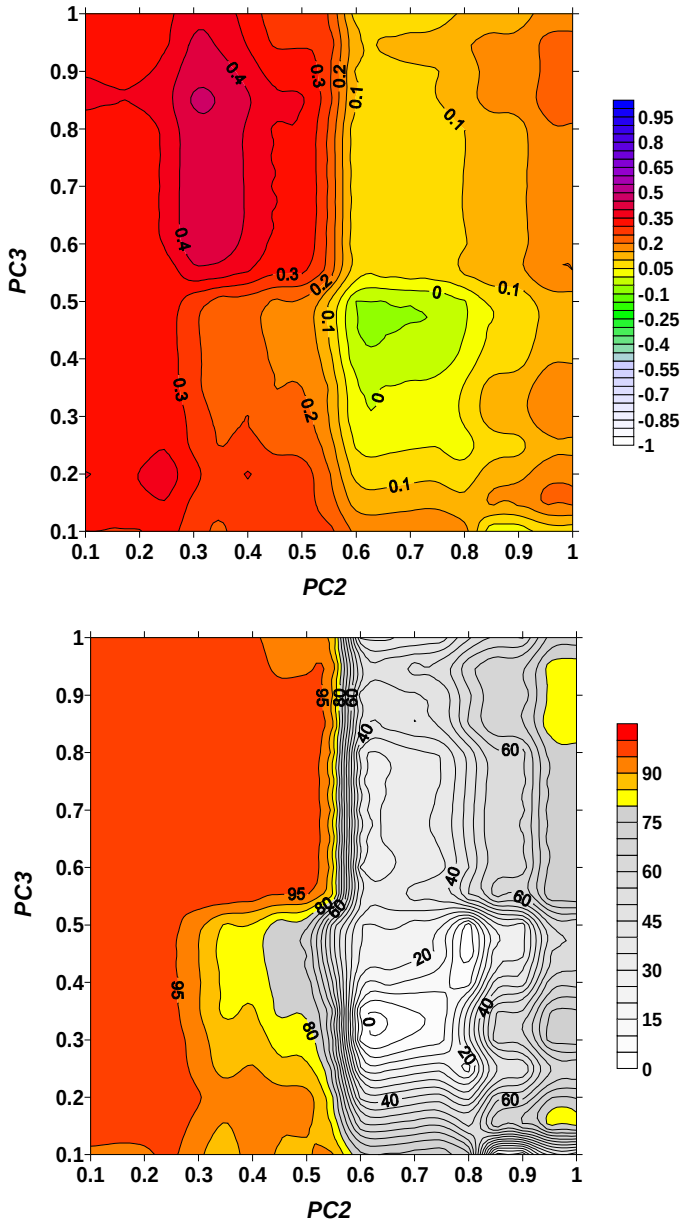

Figure 52: Correlation coefficients between the onset dates of two regions using varying γ values from 0.1 to 1.0 (top) and level of significance (bottom) for selected PC combinations (LAUX et al., 2008).

A bootstrap test was applied to check the significance of the correlation coefficient. Therefore, the ORS dates of one region were hold constant, and the ORS dates of the other region were permuted against it. The correlation coefficient between the permuted and the non-permuted variable were calculated. As the two variables are randomly paired, the expected value for the Pearson correlation coefficient is 0. By repeating this process a large number of times (1000 bootstrap realizations), a sampling distribution of r was built up (Figure 53).

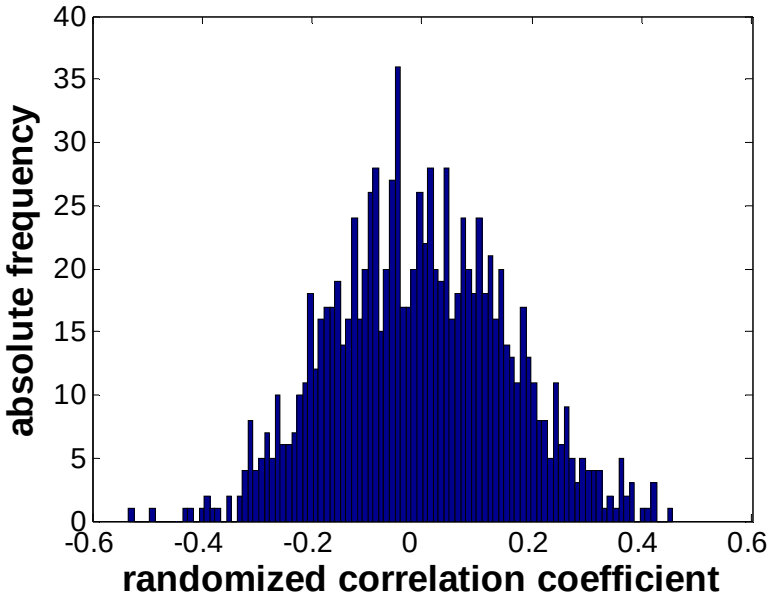

Figure 53: Sampling distribution of randomized correlation coefficients permuting region PC3 against onset dates of region PC2 using 100 bins. The correlation coefficient between the onset dates of the two regions is 0.46.

The realizations are found to be nearly symmetrical around 0.0 and the number of the 1000 realizations exceeding the absolute amount of the highest correlation coefficient (referred to Figure 52) is counted in order to derive the level of significance for the correlation coefficient. Table 16 is listing the four regression models, the best mutual γ combinations, the correlation coefficients between the regions and their level of significances derived by the bootstrap test.

The onset of the rainy season of PC3 is best to estimate the onset of PC2, PC5, and PC1. The onset of PC4 can be estimated with PC1's onset. The respective regression equations, correlation coefficients, and are listed in:

No	Target PC	Indep. PC	γ Target PC	γ Indep. PC	Regression Equation	r	Level of sig. [%]
M1	PC5	PC3	0.35	0.3	PC5 = 52.36 + 0.61 PC3	0.52	100
M2	PC2	PC3	0.3	0.85	PC2 = 44.33 + 0.57 PC3	0.46	99.9
M3	PC1	PC3	0.2	0.2	PC1 = 78.64 + 0.80 PC3	0.57	100
M4	PC4	PC1	1	0.8	PC4 = 119.7 + 0.40 PC1	0.47	99.9

Table 16: Model performances of the four regression models and results of the significance test for the correlation coefficient (LAUX et al., 2008).

The time series of the Julian onset dates can be treated as stochastic independent, since they contain annual values. The quality of the regression model can be expressed via the

R^2, which represents the explained variance fraction and the significance is verified using F-test. The Durbin-Watson test was applied in order to check the autocorrelation and the independence of the residuals. Values between 1.5 and 2.5 can be regarded as independent whereas values next to zero and four are strongly autocorrelated (DURBIN & WATSON, 1950). The non-parametric and distribution free K-S test was applied to check if the residuals are normal distributed, which is a necessary prerequisite for the correctness of the F-test. The K–S test essentially looks at the most extreme absolute deviation and determines the probability that this deviation could be explained by a normally distributed data set. The value listed as asymptotical significance (2-tailed) gives this probability (P) as a number between 0 and 1. A value of 0.05, for instance, means that only 5% of normally distributed data sets are expected to yields deviations as large as that reported for the extreme absolute deviation. In general, a 2-tailed asymptotical significance value of 0.05 is considered good evidence that the data set is not normally distributed. A value greater than 0.05 implies that there is insufficient evidence to suggest that the data set is not normally distributed, but in turn, it does not provide evidence that the data set is normally distributed. Quality parameters of the four regression models and the test of stochastic independence are summarized in Table 17:

Model			**Residuals**	
Number	**R^2**	**Signif. (%)**	**D-W**	**K-S test (asymp. sig.)**
M1	0.27	99	1.58	0.64
M2	0.21	99	2.14	0.47
M3	0.33	99	1.57	0.97
M4	0.22	99	2.18	0.27

Table 17: Quality parameters of the 4 regression models and test of stochastic independence and normal distribution of the residuals.

6.3 Linking the ORS with Atmospheric Weather Patterns

Within this section, a methodology is presented which is conditioning the single event ORS to daily large-scale atmospheric circulation using multi objective fuzzy rule based classification (MOFRBC) of meteorological anomaly fields. These fuzzy rules are obtained using a simulated annealing optimization of the classification performance. Bootstrapping resampling scheme has been applied in order to check the significance of the results. A five day period (+/- 2 days around the onset date) and two further classes (dry and wet) with different weights are then linked to the large-scale circulation patterns. For details concerning the setup of the classification, the reader is referred to Chapter 3.5.3. Performing frequency analysis in combination with bootstrapping scheme is assisting to detect highly responsible patterns for the onset of the rainy season. Investigations of all the potential predictor variables within the five different regions, only two significant patterns have been found to be related to the onset of the rainy. The

classification scheme for the eastward component of the moisture flux in 500hPa separates the onset class more clearly than all other variables. A significant feature could be found for the regions associated to PC1 and PC2. For the region associated to PC1, CP5 is related strongly to the onset of the rainy season. Table 18 shows the relative occurrence frequency, the occurrence frequency for the onset class and the quality parameter $O_{P(ONSET)}$ for each CP:

MF_U (500hPa), PC1	rel. Frequency [%]	cond. Frequency [%]	$O_{p(ONSET)}$
CP1	16.77	15.38	0.92
CP2	0.63	0.00	0
CP3	3.16	4.62	1.46
CP4	31.34	25.64	0.82
CP5	**4.55**	**11.28**	**2.48**
CP6	12.57	18.46	1.47
CP7	15.63	20.00	1.28
CP8	0.60	0.00	0
CP9	2.49	0.00	0
CP10	12.27	4.62	0.38

Table 18: Quality measures for u-componental moisture flux in 500hPa level conditioned on onset of the rains in PC1 (LAUX et al., 2007).

Figure 54 (left) shows the mean normalized distribution of CP5, averaged over 1961-1999. In contrast to the mean normalized distribution of all other patterns, CP5 shows a strong positive anomaly over Egypt. 500 bootstraps of CP time series holding the same conditional occurrence probabilities were generated. Figure 54 (right) is depicting the quality criterion $O_{P(ONSET)}$ for each realization. Since $O_{P(ONSET)}$ of CP5 exceeds the values of all realizations, it can be seen to be significant. Sea Surface Temperature is holding no significant features within Domain1. For Domain2, covering the tropical south Atlantic, the Skin Temperature T_{Skin} is revealing a suited predictor variable for the onset of the rainy season in the coastal region (PC2). Table 19 is pointing at the strongest relationship of CP8 with the monsoon's onset in this region:

T_{Skin}, PC2	Rel. Frequency [%]	cond. Frequency [%]	$O_{p(ONSET)}$
CP1	8.21	10.53	1.28
CP2	4.57	2.63	0.58
CP3	6.92	10.00	1.45
CP4	20.30	15.26	0.75
CP5	13.20	17.37	1.32
CP6	9.02	5.26	0.58
CP7	10.68	3.68	0.35
CP8	**9.50**	**17.89**	**1.88**
CP9	7.02	5.26	0.75
CP10	10.58	12.11	1.14

Table 19: Quality measures for T_{Skin} conditioned on onset of the rains in PC2 (LAUX et al., 2007).

The mean normalized T_{Skin} distribution of CP8 (Figure 55, left) is offering the largest positive anomalies in the Atlantic Ocean, with a maximum value around 18°W 10°S. Figure 55 (right) proves significance for this pattern.

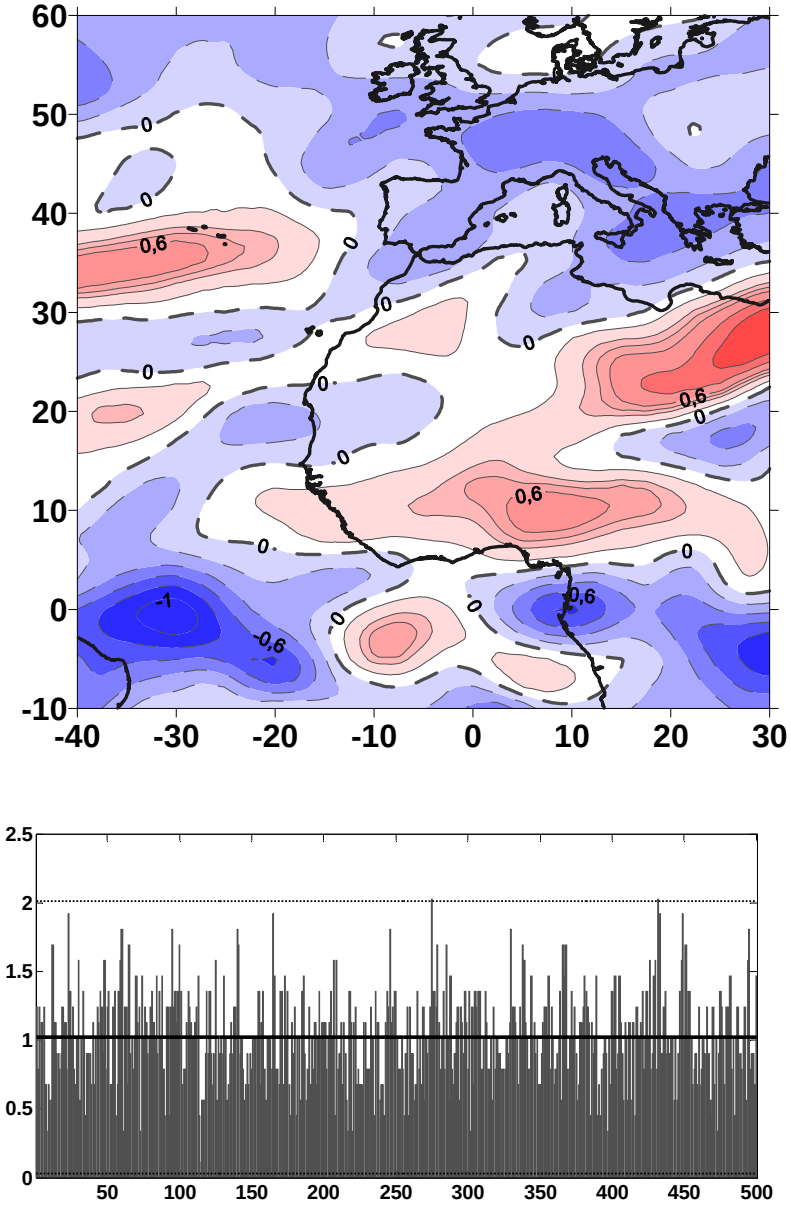

Figure 54: Mean normalized MF_U distribution in 500hPa of CP5 associated to the start of the rains in PC1 (top). Bootstrapping scheme for CP5 and MF_U in 500hPa conditioned on the onset of the rains in PC1. 500 realizations of $O_{P(ONSET)}$ were calculated and compared to $O_{P(ONSET)}$ for CP5 (2.48). The solid line represents the mean value and the dashed line the 3s value of $O_{P(ONSET)}$ for all realizations (bottom), (LAUX et al., 2007).

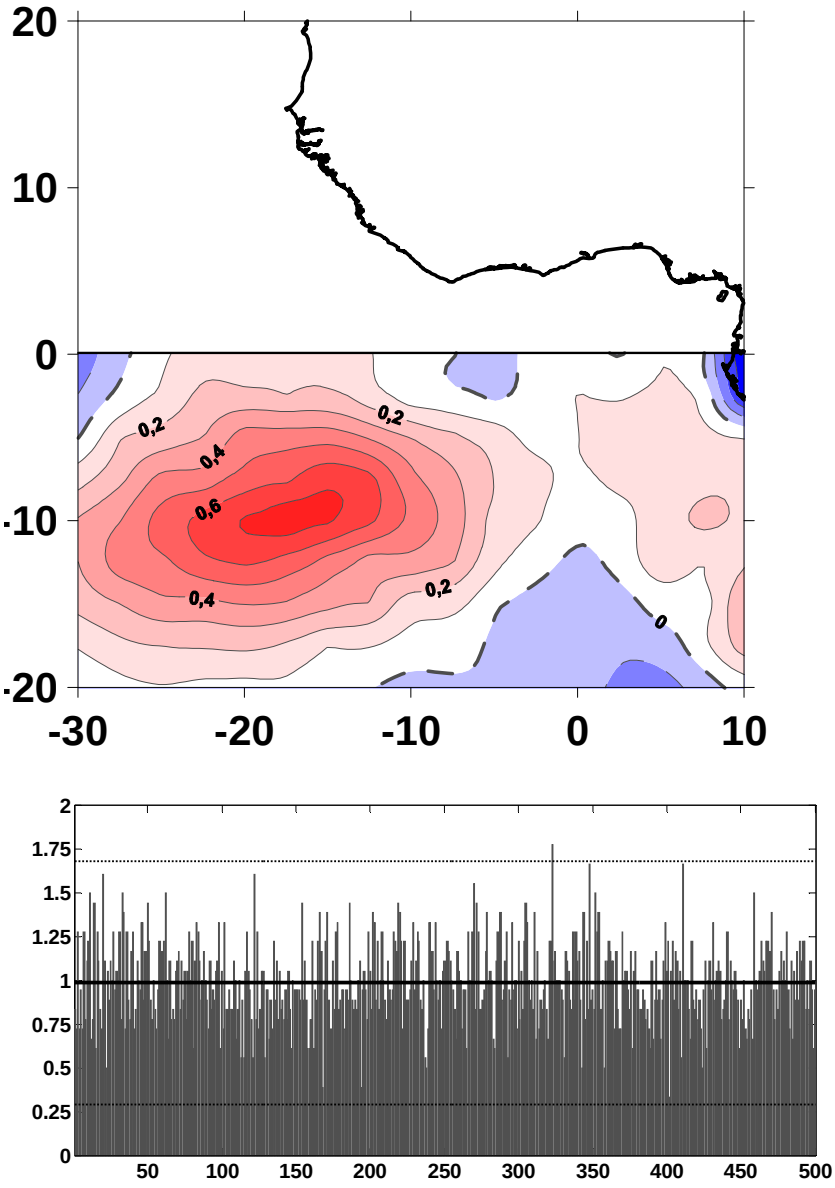

Figure 55: Mean normalized T_{Skin} distribution of CP8 associated to the start of the rains in PC2 (top). Bootstrapping scheme for CP8 and SST conditioned on the onset of the rains in PC2. 500 realizations of $O_{P(ONSET)}$ were calculated and compared to $O_{P(ONSET)}$ for CP8 (1.88). The solid line represents the mean value and the dashed line the 3s value of $O_{P(ONSET)}$ for all realizations (bottom), (LAUX et al., 2007).

6.4 Summary of Chapter 6

- LDA is a potentially useful tool to judge day by day whether the rainy season for the current year has already begun. Hit ratios of ~80% depending on the region can be reached for the ORS, whereas the prior probability is ~7%.

- LRA can potentially predict the onset dates a few weeks ahead under the assumption of the onset date of one region being already known. The predictive

power of the models is rather modest. The fractions of the explained variance are ranging from 21% to 33% for the different models.

- The multi objective fuzzy-rule based classification is a valuable methodology for linking meteorological parameters to the single event ORS in the Volta Basin. Moisture flux in 500hPa and skin temperature in the tropical Atlantic region is found to be significantly linked to the ORS. Classifying daily GFS fields of the most suited predictors can help to decide whether the rainy season has already begun or not. Similar to the LDA, however, no lead time can be obtained.

Chapter 7

7. Downscaling of Precipitation in the Volta Basin

Rainfall information is of crucial interest for a lot of applications in hydrology and agriculture. Most of these applications, like e.g. the investigation of impacts of climate change on precipitation and temperature require regional or local information. Global Circulation Models (GCMs), driven by different scenarios can be generally used for that purpose. According to the IPCC Third Assessment Report (2001), the uncertainties of their outputs are mainly due to the five key factors:

i) Uncertainties in future emissions of greenhouse gases (GHG)

ii) Uncertainties in converting emissions to GHG concentrations

iii) Uncertainties in converting concentrations to radiative forcing

iv) Uncertainties in modeling climate response to a given forcing

v) Uncertainties in converting model response into inputs for impact studies.

While the output of GCM simulation capture a large part of the uncertainties in iv) and v), they do not encapsulate the range of uncertainties in i), ii), and iii). For this reason, various scenarios should optimally be encapsulated to estimate the range of the climate change signal.

Due to the too coarse spatial resolution of climate model outputs, they cannot be directly used for hydrological or agro-meteorological impact studies. Therefore, downscaling techniques can be applied in order to transfer the large-scale GCM output to local-scale variables. Generally, there are two different approaches in use: the first is the dynamical downscaling (DDS), where deterministic regional climate models are nested into GCMs (e.g. YARNAL et al., 2001; BLÖSCHL, 2005). For this purpose, just the initial and boundary conditions are taken from the GCM to drive the regional climate model. The second method is the statistical downscaling (SDS), often referred to empirical downscaling in literature. Figure 56 is illustrating schematically the basic differences between DDS and SDS. Probably the most crucial factor with respect to impact studies is that SDS methodologies are able to derive the information directly from large-scale to site-scale. Using DDS, several nesting steps are normally required to obtain the local- or site-scale information. In comparison to DDS, SDS is computationally

inexpensive and can be applied rapidly to output from different GCM experiments. However, the shortcomings of the SDS should also be stressed: The prescription, that the relationship found for present-day climate also holds under the different forcing conditions of possible future climates (the *"Stationarity-Prerequisite"*) is difficult to verify. For very simple SDS methodologies, evidence of non-stationarity characteristics has been found (e.g. MURPHY, 1999, 2000). They also cannot account for possible systematic changes in regional forcing conditions or feedback processes.

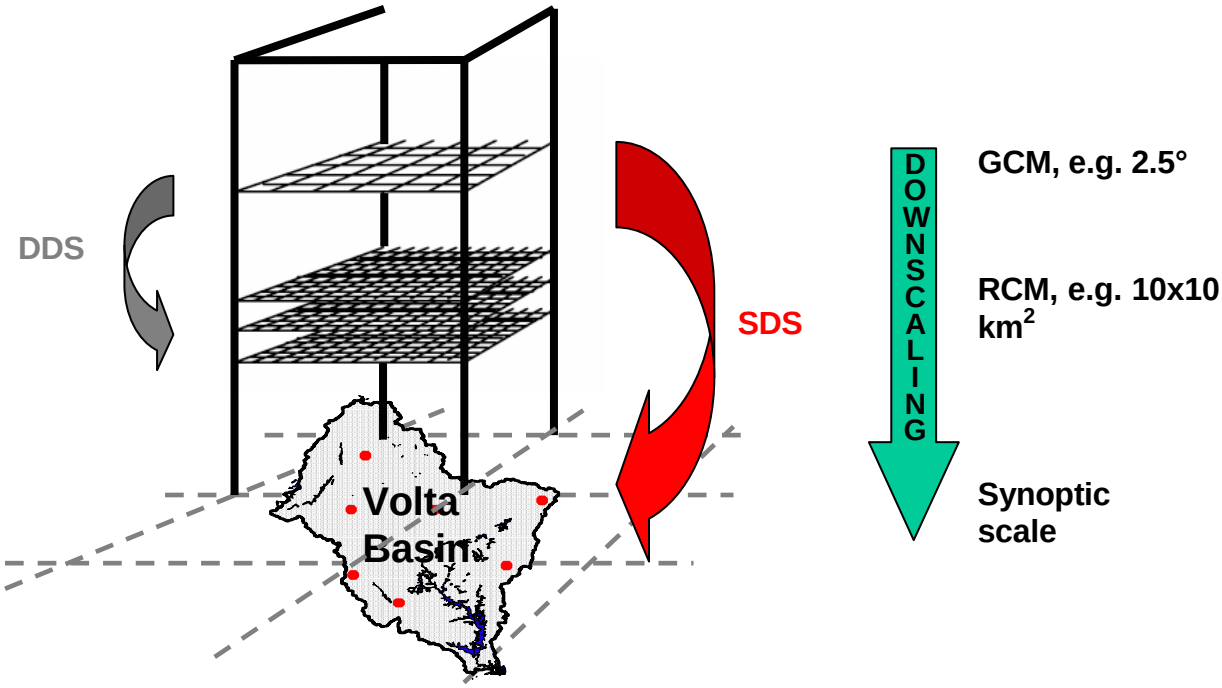

Figure 56: Schematic illustration of Dynamical Downscaling (DDS) and Statistical Downscaling (SDS).

7.1 Statistical Downscaling Methodologies

Due to the coarse resolution of GCMs, it is not possible to derive precipitation information for regional or local scale directly from GCM precipitation field. However, statistical downscaling techniques - besides exist dynamical and hybrid approaches - are exhibiting one possible solution using suitable predictor fields which are then connected to regional or local precipitation features. The concept of statistical downscaling (SDS) is based on the assumption that regional climate is conditioned by the large-scale climatic state and the regional/local physiographic features such as topography, land-sea distribution and land use (VON STORCH, 1995).

First, SDS seeks for the quantitative relationships between the observed large-scale and regional climate and, then, determines a statistical model, which relates large-scale climate variables predictors to regional and local variables predictand. Feeding large-scale output of a GCM into the statistical model, the corresponding local climate

characteristic can be estimated. Concerning the history of SDS for hydrological applications, the research followed three routes. The first has been driven by the need for estimating catchments averages of extreme rainfall from point data for hydrological design, the second from the interest of estimating daily rainfall from monthly data both in applied and theoretical contexts, and the third has triggered by the need of deriving local rainfall from average rainfall over large scale model output, provided by GCMs, especially for climate impact studies (BLÖSCHL, 2005). In practice, several statistical downscaling methodologies exist to bridge the gap between what general circulation models are able to simulate with a certain accuracy and what is needed for impact studies (e.g. HEWITSON & CRANE, 1996, ZORITA & VON STORCH, 1999, MURPHY, 1999 & 2000). They can be divided into three principal categories similar to those used by GIORGI et al. (2001):

- Weather- or circulation pattern classification algorithms. Circulation classifications are typically defined by applying clustering techniques to atmospheric fields (e.g. HUTH, 2000) and then define the local climate or hydrological state in dependence of the weather class (HEWITSON & CRANE, 1996; BÁRDOSSY et al., 1995; JACOBEIT et al., 2006).

- Regression models: Linear or non-linear relationships between predictand and predictors are established. Commonly applied methods include multiple regressions (e.g. MURPHY, 1999), artificial neural networks (e.g. CRANE AND HEWITSON, 2002), non-parametric models (CORTE-REAL et al., 1995) and canonical correlation analysis (e.g. JACOBEIT et al., 2003A; JACOBEIT et al., 2006).

- Weather generators: Weather generators replicate the statistical attributes of a local climate variable like mean or variance, but not observed sequences of events (WILKS & WILBY, 1999). Their parameters can, however, be estimated using GCM data as a guide. Typically, they are based on Markov Chain processes (SEMENOV & BARROW, 1997; WILKS AND WILBY, 1999). Most of them focus on the daily time scales, as required by many impact models, even subdaily models are available (e.g. KATZ & PARLANGE, 1995).

7.2 Screening of Suitable Predictor Variables

Theory and practice of statistical downscaling are well described in literature (e.g. GIORGI & MEARNS, 1991; WILBY & WIGLEY, 1997 & 1999). However, there is just little consensus about the choice of the predictor variables (WILBY & WIGLEY, 2000) and a comprehensive prior screening analyses is seldom presented. Various demands on the predictor should be fulfilled. According to WILBY et al. (1998) and GIORGI et al. (2001), an ideal predictor should:

- be physically and conceptually sensible

- be continuous
- be accurately modeled by GCMs
- be strongly correlated to the predictand
- hold a temporally stationary link with the predictand
- preserve observable correlations between downscaled parameters
- be sensitive to greenhouse-gas forcing

The following factors, which are potentially affecting the performance of precipitation downscaling using the MOFRBC, have been identified:

- Number of predictor variables in certain vertical levels, which should be physically related to the predictand, and their potential combinations
- Domain (location and size) and spatial resolution of the predictor variable
- Number of CPs
- Consideration of different seasons.

Due to the huge number of combinatorial possibilities concerning the potential influencing factors on the result of the downscaling procedure, the screening analysis necessitates a few simplifications. Table 1 and Table 3 (Chapter 3.3.3) are summarizing the two slightly different setups used for this analysis. The analyses have been carried out within a sector from 40°W to 30°E and 10°S to 60°N, covering a large area of the North Atlantic. Preliminary investigations, correlating monthly areal precipitation within a sector of the Volta Basin from 1°W to 3°E and 5°N to 11°N with reconstructed global gridded SLP and SST anomaly data sets, showed correlation patterns in the Mediterranean area and the North Atlantic (Figure 57). For the SST, also a small domain from 30°W to 10°E and 20°S to 0°N has been chosen to reduce the influence of potentially disturbing regions. Within this domain, the highest correlation coefficients have been found (Figure 57, bottom).

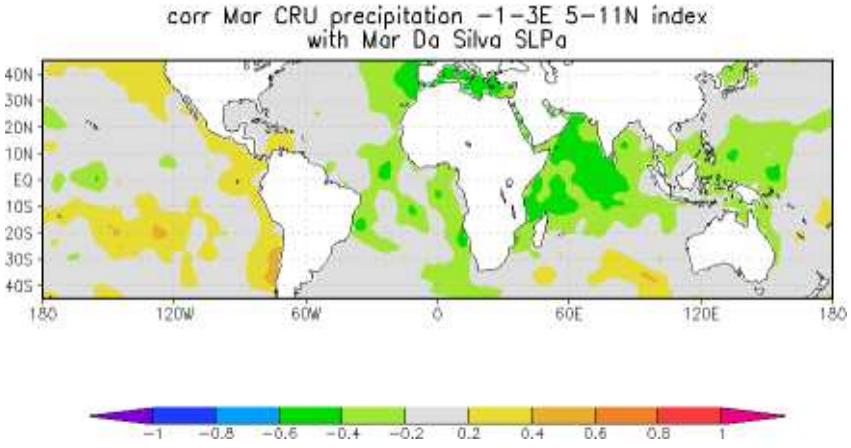

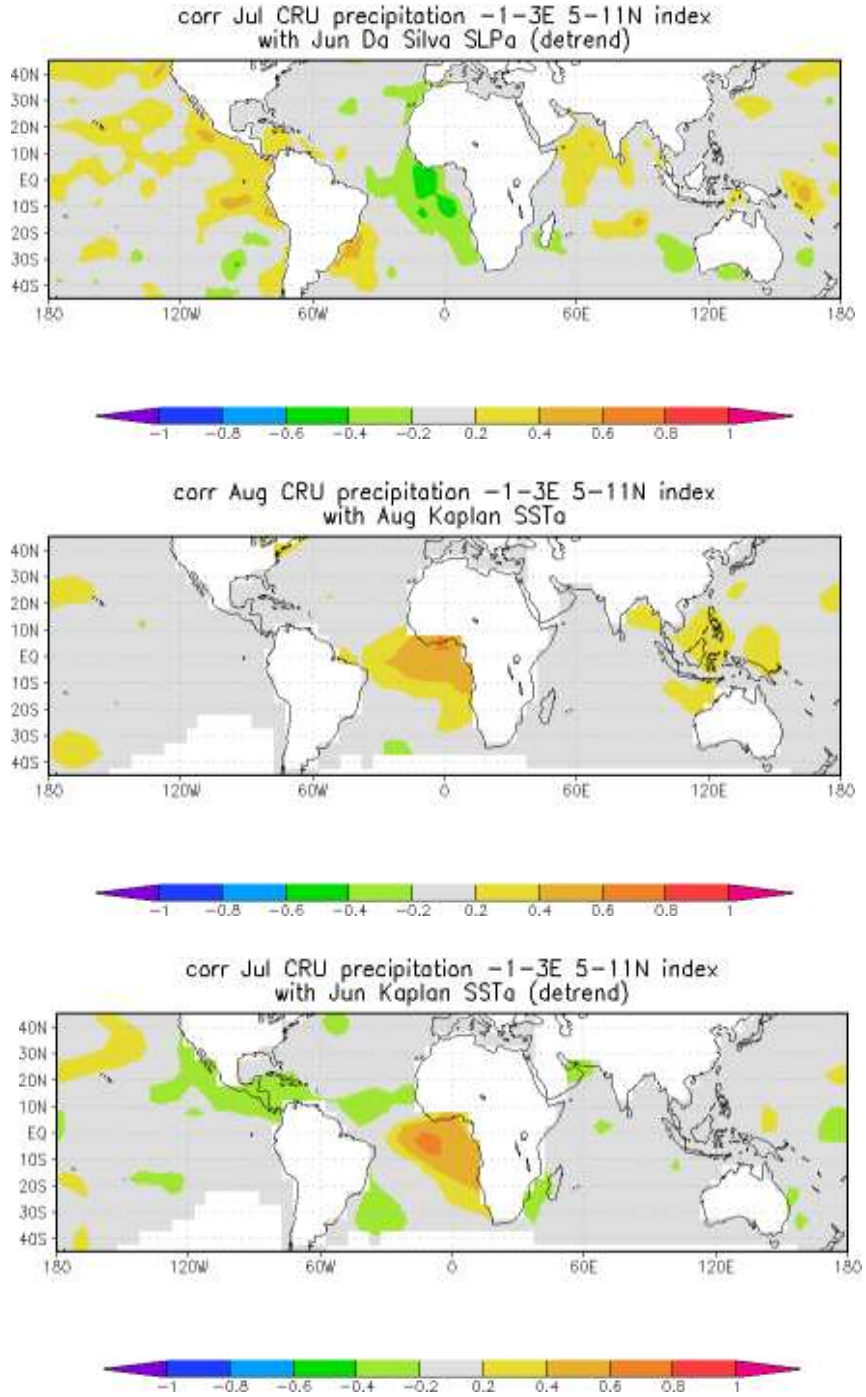

Figure 57: Pearson correlation coefficients between reconstructed monthly SLPa (top) and SSTa (bottom) fields (1961-1990) and monthly rainfall amount within a sector of the Volta Basin (1°W to 3°E and 5°N to 11°N).

At first, all the simulations have been performed using 9 predefined CPs. For the most promising variables, additional experiments of 5, 7 and 11 predefined CPs were conducted. In order to evaluate the influence of the season, two different temporal modes were analyzed: i) the whole year, and ii) the mean regional rainy seasons' length (Table 20) following Figure 23 (right).

	PC1	PC2	PC3	PC4	PC5
Rainy Season (DOY)	140-282	96-303	75-319	186-265	101-301

Table 20: Mean regional rainy seasons' lengths for PC1-PC5. Breaks within the rainy season (Little Dry Season) are not excluded from the calculation.

To judge the performance of the different variables, the wetness index has been used. For each combination, the difference between highest and the lowest wetness index of the used weather pattern set has been calculated. The unclassified CP has been excluded from this calculation. The higher the difference, the higher is the discriminative power of dry and wet circulation patterns. Table 21 is showing the most suited predictor variables for precipitation downscaling during the rainy season. 4 regions are showing the best results using either the eastward component of moisture flux at 500hPa or at 850hPa level as predictor variable. Solely for PC4, the sea level pressure field reveals better results. The variables holding the highest differences (Table 22) are highlighted in bold. With exception of PC5, 11 CPs (10 defined plus 1 undefined CP) are found to perform best.

No CPs	PC1	PC2	PC3	PC4	PC5
5 CPs	MF_U(500)	SST_TSA	MF_U(500)	MF_U(300)	MF_U(500)
7 CPs	MF_U(500)	MF_U(500)	SST_TSA	MF_U(500)	**MF_U(850)**
9 CPs	MF_U(500)	MF_U(850)	MF_U(300)	MF_U(500)	MF_U(500)
11 CPs	**MF_U(500)**	**MF_U(850)**	**MF_U(850)**	**SLP**	MF_U(500)
13 CPs	MF_U(500)	MF_U(850)	MF_U(300)	SLP	MF_U(500)

Table 21: Most suited predictor variables for downscaling rainfall during the rainy season using MOFRBC. The "best" predictor is depending strongly on the region and the number of CPs.

No CPs	PC1	PC2	PC3	PC4	PC5
5 CPs	0.69	0.42	0.23	0.55	0.2
7 CPs	0.89	0.47	0.23	0.56	**0.5**
9 CPs	0.68	1.14	0.71	1.75	0.43
11 CPs	**1.25**	**2.4**	**4.59**	**2.42**	0.49
13 CPs	0.78	1.00	1.23	1.7	0.41

Table 22: Difference between highest and the lowest wetness index during the rainy season for each PC and different numbers of CPs. The highest values for each PC are highlighted in bold.

Very similar results in terms of predictor screening have been obtained for the analysis of the whole year. Table 23 and Table 24 are summing up the results. Better results have been obtained for PC5 in comparison to the analysis of the rainy season. With exception of PC4, also 11 CPs is the best number of CPs for downscaling.

No CPs	PC1	PC2	PC3	PC4	PC5
5 CPs	MF_U(500)	MF_U(500)	SLP	MF_U(500)	MF_U(500)
7 CPs	MF_U(500)	MF_U(300)	SLP	**MF_U(500)**	MF_U(500)
9 CPs	MF_U(500)	MF_U(850)	MF_U(300)	MF_U(500)	MF_U(500)
11 CPs	**MF_U(500)**	**MF_U(300)**	**MF_U(300)**	MF_U(500)	**MF_U(500)**
13 CPs	MF_U(500)	MF_U(850)	MF_U(850)	MF_U(500)	MF_U(500)

Table 23: Most suited predictor variables for downscaling rainfall during the whole year using MOFRBC. The "best" predictor is depending strongly on the region and the number of CPs.

No CPs	PC1	PC2	PC3	PC4	PC5
5 CPs	2.09	0.34	0.25	1.68	0.69
7 CPs	2.48	0.49	0.34	**3.50**	1.40
9 CPs	2.14	0.90	0.59	2.90	1.19
11 CPs	**2.83**	**1.26**	**1.08**	2.21	**1.98**
13 CPs	1.90	0.87	0.45	1.87	1.21

Table 24: Difference between highest and the lowest wetness index during the whole year for each PC and different numbers of CPs. The highest values for each PC are highlighted in bold.

7.3 Simulating Precipitation Time Series using MOFRBC and LARS-WG – a case study for PC2

Especially in areas with low rainfall measurement density, rainfall modelling using large-scale GCM information exhibits the possibility to generate past or future rainfall time series on plot scale. However, the generation of daily precipitation series is a difficult task due to the chaotic and non-linear characteristics of precipitation, its spatial and temporal intermittency and variability of daily rainfall data (BÁRDOSSY et al., 2001; STEHLÍK & BÁRDOSSY, 2002). The spatial characteristics of rainfall are strongly depending on the time scale. For daily time scale e.g., precipitation is more intermittent than for weekly, monthly or annual scales (KATZ & ZHENG, 1999). Any causes for spatial and temporal intermittency in West Africa are based on the movement of the ITCZ, which is causing one or two rainy seasons depending on the latitude, and meso-scale convective cells (i.e. squall lines) associated with the bulk of annual rainfall for many regions.

While modeling attempts of annual and monthly totals can achieved by means of simple autoregressive moving average (ARMA) models and Markov models, daily series cannot be generated using these classical approaches since they assume continuous and mostly normal distributed variables (STEHLÍK & BÁRDOSSY, 2002). Daily precipitation series are discrete to describe dry and wet spells and continuous to describe precipitation totals on wet days. Approaches for modeling of daily precipitation are ranging from multivariate regression models (BÜRGER, 2002; HUTH & KYSELÝ, 2000) to Markov models for simulating occurrence and duration of precipitation (e.g. FOUFOULA-GEORGIOU & LETTENMAIER, 1987) to stochastic models based on circulation patterns (KATZ & PARLANGE, 1993 & 1996; BÁRDOSSY et al., 2001; STEHLÍK & BÁRDOSSY, 2002).

Rainfall has been simulated using a multivariate stochastic simulation model driven by time series of objectively classified CPs, described in Chapter 3.5. First, the CP classification has been carried out exemplarily for five test sites located in region PC2 using the eastward component of moisture flux in 300hPa as predictor for rainfall of the whole year. The model has been calibrated for the time period 1961-1990. 50 realizations of daily rainfall have been simulated for the period 1991-1999. Figure 58 shows the results for the modelled time series of daily precipitation. Additional modelled precipitation time series can be found in Appendix 6. Although the extreme values are not captured well, the annual cycle of rainfall is matched. Generally, the model slightly tends to underestimate the rainfall.

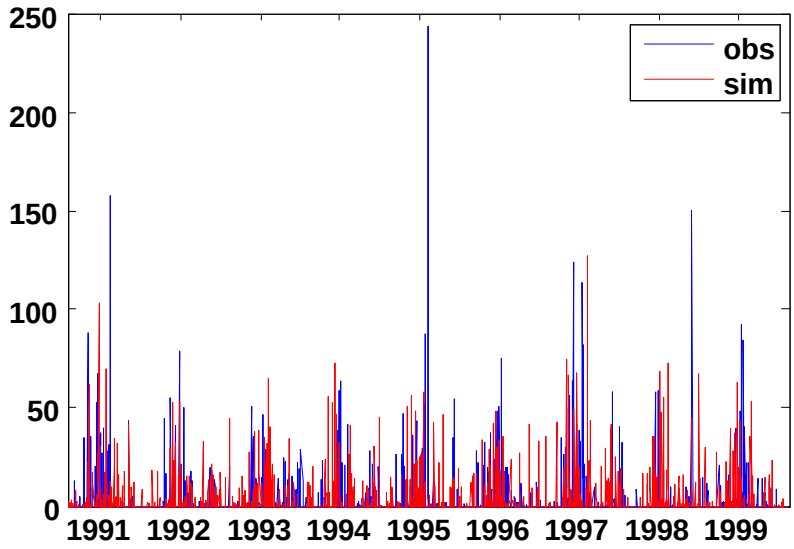

Figure 58: Observed (blue bars) versus simulated (red bars) daily precipitation during the validation period (1991-1999) at Accra using CP conditional stochastic simulation.

Figure 59 illustrates exemplarily the relationship between number of rainy days and rainfall amount at Accra aggregating the daily precipitation to monthly values. The annual cycle of the simulated values is in good agreement to the observed ones. Both values can be captured well by the simulation, and their Pearson correlation coefficient exceeds 0.95 for the observations as well as for the simulation. It should be mentioned, that the maximum of the rainfall amount in the major rainy season is shifted for one month. For the simulation, the major peak takes place in May whereas the observation shows the major peak in June.

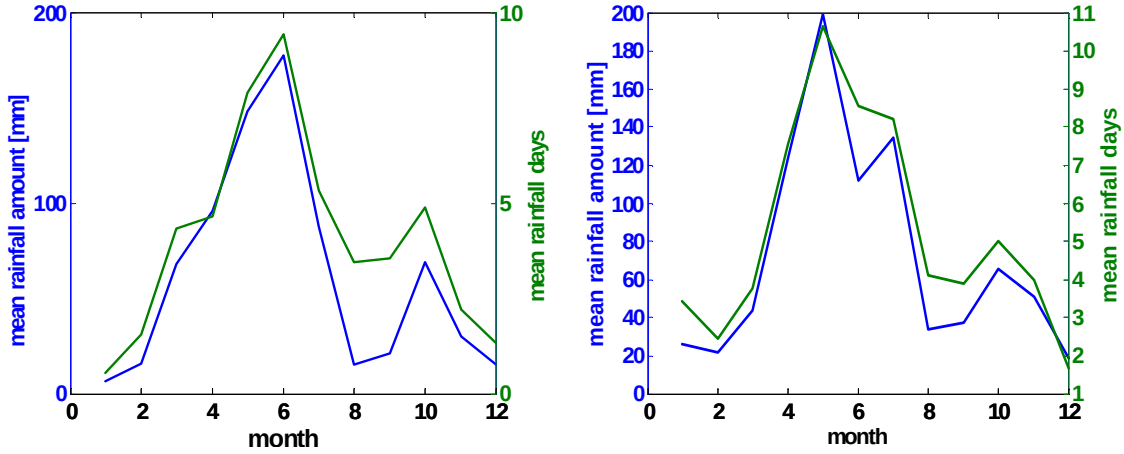

Figure 59: Observation (left) and simulation (right) of mean rainfall amount and number of rainy days at Accra during the validation period (1991-1999) using stochastic CP conditional rainfall simulation.

The simple stochastic weather generator LARS-WG has also been used to generate daily rainfall for the 5 test sites. LARS-WG is described in Chapter 3.3.5. In comparison to the CP driven model, the LARS-WG shows a better agreement of the precipitation amounts for the major rainy season, but shows minor performance for the little rainy season from September to October (Figure 60).

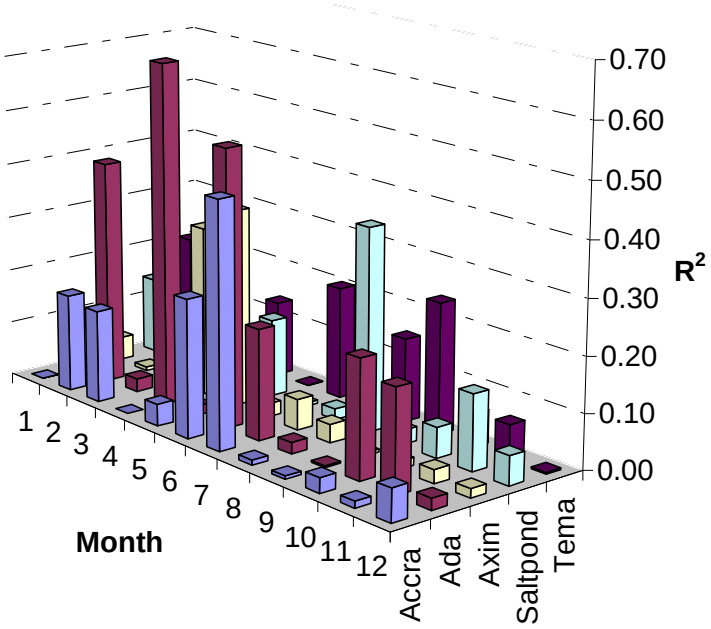

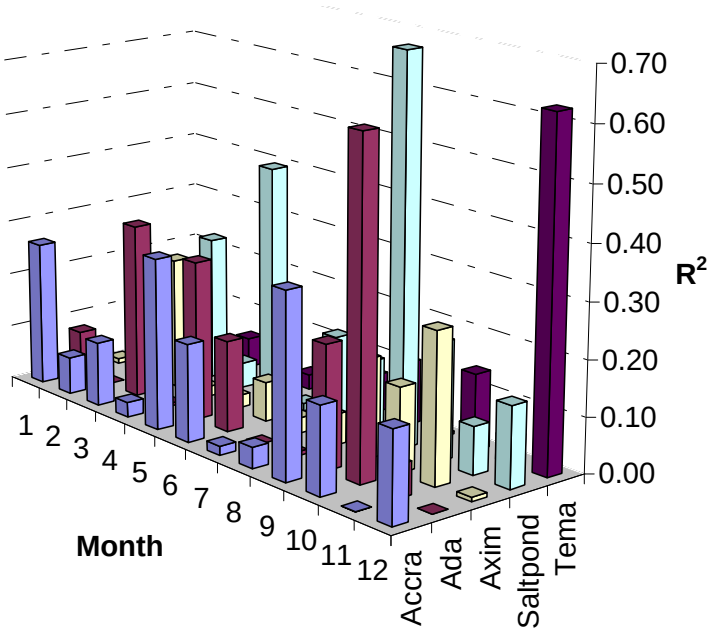

Figure 60: Monthly resolved coefficient of determination (R^2) for the rainfall simulation using LARS-WG (top) and the multivariate stochastic rainfall simulation model (bottom) at 5 test sites in the coastal region PC2 and for the validation period (1991-1999).

7.4 Summary of Chapter 7

- Under all investigated variables, the eastward component of moisture flux in 300hPa and 500hPa delivers the most promising results for statistical downscaling of precipitation within the Volta Basin. In most of the cases 12 predefined rules deliver the best discrimination between wet and dry CPs.

- In most of the cases, 11 predefined rules (weather patterns) revealed to most discriminative power between wet and dry CPs.

- LARS-WG and the multivariate stochastic simulation model are feasible tools for generating daily rainfall time series. In a case study for the coastal region PC2, LARS-WG performs better for the first rainy season than the sophisticated CP conditional rainfall simulation model. For the second rainy season, the situation is reversed.

Chapter 8

8. Assessing the Impact of Climate Change in the Volta Basin

Climate change is the result of an internal and external variability of the climatic system, both of natural and anthropogenic reason. The latter consists mainly of variations in incoming solar radiation as a consequence of changes in solar activity and the sunspot cycle (e.g. RIND et al., 1999; SHINDELL et al., 1999). The human impact on climate change among the bulk of scientists is without controversy. In this context, an increase of global mean temperature of ~0.6 +/- 0.2 Kelvin since the industrial era has been observed (HOUGHTON et al., 2001) and a warming of ~ 6 Kelvin compared to the last ice age is in store. Warming, in turn, will impact rainfall patterns, partly because warmer air holds more moisture, and also because the uneven distribution of warming around the world will lead to shifts in large-scale weather regimes. Most climate models predict decreasing rainfall amounts in the subtropics, induced through changes in circulation patterns. There is more uncertainty about changes in rainfall in the tropics mainly because of complicated interactions between climate change and natural cycles like e.g. the El Niño.

A meaningful assessment of the impacts of climate change will include a thorough assessment of the impact response to present-day or recent climate conditions in addition to an assessment of its response to a climate future. Specification of the present-day or baseline climate is therefore just as important as the specification of the scenarios of climate change. The IPCC recommends that, where possible, 1961-1990 (the most recent 30-year climate 'normal' period) should be adopted as the climatological baseline period in impact and adaptation assessments. This period has been selected since it is considered to:

- be representative of the present-day or recent average climate in the study region
- be of a sufficient duration to encompass a range of climatic variations, including a number of significant weather anomalies
- cover a period for which data on all major climatologic variables are abundant, adequately distributed over space and readily available

- include data of sufficiently high quality for use in evaluating impacts
- be consistent or readily comparable with baseline climatology used in other impact assessments[15].

In order to assess the impact of climate change for a certain region, scenario driven GCMs can be either dynamically or statistically downscaled (Chapter 7). BROOKS (2004) gives a comprehensive overview of recent research basing on climate change scenarios in the Sahel. More recently, JUNG (2006) performed dynamical regional downscaling of ECHAM4 data driven by the IS92a scenario for the Volta Basin using the mesoscale meteorological model MM5. Comparing the two 10-years time slices 1991-2000 and 2030-2039, an increase of annual precipitation amount of ~ 5%, and a spatially highly heterogeneous precipitation change, ranging from -20% to +50% was observed. Using a similar ORS definition, JUNG (2006) found a delay of the mean ORS dates for the Sahel and the Guinea coast region within the future period.

High uncertainties are expected to accompany regional climate modelling. Authors like e.g. HULME (2001) or BROOKS (2004) even concluded that it is unwise to predict regional trends with current climate models. The only consensus of diverse studies dealing with regional climate modelling in West Africa seems to be that increased temperature due to the increasing CO_2 concentration can cause a northward shift of the West African Monsoon. Furthermore, an increased physiological production, with a positive feedback loop between increasing vegetation cover and precipitation, is expected.

In the following, several aspects of rainfall variability of the past but also of the future in the Volta Basin are presented. Rainfall variability is especially referred to the ORS and the frequency change of wet and dry weather patterns. The past time slice of real climate (represented by the NCEP/NCAR reanalysis data) from 1961-1990 is compared to the time period 2011-2040 represented by the ECHAM5-A1B emission scenario. Since the difference of CO_2 is expected not to differ excessively during the selected time slices, one scenario is found to be adequate. Due to its comparatively moderate global CO_2 concentrations the A1B scenario has been chosen.

[15] http://www.cics.uvic.ca/scenarios/index.cgi?More_Info-Baseline_Climates/

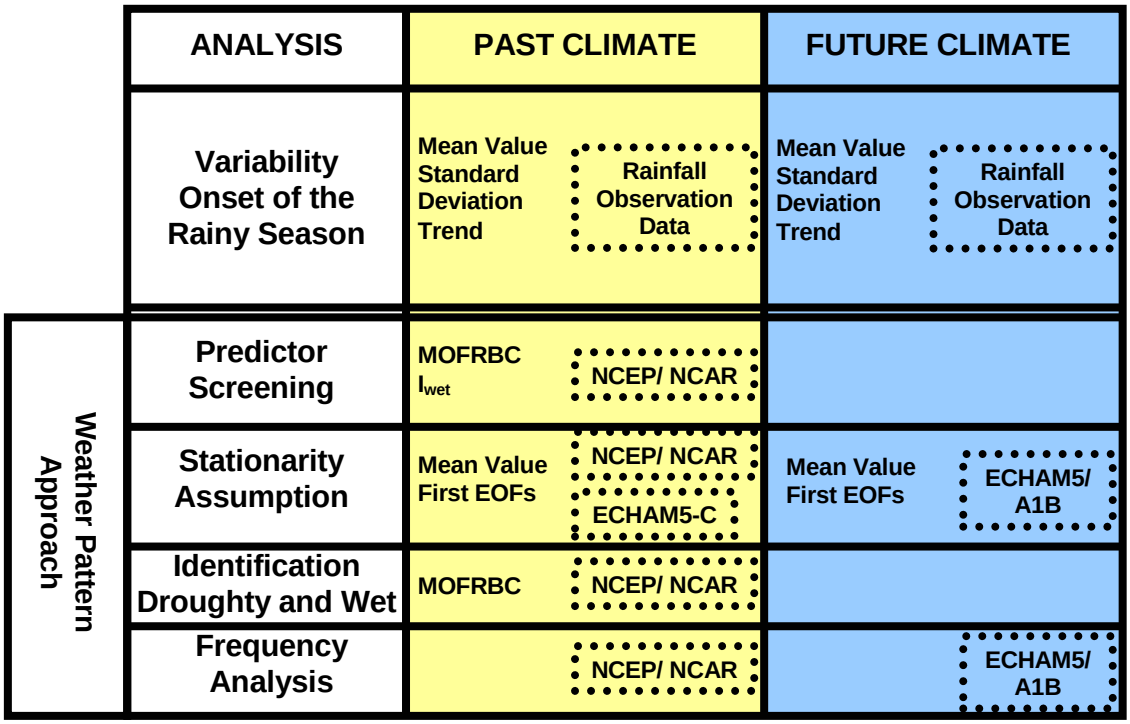

Figure 61: Schematic overview of the performed analyses with respect to climate change in the Volta Basin. The performed analyses can be divided into the variability of the onset of the rainy season (top row) and the weather pattern approach (bottom row). For each analysis, the underlying methodologies/measures and data (dotted boxes) used for analyzing the past (yellow column) and the future (blue column) climate are presented.

8.1 Impacts of Climate Change in a Past Climate

In the following subsections, the impact of climate change for the past is elaborated. Chapter 8.1.2 is dealing with the interannual variability of the past ORS dates. The identification of wet and droughty weather patterns is described in Chapter 8.1.3 and the frequency change of these weather patterns is presented in Chapter 8.1.4. Trend analysis of meteorological and hydrological measures has already been given in Chapter 2.6.

8.1.1 Intra-annual Rainfall Variability

The regional intra-annual rainfall variability is given in Chapter 2.3. In this section, the expected regional rainfall variability of the future time slice (2011-2040) is compared to the past (measured) rainfall variability of the time slice 1961-1990 (Figure 62). Clear variations in timing of the rains and rainfall amount are found for the different regions. For all the regions, the number of rainy days is changing in accordance with the rainfall amounts. Especially for the drought prone regions PC1 and PC4, the rainfall amounts are decreasing. For the southern and central regions, rainfall amount is decreasing during the first (major) rainy season and increasing during the minor season in autumn.

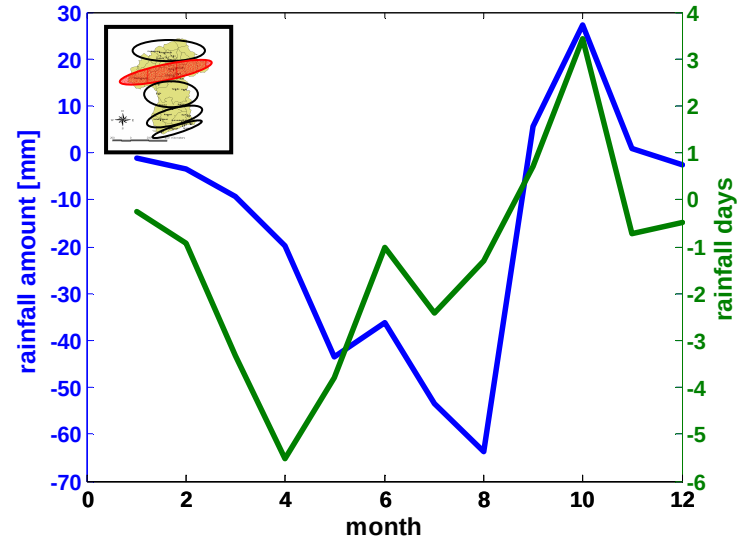
rainfall amount [mm]
rainfall days
month
30
20
10
0
-10
-20
-30
-40
-50
-60
-70
4
3
2
1
0
-1
-2
-3
-4
-5
-6
0
2
4
6
8
10
12

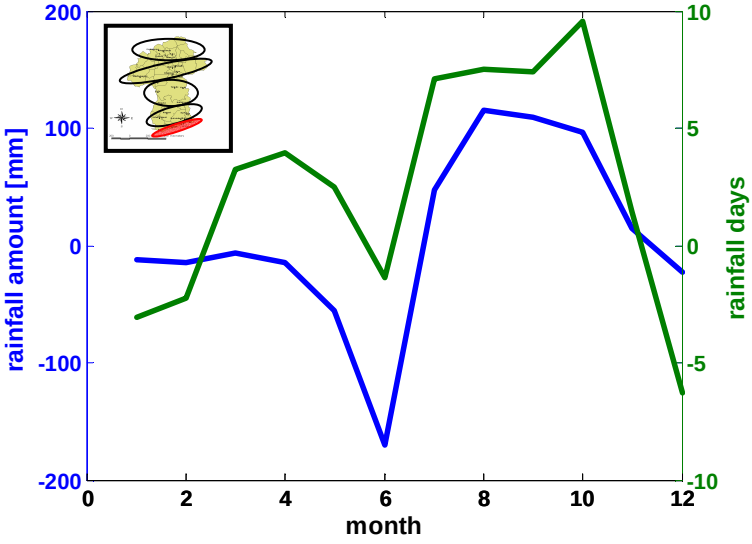
rainfall amount [mm]
rainfall days
month
200
100
0
-100
-200
10
5
0
-5
-10
0
2
4
6
8
10
12

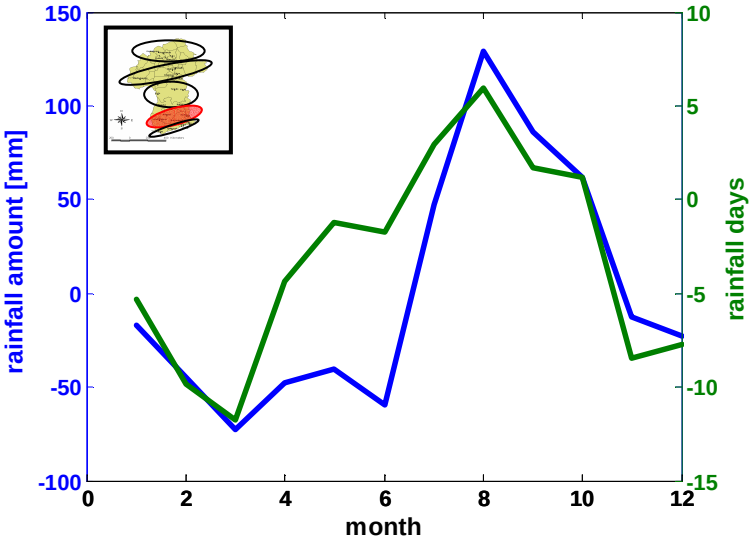
rainfall amount [mm]
rainfall days
month
150
100
50
0
-50
-100
10
5
0
-5
-10
-15
0
2
4
6
8
10
12

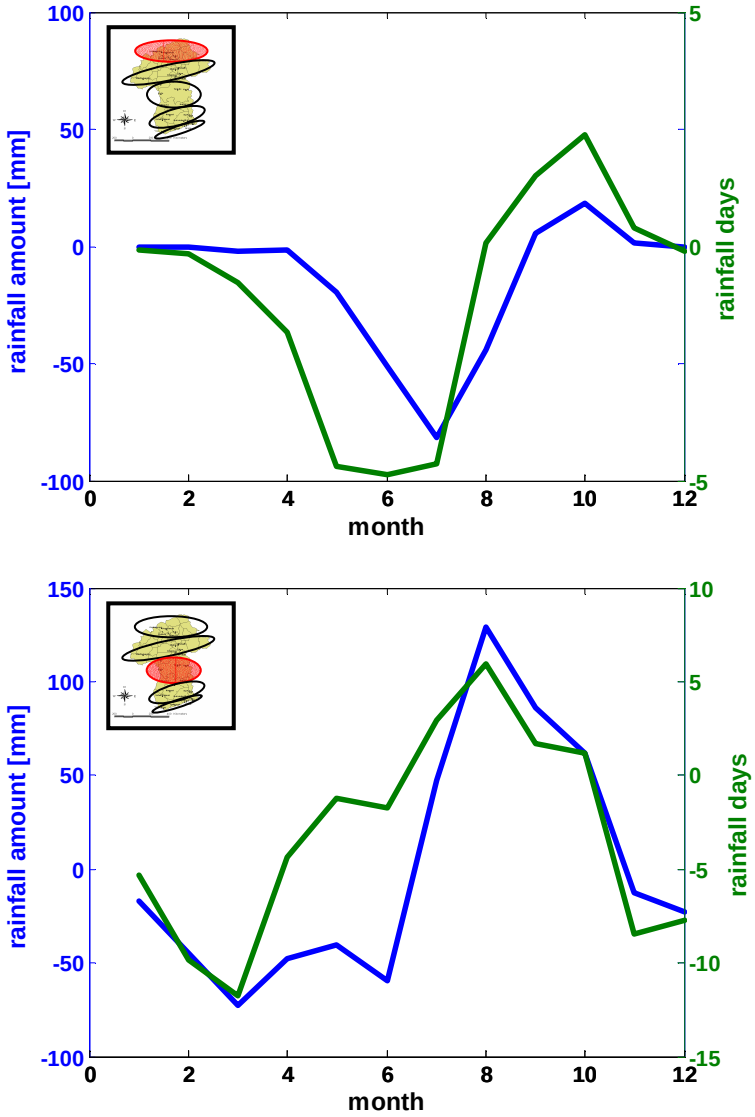

Figure 62: Difference between rainfall amount and number of rainy days of expected climate (2011-2040) and past climate (1961-1990) for the regions PC1-PC5. The location of the respective region is highlighted.

8.1.2 Interannual Variability of the Past ORS

Regional Dates of the ORS have been calculated for the 5 selected regions within the Volta Basin (see therefore Figure 11) from 1961-2001. Each region is representing an area with specific temporal rainfall characteristics (Chapter 4). First, the mean regional rainfall time series have been calculated averaging all the stations belonging to the respective region. Second, these regional time series have been used as input for both ORS-Definitions (Chapter 4.1.3). In order to receive comparable trends between the different regions a γ threshold of 0.4 was taken for Definition1. In order to reduce the systematic difference between Definition1 and Definition2 due to the different number of definition arguments, a threshold of $0.4^{2/3}$ was taken for Defintion1.

Figure 63 shows the interannual variations of the ORS dates from 1961 – 2001 using Definition1 and Definition2 and their respective linear regression functions. Both definitions are described in Chapter 4. Except for region PC4 and Definition2 positive trends towards a delayed ORS with high interannual fluctuations were observed.

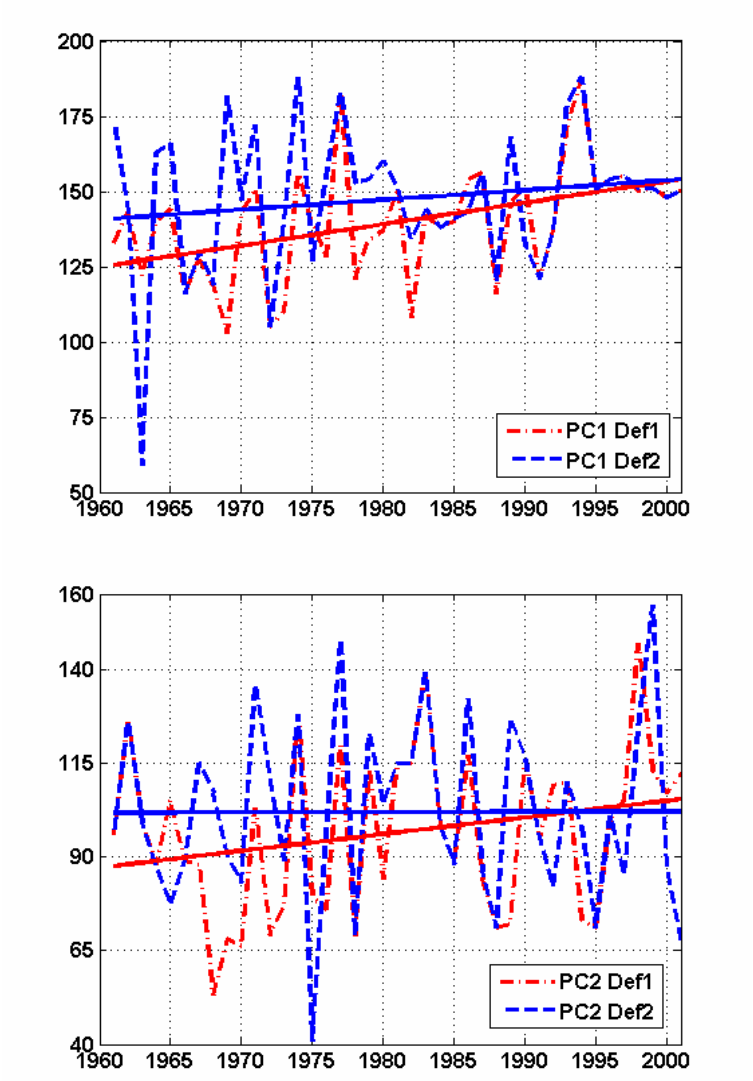

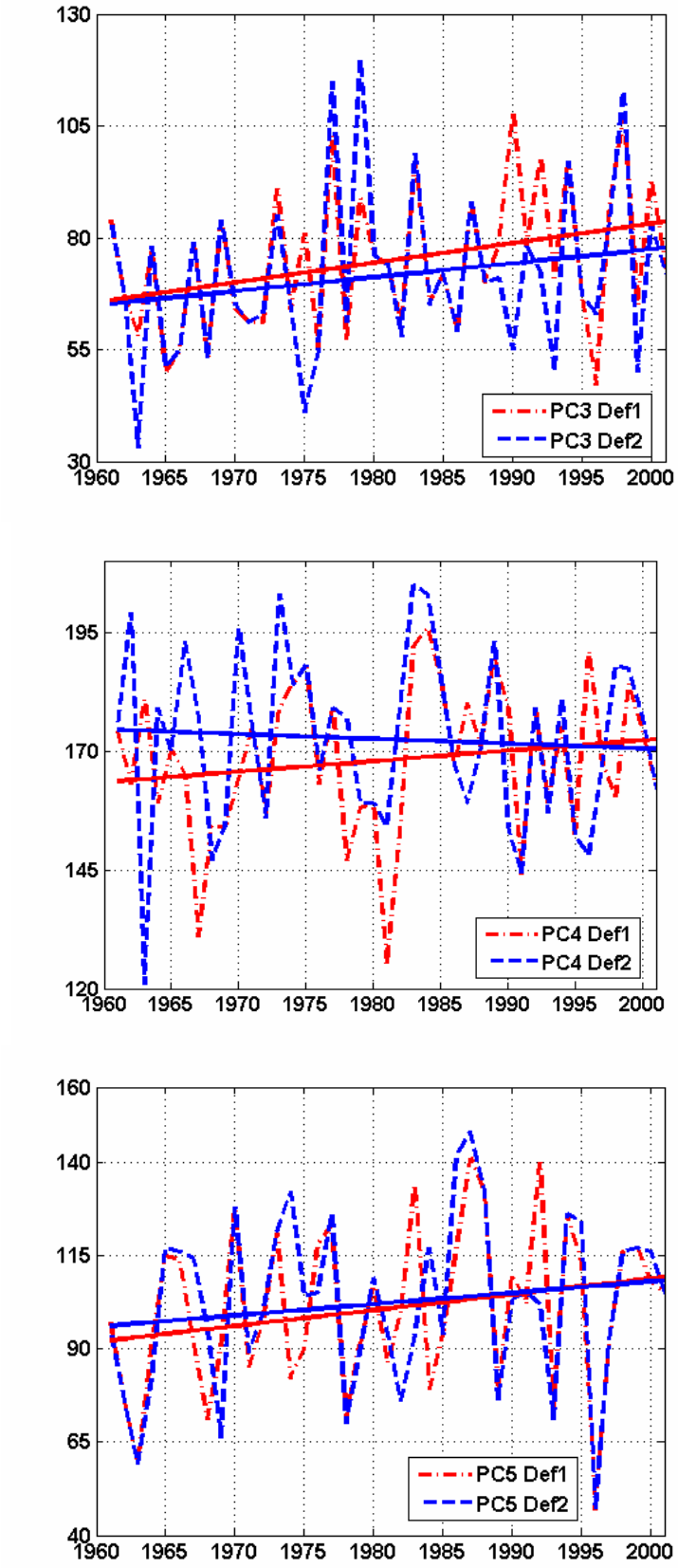

Figure 63: Onset dates [DOY] of the major rainy season, calculated for the 5 rainfall regions using Definition1 and Definition2 (dashed lines) and linear trend lines (solid lines).

Figure 64 shows the sequence of the annual ORS dates for the 5 regions of the Volta Basin using Definition1. The results are presented as classes of the ORS dates, basing on the exceedance probabilities of the ORS dates (Chapter 5.5). For this reason, the cumulative distribution functions have been calculated and the series have been classified into EARLY (exceeded in 75% - 100% of years), NORMAL (exceeded in 25% - 75% of all years), and LATE ORS (exceeded in 0%–25% of all years) for each region. Neighbouring regions show similar characteristics in the ORS dates.

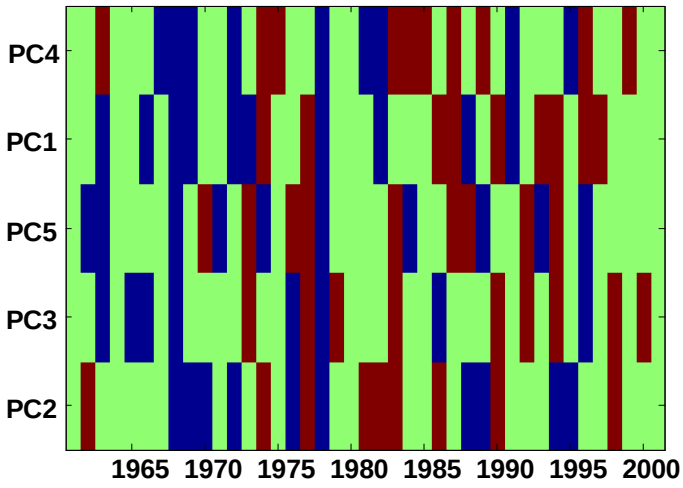

Figure 64: Interannual variability of the ORS classes EARLY (blue), NORMAL (green) and LATE (red) from 1961-2001 using Definition1. The regions PC1-PC5 are arranged due to the geographic location of the regions within the Volta Basin.

Table 25 is summarizing the mean onset dates, standard deviations, linear trends and the significance levels for each region:

Definition1	Mean onset [Julian day]	Standard dev. [days]	Trend [days/year]	Signif. [%]
PC1	140	19	0.71	99
PC2	96	22	0.45	88
PC3	75	16	0.44	96
PC4	168	16	0.22	70
PC5	101	22	0.42	99
Definition2	**Mean onset [Julian day]**	**Standard dev. [days]**	**Trend [days/year]**	**Signif. [%]**
PC1	147	24	0.32	80
PC2	102	24	0.01	20
PC3	71	19	0.31	80
PC4	172	19	-0.10	62
PC5	102	23	0.30	79

Table 25: Mean onset dates, standard deviations, trends, and their significances for the 5 regions, using Definition1 and Definition2.

In the same manner as for the station based approach, both definition reveal similar mean values and standard deviations of the onset dates. The magnitude of the trends is strongly depending on the regionalization, e.g. combining the two northernmost regions PC1 and PC4 to one region, the trend would be more balanced. Generally, Definition1 yields higher significances of the trends than Definition2. When looking at the time series of the onset dates (Figure 63), the smallest agreement of onset dates using both definitions is reached with PC2 and PC4. For PC4, for instance, the onset in 1963 takes place on Julian day No. 181 according to Definition1. When applying Definition2, the onset takes place 60 days earlier. To find out which γ criterion is mainly responsible for the positive trends (delayed onset dates) and since our focus is lying on Definition2, the relationship between the two γ criteria has been investigated, and linear trends of the amount of regional precipitation and the number of wet days have been analyzed. For this purpose, monthly mean values and monthly resolved values of the rainfall amount (represented by the $\gamma 1$) and the number of wet days (represented by $\gamma 2$) were calculated. Table 26 presents the Pearson correlation coefficient between the monthly rainfall amount and the mean monthly number of wet days.

Region	Correlation
PC1	0.95
PC2	0.77
PC3	0.91
PC4	0.96
PC5	0.97

Table 26: Correlation coefficients of monthly mean rainfall amount and monthly mean number of wet days (averaging time period: 1961-2000); (LAUX et al., 2008).

Except for the region corresponding to PC2, all the correlation coefficients are very high. There, heavy convective showers, associated with high amounts of rainfall and slightly increasing number of wet days, lead to lower correlation coefficients during the rainy season, especially during the May (month of the mean ORS date). Figure 65 exemplarily shows the monthly resolved correlation coefficient between rainfall amount and number of wet days for the region PC1. For May, the correlation coefficient of decreases to ~ 0.2.

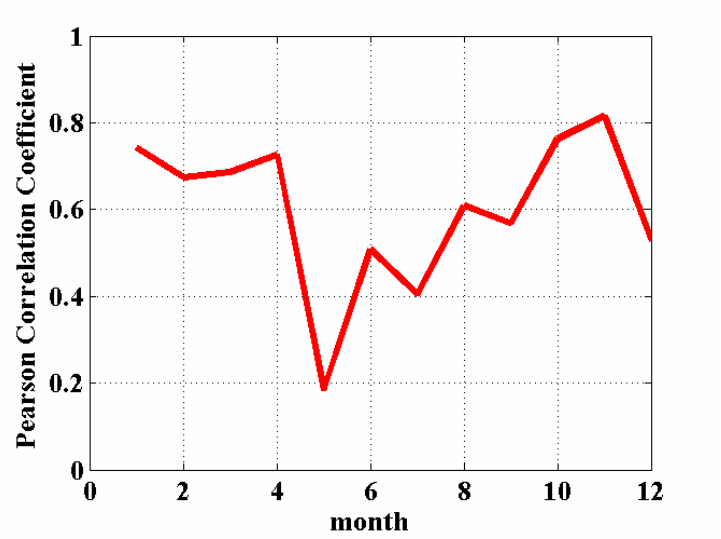

Figure 65: Monthly resolved correlation coefficient of rainfall amount and number of wet days for the region corresponding to PC1 (1961-2001); (Laux et al., 2008).

Again, trend analysis of monthly precipitation amounts and wet days was applied using linear regression analysis and verified by the F-test (see Appendix 8). Table 27 summarizes the results of the trend analysis for all regions. Both, the number of rainy days and the precipitation amounts reveal a number of significant negative trends. Overall, PC5 exhibits the most significant trends ($\alpha = 0.01$) in the number of wet days. Regarding the mean onset dates, it is presumed that for PC1, both variables might be responsible for the delayed onset. They exhibit significant and strong negative trends in April, a formerly frequent rainy season's onset month. PC2 with its normal onset dates around March displays a significant negative trend of the number of rainy days in this month and significant negative trends of precipitation one month earlier and later. PC3 having the earliest onset month with frequent starting dates in February also exhibits significant trends with high amounts of decreasing rainy days and rainfall in this month. Regarding PC4, the number of rainy days in April (trend = -0.05 days/year) seems to play a major role for the onset shift. In PC5, both parameters are important again (high negative trends in March).

	PC1		PC2		PC3		PC4		PC5	
Month	**NRD**	**RA**	**NRD**	**RA**	**NRD**	**RA**	**NRD**	**RA**	**NRD**	**RA**
1	-0.01	-0.06	-0.05	-0.44	-0.03	-0.27	0	0	-0.02	0.13
2	-0.03	-0.23	-0.04	-0.61	-0.14	-0.65	-0.01	-0.02	-0.12	-0.18
3	-0.06	-0.14	-0.08	0.03	-0.07	-0.42	-0.01	0	-0.2	-0.56
4	-0.08	-0.71	-0.06	-0.66	-0.04	0.05	-0.05	-0.21	-0.12	0.14
5	0.01	-0.15	-0.06	0.11	-0.06	-0.73	-0.06	0.14	-0.12	-0.28
6	0.02	0.28	-0.18	-6.85	-0.1	-1.04	0.01	-0.5	-0.13	0.41
7	0.02	-0.52	-0.13	-2.07	-0.06	-0.65	-0.01	-0.36	-0.13	-0.68
8	-0.02	0.75	-0.06	-0.6	0.04	-0.26	-0.04	-0.53	-0.11	-0.6
9	-0.04	-0.3	0.02	-0.38	-0.01	-0.32	-0.07	-0.39	-0.11	-0.16
10	-0.01	-0.02	0	0.36	0	-0.68	0.01	-0.14	-0.1	0.34
11	-0.05	-0.09	-0.14	-0.65	-0.1	-0.77	0	0.01	-0.13	-0.16
12	-0.02	0.02	-0.12	-0.22	-0.05	-0.02	-0.02	-0.04	-0.06	-0.2

Table 27: Monthly trends of number of rainy days (NRD) [days/year] and rainfall amounts (RA) [mm/year] for all regions. Significant values (α = 0.05) and very significant values (α = 0.01) are highlighted with light and dark grey colour. (LAUX et al., 2008).

8.1.3 Identification of Wet and Dry Weather Patterns

This subsection focuses on the identification of weather patterns, which are responsible for the major episodes, either highly favourable or unfavourable for agriculture. Special attention is given to weather patterns that tend to produce extremes in precipitation resulting in unusually wet or droughty conditions. Figure 66 is highlighting the conditional wetness index [-], the conditional precipitation amount [mm] as well as the conditional rainfall occurrence probability of 11 CPs (plus one additional pattern for the unclassified cases), illustrated exemplarily for region PC1 using eastward component of moisture flux in 500hPa as predictor. One can observe the very wet pattern CP9 leading in about 40% of all cases to rainfall with an average amount of 8mm per day. Furthermore, CP2 is relatively wet (~ 4mm per day). CP1, CP3 and CP4 are patterns which are linked to very droughty conditions. They are holding average rainfall probabilities of about 5% and mean rainfall rates of less than 1mm per day.

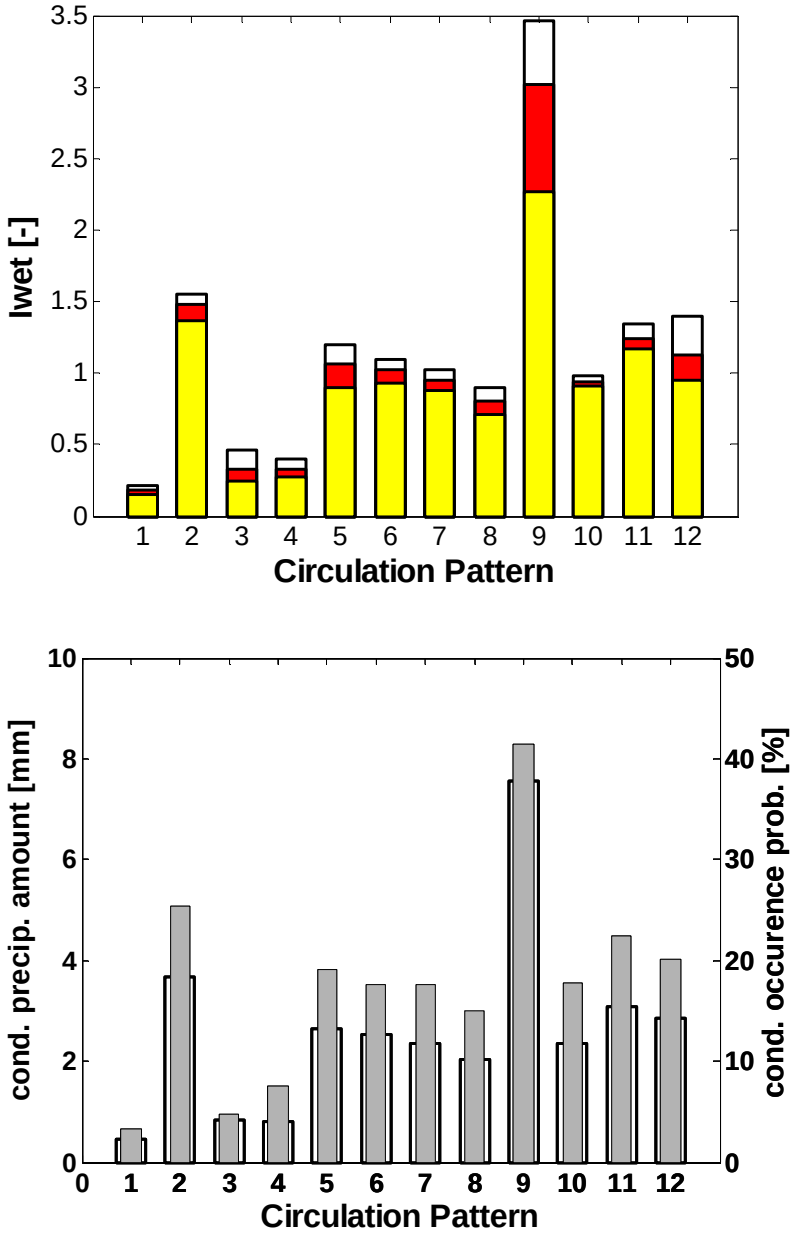

Figure 66: CP conditional mean wetness index [-] (yellow bar = minimum value, red bar = mean value, white bar = maximum value) (top); conditional precipitation amount [mm] (white bars) and conditional rainfall occurrence probability [%] (grey bars) (bottom) for region corresponding to PC1 in order to identify wet or droughty conditions. The predictor variable is the eastward component of moisture flux in 500hPa.

The wetness index of each single station within that region is showing slightly local differences (Figure 67). For CP9, e.g. the wetness index ranges from ~2.2 at Manga to ~3.5 at Niaogho. All the single stations of that region are reflecting the general tendencies of the observed (regional) wet and droughty weather patterns.

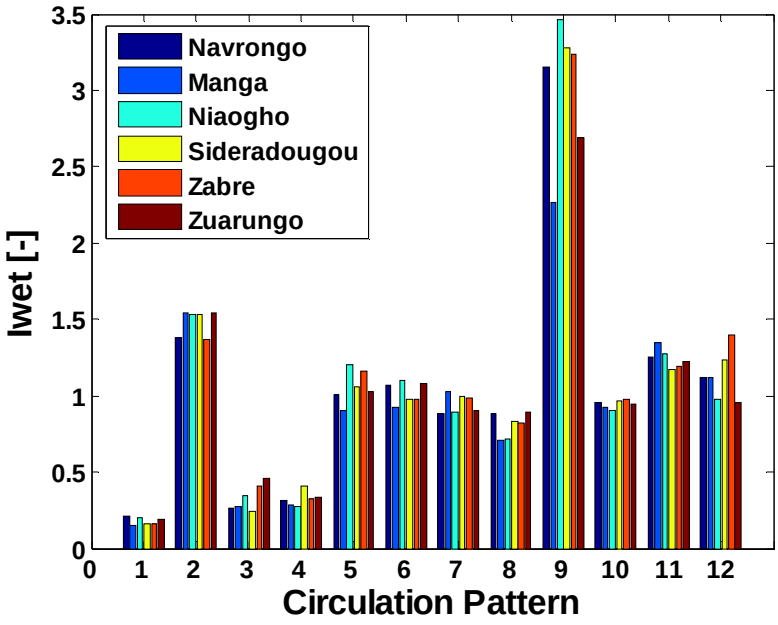

Figure 67: Wetness index of the single stations within the region corresponding to PC1. The predictor variable is the eastward component of moisture flux in 500hPa.

Figure 68 is presenting the mean anomaly distribution of the eastward component of moisture flux in 500hPa during the occurrence of the wettest (CP9) and driest (CP1) pattern. Table 28 - Table 31 are summing up the performance measures for all the regions across the Volta Basin. Table 28 is presenting the mean CP conditional wetness index [-]. Wet and dry instances of CPs for the 5 regions PC1 - PC5 are highlighted. Strong differences between the lowest and highest wetness indices and hence sharp discriminations between wet and dry patterns have been obtained for PC1, PC4 and PC5. The undefined class has been excluded from these considerations. For PC4, in which 7 CPs represent the best number of CPs, CP8 is representing the undefined class.

	PC1	PC2	PC3	PC4	PC5
CP1	**0.18**	0.91	0.95	0.68	0.71
CP2	1.48	1.11	**0.88**	1.26	0.84
CP3	0.33	1.25	**1.23**	**0.12**	0.87
CP4	0.32	0.85	0.98	2.77	0.79
CP5	1.06	0.88	0.97	1.80	1.20
CP6	1.02	1.03	1.11	1.08	1.19
CP7	0.95	**0.72**	1.00	**3.62**	**2.18**
CP8	0.81	1.08	0.98	1.45	1.11
CP9	**3.01**	0.91	0.90	-	1.28
CP10	0.94	**1.29**	1.16	-	1.14
CP11	1.24	0.92	0.98	-	**0.20**
Undef. CP	1.13	0.03	0.15	-	1.04

Table 28: Mean CP conditional wetness index [-] for the 5 regions using most suited predictor variables and number of CPs (see Table 23).

	PC1	PC2	PC3	PC4	PC5
CP1	**0.45**	2.65	3.33	1.13	2.14
CP2	3.68	3.30	**3.07**	2.10	2.58
CP3	0.82	3.60	**4.31**	**0.20**	2.60
CP4	0.81	2.44	3.40	4.74	2.39
CP5	2.64	2.56	3.38	3.01	3.63
CP6	2.54	2.90	3.87	1.81	3.61
CP7	2.36	**2.08**	3.49	**6.00**	**6.53**
CP8	2.03	3.09	3.41	2.43	3.38
CP9	**7.55**	2.61	3.14	-	3.89
CP10	2.36	**3.62**	4.10	-	3.45
CP11	3.08	2.58	3.44	-	**0.59**
Undef. CP	2.84	0.15	0.47	-	3.09

Table 29: Mean CP conditional rainfall amount [mm] for the 5 regions using most suited predictor variables and number of CPs (see Table 23).

	PC1	PC2	PC3	PC4	PC5
CP1	**3.23**	**21.20**	29.64	10.85	17.96
CP2	25.34	24.70	**28.71**	15.81	20.20
CP3	4.78	**26.13**	37.85	**1.97**	23.13
CP4	7.52	20.96	29.75	**35.00**	19.88
CP5	19.06	23.03	31.45	22.18	28.36
CP6	17.56	23.11	32.40	14.44	28.18
CP7	17.55	21.40	29.96	27.57	**49.19**
CP8	15.04	25.04	29.47	17.74	27.98
CP9	**41.49**	21.40	29.08	-	31.45
CP10	17.71	25.95	**34.62**	-	27.25
CP11	22.39	22.65	29.76	-	**5.78**
Undef. CP	20.06	6.67	28.57	-	25.73

Table 30: Mean CP conditional rainfall occurrence probability [%] for the 5 regions using most suited predictor variables and number of CPs (see Table 23).

The wettest pattern of region PC1 is revealing large anomaly differences between the European and Northern African continent (Figure 68, left). There, the gradients of the anomalies are very strong. CP2 offers a comparatively strong positive anomaly to the west of the Senegal (not shown here). The droughty patterns are differing mainly in the magnitude of the anomalies. Figure 68 (right) is presenting the most dry weather pattern conditioned to rainfall in region PC1. Generally, a tripol structure can be observed showing positive values in a zonal arranged band from 40°N up to 50°N. Negative anomalies can be found in a northern (around 60°N) and southern band around the equator.

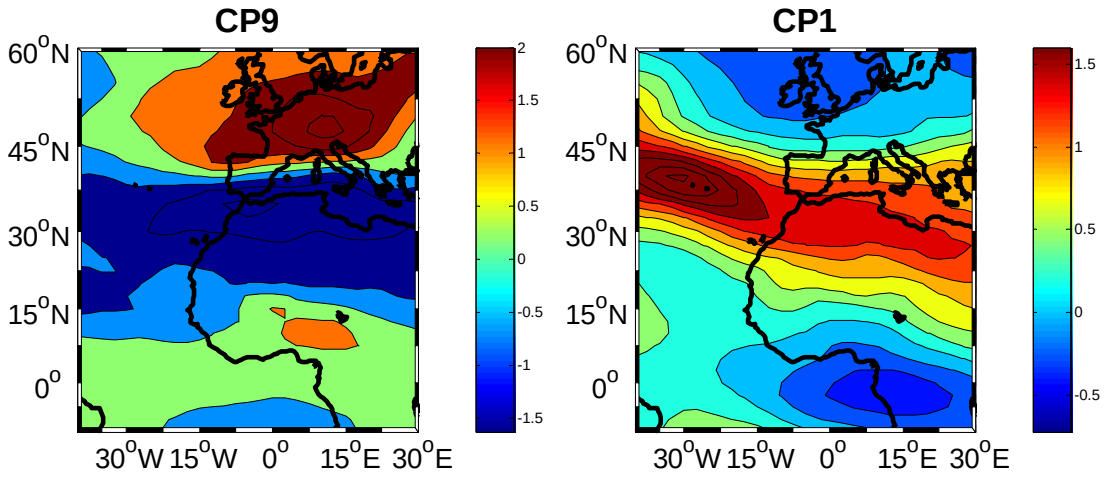

Figure 68: Mean anomalies of the eastward component of moisture flux in 500hPa corresponding to the wettest (CP9) and the driest PC (CP1) conditions within PC1.

For the southernmost regions PC2 and PC3, the eastward component of moisture flux in 300hPa has been proofed suitable to distinguish between dry and wet CPs. There, completely different mean anomalies are responsible for the wettest and driest situation (Figure 69 & Figure 70). For the regions PC4 and PC5, the wettest and driest weather patterns are similar again (Figure 71 & Figure 72).

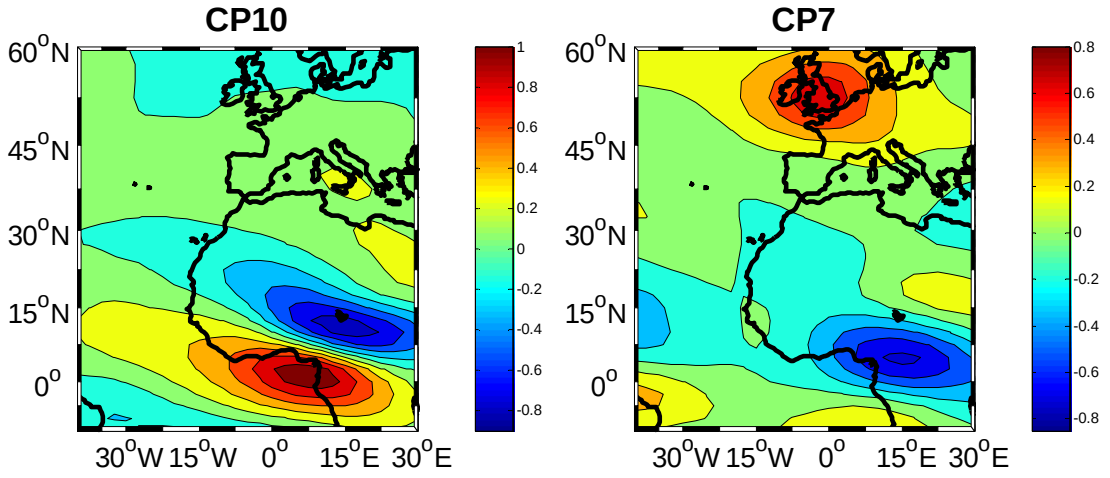

Figure 69: Mean anomalies of the eastward component of moisture flux in 300hPa corresponding to wet (CP10) and droughty (CP7) conditions within PC2.

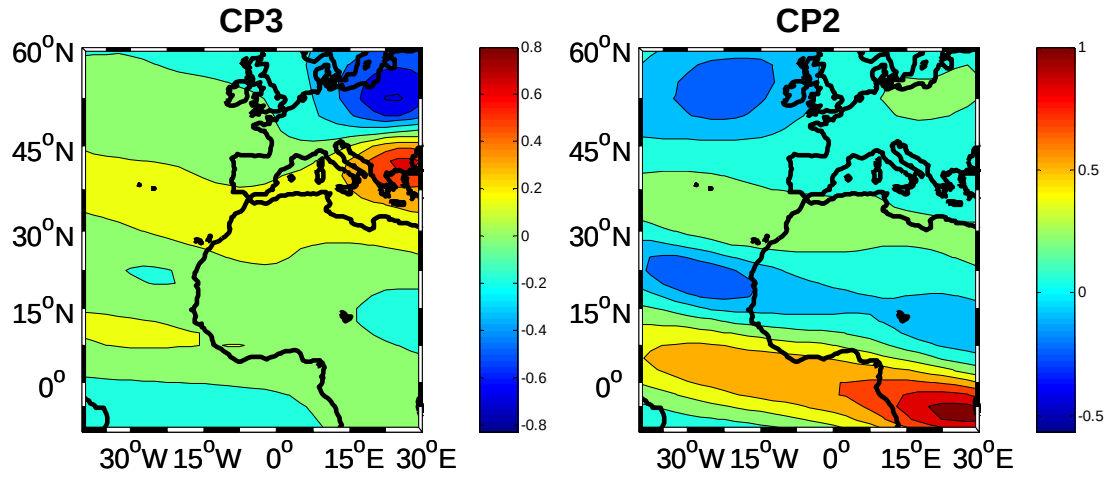

Figure 70: Mean anomalies of the eastward component of moisture flux in 300hPa corresponding to wet (CP3) and droughty (CP2) conditions within PC3.

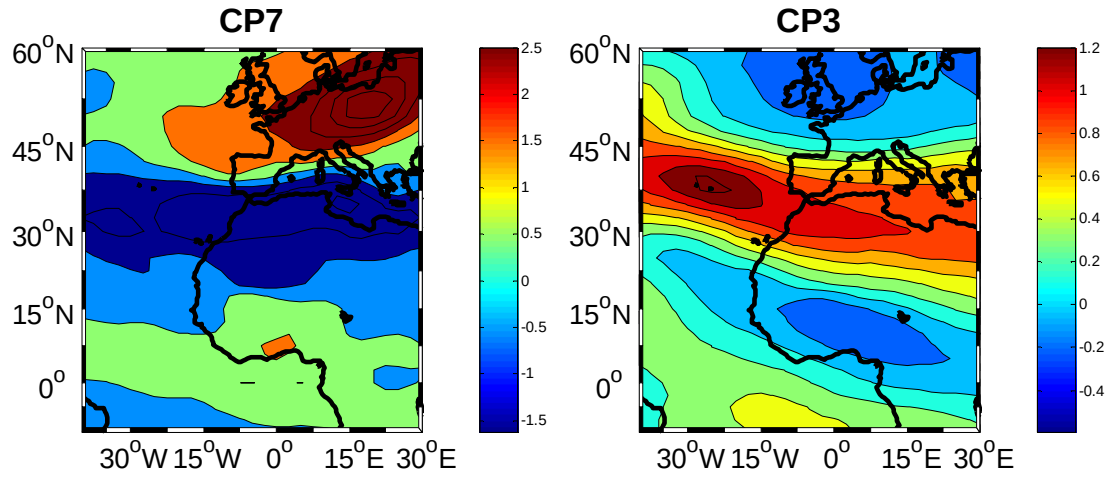

Figure 71: Mean anomalies of the eastward component of moisture flux in 500hPa corresponding to wet (CP7) and droughty (CP3) conditions within PC4.

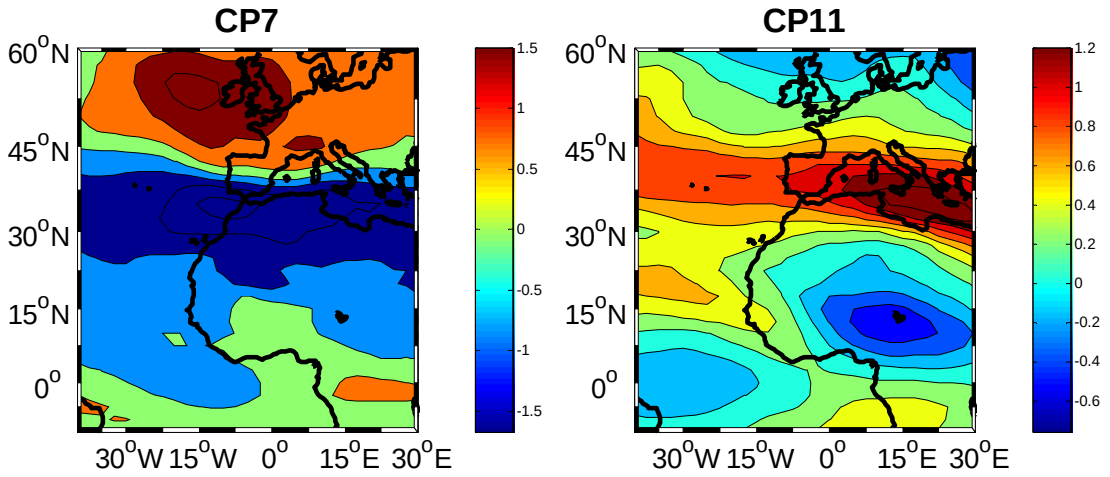

Figure 72: Mean anomalies of the eastward component of moisture flux in 300hPa corresponding to wet (CP7) and droughty (CP11) conditions within PC5.

8.1.4 Frequency Analysis of Past Weather Patterns

A change in the atmospheric circulation is often suspected to be responsible for regional climate fluctuations (e.g. LAMB, 1977). However, only few studies are dealing with time series analysis of observed atmospheric circulation patterns with respect to climate change. One reason might be that only a few long-term time series of classified atmospheric circulation patterns are available (BÁRDOSSY & CASPARY, 1990). For Central Europe the variability of the atmospheric circulation has been investigated from mid-seventeenth century (BÁRDOSSY & CASPARY, 1990; JACOBEIT, 2003A & B). BÁRDOSSY & CASPARY (1990) investigated the annual, seasonal and monthly frequencies of several European circulation types from 1881-1989. They found significant changes at all analyzed time scales. According to BECK et al. (2007), climate variation could be decomposed into two parts; one part due to frequency changes of large-scale atmospheric circulation types, and the other part due by dynamic changes within these circulation types. Within this subsection, decadal frequency variations of objective weather types in domain D1 linked to regional rainfall within the Volta Basin are analyzed from 1961-1990.

Figure 73 is illustrating the regional decadal frequencies of weather patterns for the 5 regions during the time slices 1961-1970, 1971-1980 and 1981-1990. Remarkably changes in the occurrence frequencies can be observed in many cases, e.g. CP1 of region PC3 is decreased approximately 50% in 1971-1980 and 1981-1990 compared to 1961-1960.

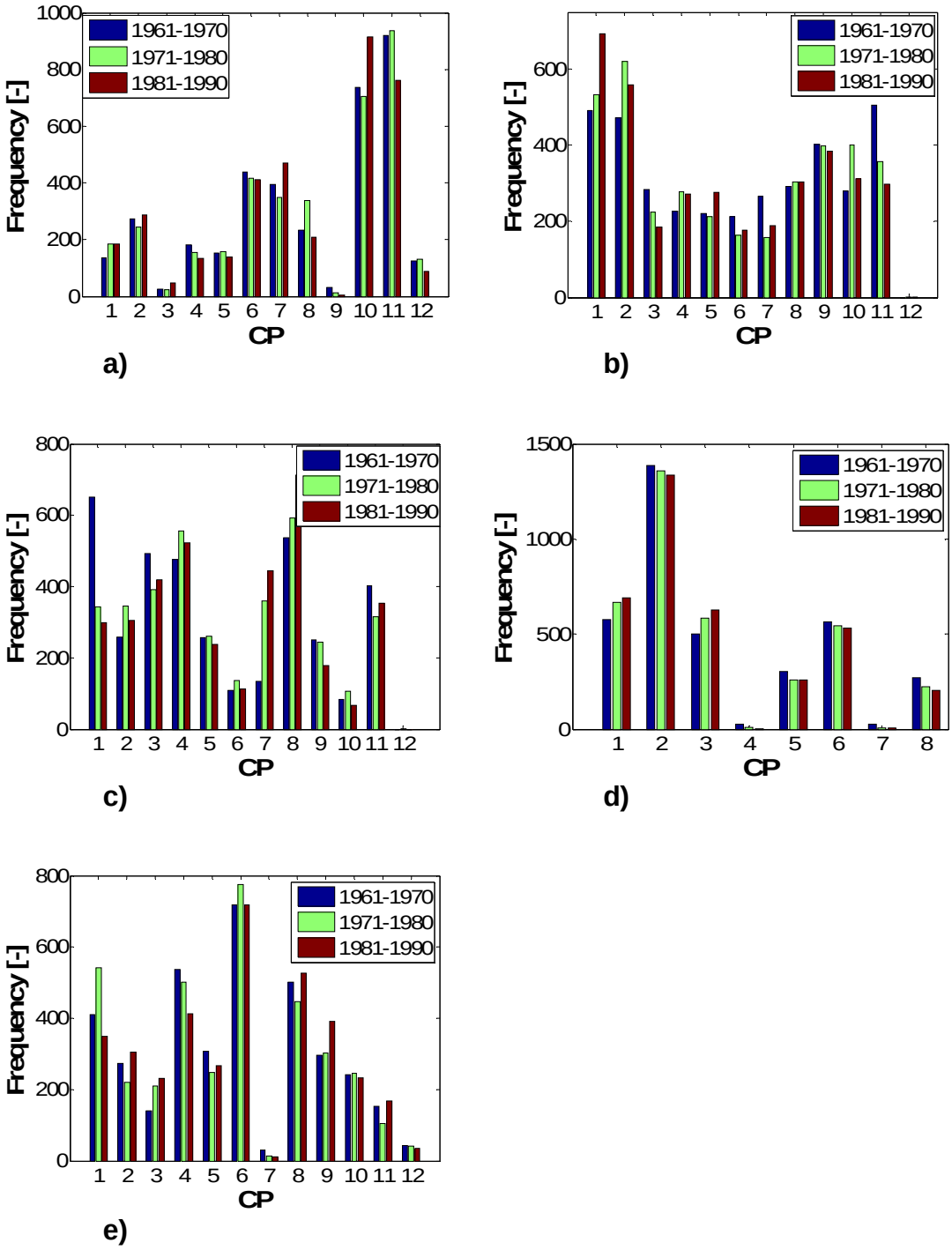

Figure 73: Decadal frequencies of past weather patterns for a) PC1, b) PC2, c) PC3, d) PC4, and e) PC5 for the periods 1961-1970, 1971-1980 and 1981-1990. The weather patterns for each region have been obtained using the most suited predictor variables (see therefore Table 22).

Generally, it can be maintained, that the occurrence frequency of the wettest weather pattern, compared to the driest pattern (Figure 74), is reduced. This is due to the fact that the dry pattern can occur during the wet and the dry seasons. The annual frequencies of the driest and wettest patterns in both regions are reflecting the regional patterns of the

EDI, presented in Chapter 5.4. For the region PC1 e.g., the wettest pattern (Figure 68, left) is missing completely during the severe drought in the 1980s. At the same time, the droughty pattern occurred comparatively frequent.

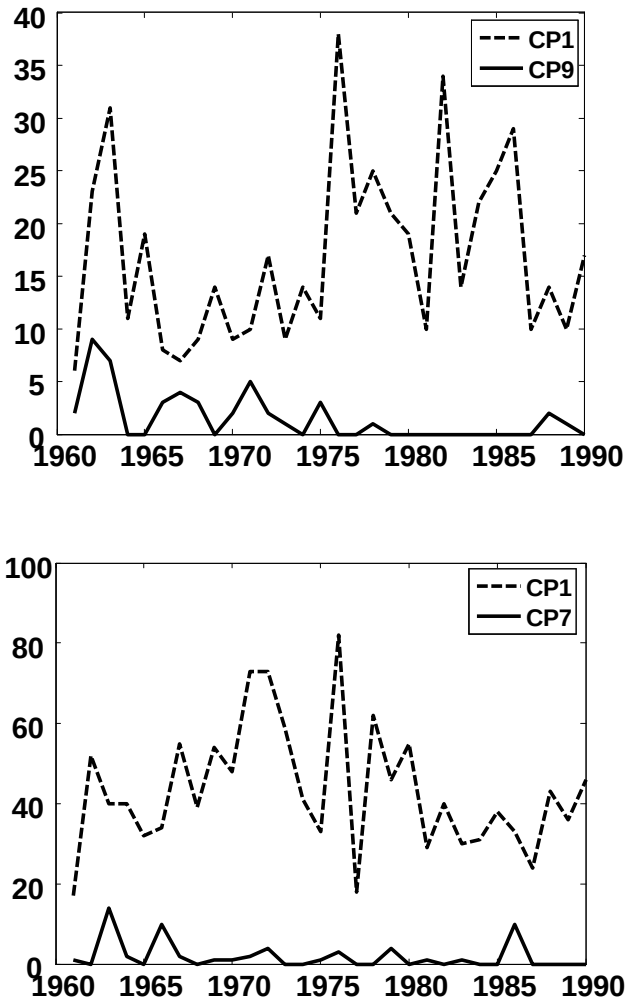

Figure 74: Interannual absolute frequencies of past drought and wet weather patterns for PC1 (top) and PC5 (bottom).

8.2 Impacts of Climate Change in a Future Climate

The impact of climate change in the future time slice 2011-2040 has been investigated in terms of ORS and weather pattern frequencies. Prior to the application of the weather pattern classification to future GCM output, the *stationarity prerequisite* must be checked. For the calculation of future weather pattern frequency, the optimized fuzzy-rules of the past calibration period 1961-1990 must be used in order to allow the direct comparison of the occurrence frequencies. A preliminary study of the mean values of both time slices and main variability modes has been applied to the most suited predictor variables (see therefore Chapter 7.2) to investigate the *stationarity prerequisite* (Chapter 8.2.1). The

trend analysis of future ORS is discussed in Chapter 8.2.2., and the frequency change of selected regions is given in Chapter 8.2.3.

8.2.1 The Stationarity-Prerequisite

To answer the question weather is it possible to apply relationships between the present-day large-scale climates to future periods (the *stationarity prerequisite*), two different aspects has been investigated:

- A comparison of the mean values of the most suited predictor variables of the NCEP/NCAR reanalysis data and the ECHAM5/MPI-OM control run for the baseline period (1961-1990) and the future time slice (2011-2040).

- An assessment of the main variability structure of the most suited predictor variables of the NCEP/NCAR reanalysis data and the ECHAM5/MPI-OM control run for the baseline period (1961-1990) and the future time slices (2011-2040).

According to Table 23, the most suited predictor variables are the eastward component of moisture flux in 300hPa and 500hPa. For that reason, they are analyzed more detailed in terms of mean values and variability structure.

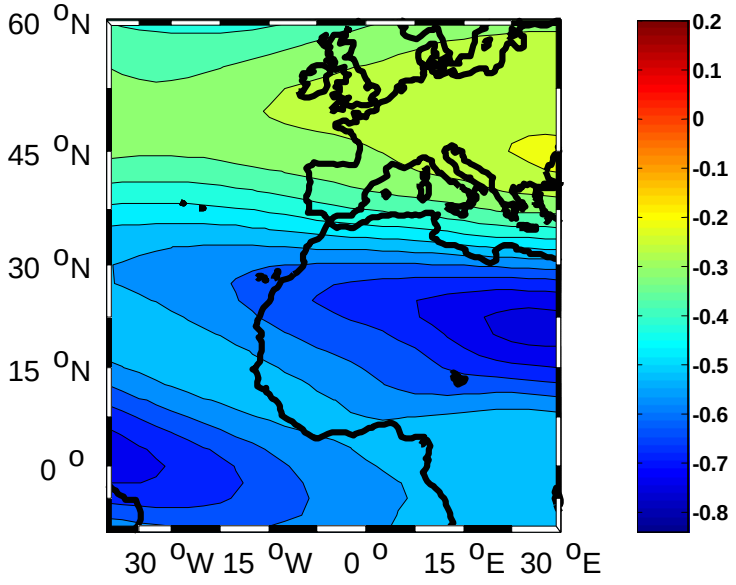

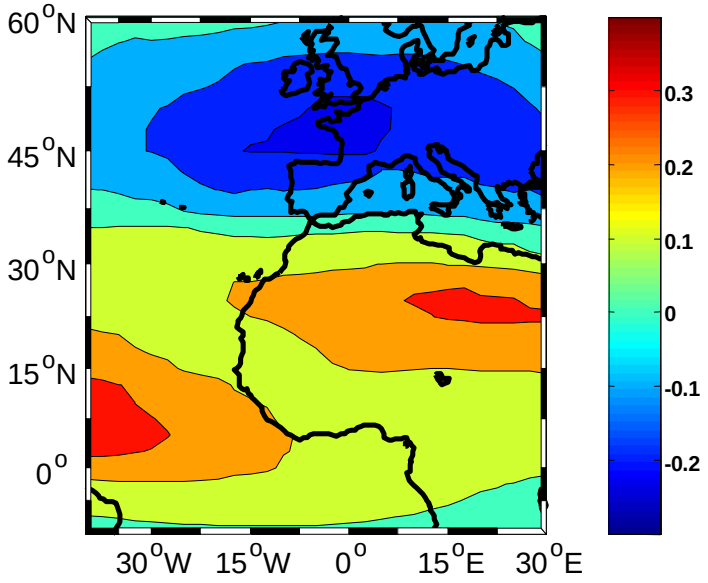

Figure 75: Mean eastward component of moisture flux in 300hPa corresponding to the NCEP/NCAR reanalysis data (top) and the ECHAM5/MPI-OM control run (bottom) for the baseline period (1961-1990). The mean values have been divided by 100.

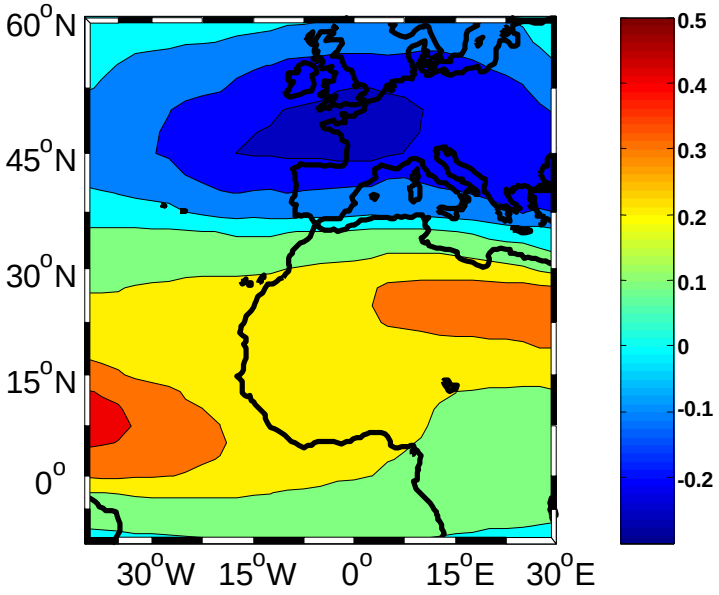

Figure 76: Mean eastward component of moisture flux in 300hPa corresponding to the ECHAM5/MPI-OM A1B scenario of the period 2011-2040. The mean values have been divided by 100.

Figure 75 is indicating the differences between the mean values of the eastward component of moisture flux in 300hPa between the NCEP reanalysis data and the

ECHAM5/MPI-OM control run of that period. One can recognize a tripole structure in both datasets; however the mathematical sign of the magnitude is reversed. The magnitude over the European continent is weakened in the reanalysis data compared to the ECHAM5 dataset. Comparing ECHAM5/MPI-OM control experiment of the baseline with the A1B scenario of the period 2011-2030, the data are found to be in good agreement (Figure 76). The 5 leading modes of reanalysis data and ECHAM5 control run generally show a good consistency. While EOF1 to EOF4 are characterized by alternate zonal belts of positive and negative loadings induced by the eastward wind speed, EOF5 shows a diagonal structure. Also, profound differences in the magnitude of the loadings can be found (Figure 85, Appendix 5).

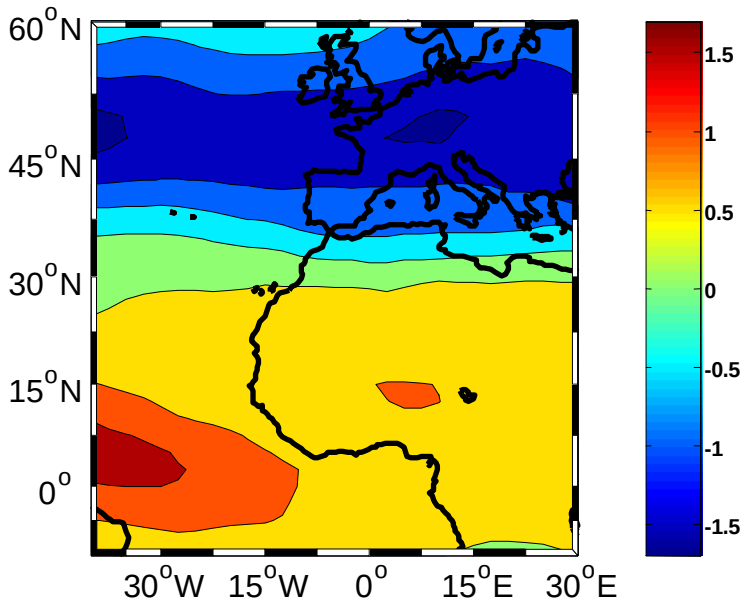

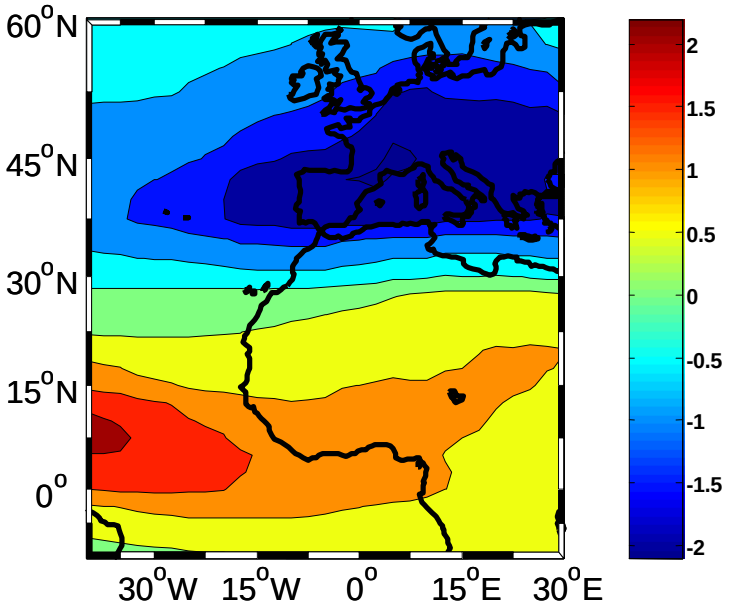

Figure 77: Mean eastward component of moisture flux in 500hPa corresponding to the NCEP/NCAR reanalysis data (top) and the ECHAM5 control run (bottom) for the baseline period (1961-1990); the mean values have been multiplied by 100.

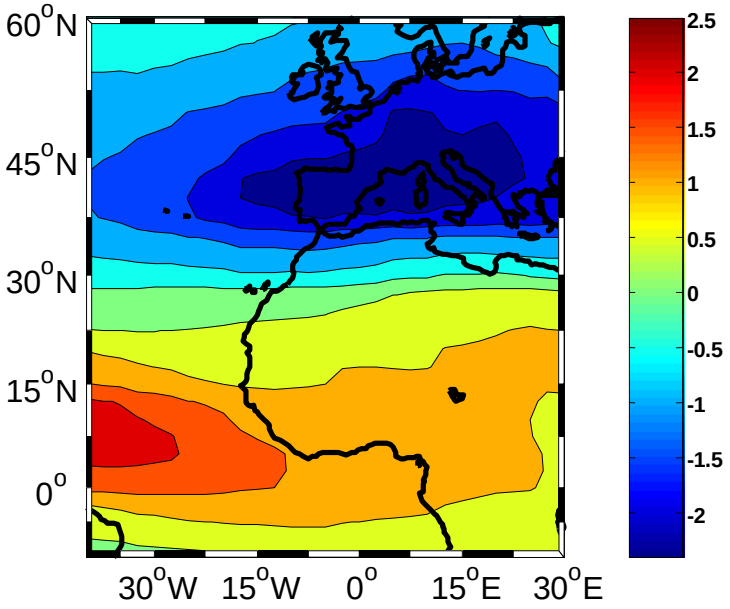

Figure 78: Mean eastward component of moisture flux in 500hPa corresponding to the ECHAM5/MPI-OM A1B scenario of the period 2011-2040. The mean values have been multiplied by 100.

For the eastward component of moisture flux in 500hPa, reanalysis and both ECHAM5 scenario, as well as control experiment can be treated as consistent. The mean values are showing a similar structure with similar magnitudes (Figure 77 & Figure 78) and the main variability patterns of the control run resemble the reanalysis data even though the EOFs are differing slightly in the magnitude (Figure 86, Appendix 5). The 5 leading EOFs of the eastward component of moisture flux in 500hPa explain a greater fraction of the total variance than for the EOFs in the 300hPa level. For both variables, no clear leading EOF pattern can be observed. This is due to the fact that most of the variability is a result of the displacement of the ITCZ. In concordance to the movement of the ITCZ, the belts with high and low wind speeds are moving up and down within the year.

8.2.2 Comparison of Past and Future Distributions of ORS Dates

Artificial regional precipitation time series have been generated for the future time slice 2001-2040 using daily ECHAM5 rainfall fields driven by the A1B scenario. The weather generator LARS-WG has been used for that purpose. A short recipe how to include climate change is given in Chapter 3.3.5. It is worthy to note, that the generated time series cannot be treated as predicted rainfall time series. Therefore, also the illustrated annual rainy seasons' onset dates cannot be seen as real onset dates. However, the relative changes in the distribution of the ORS dates can be trusted under consideration of the general uncertainties (as discussed briefly in Chapter 7). Even though the calculated regional ORS time series for the future climate should not be taken for true,, they are listed in Appendix 7. Just weak significant linear trends have been found. The distributions of the 2001-2040 onset dates, again with exception of PC2, compared to the baseline period 1961-1990 are generally shifted towards later onset dates (Figure 79). The strongest shift can be observed in the middle belt of the Volta Basin (PC3), where the trend is relatively moderate for the baseline period.

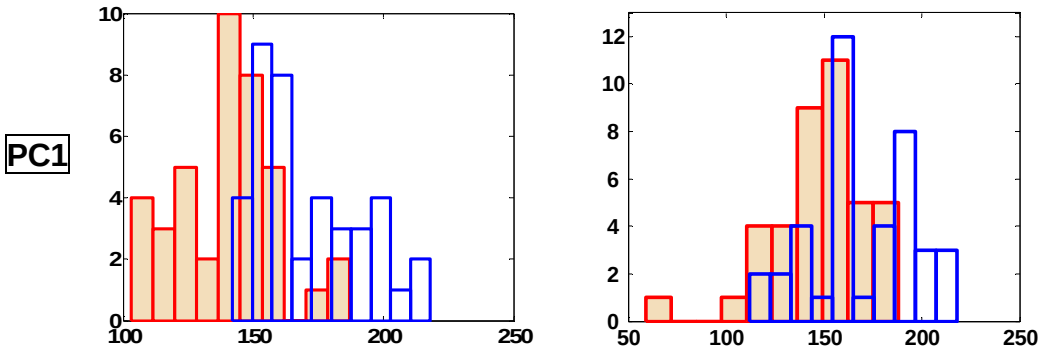

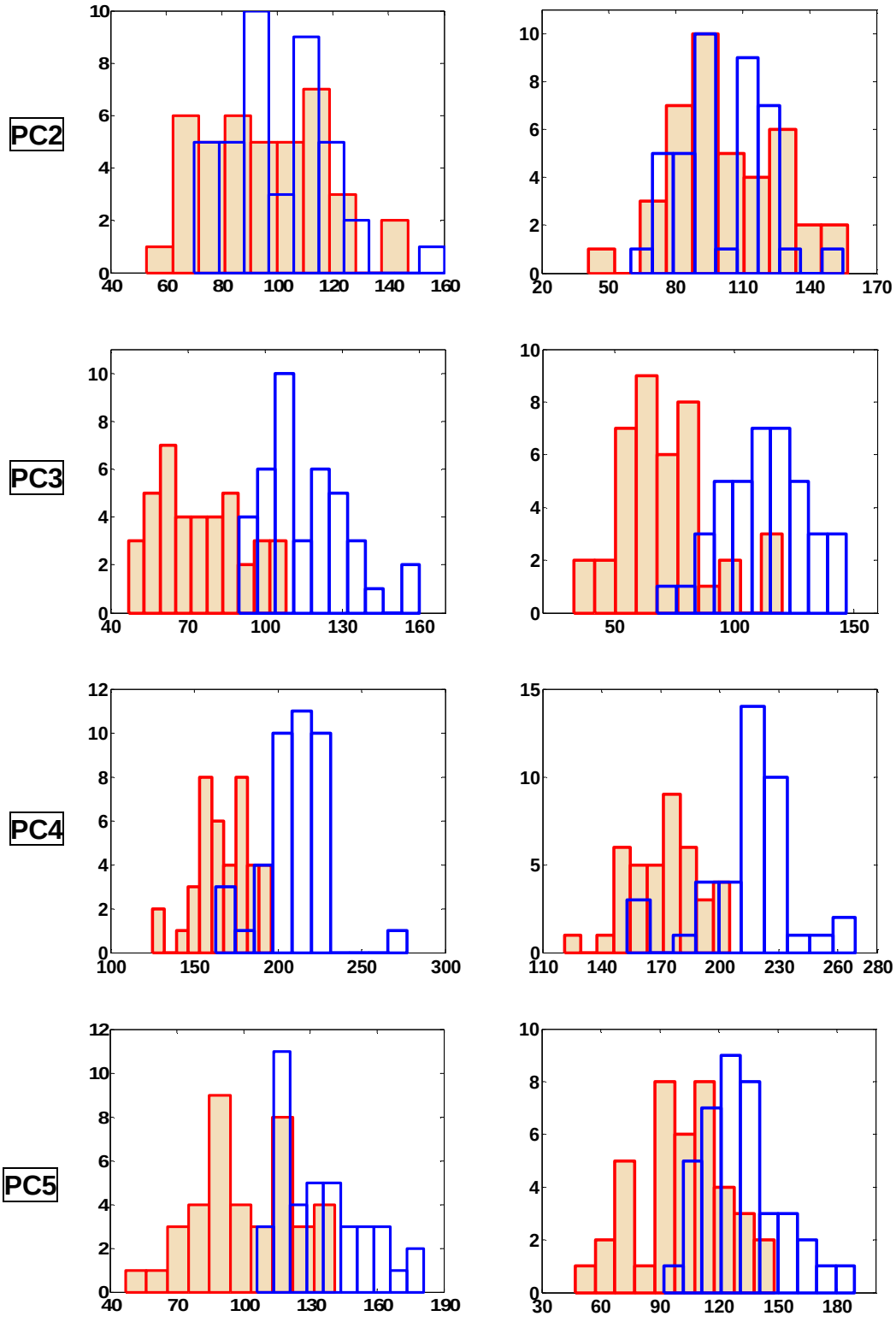

Figure 79: Histogram of the onset dates [Julian Day] from 1961-2000 (red bars) and 2001-2040 (blue bars) using Definition1 (left) and Definition2 (right) for PC1-PC5.

Table 31 is presenting the regional mean onset dates and their standard deviations for the period 2001-2040. The differences to the past mean onset dates are ranging from ~ 40 days for the northernmost region PC4 to ~ 1 week for the southernmost region PC2. Slightly differences can be observed for the different definitions.

Definition1	Mean onset (Julian day)	Standard dev. (days)
PC1	171	21
PC2	101	19
PC3	112	36
PC4	209	21
PC5	135	19
Definition2	**Mean onset (Julian day)**	**Standard dev. (days)**
PC1	170	27
PC2	100	20
PC3	112	17
PC4	215	23
PC5	131	20

Table 31: Mean regional onset dates [Julian Day] and standard deviation [days] for future time slice 2001-2040 using A1B scenario driven rainfall fields of ECHAM5.

Since the control runs establish the basic climate of the model, its ability to resemble the past should be evaluated at first. Control runs are long integrations where the model input forcings (solar irradiance, sulfates, ozone, greenhouse gases) are held constant and are not allowed evolving with time. Usually the input forcings are held fixed[16] either at present day values (i.e., for year 2000) or pre-industrial values (i.e., for 1870). For this reason, the mean values and the first 5 leading EOFs of the eastward component of moisture flux in 500hPa and 300hPa at 12:00 UTC has been compared for the ECHAM5 control run as well as for the NCEP/NCAR reanalysis data from 1961-1990.

8.2.3 Frequency Change of Weather Patterns in a Future Climate

Figure 80 is illustrating the relative change in the occurrence frequencies [%] of weather patterns linked to precipitation in different regions of the Volta Basin. For the regions corresponding to PC2, PC3 and PC4 (not shown here), the number of unclassified cases is increasing radically in the future time slice (2001-2040). This means that the fuzzy rules obtained for the classification of weather patterns for the baseline period are not optimally set for future classification. This is potentially because of the different mean values of the eastward component of moisture flux in 300hPa comparing the NCEP/NCAR reanalysis data and the ECHAM5/MPI-OM control run.

[16] In this context, "fixed" can have two different meanings. The solar forcing values are held fixed a constant, non varying number. The sulfate, ozone and greenhouse gases values, however, are fixed to continually cycle over the same 12-month input dataset every year.

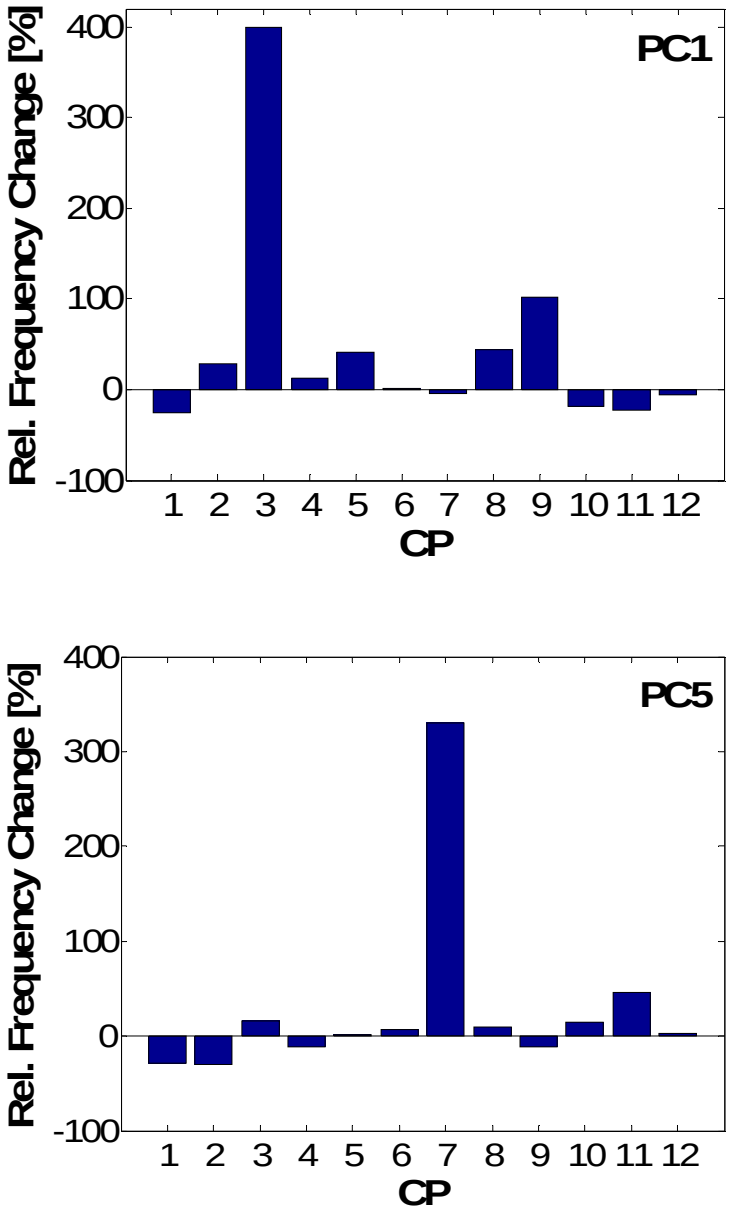

Figure 80: Relative change in the occurrence frequency of weather patterns linked to precipitation in PC1 (top) and PC5 (bottom) between reference period (1961-1990) and future period (2011-2040). The predictor variables for CPA are the eastward component of Moisture Flux in 500hP.

8.3 Summary of Chapter 8

- As speculated by farmers in the Volta Basin, very significant positive trends within the past ORS dates have been found. The trends are depending on the region. The strongest trend has been detected for region PC1, leading to a delay of around 30 days within 40 years.

- Mean monthly rainfall amount and mean monthly number of wet days are highly correlated, excepted for region PC2. There, the Pearson correlation coefficient is medium high (0.77). A monthly resolved trend analysis revealed more significant trends in the number of rainy days than in the rainfall amounts.

- For the northernmost regions (PC1, PC4 & PC5) the identified weather patterns, which are linked to dry and wet conditions are very consistent, whereas for the southern regions (PC2 and PC3), differing patterns are retained for the driest and wettest situation.

- Decadal as well as interannual variations in the occurrence frequency of the driest and wettest weather patterns can be detected.

- During the severe past drought of the 1980ies, the wettest weather patterns are missing (PC1) or reduced (PC5).

- The control run of the ECHAM5/MPI-OM is in concordance with the NCEP/NCAR reanalysis data for the baseline period in terms of the mean values and the leading modes of the eastward component of moisture flux in 500hPa. For the eastward component of moisture flux in 300hPa, the mean values are differing remarkably in their mathematical sign.

- The classification of the future period (2011-2030) cannot be applied for PC2, PC3 and PC4, because of the huge increase of cases to the undefined class using the optimized rule vector of the baseline period. For PC1 and PC5, however, they can be used. Within these regions, the extreme weather patterns, related both to wet and dry weather conditions, are increasing tremendously.

- According to the moderate scenario A1B, the ORS dates of almost all regions will experience a remarkable shift. The only exception is the coastal region PC2.

- Especially for the drought prone regions PC1 and PC4, decreasing rainfall amounts are expected. For the southern and central regions, rainfall amount is decreasing during the first (major) rainy season and increasing during the minor season in autumn

Chapter 9

9. Rainfall Variability and Agricultural Crop Yield Relationships

9.1 Introduction

More than 80% of the West African Sahel's population is rural, involved in agriculture and stock-farming. These two sectors are contributing to almost 35% of the countries' gross domestic product (GDP). Therefore, it is obvious, that climate change might seriously affect the economies of West African Sahelian countries (MOHAMED *et al.*, 2002). For West Africa and especially the Sahel zone, rainfall is the dominant climatic factor, which influences to a certain degree other factors, such as evaporation, temperature, solar radiation, wind and humidity and eventually agricultural production. Especially, in the very dry northern region of the Volta Basin, crop yield is depending primary on the seasonal or annual rainfall amount. In the southern parts, crop yields are expected to be more strongly related e.g. to the length of the rainy season (e.g. SIVAKUMAR, 1988; CHAMBERLIN & DIOP, 1999). However, additional non-climatological input factors as e.g. policies or agricultural technology can have strong effects on agricultural production.

9.2 Methodology

Statistical investigations have been carried out to reveal how crop yield variation is related to rainfall variability. Crop yield, which is an integrated measure of acreage and productivity, is expected to be stronger influenced by rainfall variability than acreage or productivity alone. First, the Pearson correlation analysis between crop yield and rainfall parameters has been conducted. The rainfall parameters are:

i) the annual rainfall amount (ARA)

ii) the number of rainy days (NRD)

iii) the onset of the rainy season (ORS) following Definition2 (Chapter 4.1.3)

iv) the cessation of the rainy season (CRS) (Chapter 4.1.4)

v) the length of the rainy season (LRS), calculated as CRS - ORS

vi) the annual mean of the EDI (MAEDI), (see Chapter 3.6.1).

In the last step, the relationship between yield of various crops varieties and climate variability has been assigned using a stepwise linear regression approach. Since rainfall is of very high spatial variability and the crop yield data are solely available for various districts across the Volta Basin, the analysis has been performed on regional scale. Therefore, crop yield data of 122 districts of the Volta Basin have been assigned to the respective rainfall region (see therefore Chapter 4.2).

The best informative predictor variable(s) for each regression model, using stepwise regression methodology, have been selected. Potential predictors were rejected which do not significantly contributing to the model (maximum p-value for a predictor = 0.05). In the case that two or more variables are added to the model, the analysis of potential collinearity by using e.g. the tolerance or the VIF value has been performed. For the multivariate cases, the predictor variables have been standardized to compare their influences to the dependent variable. The model performance is evaluated using the coefficient of determination. It expresses the explained fraction of variability in a data set. Due to a small number of cases, the adjusted coefficient of determination has also been calculated. Its value is a more realistic expression of the explained variance fraction, because it reduces the effects of variance within the data, which are simply due to chance. Furthermore, the regression line might be extremely biased by one or more outliers. Therefore, an additional robust algorithm, which uses iteratively re-weighted least squares with a bi-square weighting function, has been performed (e.g. STREET, J. O., 1988).

In order to draw inferences of a population from a sample, some prerequisites have to be checked. For each model, the residuals have been analyzed towards normality, homoscedasticity and autocorrelation.

9.3 Results

Intercorrelations of the predictor variables for each rainfall region PC1 - PC5 have been investigated and summed up schematically in Table 32:

	ORS	CRS	LRS	ARA	NRD
ORS	**1**				
CRS	**-**	**1**			
LRS	**++**	**++**	**1**		
ARA	**~**	**~**	**+**	**1**	
NRD	**~**	**~**	**~**	**+**	**1**

Table 32: Schematic representation of the correlation between various rainfall variables (++ very high positive correlation, + high positive correlation, ~ mean positive or negative correlation, - high negative correlation, -- very high negative correlation).

Very high positive correlations between LRS and ORS as well as LRS and CRS can be found. Additionally, the ARA is strongly correlated with the LRS and the NRD. The ORS and CRS shows strong negative correlations. It has to be noted, that the ORS is just an artificial date and is thus not necessarily coinciding with the actual planting date. For this study, no reliable information about the actual planting dates has been available.

Table 33 is summing up the results of the stepwise linear regression analysis. In nearly all the cases, solely one predictor variable has been chosen to model the relationship between crop yield and rainfall parameter. The adjusted coefficients of determination are ranging from 0.27 to 0.76. The annual rainfall amount (ARA) is the most frequently used variable for prediction. In a few cases, the regression line is extremely biased by one or two outliers. Then, the robust algorithm should be preferred. The regression coefficients of all models are listed in Table 33. The least-squares regression approach is represented through the slope β and the intercept Y, whereas the robust regression is using the parameters β_{rob} and Y_{rob}.

Crop	PC	Prec	R^2	Adjusted R^2	F-Ratio	β	Y	β_{rob}	Y_{rob}
Maize	1	NRD	0.42	0.38	10.05	20.88	-696.20	17.30	-389.42
	2	-	-	-	-	-	-	-	-
	3	ARA	0.68	0.64	16.66	0.00	0.87	0.00	0.90
	4	ARA	0.71	0.69	39.71	1.88	-434.32	1.86	-419.31
		ARA				0.00		0.00	
	5	NRD	0.83	0.76	17.63	0.01	-0.26	0.01	-0.22
Millet	1	ORS	0.52	0.49	15.33	-3.80	1280.43	-3.71	1266.57
		ARA				1.34		1.37	
	4	NRD	0.68	0.62	16.13	-6.96	226.00	-7.08	220.04
	5	-	-	-	-	-	-	-	-
Sorghum	1	LRS	0.57	0.54	18.69	3.73	438.91	3.75	435.63
	4	ARA	0.55	0.52	19.27	0.84	92.16	0.85	85.15
	5	NRD	0.70	0.66	18.41	0.01	-0.35	0.01	-0.14
Rice	1	NRD	0.33	0.28	6.89	27.52	-890.15	29.53	-1067.32
	2	LRS	0.43	0.36	6.03	-0.01	3.79	-0.01	3.78
	3	-	-	-	-	-	-	-	-
	4	CRS	0.31	0.27	7.27	25.40	-5487.09	22.83	-4837.34
	5	ARA	0.46	0.39	6.82	0.00	1.77	0.00	1.52
Cotton	1	-	-	-	-	-	-	-	-
	4	-	-	-	-	-	-	-	-
Groundnut	1	-	-	-	-	-	-	-	-
	4	ARA	0.57	0.54	21.05	1.47	-244.68	1.48	-249.09
	5	ARA	0.46	0.39	6.82	0.00	1.77	0.00	1.52
Beans	1	-	-	-	-	-	-	-	-
	4	ARA	0.53	0.50	18.11	1.72	-425.78	1.76	-453.35
Cocoyam	2	MAEDI	0.77	0.74	27.02	0.15	4.34	0.15	4.35
	3	NRD	0.60	0.54	11.75	0.03	2.27	0.03	2.15
	5	LRS	0.70	0.66	18.65	0.02	1.88	0.02	1.86

Yam	2	ORS	0.60	0.55	12.07	-0.01	6.10	-0.01	6.08
	3	MAEDI	0.63	0.58	13.35	2.27	10.03	2.29	10.03
	5	ORS	0.51	0.44	8.17	-0.02	13.28	-0.02	13.34
Cassava	2	-	-	-	-	-	-	-	-
	3	-	-	-	-	-	-	-	-
	5	ARA	0.48	0.41	7.25	0.01	3.30	0.01	3.20
Plantain	2	-	-	-	-	-	-	-	-
	3	-	-	-	-	-	-	-	-
	5	LRS	0.43	0.36	6.03	0.02	2.71	0.02	2.75

Table 33: Results of the linear regression analysis. ('-' is indicating that no suitable predictor variable could be found to build a regression model).

Figure 81 is illustrating the regression model of the annual rainfall amount and the yield of sorghum within region PC4 exemplarily. The used model explains 52% of the total variance.

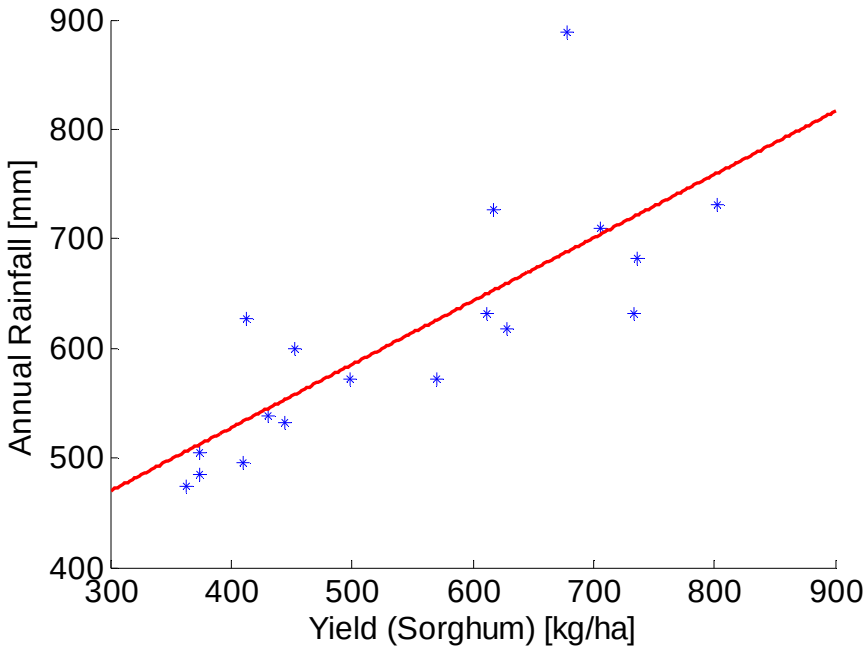

Figure 81: Relationship between annual rainfall [mm] and crop yield of Sorghum within region PC4. Adjusted R^2 of the regression = 0.52.

Two multivariate regression models have been established. For the prediction of maize yield for PC5 as well as millet yield for PC4 (Figure 82), the two predictors ARA and NRD have been used respectively. Despite of the observed intercorrelations of ARA and NRD (Table 32), multi-collinearity can be excluded (tolerance value ~ 1). The linear regression model illustrated in Figure 82 explains 76% of the total variance using the robust algorithm.

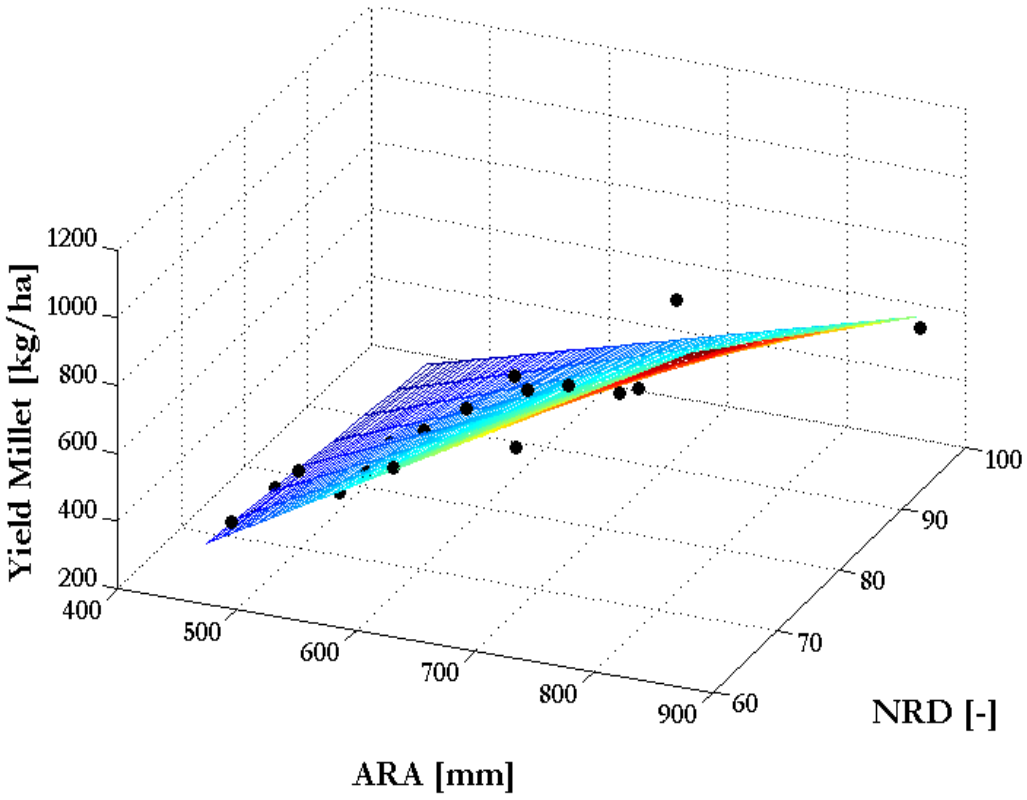

Figure 82: Millet yield as a function of ARA [mm] and NRD [-] within PC4. Adjusted R^2 of the regression = 0.76.

9.4 Conclusions

Several models between crop yield and rainfall variability parameters have been identified. Since all the assumptions for the model residuals are fulfilled, inferences from the sample can be transferred to the population. However, the detected models have to be applied with caution, especially when they are projected to future climate:

- The most prominent criticisms are the “black-box” nature of these models and difficulties of separating the yield changes due to climate from different factors, e.g. differences in land management strategies or technology (fertilizers).

- Statistical significance is depending of the sample size. As the data availability for crop yield is rather small (Burkina Faso: 1984-2001; Ghana: 1991-2001), the reliability of the climate-crop yield relationships is limited. The statistical reliability of the climate-crop yield relationships is generally higher for the regions PC1 and PC4 (Burkina Faso).

- For sake of simplicity, crop yield - rainfall variability models are often assumed to be linear. Thus, regression models appear to be more appropriate for studying the effect of current and past climate variability than the potential effects of climate change, since the latter involves extrapolation beyond the range of present-day climate used to specify the model.

Dynamic crop models, which are accounting for the fundamental biophysical mechanisms between crop response and climate factors, are more appropriate tools to estimate the effect of climate change on crop yields. Nonetheless, regression models have been found to be useful for testing the potential effects of relatively small changes in climate variables (ROSENZWEIG, C. & HILLEL, D., 1998).

Chapter 10

10. Summary & Outlook

Water availability plays a vital role in the promotion of economic growth and reduction of poverty in the Volta Basin. There is a rapidly increasing demand for water due to the increasing population pressure and the corresponding intensification of different competing sectors like e.g. hydropower generation, agriculture, mining, and domestic and industrial consumption. The strongly increasing demand of water - also in course with possible climate change - may aggravate water scarcity in future, which already exists under present-day conditions in the Volta Basin.

The agricultural sector is known to be highly vulnerable to climate change, not at least due to the mainly practiced rain-fed farming in the Volta Basin. High rainfall variability of the past often led to shortages in food supply and famines, especially in the Sahel. However, unlike the temperature, a trend analysis of rainfall data revealed no clear signal within the Volta Basin. Positive, as well as negative precipitation trends have been detected in the past. West African farmers reported of an increasing variability of the ORS, attributed to the most import variable for agriculture. Wrong decisions of the planting time, often led to total crop failure in the past, accompanied with re-sowing and high economic loss for the farmers. Therefore, their interest in scientific based prediction methods is increasing. They begin to perceive traditional decision criterions as becoming less reliable due to the increased rainfall variability.

In the context of that doctoral thesis, several aspects of the regional rainfall variability in the Volta Basin were investigated to establish groundwork for agricultural decision support. Basing on Figure 9, the results are summarized and discussed towards usability for a decision support system and include:

The development of an agricultural meaning ORS definition: Two different onset definitions were developed and applied, one for the now- and *forecasting of the planting dates* for the current season, the second one solely for ex-post application accounting additionally for a very important criterion ensuring the survival of the seedlings in the early stage of growing. In conjunction with the *impacts of climate change on rainfall variability*, the variability of past ORS dates has been analyzed to verify farmers' speculations about a possible delay of the ORS within the past decades in West Africa. Performing trend analysis, a delay of the regional ORS dates could be proofed. For the northernmost region, a delay of 35 days within 40 years was observed. The flexibility of

both definitions has been achieved by introducing fuzzy-logic based membership functions. This approach can be easily adapted to the requirements of diverse crops and different rainfall conditions.

Nowcasting of planting dates: First, *Linear Discriminant Analysis* (LDA) has been used to judge day by day whether or not the rainy season has already started. The methodology performs well, but the hit ratio of the classification is strongly depending on the region and the threshold value for the fuzzy-logic definition of the ORS. With a prior probability of ~ 7%, the hit ratios for the correct identification of the ORS range from ~ 56% within the southernmost region PC2 to ~ 79% within the northernmost region PC4. As a disadvantage one can designate the missing lead time.

Second, *Multi Objective Fuzzy Logic Based Classification* (MOFRBC) has been applied to identify weather patterns using large-scale meteorological fields, which are significantly linked with the regional ORS. Only two significant patterns could be identified:

i) For the southernmost region PC2, the skin temperature T_{SKIN} of the tropical southern Atlantic seems to play an important role for the ORS. During the regional ORS within PC2, a strong positive anomaly with its centre around 20°W10°S is establishing.

ii) The regional ORS of PC5, located in the centre of the Volta Basin, is significantly linked with the horizontal component of moisture flux in 500hPa. A very strong positive anomaly with its centre over Egypt and a relatively strong anomaly eastward of the Volta Basin are prevailing. This pattern can be physically explained with the occurrence of squall lines propagating eastwards over the Volta Basin. This speculation is confirming findings of OMOTOSHO (1984), who attributes the central part of Ghana as the region with the most squall line frequency. The squall line induced annual rainfall fraction is estimated to range between 50% and 80%. As the definition for the ORS does not account for the different sources of rainfall (Chapter 2.3.1), further analysis considering e.g. rainfall intensities for discrimination of the different rainfall mechanisms would be necessary.

Due to the good performance of the LDA and the easy-accessible data basis (measured rainfall at 29 different sites in the Volta Basin), this method is well suited to get implemented into a DSS. However, no lead time is obtained from this methodology. The fact, that only two significant weather patterns have been detected, reduces the practical usability of the MOFRBC method for the DSS. In addition to that, only probabilistic statements about the occurrence of the regional ORS could be given due to the non-uniqueness of the occurrence of these patterns during the year. The application

of MOFRBC requires modeled and thus less reliable input data. In the same manner as the LDA, no lead time for the planting preparation can be obtained. Therefore, it can be summarized that the modified MOFRBC scheme for the prediction of the ORS is of minor importance for the integration in the DSS. However, it is important for the assessment of the impacting factors on rainfall variability and more specific, for the ORS.

Forecasting of planting dates: Linear Regression Analysis (LRA) has been applied and four linear regression models have been built up to estimate the regional planting date-oriented ORS, which is following roughly the movement of the ITCZ. The performance of the LRA is strongly depending on the threshold value of the ORS definition and rather limited compared to the LDA. The used models explain between 21% and 33% of the variability. Due to this reduced performance, it is recommended to apply the LRA solely in conjunction with the LDA. The LRA is restricted for the estimation of the regional onset dates for the current year. Extrapolations to years in the future are not allowed. Just as the LDA, this approach is relying solely on measured and easy accessible rainfall data, and can be easily implemented into the DSS. A benefit can be seen in the obtained lead time for the planting preparations.

Impacts of climate change on rainfall variability: The impact of climate change on the rainfall variability has been evaluated applying numerous methodologies for different purposes:

i) Risk mapping basing on past rainfall data to answer the crucial question *when*, *where* and *what* to plant.

- Maps of long-term ORS dates (mean and standard deviation): These maps can be used as a rough guess for the planting date under co-consideration of the standard deviation. High standard deviations are generally accompanied with a high risk of total crop failure, which could be localized e.g. for the southernmost region PC2. Unlike the ORS, the standard deviations of the cessation dates are comparatively low. ORS, CRS as well as the LRS reveal partly high regional differences.

- Maps of long-term CRS and LRS dates (mean and standard deviation): Maps showing the regional differences in terms of mean value and the standard deviation of the cessation and the length of the rainy season have been derived.

- Maps of the minimum dry spell probability and risk of crop failure: Risk mapping of dry spell occurrence probability - accounting for the *false start* criterion of the ORS definition - has been performed. For regions showing high dry spell probability like e.g. the western part of region PC5, irrigation

strategies would be beneficial to reduce the risk of crop failure and thus enhance food security. A map illustrating the date of the minimum dry spell occurrence probabilities has been derived as additional information for decision support of the optimal planting time. Dry spell probability and the derived minimum dry spell probability map should be additionally consulted for the prediction of the planting time, as the *false start* criterion is of crucial importance for the survival of the seedlings and cannot be implemented directly to the ORS definition in the predictive mode.

- Regional exceedance probability plots and return periods for EARLY, NORMAL and LATE ORS dates.

All the derived maps provide important information concerning the question *when*, *where* and *what* to plant and are therefore important tools for agricultural decision support in the Volta Basin. A major shortcoming is the sparse density of the observation network accompanied with a limited reliability of the interpolated maps. Edaphic information is of similar importance for this concern and should, if available, also be considered to answer this question.

ii) Drought features: A drought definition basing on the *Effective Drought Index* EDI has been developed and applied. Basing on this definition, the important drought features like the drought duration, drought intensity and drought interarrival times could be derived. Depending strongly on the region, drought duration is varying between 72 and 116 [days], drought intensity between 56 and 84 [cum. EDI], and drought interarrival time between 143 and 204 [days]. Accounting for the mutual dependence structure of drought duration and drought intensity by means of a Clayton Copula approach, the regional return periods could be derived more reliably. These variables are of immense importance for agricultural planning.

The development of a quantitative drought definition approach and the performed drought modelling provides a first, but necessary step towards drought monitoring and the development of drought mitigation strategies in the Volta Basin.

iii) Past and future CP frequency: The impact of global climate change on the occurrence frequency of weather patterns in the Volta Basin has been analyzed. The MOFRBC has been used for the objective classification of weather patterns conditioned to local rainfall (observation time series). For this reason, the eastward component of moisture flux in 300hPa and 500hPa proofed suitable as predictor variables. A comparison of the ECHAM5/MPI-OM control run and the NCEP/NCAR reanalysis data of the baseline period 1961-1990 revealed good concordance of the mean values and the leading EOFs for the eastward

component of moisture flux in 500hPa. The eastward component of moisture flux in 300hPa showed differences in terms of a reversed sign of the mean field under maintenance of the pattern structure. The reasons could not be identified. After the classification, the time series of daily weather patterns have been derived. Comparing the past (1961-1990) with the future (2011-2040) CP occurrence frequencies, a drastic increase of droughty and wet patterns for region PC1 and PC5 have been found for the future time slice. In the regions PC2, PC3 and PC4, the number of unclassified cases is increasing drastically for the future time slice, for PC2 and PC3 probably due to the non-concordance of the ECHAM5/MPI-OM control run and the NCEP/NCAR reanalysis data. For the northernmost region PC4, where the moisture flux in the 500hPa level has been used for classification, an alteration (non-stationarity) of the past weather patterns can be concluded.

iv) Past and future dates of ORS: For the generation of artificial time series of rainfall, the LARS-WG and the CP conditional rainfall simulation methodology MOFRBC have been tested for five test sites in PC2. Both, the CP conditional rainfall simulation and the LARS-WG weather generator are found to be adequate for rainfall generation. For the validation period 1991-1999, the simple LARS-WG performs even better for the major rainy season, and the performance of MOFRBC is better for the minor rainy season. The relatively good fit of the LARS-WG can be explained due to the fact that LARS-WG replicates the mean monthly statistics of the predictand of the calibration period. Within a month, a time series is generated on the basis of the monthly distributions of the lengths of continuous sequences of wet and dry days, but the beginning of the series is chosen randomly. If the monthly statistics of the predictand remains stable over time, a relatively good agreement between simulated and measured time series can be archived. The CP conditional rainfall simulation scheme utilizes the relationship between the atmosphere and the meteorological state of the predictand for the simulation. Although this relationship is just empirically, the reliability of the results especially in terms of the timing of rainfall events can be judged higher than those of the stochastic weather generator.

v) Comparison of past and future intra-annual rainfall distribution: A weather generator was used to derive the regional intra-annual rainfall distribution. It is found that the number of rainy days will change in accordance to the rainfall amount. Especially for the drought prone regions PC1 and PC4, the rainfall amounts are decreasing. For the southern and central regions, rainfall amount is decreasing during the first (major) rainy season and increasing during the minor season in autumn leading to a more favourable situation for agriculture.

vi) The following problems should be mentioned in the context of statistical downscaling of rainfall in the Volta Basin:

- High complexity of rainfall variability: numerous rainfall affecting and modifying influences have been identified (e.g. TSA, MEI, squall lines, movement of the ITCZ).

- Reduced quality of the large-scale GCM output: inhomogeneities within the reanalysis data and non-consistency of reanalysis data and the ECHAM5 control run (Chapter 8.2.1).

- Limited experience with weather typing for statistical downscaling of rainfall on daily time scale: only a limited number of studies of rainfall modeling for West Africa exist in literature, and no well-established weather classification system exists, like e.g. the *Großwetterlagen* for Central Europe (HESS & BREZOWSKY, 1977).

In Chapter 10, stepwise linear regression analysis has been carried out to check whether or not regional crop yield can be modelled by means of rainfall variability. Rainfall variability has been assessed in terms of the annual rainfall amount, the number of rainy days, the onset, cessation and length of the rainy season and the annual mean of the monthly averaged Effective Drought Index. Regression models, which explain up to 80% of the total variance of crop yield, could be established. The annual rainfall amount is the most frequent used predictor variable for this purpose. Due to the limited sample size, the found relationships should not be applied without caution.

OUTLOOK: The developed methodologies, especially concerning the prediction of the regional ORS should be applied and tested for future periods in the Volta Basin. This should be done by the respective farming management authorities in Ghana and Burkina Faso. For this reason, the developed methodologies were transferred to stakeholders in Ghana and Burkina Faso. A training workshop was held in January 2008 at the *United Nations University Institute for Natural Resources* (UNU-INRA) in Accra (Ghana) and at the Direction *Générale des Ressources en Eau* (DGRE) in Ouagadougou (Burkina Faso).

Extending the analysis to further drought-prone Sahelian countries could be beneficial for the local agricultural and water management authorities. In this context, the application and improvement of the ORS definition is intended. As an alternative of adjusting the membership functions of the ORS definition using values from literature, an optimization of the definition towards the annual crop yield could be performed. Dynamical vegetation models (like e.g. CropSyst) could be driven for that purpose using the simulated crop yield as objective function. In this way, the “optimal” crop

requirements for a certain location could be identified. A shortcoming of this alternative is the extensive information required for dynamical modeling (soil physical and soil chemical properties, annual management, etc.). For the Volta Basin these information were not available, however, a case study for Cameroon is in preparation.

More emphasis should be given to climate change and its impacts on agriculture. Therefore, more scenarios should be considered in order to encapsulate the range of uncertainties. Reliable estimation of future drought probabilities, for example, is a necessary step towards the development of adaptation and mitigation strategies.

TABLE OF LITERATURE

ACHEAMPONG, P.K. (1988): Water Balance Analysis for Ghana. *Geography*, **73**:125-131.

ADIKU, S. G. K.; STONE, R. C. (1995): Using the Southern Oscillation index for improving rainfall prediction and agricultural water management in Ghana. *Agricultural Water Management*, **29**:85-100.

ADIKU, S. G. K. (2003): Exploring options for improving crop productivity within some farming zones of Ghana using coupled climatic-crop models. START, Washington DC, USA. Final report. (http://www.start.org/Program/PDF_Program_Reports/AI_final_reports/AI_1/Adiku_Finalreport.doc).

ATI, O. F.; STIGTER, C. J.; & OLADIPO, E. O. (2002): A comparison of methods to determine the onset of the growing season in Northern Nigeria. *International Journal of Climatology*, **22**:731-742.

BÁRDOSSY, A.; & PLATE, E. J. (1991): Modeling Daily Rainfall using a Semi-Markov Representation of Circulation Pattern Occurrence. *Journal of Hydrology*, **122**:731-742.

BÁRDOSSY, A.; & PLATE, E. J. (1992): Space-time model of daily rainfall using atmospheric circulation patterns. *Water Resources Research*, **28**:1247-1259.

BÁRDOSSY, A.; DUCKSTEIN, L.; & BOGÁRDI, I. (1995): Fuzzy rule based classification of atmospheric circulation patterns. *International Journal of Climatology*, **15**:1087-1097.

BÁRDOSSY, A.; & CASPARY, H. J. (2001A): Detection of Climate Change in Europe by analyzing European atmospheric circulation patterns from 1881-1989. *Theoretical and Applied Climatology*, **42**:155-167.

BÁRDOSSY, A.; STEHLIK, J.; & CASPARY, H. J. (2001B): Generating of areal precipitation series in the upper Neckar catchment. *Physics and Chemistry of the Earth*, **9**:683-687.

BÁRDOSSY, A.; STEHLÍK, J.; & CASPARY, H.-J. (2002): Automated objective classifcication of daily circulation patterns for rainfall and temperature downscaling based on optimised fuzzy rules. *Climate Research*, **23**:11-22.

BÁRDOSSY, A.; & FILIZ, F. (2005): Identification of flood producing atmospheric circulation patterns. *Journal of Hydrology*, **313**:48-57.

BECK, C.; JACOBEIT, J.; & JONES, P. D. (2007): Frequency and within-type variations of large-scale circulation types and their effects on low-frequency climate variability in central Europe since 1780. *International Journal of Climatology*, **4**:473-491.

BEER, T.; GREENHUT, G. K.; & TANDOH, S. E. (1977): Relations between the Z criterion for the subtropical high, Hadley cell parameters and the rainfall in Northern Ghana. *Monthly Weather Review*, **105**:849-855.

BENOIT, P. (1977): The start of the growing season in northern Nigeria. *Agricultural Meteorology*, **18**:91-99.

BERAN, M. A.; & RODIER, J. A. (1985): Hydrological aspects of Drought. *WMO-UNESCO Panel Report. Studies and Reports in Hydrology*. UNESCO Press, Paris.

BLÖSCHL, G. (2005): Statistical upscaling and downscaling in hydrology. *Encyclopedia of Hydrological Sciences*. Anderson, M. G. (ed.), J. Wiley & Sons, Chichester.

BROOKS, N. (2004): Droughts in the African Sahel: Long term perspectives and future prospects. *Tyndall Centre Working Paper,* **(61)**:31.

BÜRGER, G. (2002): Selected precipitation scenarios across Europe. *Journal of Hydrology,* **262**:99-110.

CAHALAN, R. F.; WHARTON, L. E.; & WU, M. -L. (1996): Empirical orthogonal functions of monthly precipitation and temperature over the United States and homogeneous stochastic models. *Journal of Geophysical Research*, **26**:309-318.

CANCELLIERE, A.; & SALAS, J. D. (2004): Drought length properties for periodic-stochastic hydrologic data. *Water Resources Research*, **40**:W02503.

CHAMBERLIN P.; & DIOP, M. (1999): Inter-relationships between groundnut yield in Senegal, Interannual rainfall variability and sea surface temperatures. *Theoretical and Applied Climatology*, **63**:163-181.

CHAMBERLIN P.; & DIOP, M. (2003): Application of daily rainfall principal component analysis to the assessment of the rainy season characteristics in Senegal. *Climate Research*, **23**:159-169.

CORTE-REAL, J.; ZHANG, X.; & WANG, X. (1995): Downscaling GCM information to regional scales: a non-parametric multivariate regression approach. *Climate Dynamics*, **7**:413-424.

DASILVA, A. M.; YOUNG, C.C.; & LEVITUS, S. (1994): *Atlas of surface marine data*. **Vol.1**, Algorithms and procedures, NOAA Atlas Series, 6, 74 pp, NOAA, Washington, D.C.

DAVIDSON, N. E.; MCBRIDE, J. L.; & MCAVANEY, B. J. (1983): The onset of the Australian monsoon during winter MONEX: Synoptic aspects. *Monthly Weather Review* **111**:496-516.

DRACUP, J. A. (1980A): On the definition of droughts. *Water Resources Research*, **16**:297-302.

DRACUP, J. A. (1980B): On the statistical characteristics of drought events. *Water Resources Research*, **16**:289-296.

DROBINSKI, P.; SULTAN, B.; & JANICOT, S. (2005): Role of the Hoggar massif in West African monsoon onset. *Geophysical Research Letter*, **32**:L01705.

DURBIN, J.; & WATSON, G. S. (1950): Testing for serial correlation in least squares regression. *Biometrika*, **37**:409-428.

ELDRIDGE, R. H. (1957): A synoptic study of West African disturbance lines. *Quarterly Journal of the Royal Meteeorological Society*, **83**:303-314.

FINK, A.; & REINER, A. (2003): Spatio-temporal Variability of the Relation between African Easterly Waves and West African Squall Lines in 1998 and 1999. *Journal of Geophysical Research*, **108**(D11), 4332.

FONTAINE, B.; PHILIPPON, N.; TRZASKA, S.; & ROUCOU, P. (2002): Spring to summer changes in the West African monsoon through NCEP/NCAR reanalyses (1968–1998), *Journal of Geophysical Research*, **107**(D14), 4186.

GRAEF, F.; & HAIGIS, J. (2001): Spatial and temporal rainfall variability in the Sahel and effects on farmers' management strategies. *Journal of Arid Environments*, **48**(2):221-231.

GIANNINI, A.; SARAVANAN, R.; & CHANG, P. (2003): Oceanic forcing of Sahel rainfall on interannual to interdecadal time scale. *Science*, **302**:1027-1030.

GIORGI, F.; & MEARNS, L. O. (1991): Approaches to regional climate change simulation: A review, *Reviews of Geophysics*, **29**:191-216.

GIORGI, F. et al. (2001): Regional climate information – evaluation and projections. Chapter 10 in Climate Change 2001: The Scientific Basis. Third Assessment Report of the Intergovernmental Panel on Climate Change (IPCC), Cambridge University Press, Camebridge, U.K., 583-638.

HAHN, G. J.; & SHAPIRO, S. S. (1994): Statistical Models in Engineering. John Wiley & Sons, New York, 1994.

HASTENRATH, S. (2000): Interannual and longer term variability of upper-air circulation over the tropical Atlantic and West Africa in boreal summer. *International Journal of Climatology*, **20**:1415-1430.

HAYWARD, D.; & OGUNTOYINBO, J. (1987): Climatology of West Africa. Hutchindson.

HENDON, H. H.; & LIEBMANN, B. (1990): A composite study of onset of the Australian summer monsoon. *Journal of the Atmospheric Sciences*, **47**:2909-2923.

HESS, P.; & BREZOWSKY, H. (1977): Katalog der Großwetterlagen Europas 1881-1976. *Ber. Dt. Wetterd.*, **15** (113).

HESS, T. M.; STEPHENS, W.; & MARYAH, U. M. (1995): Rainfall trends in the North East Arid zone of Nigeria 1961-1990. *Agricultural and Forest Meteorology*, **74**:87-97.

HEWITSON, B.; & CRANE, R. (1996): Climate downscaling: techniques and application. *Climate Research*, **7**:85-95.

HEWITSON, B. C., CRANE, R. G. (2002): Self-organizing maps: applications to synoptic climatology. *Climate Research*, **22**:13-26.

HOLLAND, P. W.; & WELSCH, R. E. (1977): Robust Regression Using Iteratively Reweighted Least-Squares, *Communications in Statistics: Theory and Methods*, **A6**:813-827.

HOLLAND, G. J. (1986): Interannual variability of the Australian summer monsoon at Darwin: 1952-82. *Monthly Weather Review*, **114**:594-604.

HOTELLING, H. (1935): The most predictable criterion. *Journal of Educational Psychology*, **26**:139-142.

HOUGHTON, J.T., et al., EDS., 2001: *Climate Change 2001: The Scientific Basis.* Cambridge Univ. Press, Cambridge.

HULME, M. (1992): Rainfall changes in Africa: 1931-1960 to 1961-1990. *International Journal of Climatology*, **7**:685-699.

HULME, M. (2001): Climate Perspectives on Sahelian desiccation: 1973-1998. *Global Environmental Change*, **11**:19-29.

HUTH, R.; & KYSELÝ, J. (2000): Constructing site specific climate change scenarios on a monthly scale using statistical downscaling. *Theoretical and Applied Climatology*, **66**:13-27.

HUTH, R. (2000): A circulation classification scheme applicable in GCM studies. *Theoretical and Applied Climatology,* **67**:1-18.

ILESANMI, O. O. (1972): An empirical formulation of the onset, advance and retreat of rainfall in Nigeria. *Journal of Tropical Geography*, **34**:17-24.

IPCC (2001): Climate Change 2001: Impacts, Adaptation, And Vulnerability: Contribution Of Working Group II To The Third Assessment Report of the IPCC. Cambridge University Press, Cambridge.

JACOBEIT, J. (2003A): Links between flood events in central Europe since AD 1500 and large-scale atmospheric circulation modes. *Geophysical Research Letters*, **4**:1172.

JACOBEIT, J. (2003B): Atmospheric circulation variability in the North-Atlantic-European area since the mid-seventeenth century. *Climate Dynamics*, **4**:341-352.

JACOBEIT, J.; & DÜNKELOH, A. (2003C): Zirkulationsdynamik mediterraner Niederschlagsschwankungen - kanonische Korrelationsanalyse für das Winterhalbjahr seit Mitte des 20. Jahrhunderts. - In: Beiträge zur Klima- und Meeresforschung; von Chmielewski, F. - M.; & Foken, T. (eds.); Berlin und Bayreuth, 39-49.

JACOBEIT, J.; PHILIPP, A.; & NONNENMACHER, M. (2006): Atmospheric circulation dynamics linked with prominent discharge events in Central Europe. *Hydrological Sciences Journal*, **5**:946-965.

JANICOT, S.; MORON, V.; & FONTAINE, B. (1996): Sahel droughts and ENSO dynamics. *Geophysical Research Letters*, **23**:515–518.

JUDGE, G. G.; HILL, R. C,; GRIFFITHS, W. E.; LUTKEPOHL, H.; & LEE, T.-C. (1988): Introduction to the Theory and Practice of Econometrics. Wiley: New York.

JUNG, G. (2006): Regional Climate Change and the Impact on Hydrology in the Volta Basin of West Africa. Doctoral thesis.

KAISER, H. F. (1958): The varimax criterion for analytic rotation in factor analysis. *Pyrometrical*, **23**:187-200.

KALNAY ET AL. (1996): The NCEP/NCAR 40-year reanalysis project. *Bulletin of the American Meteorological Society*, **77**:437-470.

KAPLAN, A.; KUSHNIR, Y.; & CANE, M. A. (2000): Reduced space optimal interpolation of historical marine sea level pressure. *Journal of Climatology*, **13**:2987-3002.

KAPLAN, A.; CANE, M.; KUSHNIR, Y.; CLEMENT, A.; BLUMENTHAL, M.; & RAJAGOPALAN, B. (1998): Analyses of global sea surface temperature 1856-1991. *Journal of Geophysical Research*, **103**(18):567-589.

KASEI, C. N.; & AFUAKWA, J. J. (1991): Determination of optimum planting date and growing season of maize in the northern savannah zone of Ghana; Soil Water Balance in the Sudan Sahelian Zone. *Proceedings of the Niamey Workshop*, February 1991. IAHS Publ. no. 199.

KATZ, R. W.; & PARLANGE, M. B. (1993): Effects of an index of atmospheric circulation on stochastic properties of precipitation. *Water Resources Research*, **29**:2335–2344.

KATZ, R. W.; & PARLANGE, M. B. (1995): Generalizations of Chain-Dependent Processes: Application of Hourly Precipitation. *Water Resources Research*, **31**(5):1331-1341.

KATZ, R. W.; & ZHENG, X. (1999): Mixture Model for overdispersion of precipitation. *Climate Change*, **8**:2528–2537.

KAMARA, S. I. (1986): Origins and Types of Rainfall in West Africa. *Weather*, **41**:48-56.

KLIWA (2002): Langzeitverhalten der Hochwasserabflüsse in Baden-Württemberg und Bayern – *KLIWA Berichte*, Heft 2, Landesanstalt für Umweltschutz Baden-Württemberg; Bayerisches Landesamt für Wasserwirtschaft; & Deutscher Wetterdienst (eds.).

KOWALL, J. A.; & KASSAM, A. H. (1978): Agricultural Ecology of Savannah - a study of West Africa. Oxford University Press.

KUNSTMANN, H.; & JUNG, G. (2007): Agricultural Influence of soil-moisture and land use change on precipitation in the Volta Basin of West Africa. *Intl. J. River Basin Management*, **5**(1):9–16.

LAMB, H. H. (1977): Climate present, past and future Volume 2: Climatic history and the future. Methuen & co Ltd, London.

LAMB, P. J.; & PEPPLER, R. A. (1992): Further case studies of tropical Atlantic surface atmospheric and oceanic patterns associated with sub-Saharan drought. *Journal of Climate,* **5:**476-488.

LAUX, P.; KUNSTMANN, H.; & BÁRDOSSY A. (2007): Linking the West African monsoon's onset with atmospheric circulation patterns. Quantification and Reduction of Predictive Uncertainty for Sustainable Water Resource Management. IAHS Publ. **313**:40-50.

LAUX, P.; KUNSTMANN, H.; & BÁRDOSSY A. (2008): Predicting the Regional Onset of the Rainy Season in West Africa. *International Journal of Climatology*, **28**(3):329-342.

LE BARBÉ, L.; & LEBEL, T. (1997): Rainfall climatology of the Hapex-Sahel region during the years 1950–1990. *Journal of Hydrology*, **188–189**:43-73.

LEROUX, M. (2001): The Meteorology and Climate of Tropical Africa. Springer - Praxis books in environmental sciences, London.

L'HOTE, Y. E. M., G. (1995). Carte Afrique de l'Ouest et centrale: Precipitations moyennes annuelles (periode 1951-1989). (1995). Carte Afrique de l'Ouest et centrale: Precipitations moyennes annuelles (periode 1951-1989). Paris, ORSTOM Institut de recherche pour le developpement.

LI, K. Y.; COE, M. T.; RAMANKUTTY, N.; & DE JONG, R. (2007): Modeling the hydrological impact of land-use change in West Africa. *Journal of Hydrology***, 337**(3-4):258-268.

LISTER, D. H.; & PALUTIKOV, J. P. (2001): Seasonal climate forecasting for West Africa: a review. CLIMAG-West Africa.
(Deliverable 4, http://www.ibimet.cnr.it/Case/climag/download/Deliverable_D4.pdf).

LOS, S. O.; WEEDON, G. P.; NORTH, P. R. J.; KADUK, J. D. ; TAYLOR, C. M.; & COX, P. M. (2006): An observation-based estimate of the strength of rainfallvegetation interactions in the Sahel, Geophysical Research Letters, **33**, L16402.

MALHI, Y.; & WRIGHT, J. (2004): Spatial Patterns and Recent Trends in the Climate of Tropical Rainforest Regions, *Philosophical Transactions of the Royal Society of London,* **359**:311-329.

MATULLA, C.; & HAAS, P. (2003): Prädiktorsensitives Downscaling gekoppelt mit Wettergeneratoren: saisonale und tägliche CC-Szenarien in komplex strukturiertem Gelände. *GKSS-Report* 2003/24.

MARTIN, N. (2005): Development of a water balance for the Atankwidi catchment, West Africa – A case study of groundwater recharge in the semi-arid climate. PhD thesis; Georg-August Universität Göttingen.

MARX, A.; KUNSTMANN, H.; SCHÜTTEMEYER, D.; & MOENE, A. F. (2007): Uncertainty analysis for satellite derived sensible heat fluxes and scintillometer measurements over Savannah environment and comparison to mesoscale meteorological simulation results. *Agricultural and Forest Meteorology*, (in press), doi:10.1016/j.agrformet.2007.11.009.

MASON, S. J. (1998): Seasonal forecasting of South African rainfall using a non-linear discriminant analysis model. *International Journal of Climatology*, **18**:147-164.

MATHIER, L. (1992): The use of geometric and gamma-related distributions for frequency analysis of water deficit. *Hydrology and Hydraulics*, **6**:239-254.

MCGREGOR, G. R.; & NIEUWOLT, S. (1998): Tropical climatology. Chichester, New York, Weinheim, Brisbane, Singapore, Toronto.

MCMAHON, T. A.; & DIAZ ARENAS, A. (1982): Methods of computation of low streamflow, *Studies and Reports in Hydrology 36*. UNESCO Paris 95, France.

MOHAMED, A. B.; VAN DUIVENBOODEN, N.; & ABDOUSSALLAM, S. (2002): Impact of Climate Change on Agricultural Production in the Sahel – Part 1. Methodological Approach and Case Study for Millet in Niger. *Climatic Change*, **54**(3): 327-348.

MORID, S., SMAKHTIN, V.; BAGHERZADEH, K. (2007): Drought forecasting using artificial neural networks and time series of drought indices. *International Journal of Climatology*, (in press), doi:10.1002/joc.1498.

MORID, S., SMAKHTIN, V.; MOGHADDASI, M. (2006): Comparison of seven meteorological indices for drought monitoring in Iran. *International Journal of Climatology*, **26**(7):971-985.

MURPHY, J. M. (1999): An evaluation of statistical and dynamical techniques for downscaling local climate. *Journal of Climate*, **12**:2256-2284.

Murphy, J. M. (2000): Predictions of climate change over Europe using statistical and dynamical downscaling techniques. *Inernational Journal of Climatology*, **20**:489-501.

NAKICENOVIC, N.; & SWART (2000): Special Report on Emission Scenarios. A special report of Working Group III for the Integovernmental Panel on Climate Change. Cambridge University Press, 599 pp.

NEUMANN, R.; JUNG, G.; LAUX, P.; & KUNSTMANN, H. (2006): Climate trends of temperature, precipitation and river discharge in the Volta Basin of West Africa. *International Journal of River Basin Management*, **5**:17-30.

NICHOLSON, S. E. (1994): Recent rainfall fluctuations in Africa and their relationship to past conditions over the continent. *The Holocene*, **4**:121-131.

NICHOLSON, S. E. (2001): Climatic and environmental change in Africa during the last two centuries. *Climate Research*, **17**:123-144.

NICHOLSON, S. E. (2005): On the question of the recovery of the rains in the West African Sahel. *Journal of Arid Environments*, **63**:615-641.

OGUNTUNDE, P. G. (2004): Evapotranspiration and complimentary relations in the water balance of the Volta Basin: Field measures and GIS-based regional estimates. Ecology and Development Series No. 22; Cuvillier Verlag Göttingen.

OMOTOSHO, J. B. (1984): Spatial and seasonal variations of line squalls over West Africa. *Archiv für Meteorologie, Geophysik und Bioklimatologie,* **A33**:143-150.

OMOTOSHO, J. B. (1985): The separate contributions of squall lines, thunderstorms and the monsoon to the total rainfall in Nigeria. *Journal of Climatology*, **5**:543-552.

OMOTOSHO, J. B. (1990): Onset of thunderstorms and precipitation over Northern Nigeria. *International Journal of Climatology*, **10**:840-860.

OMOTOSHO, J. B. (1992): Long-range prediction of the onset and end of the rainy season in the West African Sahel. *International Journal of Climatology*, **12**:369-382.

OPOKU-ANKOMAH, Y.; & CORDREY, I. (1994): Atlantic sea surface temperatures and rainfall variability in Ghana. *Bulletin of the American Meteorological Society*, **7**:551-557.

ÖZELKAN, E. C., GALAMBOSI, A., DUCKSTEIN, L., & BÁRDOSSY, A. (1998): A multi-objective fuzzy classification of large scale atmospheric circulation patterns for precipitation modelling, *Applied Mathematics and Computation*, **91**:127-142.

PALMER, W. C. (1965): Meteorological drought. Research Paper No. 45. U.S. Department of Commerce Weather Bureau, Washington, D.C.

PALMER, T.N.; BRANKOVIC, C.; VITERBO, P.; & MILLER, M. J. (1992): Modeling interanual variations of summer monsoons. *Journal of Climate*, **5**:399-417.

PANAGOULIA, D.; BÁRDOSSY, A.; & LOURMAS, G. (2006A): Diagnostic statistics of daily rainfall variability in an evolving climate. *Advances in Geosciences*, **7**:349-354.

PANAGOULIA, D.; GRAMMATIKOGIANNIS, A.; & BÁRDOSSY, A. (2006B): An automated classification method of daily circulation patterns for surface climate data downscaling based on optimized fuzzy rules. *Global NEST Journal*, **8**(3):218-223.

PAETH, H., & HENSE, A. (2003): Seasonal forecast of sub-sahelian rainfall using cross validated model output statistics. *Meteorologische Zeitschrift*, **12**(3):157-173.

PEARSON, K. (1902): On lines and planes of closest fit to systems of points in space; *Philosophical Magazine*, **2**:559-572.

PRESS, W. A.; TEUKOLSKY, S. A.; VETTERLING, W. T.; & FLANNERY B. P. (1988): Numerical recipes in C; Cambridge: University Press; 994p.

POCCARD, I.; JANICOT, S.; & CAMBERLIN, P. (2000): Comparison of rainfall structures between NCEP/NCAR reanalyses and observed data over tropical Africa. *Climate Dynamics*, **12**:897-915.

POHLMANN, H.; & GREATBATCH, R. J. (2006): Discontinuities in the late 1960's in different atmospheric data products. *Geophysical Research Letters,* **33**(22):L22803.

PROSPERO, J. M.; & NEES, R. T. (1977): Dust concentration in the atmosphere of the equatorial North Atlantic; possible relationship to Sahelian drought. *Science* **196**:1196-1198.

RIND, D.; LEAN, J.; & HEALY, R. (1999): Simulated time-dependent climate response to solar radiative forcing since 1600. *Journal of Geophysical Research*, **104**:1973-1990.

ROECKNER, E.; LAUTENSCHLAGER, M.; & SCHNEIDER, H. (2006a): IPCC-AR4 MPI-ECHAM5_T63L31 MPI-OM_GR1.5L40 SRESB1 run no.1: atmosphere 6 HOUR values MPImet/MaD Germany. (doi: 10.1594/WDCC/EH5-T63L31_OM GR1.5L40_B1_1_6H).

ROECKNER, E.; LAUTENSCHLAGER, M.; & SCHNEIDER, H. (2006b): IPCC-AR4 MPI-ECHAM5_T63L31 MPI-OM_GR1.5L40 SRESA1B run no.1: atmosphere 6 HOUR values MPImet/MaD Germany. (doi: 10.1594/WDCC/EH5-T63L31_OM-GR1.5L40_A1B_1_6H).

RONCOLI, C.; INGRAM, K.; & KIRSHEN P. (2002): Reading the Rains: Local Knowledge and Rainfall Forecasting in Burkina Faso. *Society and Natural Resources*, **15**:409-427.

ROSENZWEIG, C.; & HILLEL, D. (2000): Soils and global climate change: challenges and opportunities. *Soil Science*, **165**(1):47-56.

ROUX, F.; TESTUD, J.; PAYEN, M., & PINTY, B. (1984): West African squall-line thermodynamic structure retrieved from Dual-Doppler Radar observations. *Journal of the Atmospheric Sciences,* **41**:3104-3121.

ROWELL, D. P.; & MILFORD, J. R. (1993): On the generation of African squall lines. *Journal of Climatology,* **6**:1181-1193.

SARI, (2006): Personal communication with Dr. Mathias Fosu from the Savannah Agricultural Research Institute (Ghana).

SARRIA-DODD, D. E.; & JOLLIFFE, I. T. (2001): Early detection of the start of the wet season in semiarid tropical climates of western Africa. *International Journal of Climatology*, **21**:1251-1262.

SALAMON, P.; SIBANI, P.; & FROST, R. (2000): Facts, Conjectures, and Improvements for Simulated Annealing. SIAM Monographs on Mathematical Modeling and Computation. Philadelphia.

SALVADORI, G. (2004): Bivariate return periods via 2-Copulas. *Statistical Methodology*, **1**:129-144.

SALVADORI, G.; DEMICHELE, C.; KOTTEGODA, N. T.; & ROSSO, R. (2007): Extremes in nature. An approach using copulas. WST Library Series, Vol. 56, Springer, 2007.

SARI (2006): Personal communication with Dr. Mathias Fosu, Savanah Research Institute, Tamale (Ghana).

SHINDELL, D. T.; RIND, D.; BALACHANDRAN, N. K.; LEAN, J.; & LONERGAN, P. (1999): Solar variability, ozone and climate. *Science*, **284**:305-308.

SEMENOV, M. A.; & BARROW, E. M. (1997): Use of a stochastic weather generator in the development of climate change scenarios. *Climatic Change*, **35**:397-414.

SEMENOV, M. A.; BROOKS, R. J.; BARROW, E. M.; & RICHARDSON, C. W. (1998): Comparison of the WGEN and LARS-WG stochastic weather generators for diverse climates. *Climate Research*, **10**:95-107.

SEMENOV, M. A.; BROOKS, R. J. (1999): Spatial interpolation of the LARS-WG stochastic weather generator in Great Britain. *Climate Research*, **11**:137-148.

SHIAU, J.-T.; FENG, S.; & NADARAJAH, S. (2007): Assessment of hydrological droughts for the Yellow River, China, using copulas. *Hydrological Processes*, **16**:2157-2163.

SIVAKUMAR, M. V. K. (1988): Predicting rainy season potential from the onset of rains in Southern Sahelian and Sudanian climatic zones of West Africa. *Agricultural and Forest Meteorology*, **42**:295-305.

SIVAKUMAR, M. V. K. (1992A): Climate change and implications for agriculture in Niger; *Climatic Change*, **20**(4):297-312.

SIVAKUMAR, M. V. K. (1992B): Empirical Analysis of Dry Spells for Agricultural Applications in West Africa; *Journal of Climate*, **5**(5):532-540.

SKLAR, A. (1959) : Fonctions de répartition à *n* dimensions et leurs marges. Publications de l'Institut de Statistique de L'Université de Paris, **8**:229-231.

SMAKHTIN, V. U.; & HUGHES, D. A. (2007): Automated estimation and analyses of meteorological drought characteristics from monthly rainfall data. *Environmental Modelling & Software*, **22**(6):880-890.

STEHLÍK, J.; & BÁRDOSSY, A. (2002): Multivariate stochastic downscaling model for generating daily precipitation series based on atmospheric circulation. *Journal of Hydrology*, **256**:120-141.

STEHLÍK, J.; & BÁRDOSSY, A. (2003): Statistical comparison of European circulation patterns and development of a continental scale classification. *Theoretical and Applied Climatology*, **76**:31-46.

STERN, R. D.; DENNETT, M. D.; & DALE, I. C (1982A): Analyzing daily rainfall measurements to give agronomically useful results: Direct methods. *Methodology of Experimental Agriculture*, **17**:223-236.

STERN, R. D., & COE, R. (1982B): The Use of Rainfall Models in Agricultural Planning. *Agricultural Meteorology*, **26**:35-50.

STREET, J. O.; CARROLL, R. J.; & RUPPERT, D. (1988): A Note on Computing Robust Regression Estimates via Iteratively Reweighted Least Squares. *The American Statistician*, **42**:152-154.

SULTAN, B.; & JANICOT, S. (2000): Abrupt shift of the ITCZ over West Africa and intraseasonal variability. *Geophysical Research Letters*, **27**:3353-3356.

SULTAN, B.; JANICOT, S.; & DIEDHIOU, A. (2003A): The West African Monsoon Dynamics, Part I: Documentation of Intraseasonal Variability. *Journal of Climate*, **16**:3389-3406.

SULTAN, B.; & JANICOT, S. (2003B): The West African Monsoon Dynamics, Part II: The "Preonset" and "Onset" of the Summer Monsoon; *Journal of Climate*, **16**:3407-3427.

STEWART, J. I. (1991): Principles and performance of response farming. *Climatic Risk in Crop Production. Models and Management for the Semi-Arid Tropics and Sub-Tropics*, Ford, W.; Muchow, R. C.; & Bellamy, Z. A. (eds). CAB International. Wallingford.

TRAORÉ, P. C. S.; KOURESSY, M.; VAKSMANN, M.; TABO, R.; MAIKANO, I.; TRAORÉ, S. B.; & COOPER P. (2007): What Is Different about Sudano-Sahelian West Africa*?*; Climate Application and Agriculture, Sivakumar, M. V. K.; & Hansen, J. (eds.). Springer Berlin Heidelberg.doi:10.1007/978-3-540-44650-7_19.

TROUP, A. J. (1961): Variations in upper tropospheric flow associated with the onset of the Australian summer monsoon. *Indian Journal of Meteorology and Geophysics*, **12**: 217-230.

USMAN, M. T.; ARCHER, E.; JOHNSTON P.; & TADROSS, M. (2005): A conceptual framework for enhancing the utility of rainfall hazard forecasts for agriculture in marginal environments. *Natural hazards*, **34**:111-129.

UVO, C.; & BERNDTSSON, R. (1996): Regionalization and spatial properties of Ceará State rainfall in northeast Brazil. *Journal of Geophysical Research*, **101**:4221-4233.

VON STORCH, H., 1995: Inconsistencies at the interface of climate impact studies and global climate research. *Meteorol. Zeitschrift*, **4**:72-80.

WALTER, M. W. (1967): Length of the rainy season in Nigeria. *Nigerian Geographical Journal*, **10**:123-128.

WARD, M. N.; & FOLLAND, C. K. (1991): Prediction of seasonal rainfall in the north Nordeste of Brazil using eigenvectors of sea-surface temperatures. *International Journal of Climatology*, **11**:711-743.

WETTERHALL, F.; BÁRDOSSY, A.; CHEN, D.; HALLDIN, S.; XU, C.-Y. (2006): Daily precipitation downscaling techniques in three Chinese regions. *Water Resources Research*, **42**:W11423.

WILBY R. L.; & WIGLEY T. M. L. (2000): Precipitation predictors for downscaling: observed and general circulation model relationships. *International Journal of Climatology*, **20**:641-661.

WILKS, D. S.; & WILBY, R. L. (1997): Downscaling general circulation model output: a review of methods and limitations. *Progress in Physical Geography*, **21**:530-548.

WILKS, D. S.; & WILBY, R. L. (1999): The weather generation game: a review of stochastic weather models. *Progress in Physical Geography*, **23**:329-357.

WILKS, D. (2006): Statistic Methods in the Atmospheric Sciences; Academic Press.

WILSON, J. W.; & SCHREIBER, W. E. (1986): Initiation of convective storms at radar-observed boundary-layer convergence lines. *Monthly Weather Review*, **114**:2516-2536.

YARNAL, B.; COMRIE, A. C.; FRAKES, B.; & BROWN, D. P. (2001): Developments and prospects in synoptic climatology. *International Journal of Climatology*, **21**:1923-1950.

ZEHE, E.; SINGH, A. K.; & BÁRDOSSY, A. (2006A): Modelling of monsoon rainfall for a mesoscale catchment in North-Wesz India I: assessment of objective circulation patterns. *Hydrology and Earth System Sciences*, **10**:797-806.

ZEHE E.; SINGH, A.; & BÁRDOSSY, A (2006B): Modelling of monsoon rainfall for a mesoscale catchment in North-West India II: Stochastic rainfall simulations. *Hydrology and Earth System Sciences*, **10**:807-815.

ZENG, N. (2003): Atmospheric science: drought in the Sahel. *Science*, **302**:999-1000.

ZORITA, E.; & VON STORCH, H. (1999): The analog method - a simple statistical downscaling technique: comparison with more complicated methods. *Journal of Climate*, **12**:2474-2489.

APPENDIX 1

Location	Method	Predictors	Predictands	Reference
Germany	Weather Patterns	Baur weather classes	Precipitation	Bárdossy & Plate (1991)
Germany	CP conditional stochastic model	GHP(500hPa)	Precipitation	Bárdossy & Plate (1992)
USA	MOFRBC	CPs in 500hPa	Precipitation	Özelkan et al. (1998)
Germany	MOFRBC	GHP(500hPa)	Precipitation	Bárdossy et al. (2001)
Germany, Greece	MOFRBC	GHP(500hPa)	Precipitation	Stehlík & Bárdossy (2002)
Germany, Greece, UK	MOFRBC	GHP(500hPa) GHP(700hPa) MSLP	Precipitation	Stehlík & Bárdossy (2003)
Germany, Greece	MOFRBC	GHP500 GHP700	Precipitation Temperature	Bárdossy et al. (2002)
France, Spain	MOFRBC	SLP	Discharge	Bárdossy & Filiz (2005)
India	MOFRBC	GHP500	Precipitation	Zehe et al. (2006A)
India	CP conditional stochastic model	GHP500	Precipitation	Zehe et al. (2006B)
Greece	CP conditional stochastic model	GHP700	Precipitation	Panagoulia et al., (2006A)
Greece	MOFRBC	GHP700	Precipitation Temperature	Panagoulia et al. (2006B)
China	CP conditional stochastic model	GHP (1000, 850, 700, 500hPa) SH(850, 700, 500hPa) u(850, 700, 500hPa)	Precipitation	Wetterhall et al. (2006)

Table 34: Selected case studies using MOFRBC or a CP conditional stochastic model for statistical downscaling.

APPENDIX 2

Station	pc1	pc2	pc3	pc4	pc5
Accra	**0.80**	0.00	0.03	0.04	0.14
Ada	**0.66**	0.00	0.01	0.07	0.13
Akuse	0.40	-0.03	0.09	-0.01	**0.50**
Axim	**0.51**	0.02	-0.02	0.10	0.14
Bole	0.07	0.05	0.08	**0.66**	0.10
Ho	0.22	-0.01	0.06	0.09	**0.58**
Kete-Krachi	0.04	0.07	0.06	**0.47**	0.25
Koforidua	0.28	-0.02	0.09	-0.01	**0.60**
Kumasi	0.02	0.04	-0.01	0.15	**0.67**
Navrongo	0.02	0.11	**0.70**	0.20	-0.01
Saltpond	**0.69**	0.02	0.00	0.04	0.11
Sefwi-Bekwai	0.12	0.01	-0.02	0.06	**0.64**
Tamale	0.08	0.06	0.17	**0.69**	-0.02
Tema (GH)	**0.81**	0.00	0.02	0.01	0.13
Wa	0.04	0.06	0.36	**0.54**	0.04
Wenchi	0.02	0.02	-0.08	**0.45**	0.40
Yendi	0.07	0.06	0.15	**0.65**	-0.02
Kpeve	0.12	0.01	**0.63**	0.03	0.11
Zuarungo	**0.54**	-0.08	-0.07	0.21	0.03
Ejura	-0.01	-0.02	**0.74**	0.01	0.00
Kaya	0.01	**0.59**	0.25	0.05	0.01
Manga	0.00	0.21	**0.73**	0.07	0.05
Niaogho	0.00	0.21	**0.67**	0.07	0.04
Ouahiguoya	-0.01	**0.73**	0.10	0.08	0.02
Seguenega	0.01	**0.73**	0.09	0.03	0.01
Sideradougou	0.03	0.18	**0.28**	0.20	0.03
Tema (BF)	0.02	**0.65**	0.19	0.03	0.00
Zabre	0.01	0.10	**0.74**	0.18	0.03
Gourcy	0.00	**0.75**	0.08	0.11	-0.01

Table 35: Classification of each rainfall observation site to one region using Pearson correlation coefficient between precipitation time series of 29 observation stations and the 5 retained principal components applying S-mode PCA basing on the correlation matrix.

APPENDIX 3

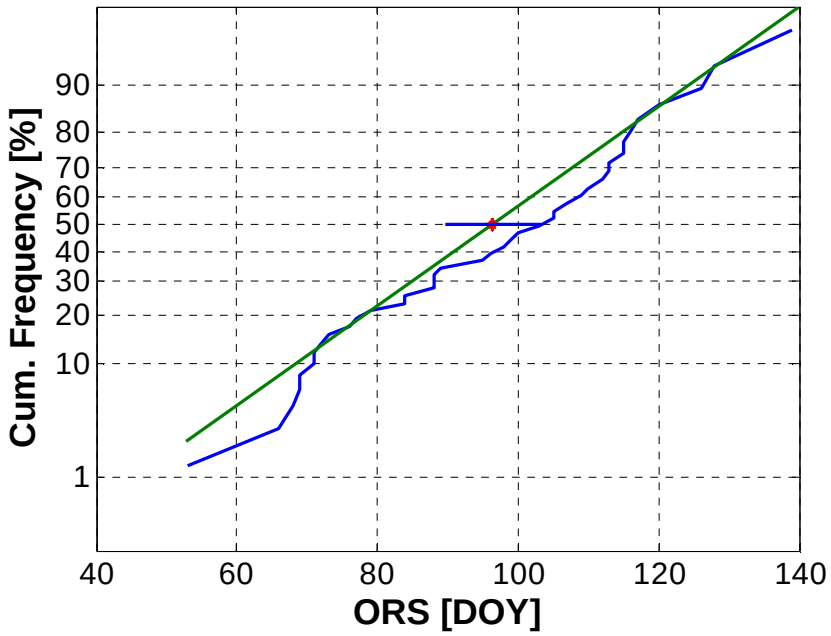

a)

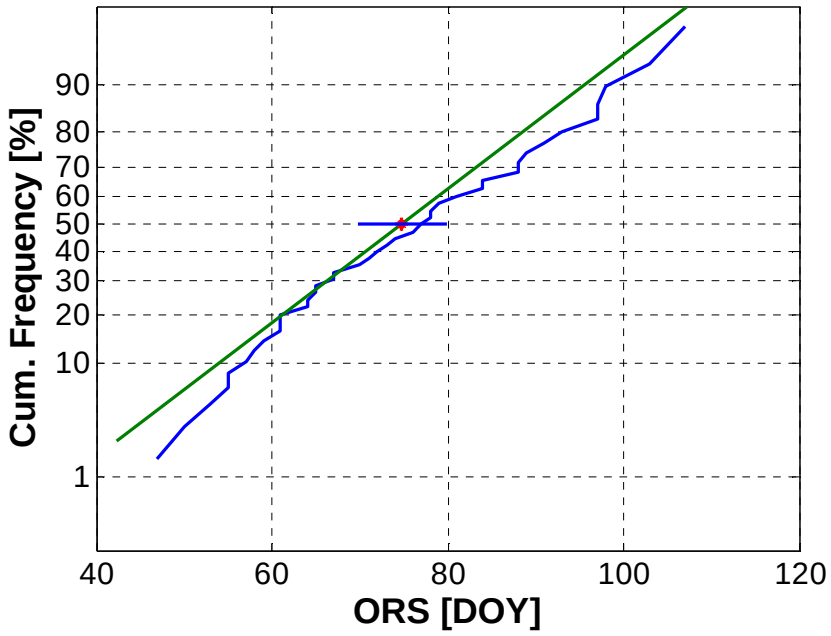

b)

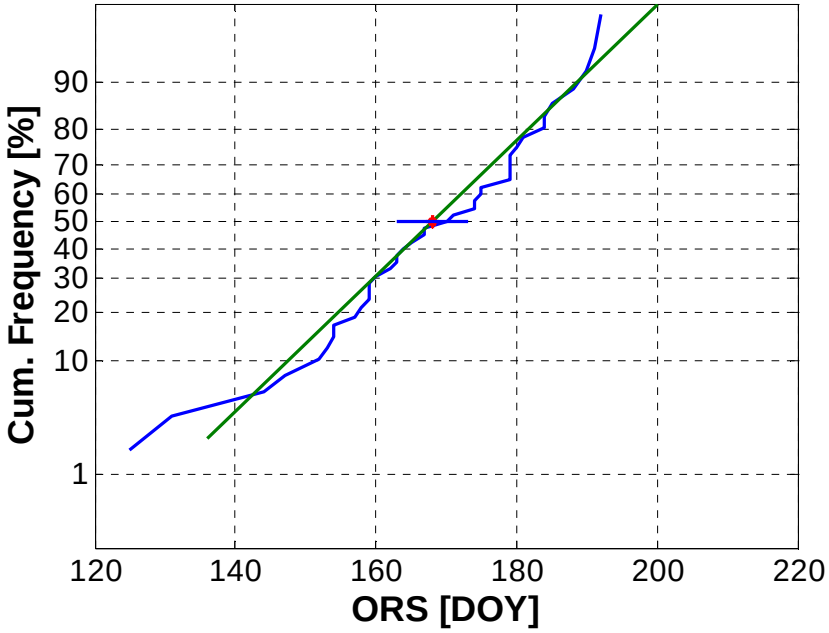

c)

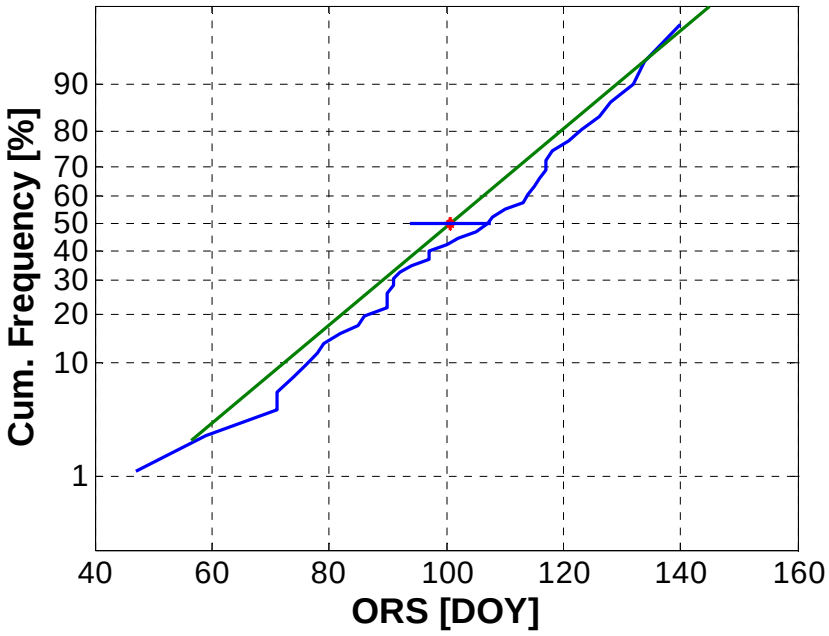

d)

Figure 83: Cumulative distribution functions of the ORS dates (blue line) from 1961-2001: a) PC2, b) PC3, c) PC4 and d) PC5. The red asterisk (blue horizontal line) indicates the mean (two standard error bar), the green line indicates normal distribution of the data.

APPENDIX 4

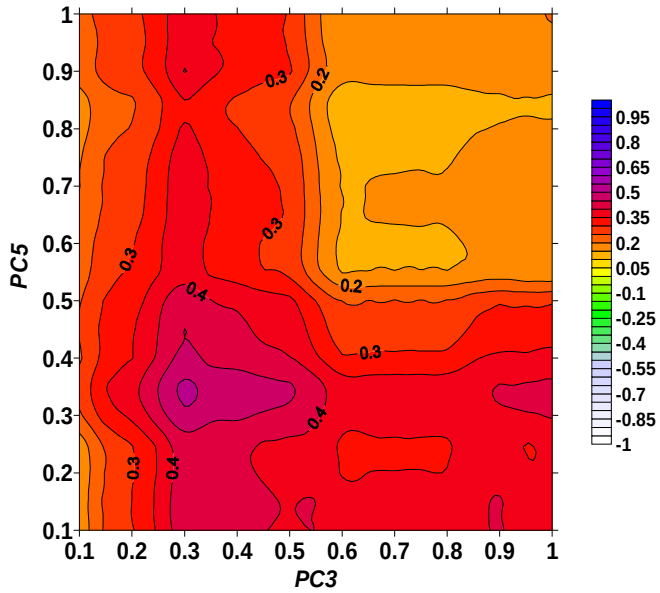
PC5
PC3
0.95
0.8
0.65
0.5
0.35
0.2
0.05
-0.1
-0.25
-0.4
-0.55
-0.7
-0.85
-1

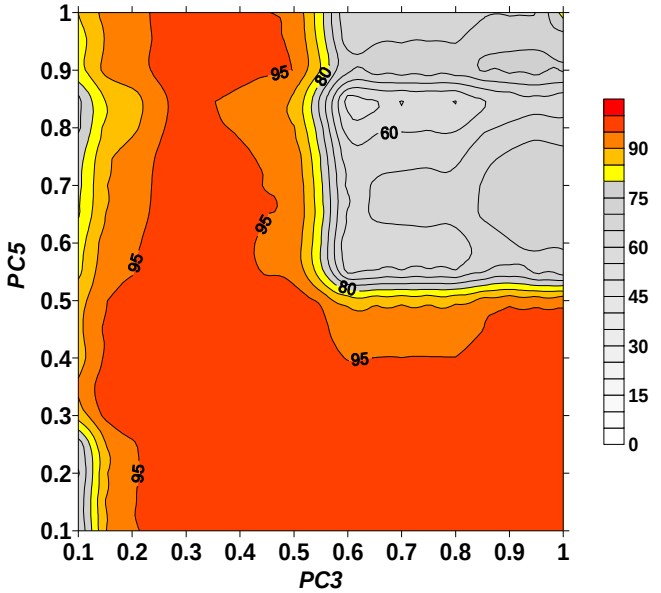
PC5
PC3
90
75
60
45
30
15
0

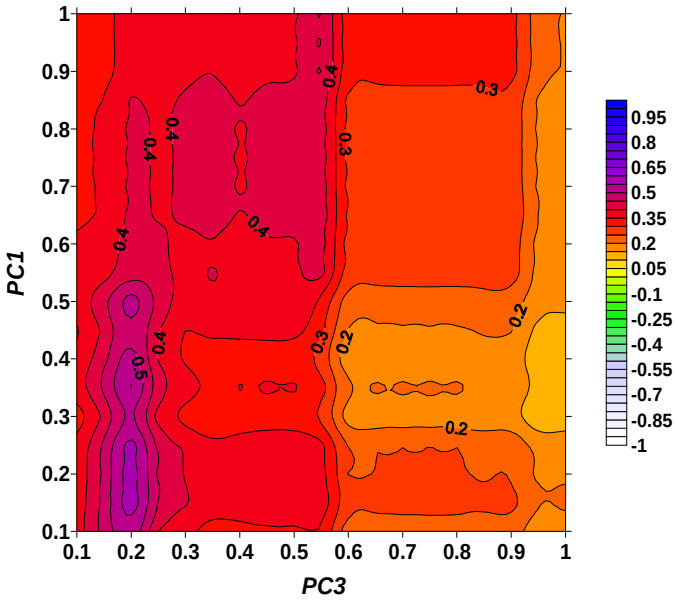
PC1
PC3
0.95
0.8
0.65
0.5
0.35
0.2
0.05
-0.1
-0.25
-0.4
-0.55
-0.7
-0.85
-1

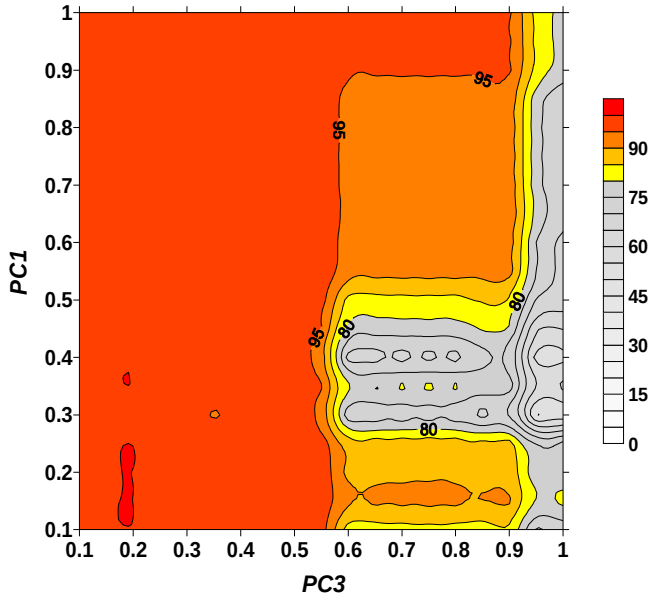
PC1
PC3
90
75
60
45
30
15
0

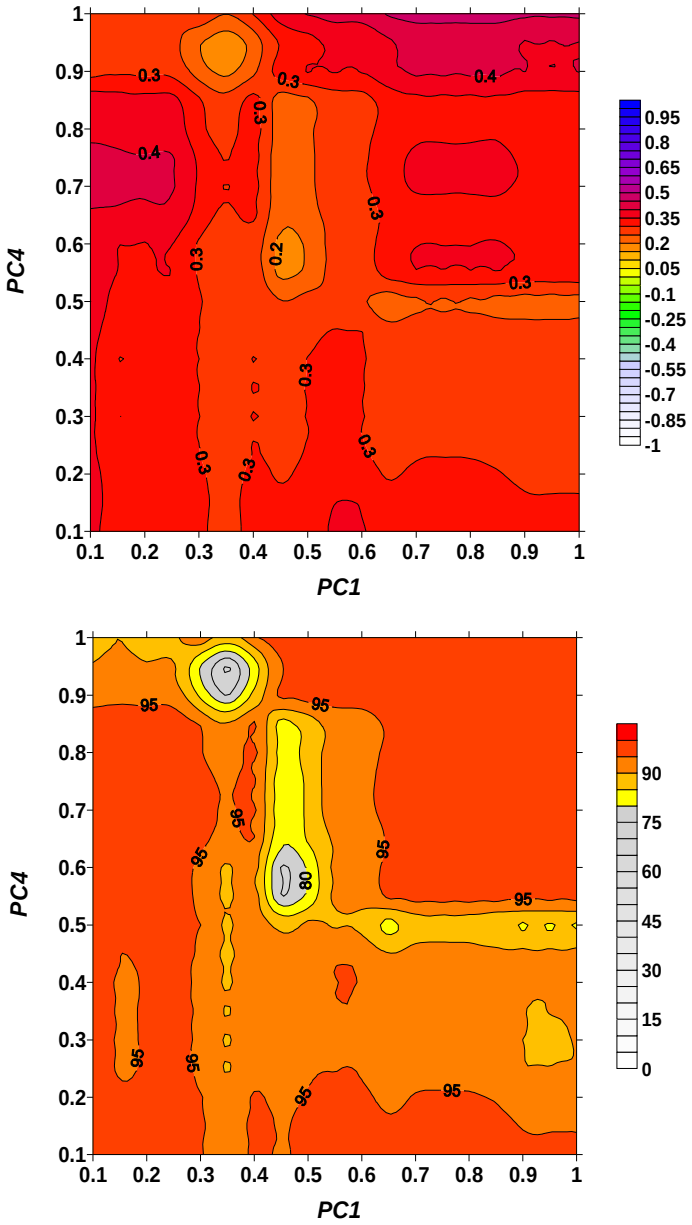

Figure 84: Pearson correlation coefficients between the onset dates of two regions using varying γ values from 0.1 to 1.0 (top) and level of significance (bottom) for selected PC combinations (source: Laux et al., 2008).

APPENDIX 5

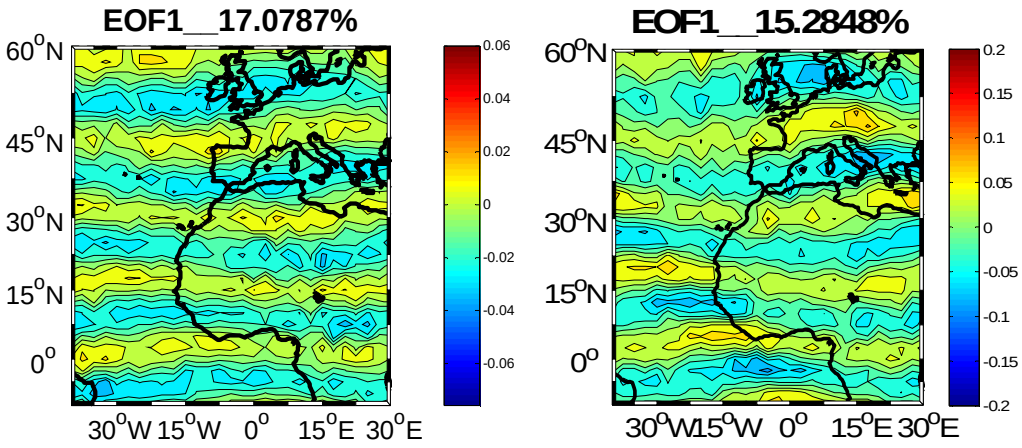
EOF1__17.0787%
60°N
45°N
30°N
15°N
0°
30°W 15°W 0° 15°E 30°E
0.06
0.04
0.02
0
-0.02
-0.04
-0.06

EOF1__15.2848%
60°N
45°N
30°N
15°N
0°
30°W15°W 0° 15°E 30°E
0.2
0.15
0.1
0.05
0
-0.05
-0.1
-0.15
-0.2

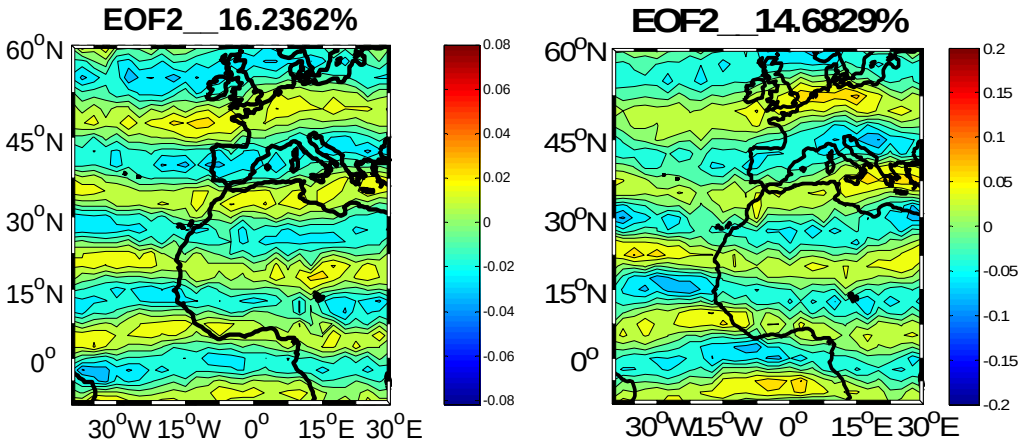
EOF2__16.2362%
60°N
45°N
30°N
15°N
0°
30°W 15°W 0° 15°E 30°E
0.08
0.06
0.04
0.02
0
-0.02
-0.04
-0.06
-0.08

EOF2__14.6829%
60°N
45°N
30°N
15°N
0°
30°W15°W 0° 15°E 30°E
0.2
0.15
0.1
0.05
0
-0.05
-0.1
-0.15
-0.2

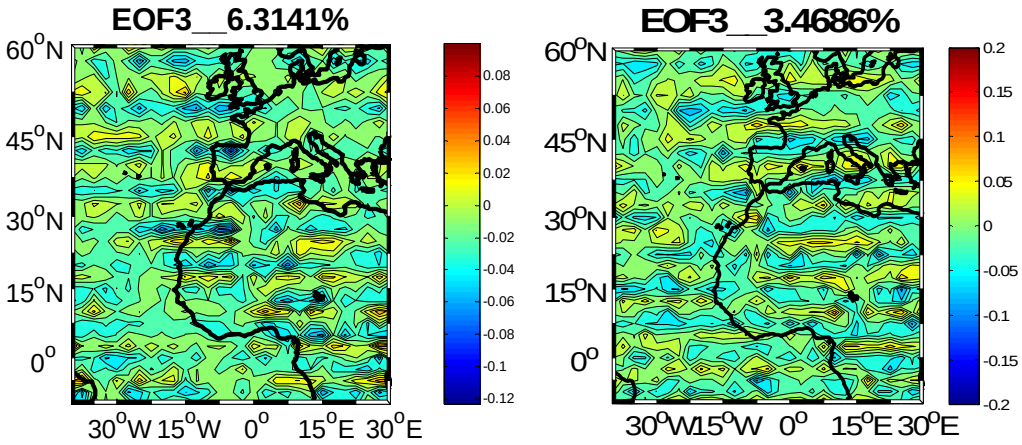
EOF3__6.3141%
60°N
45°N
30°N
15°N
0°
30°W 15°W 0° 15°E 30°E
0.08
0.06
0.04
0.02
0
-0.02
-0.04
-0.06
-0.08
-0.1
-0.12

EOF3__3.4686%
60°N
45°N
30°N
15°N
0°
30°W15°W 0° 15°E 30°E
0.2
0.15
0.1
0.05
0
-0.05
-0.1
-0.15
-0.2

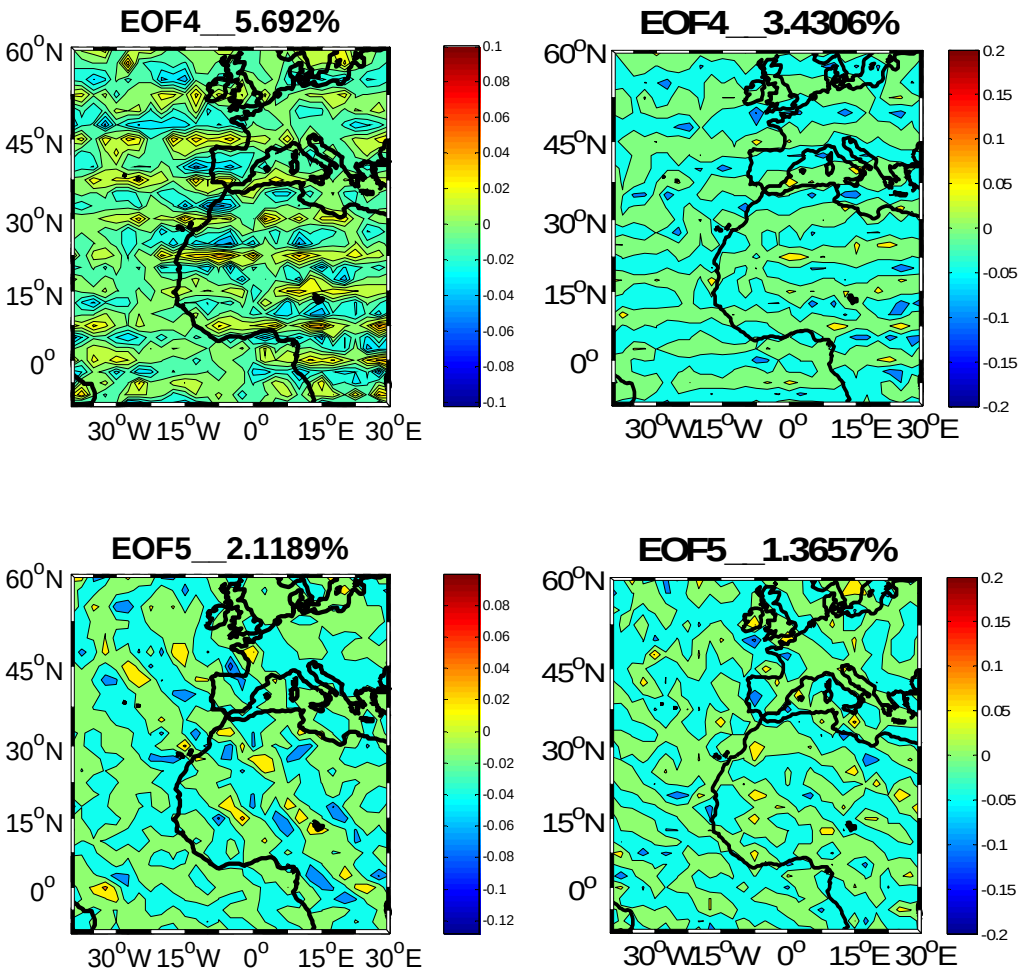

Figure 85: The 5 leading Empirical Orthogonal Functions of the mean eastward component of moisture flux in 300hPa corresponding to the NCEP/NCAR reanalysis data (left) and the ECHAM5/MPI-OM control run (right) for the baseline period 1961-1990.

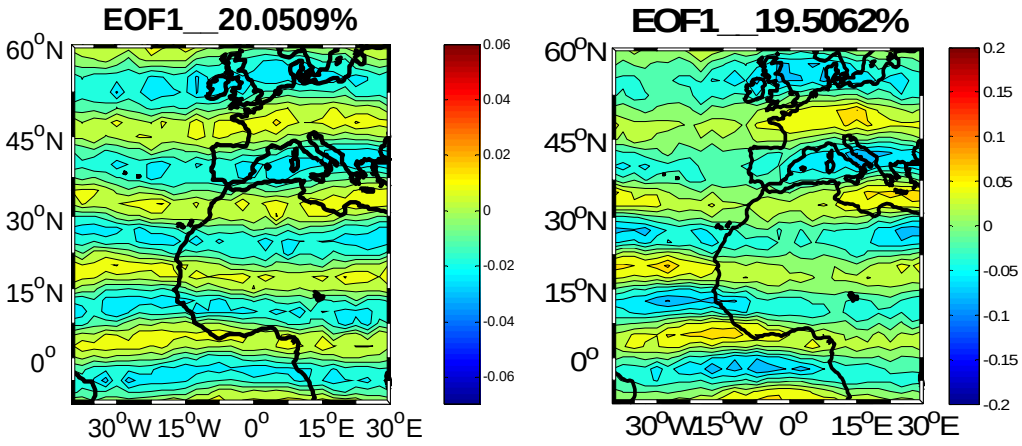
EOF1__20.0509%
60°N
45°N
30°N
15°N
0°
30°W 15°W 0° 15°E 30°E
0.06
0.04
0.02
0
-0.02
-0.04
-0.06

EOF1__19.5062%
60°N
45°N
30°N
15°N
0°
30°W 15°W 0° 15°E 30°E
0.2
0.15
0.1
0.05
0
-0.05
-0.1
-0.15
-0.2

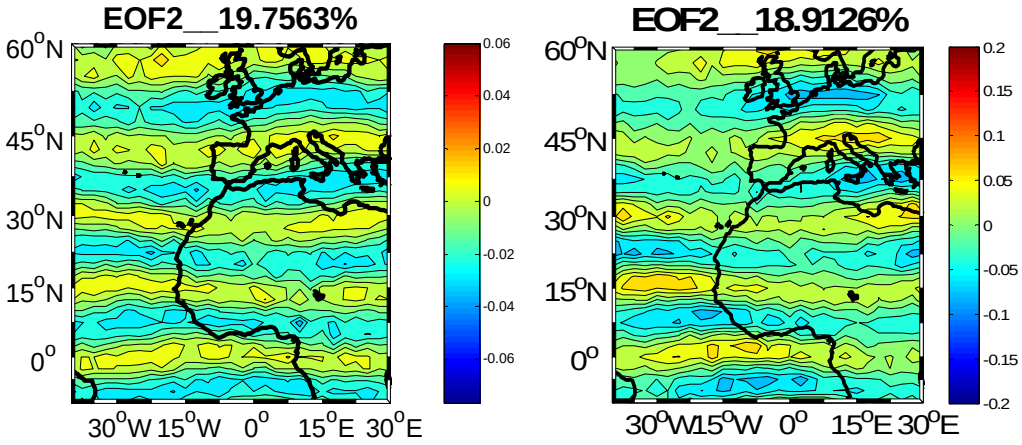
EOF2__19.7563%
60°N
45°N
30°N
15°N
0°
30°W 15°W 0° 15°E 30°E
0.06
0.04
0.02
0
-0.02
-0.04
-0.06

EOF2__18.9126%
60°N
45°N
30°N
15°N
0°
30°W 15°W 0° 15°E 30°E
0.2
0.15
0.1
0.05
0
-0.05
-0.1
-0.15
-0.2

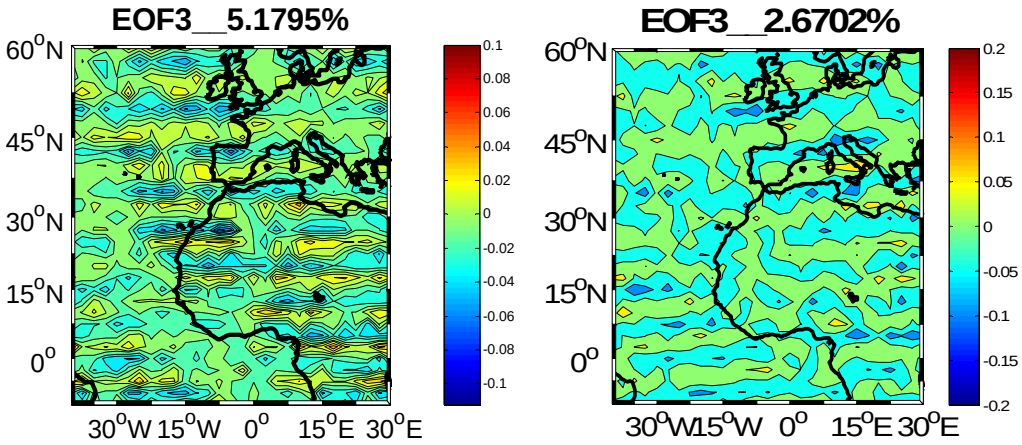
EOF3__5.1795%
60°N
45°N
30°N
15°N
0°
30°W 15°W 0° 15°E 30°E
0.1
0.08
0.06
0.04
0.02
0
-0.02
-0.04
-0.06
-0.08
-0.1

EOF3__2.6702%
60°N
45°N
30°N
15°N
0°
30°W 15°W 0° 15°E 30°E
0.2
0.15
0.1
0.05
0
-0.05
-0.1
-0.15
-0.2

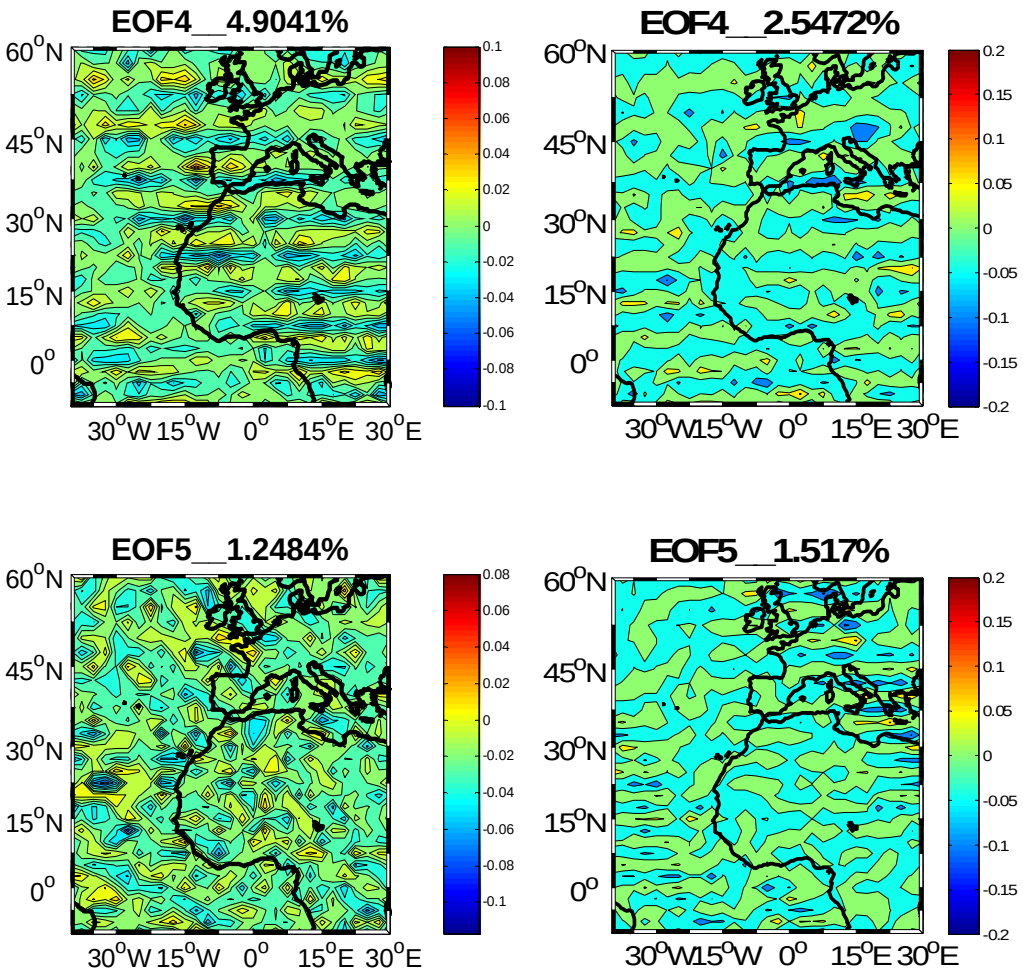

Figure 86: The 5 leading Empirical Orthogonal Functions of the mean eastward component of moisture flux in 500hPa corresponding to the NCEP/NCAR reanalysis data (left) and the ECHAM5/MPI-OM control run (right) for the baseline period 1961-1990.

APPENDIX 6

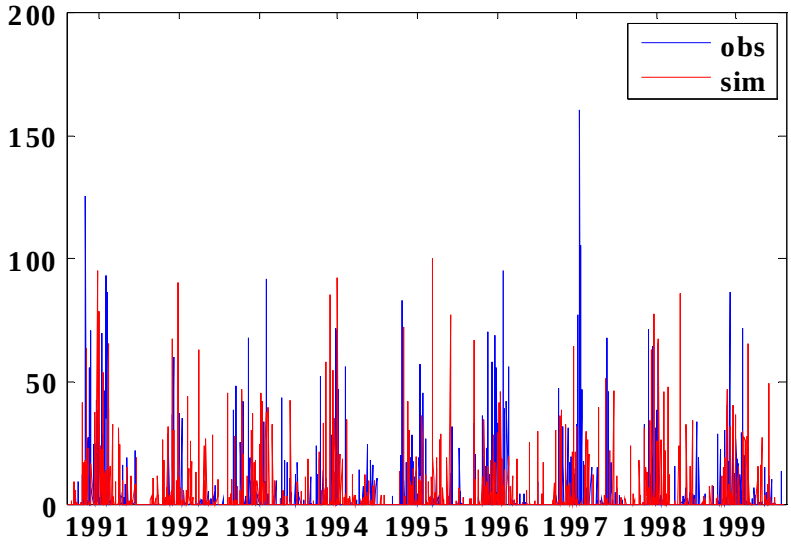

a)

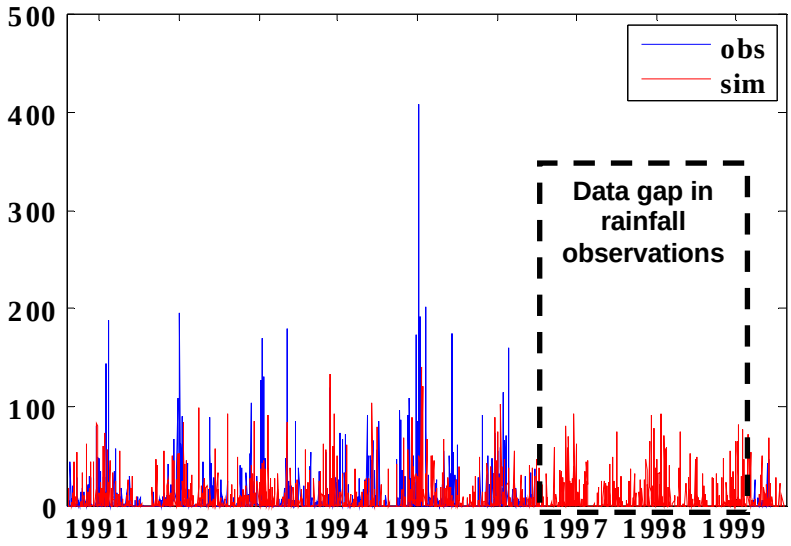

b)

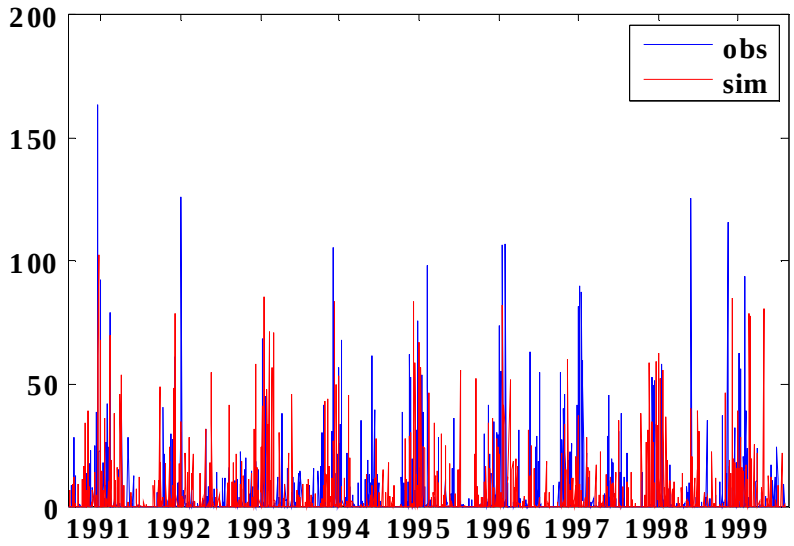

c)

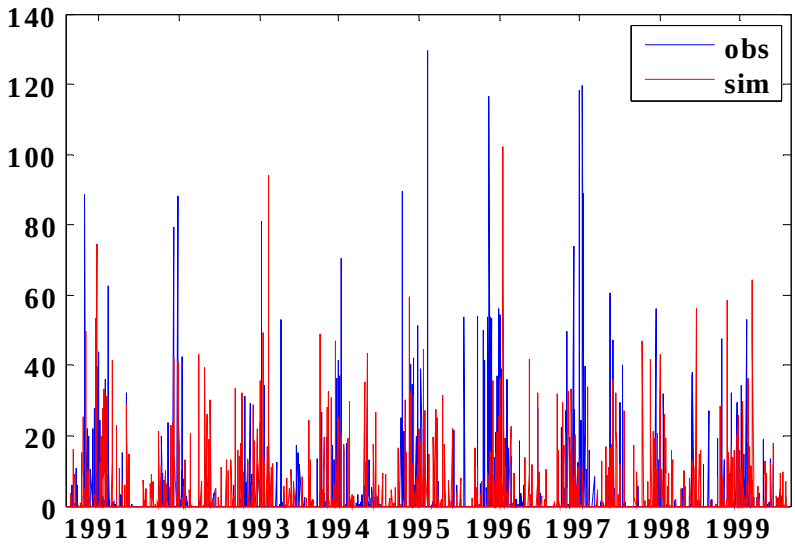

d)

Figure 87: Observed (blue bars) versus simulated (red bars) daily precipitation during the validation period (1991-1999) within PC2 using CP conditional stochastic simulation: a) Ada, b) Axim, c) Saltpond and d) Tema.

APPENDIX 7

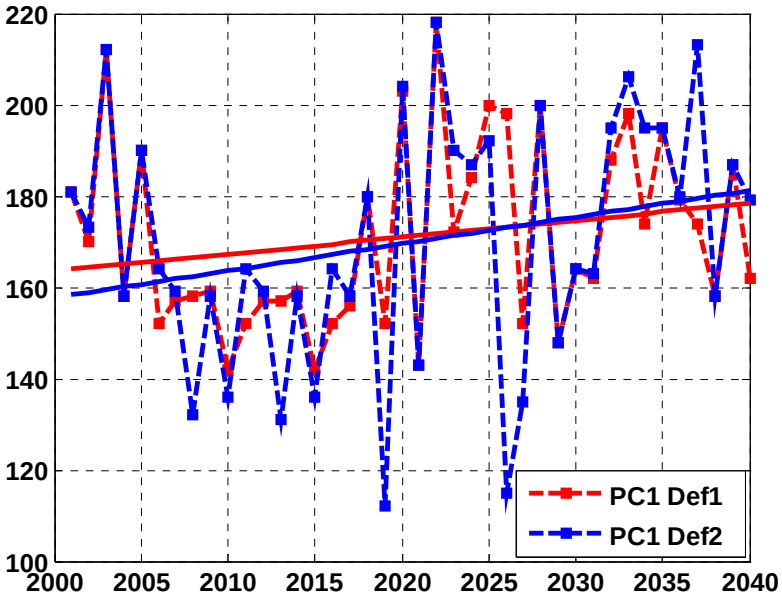
220
200
180
160
140
120
100
2000
2005
2010
2015
2020
2025
2030
2035
2040
PC1 Def1
PC1 Def2

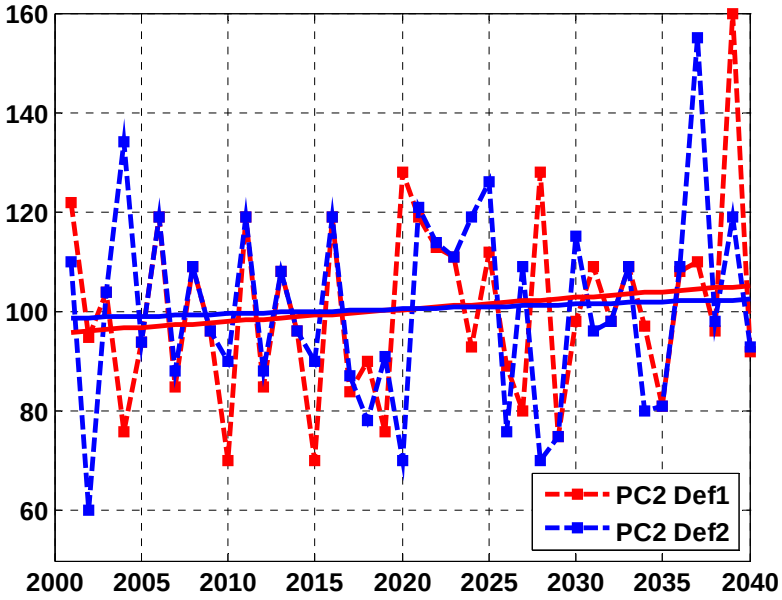
160
140
120
100
80
60
2000
2005
2010
2015
2020
2025
2030
2035
2040
PC2 Def1
PC2 Def2

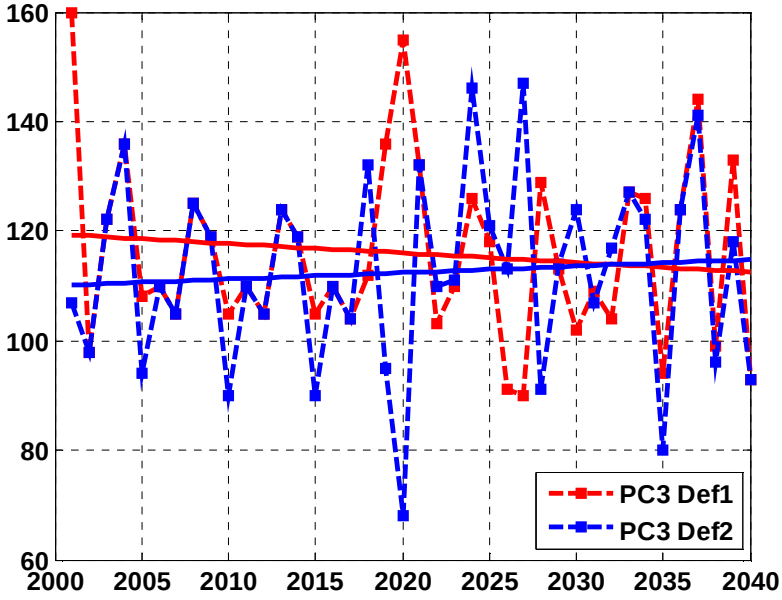
160
140
120
100
80
60
2000
2005
2010
2015
2020
2025
2030
2035
2040
PC3 Def1
PC3 Def2

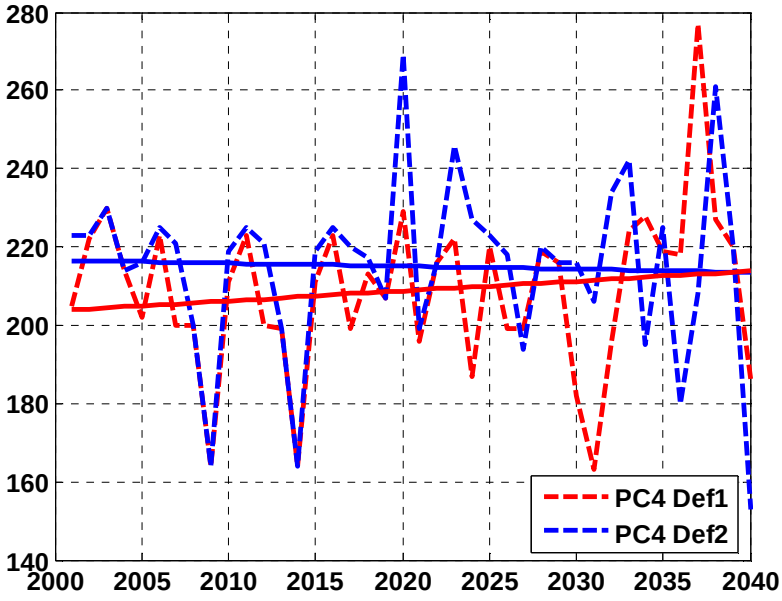
280
260
240
220
200
180
160
140
2000
2005
2010
2015
2020
2025
2030
2035
2040
PC4 Def1
PC4 Def2

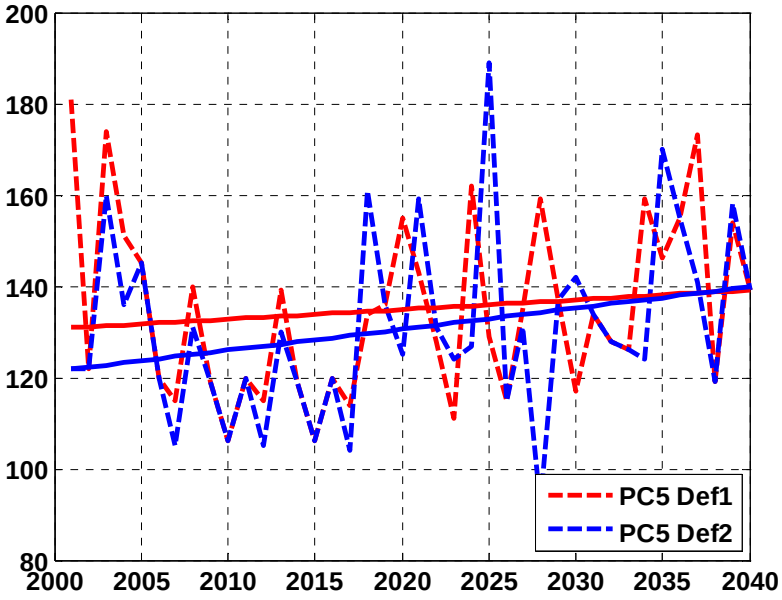

Figure 88: Estimation of future ORS dates using ECHAM5-A1B scenario.

APPENDIX 8

Inferential statistics comprises the use of statistics to make inferences concerning some unknown aspect of a population. It is distinguished from descriptive statistics. It includes hypothesis testing, which is described in the following for the applied tests. In general, hypothesis testing consists of the following steps:

1. Formulation of the test hypotheses
2. Choosing the level of significance and determine the degrees of freedom
3. Calculation the test statistics
4. Decision about the hypotheses

8.1: t - test:

The t - test can be applied to test the correlation coefficient for significance. The shape of the sampling distribution of r tends slowly towards the normal distribution with increasing sample size n.

Test hypotheses:
H_0: The correlation coefficient r is significantly different to zero
H_1: The correlation coefficient r is not significantly different to zero

Test statistics:

$$t_{emp} = \frac{r\sqrt{N-2}}{\sqrt{1-r^2}},$$

Level of significance and degrees of freedom:
The significance level α must be chosen. The degrees of freedom entering the t - distribution are N - 2.

Decision:
The hypothesis that r is significantly different from zero is rejected, if:

$$t_{emp} > t_{krit}(1-\alpha, d.f.).$$

8.2: χ^2- test:

The basic idea behind the χ^2 - test is to divide the range of the data into a number of intervals. Then the number of points that fall into each interval is compared to expected number of points for that interval if the data come from the hypothesized distribution. It can be used to test the data following any distribution. In this thesis it has been used to test whether or not the data follow a normal distribution.

Test hypotheses:

H_0: The data follow a normal distribution

H_1: The data do not follow a normal distribution

Test statistics:

For the χ^2 goodness of fit, the data is divided into k bins and the test statistic is defined as:

$$\chi^2 = \sum_{i=1}^{k} \frac{1}{E_i}(O_i - E_i)^2 ,$$

where O_i is the observed frequency for bin i and E_i is the expected frequency for bin i. The expected frequency is calculated by:

$$E_i = F(Y_u) - F(Y_l) ,$$

where F is the cumulative distribution function for the distribution being tested, Y_u is the upper limit for class i, and Y_l is the lower limit for class i.

Level of significance and degrees of freedom:

The significance level α must be chosen. The test statistic follows approximately a χ^2 distribution with (k - c) degrees of freedom where k is the number of non-empty cells and c = the number of parameters (including location and scale parameters and shape parameters) for the distribution + 1.

Decision:

The hypothesis that the distribution is from the specified distribution is rejected, if:

$$\chi^2_{emp} > \chi^2_{tab}(1-\alpha, k-c) .$$

Comments:

The primary advantage of the χ^2 goodness of fit test is that it is quite general. It can be applied for any distribution, either discrete or continuous, for which the cumulative

distribution function can be computed. This test is sensitive to the choice of bins. There is no optimal choice for the bin width (since the optimal bin width depends on the distribution). Most reasonable choices should produce similar, but not identical, results. For the chi-square approximation to be valid, the expected frequency should be at least 5. This test is not valid for small samples, and if some of the counts are less than five, you may need to combine some bins in the tails.

8.3: K-S test:

The K-S test is a nonparametric test of equality of one-dimensional probability distributions used to compare a sample with a reference probability distribution. The K-S statistic quantifies a distance between the empirical distribution function of the sample and the cumulative distribution function of the reference distribution. With some modifications it can be used to serve as a goodness of fit test. For normality testing, samples are standarised and compared with a standard normal reference distribution.

Test hypotheses:
H_0: The data follow a normal distribution
H_1: The data do not follow a normal distribution

Test statistics:
The empirical distribution function F_n for n observations x_i is defined as:

$$F_n(x) = \frac{1}{n}\sum_{i=1}^{n} I_{x_i \leq x},$$

where $I_{x_i \leq x}$ is the indicator function.The K-S statistic is given by:

$$D_n = \sup |F_n(x) - F(x)|.$$

Level of significance and degrees of freedom:
The significance level α must be chosen. The degrees of freedom entering the D-distribution are N - 2.

Decision:
The hypothesis that the distribution comes from the specified distribution is rejected, if:

$$D_n > D_{krit}(1-\alpha, d.f.).$$

8.4: Mann-Kendall Significance Test

The Mann-Kendall test was used for the determination of the level of significance of an assumed linear trend. The sum *Q* of algebraic signs of neighboring values is acquired as statistical variable:

$$Q = \sum_{i=1}^{n-1} \sum_{j=i+1}^{n} \text{sign}(x_i - x_j),$$

with Q being the variable after Mann-Kendall, and n the number of time steps (number of observational years minus the number of years that fell out due to data gaps). The variable Q is characterized as follows: for $n > 10$, Q is an approximately normal distributed random variable (Kendall, 1975) ; for the average value $\overline{Q} = 0$ holds, and the variance is given by:

$$\sigma_Q{}^2 = \frac{1}{18}(n(n-1)(2n+5)).$$

From these variables one obtains the standard normal distributed $N(0,1)$ test variable $\hat{z}$, with:

$$\hat{z} = \frac{Q}{\sigma_Q}.$$

$\hat{z}$ can be tested on significance using the two-sided test on a normal distribution. For each of the trends that were determined, the stability was evaluated using the reverse arrangement test (KLIWA, 2002). This is done step by step by calculating the slope of the trend for a one year shortened time series, starting with the complete time series. In shortening the time series it has to be made sure that the length of the time series doesn't fall below 20 years. For that purpose, the absolute trend has been calculated using equation 3.27. Then the relative trend:

$$b_r = 100 \frac{b_a}{MHW},$$

with MHW being the average of the determined maxima of the shortened observation period has been calculated. Afterwards, the determined trend slope is for each shortened time series tested on significance using the *Mann-Kendall* test on a linear trend.

8.5: Analysis of Variance (Anova) using a F-test

Another possibility to judge the significance of the trend is to perform an F-test of the MSR/MSE ratio. In order to test the null hypothesis whether the slope $b_1 = 0$, it is useful to divide the total variance $s_y^2 = \sum (y_i - \bar{y})^2 / (N-1)$ of the dependent variable into two independent parts: the variance due to the regression and the error variance $\sum \varepsilon^2 / (N-2)$.

These calculations are indicated best by the *Analysis of Variance* (ANOVA) table for linear regression. Table 36 presents the scheme of how to compute the ANOVA parameters with respect to the degrees of freedom. Under the null hypothesis of there being no effect due to the regression, the mean squares due to regression and the mean squares due to the variance result in the variance due to the error. Hence, the MSR/MSE ratio is expected to follow the F distribution, and the calculated value can be compared with the tabulated value for a certain level of significance and 1 and (N-2) degrees of freedom. If the calculated value is larger than the tabulated value, the null hypothesis is rejected and the regression is seen to be significant.

Source	Degrees of Freedom	Sum of squares	Mean squares
Regression	1	$SSR = \sum (\hat{y}_i - \bar{y})^2$	MSR = SSR / 1
Error	(N-2)	$SSE = \sum (y_i - \hat{y}_i)^2$	MSE = SSE / (N -2)
Total	(N-1)	$SST_O = \sum (y_i - \bar{y})^2$	

Table 36: Analysis of variance (ANOVA) for linear regression (SSR - Sum of squares due to regression; SSE Sum of squares due to error; SST_O - Sum of squares due to total; MSR - Mean of squares due to regression; MSE - Mean of squares due to error).

CURRICULUM VITAE

PERSONAL DATA:

Name: Patrick Laux

Date of Birth: 08.01.1976

Place of Birth: Wadern, Germany

Nationality: German

PROFESSIONAL EXPERIENCE BACKGROUND:

2009 **Post Doc Position** at the Institute for Meteorology and Climate Research in Garmisch-Partenkirchen, Forschungszentrum Karlsruhe GmbH, Germany

2004 - 2008 **PhD Position** at the Institute for Meteorology and Climate Research in Garmisch-Partenkirchen, Forschungszentrum Karlsruhe GmbH, Germany

EDUCATIONAL BACKGROUND:

1996 - 2003 Studies of **Applied Environmental Sciences** at Karl Marx University of Treves, Germany, Diploma degree (equivalent to Master degree)

Major subjects: Hydrology, Remote Sensing

Minor subjects: Meteorology, Soil Sciences and Environmental Law

Diploma Thesis: “Quantification of Chemical Parameters of Sediment Samples of the Olewiger Bach (Treves) using Reflectance Spectra Measurement. Comparison of Methods: Partial Least Squares Regression (PLSR) vs. Artificial Neural Networks (ANN)’

1982 - 1995 Primary and Secondary School

Institut für Wasserbau
Universität Stuttgart

Pfaffenwaldring 61
70569 Stuttgart (Vaihingen)
Telefon (0711) 685 - 64717/64749/64752/64679
Telefax (0711) 685 - 67020 o. 64746 o. 64681
E-Mail: iws@iws.uni-stuttgart.de
http://www.iws.uni-stuttgart.de

Verzeichnis der Mitteilungshefte

5 Plate, Erich: *Beitrag zur Bestimmung der Windgeschwindigkeitsverteilung in der durch eine Wand gestörten bodennahen Luftschicht*,
und
Röhnisch, Arthur; Marotz, Günter: *Neue Baustoffe und Bauausführungen für den Schutz der Böschungen und der Sohle von Kanälen, Flüssen und Häfen; Gestehungskosten und jeweilige Vorteile*, sowie Unny, T.E.: *Schwingungsuntersuchungen am Kegelstrahlschieber*, 1967

6 Seiler, Erich: *Die Ermittlung des Anlagenwertes der bundeseigenen Binnenschiffahrtsstraßen und Talsperren und des Anteils der Binnenschiffahrt an diesem Wert*, 1967

7 *Sonderheft anläßlich des 65. Geburtstages von Prof. Arthur Röhnisch mit Beiträgen von* Benk, Dieter; Breitling, J.; Gurr, Siegfried; Haberhauer, Robert; Honekamp, Hermann; Kuz, Klaus Dieter; Marotz, Günter; Mayer-Vorfelder, Hans-Jörg; Miller, Rudolf; Plate, Erich J.; Radomski, Helge; Schwarz, Helmut; Vollmer, Ernst; Wildenhahn, Eberhard; 1967

8 Jumikis, Alfred: *Beitrag zur experimentellen Untersuchung des Wassernachschubs in einem gefrierenden Boden und die Beurteilung der Ergebnisse*, 1968

9 Marotz, Günter: *Technische Grundlagen einer Wasserspeicherung im natürlichen Untergrund*, 1968

10 Radomski, Helge: *Untersuchungen über den Einfluß der Querschnittsform wellenförmiger Spundwände auf die statischen und rammtechnischen Eigenschaften*, 1968

11 Schwarz, Helmut: *Die Grenztragfähigkeit des Baugrundes bei Einwirkung vertikal gezogener Ankerplatten als zweidimensionales Bruchproblem*, 1969

12 Erbel, Klaus: *Ein Beitrag zur Untersuchung der Metamorphose von Mittelgebirgsschneedecken unter besonderer Berücksichtigung eines Verfahrens zur Bestimmung der thermischen Schneequalität*, 1969

13 Westhaus, Karl-Heinz: *Der Strukturwandel in der Binnenschiffahrt und sein Einfluß auf den Ausbau der Binnenschiffskanäle*, 1969

14 Mayer-Vorfelder, Hans-Jörg: *Ein Beitrag zur Berechnung des Erdwiderstandes unter Ansatz der logarithmischen Spirale als Gleitflächenfunktion*, 1970

15 Schulz, Manfred: *Berechnung des räumlichen Erddruckes auf die Wandung kreiszylindrischer Körper*, 1970

16 Mobasseri, Manoutschehr: *Die Rippenstützmauer. Konstruktion und Grenzen ihrer Standsicherheit*, 1970

17 Benk, Dieter: *Ein Beitrag zum Betrieb und zur Bemessung von Hochwasserrückhaltebecken*, 1970

18 Gàl, Attila: *Bestimmung der mitschwingenden Wassermasse bei überströmten Fischbauchklappen mit kreiszylindrischem Staublech*, 1971, vergriffen

19 Kuz, Klaus Dieter: *Ein Beitrag zur Frage des Einsetzens von Kavitationserscheinungen in einer Düsenströmung bei Berücksichtigung der im Wasser gelösten Gase*, 1971, vergriffen

20 Schaak, Hartmut: *Verteilleitungen von Wasserkraftanlagen*, 1971

21 *Sonderheft zur Eröffnung der neuen Versuchsanstalt des Instituts für Wasserbau der Universität Stuttgart mit Beiträgen von* Brombach, Hansjörg; Dirksen, Wolfram; Gàl, Attila; Gerlach, Reinhard; Giesecke, Jürgen; Holthoff, Franz-Josef; Kuz, Klaus Dieter; Marotz, Günter; Minor, Hans-Erwin; Petrikat, Kurt; Röhnisch, Arthur; Rueff, Helge; Schwarz, Helmut; Vollmer, Ernst; Wildenhahn, Eberhard; 1972

22 Wang, Chung-su: *Ein Beitrag zur Berechnung der Schwingungen an Kegelstrahlschiebern*, 1972

23 Mayer-Vorfelder, Hans-Jörg: *Erdwiderstandsbeiwerte nach dem Ohde-Variationsverfahren*, 1972

24 Minor, Hans-Erwin: *Beitrag zur Bestimmung der Schwingungsanfachungsfunktionen überströmter Stauklappen*, 1972, vergriffen

25 Brombach, Hansjörg: *Untersuchung strömungsmechanischer Elemente (Fluidik) und die Möglichkeit der Anwendung von Wirbelkammerelementen im Wasserbau*, 1972, vergriffen

26 Wildenhahn, Eberhard: *Beitrag zur Berechnung von Horizontalfilterbrunnen*, 1972

27 Steinlein, Helmut: *Die Eliminierung der Schwebstoffe aus Flußwasser zum Zweck der unterirdischen Wasserspeicherung, gezeigt am Beispiel der Iller*, 1972

28 Holthoff, Franz Josef: *Die Überwindung großer Hubhöhen in der Binnenschiffahrt durch Schwimmerhebewerke*, 1973

29 Röder, Karl: *Einwirkungen aus Baugrundbewegungen auf trog- und kastenförmige Konstruktionen des Wasser- und Tunnelbaues*, 1973

30 Kretschmer, Heinz: *Die Bemessung von Bogenstaumauern in Abhängigkeit von der Talform*, 1973

31 Honekamp, Hermann: *Beitrag zur Berechnung der Montage von Unterwasserpipelines*, 1973

32 Giesecke, Jürgen: *Die Wirbelkammertriode als neuartiges Steuerorgan im Wasserbau*, und Brombach, Hansjörg: *Entwicklung, Bauformen, Wirkungsweise und Steuereigenschaften von Wirbelkammerverstärkern*, 1974

33 Rueff, Helge: *Untersuchung der schwingungserregenden Kräfte an zwei hintereinander angeordneten Tiefschützen unter besonderer Berücksichtigung von Kavitation*, 1974

34 Röhnisch, Arthur: *Einpreßversuche mit Zementmörtel für Spannbeton - Vergleich der Ergebnisse von Modellversuchen mit Ausführungen in Hüllwellrohren*, 1975

35 *Sonderheft anläßlich des 65. Geburtstages von Prof. Dr.-Ing. Kurt Petrikat mit Beiträgen von*: Brombach, Hansjörg; Erbel, Klaus; Flinspach, Dieter; Fischer jr., Richard; Gàl, Attila; Gerlach, Reinhard; Giesecke, Jürgen; Haberhauer, Robert; Hafner Edzard; Hausenblas, Bernhard; Horlacher, Hans-Burkhard; Hutarew, Andreas; Knoll, Manfred; Krummet, Ralph; Marotz, Günter; Merkle, Theodor; Miller, Christoph; Minor, Hans-Erwin; Neumayer, Hans; Rao, Syamala; Rath, Paul; Rueff, Helge; Ruppert, Jürgen; Schwarz, Wolfgang; Topal-Gökceli, Mehmet; Vollmer, Ernst; Wang, Chung-su; Weber, Hans-Georg; 1975

36 Berger, Jochum: *Beitrag zur Berechnung des Spannungszustandes in rotationssymmetrisch belasteten Kugelschalen veränderlicher Wandstärke unter Gas- und Flüssigkeitsdruck durch Integration schwach singulärer Differentialgleichungen*, 1975

37 Dirksen, Wolfram: *Berechnung instationärer Abflußvorgänge in gestauten Gerinnen mittels Differenzenverfahren und die Anwendung auf Hochwasserrückhaltebecken*, 1976

38 Horlacher, Hans-Burkhard: *Berechnung instationärer Temperatur- und Wärmespannungsfelder in langen mehrschichtigen Hohlzylindern*, 1976

39 Hafner, Edzard: *Untersuchung der hydrodynamischen Kräfte auf Baukörper im Tiefwasserbereich des Meeres*, 1977, ISBN 3-921694-39-6

40 Ruppert, Jürgen: *Über den Axialwirbelkammerverstärker für den Einsatz im Wasserbau*, 1977, ISBN 3-921694-40-X

41 Hutarew, Andreas: *Beitrag zur Beeinflußbarkeit des Sauerstoffgehalts in Fließgewässern an Abstürzen und Wehren*, 1977, ISBN 3-921694-41-8, vergriffen

42 Miller, Christoph: *Ein Beitrag zur Bestimmung der schwingungserregenden Kräfte an unterströmten Wehren*, 1977, ISBN 3-921694-42-6

43 Schwarz, Wolfgang: *Druckstoßberechnung unter Berücksichtigung der Radial- und Längsverschiebungen der Rohrwandung*, 1978, ISBN 3-921694-43-4

44 Kinzelbach, Wolfgang: *Numerische Untersuchungen über den optimalen Einsatz variabler Kühlsysteme einer Kraftwerkskette am Beispiel Oberrhein*, 1978, ISBN 3-921694-44-2

45 Barczewski, Baldur: *Neue Meßmethoden für Wasser-Luftgemische und deren Anwendung auf zweiphasige Auftriebsstrahlen*, 1979, ISBN 3-921694-45-0

46 Neumayer, Hans: *Untersuchung der Strömungsvorgänge in radialen Wirbelkammerverstärkern*, 1979, ISBN 3-921694-46-9

47 Elalfy, Youssef-Elhassan: *Untersuchung der Strömungsvorgänge in Wirbelkammerdioden und -drosseln*, 1979, ISBN 3-921694-47-7

48 Brombach, Hansjörg: *Automatisierung der Bewirtschaftung von Wasserspeichern*, 1981, ISBN 3-921694-48-5

49 Geldner, Peter: *Deterministische und stochastische Methoden zur Bestimmung der Selbstdichtung von Gewässern*, 1981, ISBN 3-921694-49-3, vergriffen

50 Mehlhorn, Hans: *Temperaturveränderungen im Grundwasser durch Brauchwassereinleitungen*, 1982, ISBN 3-921694-50-7, vergriffen

51 Hafner, Edzard: *Rohrleitungen und Behälter im Meer*, 1983, ISBN 3-921694-51-5

52 Rinnert, Bernd: *Hydrodynamische Dispersion in porösen Medien: Einfluß von Dichteunterschieden auf die Vertikalvermischung in horizontaler Strömung*, 1983, ISBN 3-921694-52-3, vergriffen

53 Lindner, Wulf: *Steuerung von Grundwasserentnahmen unter Einhaltung ökologischer Kriterien*, 1983, ISBN 3-921694-53-1, vergriffen

54 Herr, Michael; Herzer, Jörg; Kinzelbach, Wolfgang; Kobus, Helmut; Rinnert, Bernd: *Methoden zur rechnerischen Erfassung und hydraulischen Sanierung von Grundwasserkontaminationen*, 1983, ISBN 3-921694-54-X

55 Schmitt, Paul: *Wege zur Automatisierung der Niederschlagsermittlung*, 1984, ISBN 3-921694-55-8, vergriffen

56 Müller, Peter: *Transport und selektive Sedimentation von Schwebstoffen bei gestautem Abfluß*, 1985, ISBN 3-921694-56-6

57 El-Qawasmeh, Fuad: *Möglichkeiten und Grenzen der Tropfbewässerung unter besonderer Berücksichtigung der Verstopfungsanfälligkeit der Tropfelemente*, 1985, ISBN 3-921694-57-4, vergriffen

58 Kirchenbaur, Klaus: *Mikroprozessorgesteuerte Erfassung instationärer Druckfelder am Beispiel seegangsbelasteter Baukörper*, 1985, ISBN 3-921694-58-2

59 Kobus, Helmut (Hrsg.): *Modellierung des großräumigen Wärme- und Schadstofftransports im Grundwasser*, Tätigkeitsbericht 1984/85 (DFG-Forschergruppe an den Universitäten Hohenheim, Karlsruhe und Stuttgart), 1985, ISBN 3-921694-59-0, vergriffen

60 Spitz, Karlheinz: *Dispersion in porösen Medien: Einfluß von Inhomogenitäten und Dichteunterschieden*, 1985, ISBN 3-921694-60-4, vergriffen

61 Kobus, Helmut: *An Introduction to Air-Water Flows in Hydraulics*, 1985, ISBN 3-921694-61-2

62 Kaleris, Vassilios: *Erfassung des Austausches von Oberflächen- und Grundwasser in horizontalebenen Grundwassermodellen*, 1986, ISBN 3-921694-62-0

63 Herr, Michael: *Grundlagen der hydraulischen Sanierung verunreinigter Porengrundwasserleiter*, 1987, ISBN 3-921694-63-9

64 Marx, Walter: *Berechnung von Temperatur und Spannung in Massenbeton infolge Hydratation*, 1987, ISBN 3-921694-64-7

65 Koschitzky, Hans-Peter: *Dimensionierungskonzept für Sohlbelüfter in Schußrinnen zur Vermeidung von Kavitationsschäden*, 1987, ISBN 3-921694-65-5

66 Kobus, Helmut (Hrsg.): *Modellierung des großräumigen Wärme- und Schadstofftransports im Grundwasser*, Tätigkeitsbericht 1986/87 (DFG-Forschergruppe an den Universitäten Hohenheim, Karlsruhe und Stuttgart) 1987, ISBN 3-921694-66-3

67 Söll, Thomas: *Berechnungsverfahren zur Abschätzung anthropogener Temperaturanomalien im Grundwasser*, 1988, ISBN 3-921694-67-1

68 Dittrich, Andreas; Westrich, Bernd: *Bodenseeufererosion, Bestandsaufnahme und Bewertung*, 1988, ISBN 3-921694-68-X, vergriffen

69 Huwe, Bernd; van der Ploeg, Rienk R.: *Modelle zur Simulation des Stickstoffhaushaltes von Standorten mit unterschiedlicher landwirtschaftlicher Nutzung*, 1988, ISBN 3-921694-69-8, vergriffen

70 Stephan, Karl: *Integration elliptischer Funktionen*, 1988, ISBN 3-921694-70-1

71 Kobus, Helmut; Zilliox, Lothaire (Hrsg.): *Nitratbelastung des Grundwassers, Auswirkungen der Landwirtschaft auf die Grundwasser- und Rohwasserbeschaffenheit und Maßnahmen zum Schutz des Grundwassers*. Vorträge des deutsch-französischen Kolloquiums am 6. Oktober 1988, Universitäten Stuttgart und Louis Pasteur Strasbourg (Vorträge in deutsch oder französisch, Kurzfassungen zweisprachig), 1988, ISBN 3-921694-71-X

72 Soyeaux, Renald: *Unterströmung von Stauanlagen auf klüftigem Untergrund unter Berücksichtigung laminarer und turbulenter Fließzustände*,1991, ISBN 3-921694-72-8

73 Kohane, Roberto: *Berechnungsmethoden für Hochwasserabfluß in Fließgewässern mit überströmten Vorländern*, 1991, ISBN 3-921694-73-6

74 Hassinger, Reinhard: *Beitrag zur Hydraulik und Bemessung von Blocksteinrampen in flexibler Bauweise*, 1991, ISBN 3-921694-74-4, vergriffen

75 Schäfer, Gerhard: *Einfluß von Schichtenstrukturen und lokalen Einlagerungen auf die Längsdispersion in Porengrundwasserleitern*, 1991, ISBN 3-921694-75-2

76 Giesecke, Jürgen: *Vorträge, Wasserwirtschaft in stark besiedelten Regionen; Umweltforschung mit Schwerpunkt Wasserwirtschaft*, 1991, ISBN 3-921694-76-0

77 Huwe, Bernd: *Deterministische und stochastische Ansätze zur Modellierung des Stickstoffhaushalts landwirtschaftlich genutzter Flächen auf unterschiedlichem Skalenniveau*, 1992, ISBN 3-921694-77-9, vergriffen

78 Rommel, Michael: *Verwendung von Kluftdaten zur realitätsnahen Generierung von Kluftnetzen mit anschließender laminar-turbulenter Strömungsberechnung*, 1993, ISBN 3-92 1694-78-7

79 Marschall, Paul: *Die Ermittlung lokaler Stofffrachten im Grundwasser mit Hilfe von Einbohrloch-Meßverfahren*, 1993, ISBN 3-921694-79-5, vergriffen

80 Ptak, Thomas: *Stofftransport in heterogenen Porenaquiferen: Felduntersuchungen und stochastische Modellierung*, 1993, ISBN 3-921694-80-9, vergriffen

81 Haakh, Frieder: *Transientes Strömungsverhalten in Wirbelkammern,* 1993, ISBN 3-921694-81-7

82 Kobus, Helmut; Cirpka, Olaf; Barczewski, Baldur; Koschitzky, Hans-Peter: *Versucheinrichtung zur Grundwasser und Altlastensanierung VEGAS, Konzeption und Programmrahmen*, 1993, ISBN 3-921694-82-5

83 Zang, Weidong: *Optimaler Echtzeit-Betrieb eines Speichers mit aktueller Abflußregenerierung*, 1994, ISBN 3-921694-83-3, vergriffen

84 Franke, Hans-Jörg: *Stochastische Modellierung eines flächenhaften Stoffeintrages und Transports in Grundwasser am Beispiel der Pflanzenschutzmittelproblematik*, 1995, ISBN 3-921694-84-1

85 Lang, Ulrich: *Simulation regionaler Strömungs- und Transportvorgänge in Karstaquiferen mit Hilfe des Doppelkontinuum-Ansatzes: Methodenentwicklung und Parameteridentifikation*, 1995, ISBN 3-921694-85-X, vergriffen

86 Helmig, Rainer: *Einführung in die Numerischen Methoden der Hydromechanik*, 1996, ISBN 3-921694-86-8, vergriffen

87 Cirpka, Olaf: *CONTRACT: A Numerical Tool for Contaminant Transport and Chemical Transformations - Theory and Program Documentation* -, 1996, ISBN 3-921694-87-6

88 Haberlandt, Uwe: *Stochastische Synthese und Regionalisierung des Niederschlages für Schmutzfrachtberechnungen*, 1996, ISBN 3-921694-88-4

89 Croisé, Jean: *Extraktion von flüchtigen Chemikalien aus natürlichen Lockergesteinen mittels erzwungener Luftströmung*, 1996, ISBN 3-921694-89-2, vergriffen

90 Jorde, Klaus: *Ökologisch begründete, dynamische Mindestwasserregelungen bei Ausleitungskraftwerken*, 1997, ISBN 3-921694-90-6, vergriffen

91 Helmig, Rainer: *Gekoppelte Strömungs- und Transportprozesse im Untergrund - Ein Beitrag zur Hydrosystemmodellierung*-, 1998, ISBN 3-921694-91-4, vergriffen

92 Emmert, Martin: *Numerische Modellierung nichtisothermer Gas-Wasser Systeme in porösen Medien,* 1997, ISBN 3-921694-92-2

93 Kern, Ulrich: *Transport von Schweb- und Schadstoffen in staugeregelten Fließgewässern am Beispiel des Neckars*, 1997, ISBN 3-921694-93-0, vergriffen

94 Förster, Georg: *Druckstoßdämpfung durch große Luftblasen in Hochpunkten von Rohrleitungen 1997*, ISBN 3-921694-94-9

95 Cirpka, Olaf: *Numerische Methoden zur Simulation des reaktiven Mehrkomponententransports im Grundwasser*, 1997, ISBN 3-921694-95-7, vergriffen

96 Färber, Arne: *Wärmetransport in der ungesättigten Bodenzone: Entwicklung einer thermischen In-situ-Sanierungstechnologie*, 1997, ISBN 3-921694-96-5

97 Betz, Christoph: *Wasserdampfdestillation von Schadstoffen im porösen Medium: Entwicklung einer thermischen In-situ-Sanierungstechnologie*, 1998, ISBN 3-921694-97-3

98 Xu, Yichun: *Numerical Modeling of Suspended Sediment Transport in Rivers*, 1998, ISBN 3-921694-98-1, vergriffen

99 Wüst, Wolfgang: *Geochemische Untersuchungen zur Sanierung CKW-kontaminierter Aquifere mit Fe(0)-Reaktionswänden,* 2000, ISBN 3-933761-02-2

100 Sheta, Hussam: *Simulation von Mehrphasenvorgängen in porösen Medien unter Einbeziehung von Hysterese-Effekten*, 2000, ISBN 3-933761-03-4

101 Ayros, Edwin: *Regionalisierung extremer Abflüsse auf der Grundlage statistischer Verfahren*, 2000, ISBN 3-933761-04-2, vergriffen

102 Huber, Ralf: *Compositional Multiphase Flow and Transport in Heterogeneous Porous Media*, 2000, ISBN 3-933761-05-0

103 Braun, Christopherus: *Ein Upscaling-Verfahren für Mehrphasenströmungen in porösen Medien*, 2000, ISBN 3-933761-06-9

104 Hofmann, Bernd: *Entwicklung eines rechnergestützten Managementsystems zur Beurteilung von Grundwasserschadensfällen*, 2000, ISBN 3-933761-07-7

105 Class, Holger: *Theorie und numerische Modellierung nichtisothermer Mehrphasenprozesse in NAPL-kontaminierten porösen Medien,* 2001, ISBN 3-933761-08-5

106 Schmidt, Reinhard: *Wasserdampf- und Heißluftinjektion zur thermischen Sanierung kontaminierter Standorte*, 2001, ISBN 3-933761-09-3

107 Josef, Reinhold:, *Schadstoffextraktion mit hydraulischen Sanierungsverfahren unter Anwendung von grenzflächenaktiven Stoffen*, 2001, ISBN 3-933761-10-7

108 Schneider, Matthias: *Habitat- und Abflussmodellierung für Fließgewässer mit unscharfen Berechnungsansätzen*, 2001, ISBN 3-933761-11-5

109 Rathgeb, Andreas: *Hydrodynamische Bemessungsgrundlagen für Lockerdeckwerke an überströmbaren Erddämmen*, 2001, ISBN 3-933761-12-3

110 Lang, Stefan: *Parallele numerische Simulation instätionärer Probleme mit adaptiven Methoden auf unstrukturierten Gittern*, 2001, ISBN 3-933761-13-1

111 Appt, Jochen; Stumpp Simone: *Die Bodensee-Messkampagne 2001, IWS/CWR Lake Constance Measurement Program 2001*, 2002, ISBN 3-933761-14-X

112 Heimerl, Stephan: *Systematische Beurteilung von Wasserkraftprojekten,* 2002, ISBN 3-933761-15-8

113 Iqbal, Amin: *On the Management and Salinity Control of Drip Irrigation,* 2002, ISBN 3-933761-16-6

114 Silberhorn-Hemminger, Annette: *Modellierung von Kluftaquifersystemen: Geostatistische Analyse und deterministisch-stochastische Kluftgenerierung,* 2002, ISBN 3-933761-17-4

115 Winkler, Angela: *Prozesse des Wärme- und Stofftransports bei der In-situ-Sanierung mit festen Wärmequellen,* 2003, ISBN 3-933761-18-2

116 Marx, Walter: *Wasserkraft, Bewässerung, Umwelt - Planungs- und Bewertungsschwerpunkte der Wasserbewirtschaftung,* 2003, ISBN 3-933761-19-0

117 Hinkelmann, Reinhard: *Efficient Numerical Methods and Information-Processing Techniques in Environment Water,* 2003, ISBN 3-933761-20-4

118 Samaniego-Eguiguren, Luis Eduardo: *Hydrological Consequences of Land Use / Land Cover and Climatic Changes in Mesoscale Catchments*, 2003, ISBN 3-933761-21-2

119 Neunhäuserer, Lina: *Diskretisierungsansätze zur Modellierung von Strömungs- und Transportprozessen in geklüftet-porösen Medien*, 2003, ISBN 3-933761-22-0

120 Paul, Maren: *Simulation of Two-Phase Flow in Heterogeneous Poros Media with Adaptive Methods*, 2003, ISBN 3-933761-23-9

121 Ehret, Uwe: *Rainfall and Flood Nowcasting in Small Catchments using Weather Radar*, 2003, ISBN 3-933761-24-7

122 Haag, Ingo: *Der Sauerstoffhaushalt staugeregelter Flüsse am Beispiel des Neckars - Analysen, Experimente, Simulationen -,* 2003, ISBN 3-933761-25-5

123 Appt, Jochen: *Analysis of Basin-Scale Internal Waves in Upper Lake Constance,* 2003, ISBN 3-933761-26-3

124 Hrsg.: Schrenk, Volker; Batereau, Katrin; Barczewski, Baldur; Weber, Karolin und Koschitzky, Hans-Peter: *Symposium Ressource Fläche und VEGAS - Statuskolloquium 2003, 30. September und 1. Oktober 2003,* 2003, ISBN 3-933761-27-1

125 Omar Khalil Ouda: *Optimisation of Agricultural Water Use: A Decision Support System for the Gaza Strip,* 2003, ISBN 3-933761-28-0

126 Batereau, Katrin: *Sensorbasierte Bodenluftmessung zur Vor-Ort-Erkundung von Schadensherden im Untergrund*, 2004, ISBN 3-933761-29-8

127 Witt, Oliver: *Erosionsstabilität von Gewässersedimenten mit Auswirkung auf den Stofftransport bei Hochwasser am Beispiel ausgewählter Stauhaltungen des Oberrheins*, 2004, ISBN 3-933761-30-1

128 Jakobs, Hartmut: *Simulation nicht-isothermer Gas-Wasser-Prozesse in komplexen Kluft-Matrix-Systemen*, 2004, ISBN 3-933761-31-X

129 Li, Chen-Chien: *Deterministisch-stochastisches Berechnungskonzept zur Beurteilung der Auswirkungen erosiver Hochwasserereignisse in Flussstauhaltungen,* 2004, ISBN 3-933761-32-8

130 Reichenberger, Volker; Helmig, Rainer; Jakobs, Hartmut; Bastian, Peter; Niessner, Jennifer: *Complex Gas-Water Processes in Discrete Fracture-Matrix Systems: Upscaling, Mass-Conservative Discretization and Efficient Multilevel Solution,* 2004, ISBN 3-933761-33-6

131 Hrsg.: Barczewski, Baldur; Koschitzky, Hans-Peter; Weber, Karolin; Wege, Ralf: *VEGAS - Statuskolloquium 2004,* Tagungsband zur Veranstaltung am 05. Oktober 2004 an der Universität Stuttgart, Campus Stuttgart-Vaihingen, 2004, ISBN 3-933761-34-4

132 Asie, Kemal Jabir: *Finite Volume Models for Multiphase Multicomponent Flow through Porous Media*. 2005, ISBN 3-933761-35-2

133 Jacoub, George: *Development of a 2-D Numerical Module for Particulate Contaminant Transport in Flood Retention Reservoirs and Impounded Rivers,* 2004, ISBN 3-933761-36-0

134 Nowak, Wolfgang: *Geostatistical Methods for the Identification of Flow and Transport Parameters in the Subsurface,* 2005, ISBN 3-933761-37-9

135 Süß, Mia: *Analysis of the influence of structures and boundaries on flow and transport processes in fractured porous media*, 2005, ISBN 3-933761-38-7

136 Jose, Surabhin Chackiath: *Experimental Investigations on Longitudinal Dispersive Mixing in Heterogeneous Aquifers,* 2005, ISBN: 3-933761-39-5

137 Filiz, Fulya: *Linking Large-Scale Meteorological Conditions to Floods in Mesoscale Catchments,* 2005, ISBN 3-933761-40-9

138 Qin, Minghao: *Wirklichkeitsnahe und recheneffiziente Ermittlung von Temperatur und Spannungen bei großen RCC-Staumauern*, 2005, ISBN 3-933761-41-7

139 Kobayashi, Kenichiro: *Optimization Methods for Multiphase Systems in the Subsurface - Application to Methane Migration in Coal Mining Areas*, 2005, ISBN 3-933761-42-5

140 Rahman, Md. Arifur: *Experimental Investigations on Transverse Dispersive Mixing in Heterogeneous Porous Media,* 2005, ISBN 3-933761-43-3

141 Schrenk, Volker: *Ökobilanzen zur Bewertung von Altlastensanierungsmaßnahmen,* 2005, ISBN 3-933761-44-1

142 Hundecha, Hirpa Yeshewatesfa: *Regionalization of Parameters of a Conceptual Rainfall-Runoff Model*, 2005, ISBN: 3-933761-45-X

143 Wege, Ralf: *Untersuchungs- und Überwachungsmethoden für die Beurteilung natürlicher Selbstreinigungsprozesse im Grundwasser,* 2005, ISBN 3-933761-46-8

144 Breiting, Thomas: *Techniken und Methoden der Hydroinformatik - Modellierung von komplexen Hydrosystemen im Untergrund*, 2006, 3-933761-47-6

145 Hrsg.: Braun, Jürgen; Koschitzky, Hans-Peter; Müller, Martin: *Ressource Untergrund: 10 Jahre VEGAS: Forschung und Technologieentwicklung zum Schutz von Grundwasser und Boden,* Tagungsband zur Veranstaltung am 28. und 29. September 2005 an der Universität Stuttgart, Campus Stuttgart-Vaihingen, 2005, ISBN 3-933761-48-4

146 Rojanschi, Vlad: *Abflusskonzentration in mesoskaligen Einzugsgebieten unter Berücksichtigung des Sickerraumes,* 2006, ISBN 3-933761-49-2

147 Winkler, Nina Simone: *Optimierung der Steuerung von Hochwasserrückhaltebecken-systemen,* 2006, ISBN 3-933761-50-6

148 Wolf, Jens: *Räumlich differenzierte Modellierung der Grundwasserströmung alluvialer Aquifere für mesoskalige Einzugsgebiete*, 2006, ISBN: 3-933761-51-4

149 Kohler, Beate: *Externe Effekte der Laufwasserkraftnutzung*, 2006, ISBN 3-933761-52-2

150 Hrsg.: Braun, Jürgen; Koschitzky, Hans-Peter; Stuhrmann, Matthias: *VEGAS-Statuskolloquium 2006,* Tagungsband zur Veranstaltung am 28. September 2006 an der Universität Stuttgart, Campus Stuttgart-Vaihingen, 2006, ISBN 3-933761-53-0

151 Niessner, Jennifer: *Multi-Scale Modeling of Multi-Phase - Multi-Component Processes in Heterogeneous Porous Media*, 2006, ISBN 3-933761-54-9

152 Fischer, Markus: *Beanspruchung eingeerdeter Rohrleitungen infolge Austrocknung bindiger Böden,* 2006, ISBN 3-933761-55-7

153 Schneck, Alexander: *Optimierung der Grundwasserbewirtschaftung unter Berücksichtigung der Belange der Wasserversorgung, der Landwirtschaft und des Naturschutzes*, 2006, ISBN 3-933761-56-5

154 Das, Tapash: *The Impact of Spatial Variability of Precipitation on the Predictive Uncertainty of Hydrological Models,* 2006, ISBN 3-933761-57-3

155 Bielinski, Andreas: *Numerical Simulation of CO_2 sequestration in geological formations*, 2007, ISBN 3-933761-58-1

156 Mödinger, Jens: *Entwicklung eines Bewertungs- und Entscheidungsunterstützungssystems für eine nachhaltige regionale Grundwasserbewirtschaftung*, 2006, ISBN 3-933761-60-3

157 Manthey, Sabine: *Two-phase flow processes with dynamic effects in porous media - parameter estimation and simulation,* 2007, ISBN 3-933761-61-1

158 Pozos Estrada, Oscar: *Investigation on the Effects of Entrained Air in Pipelines,* 2007, ISBN 3-933761-62-X

159 Ochs, Steffen Oliver: *Steam injection into saturated porous media – process analysis including experimental and numerical investigations*, 2007, ISBN 3-933761-63-8

160 Marx, Andreas: *Einsatz gekoppelter Modelle und Wetterradar zur Abschätzung von Niederschlagsintensitäten und zur Abflussvorhersage, 2007,* ISBN 3-933761-64-6

161 Hartmann, Gabriele Maria: *Investigation of Evapotranspiration Concepts in Hydrological Modelling for Climate Change Impact Assessment*, 2007, ISBN 3-933761-65-4

162 Kebede Gurmessa, Tesfaye: *Numerical Investigation on Flow and Transport Characteristics to Improve Long-Term Simulation of Reservoir Sedimentation*, 2007, ISBN 3-933761-66-2

163 Trifković, Aleksandar: *Multi-objective and Risk-based Modelling Methodology for Planning, Design and Operation of Water Supply Systems*, 2007, ISBN 3-933761-67-0

164 Götzinger, Jens: *Distributed Conceptual Hydrological Modelling - Simulation of Climate, Land Use Change Impact and Uncertainty Analysis*, 2007, ISBN 3-933761-68-9

165 Hrsg.: Braun, Jürgen; Koschitzky, Hans-Peter; Stuhrmann, Matthias: *VEGAS – Kolloquium 2007,* Tagungsband zur Veranstaltung am 26. September 2007 an der Universität Stuttgart, Campus Stuttgart-Vaihingen, 2007, ISBN 3-933761-69-7

166 Freeman, Beau: *Modernization Criteria Assessment for Water Resources Planning; Klamath Irrigation Project, U.S.*, 2008, ISBN 3-933761-70-0

167 Dreher, Thomas: *Selektive Sedimentation von Feinstschwebstoffen in Wechselwirkung mit wandnahen turbulenten Strömungsbedingungen*, 2008, ISBN 3-933761-71-9

168 Yang, Wei: *Discrete-Continuous Downscaling Model for Generating Daily Precipitation Time Series*, 2008, ISBN 3-933761-72-7

169 Kopecki, Ianina: *Calculational Approach to FST-Hemispheres for Multiparametrical Benthos Habitat Modelling,* 2008*,* ISBN 3-933761-73-5

170 Brommundt, Jürgen: *Stochastische Generierung räumlich zusammenhängender Niederschlagszeitreihen*, 2008, ISBN 3-933761-74-3

171 Papafotiou, *Alexandros: Numerical Investigations of the Role of Hysteresis in Heterogeneous Two-Phase Flow Systems*, 2008, ISBN 3-933761-75-1

172 He, Yi: *Application of a Non-Parametric Classification Scheme to Catchment Hydrology*, 2008, ISBN 978-3-933761-76-7

173 Wagner, Sven: *Water Balance in a Poorly Gauged Basin in West Africa Using Atmospheric Modelling and Remote Sensing Information*, 2008, ISBN 978-3-933761-77-4

174 Hrsg.: Braun, Jürgen; Koschitzky, Hans-Peter; Stuhrmann, Matthias; Schrenk, Volker: *VEGAS-Kolloquium 2008 Ressource Fläche III*, Tagungsband zur Veranstaltung am 01. Oktober 2008 an der Universität Stuttgart, Campus Stuttgart-Vaihingen, 2008, ISBN 978-3-933761-78-1

175 Patil, Sachin: *Regionalization of an Event Based Nash Cascade Model for Flood Predictions in Ungauged Basins*, 2008, ISBN 978-3-933761-79-8

176 Assteerawatt, Anongnart: *Flow and Transport Modelling of Fractured Aquifers based on a Geostatistical Approach,* 2008, ISBN 978-3-933761-80-4

177 Karnahl, Joachim Alexander: *2D numerische Modellierung von multifraktionalem Schwebstoff- und Schadstofftransport in Flüssen*, 2008, ISBN 978-3-933761-81-1

178 Hiester, Uwe: *Technologieentwicklung zur In-situ-Sanierung der ungesättigten Bodenzone mit festen Wärmequellen,* 2009, ISBN 978-3-933761-82-8

179 Laux, Patrick: *Statistical Modeling of Precipitation for Agricultural Planning in the Volta Basin of West Africa,* 2009, ISBN 978-3-933761-83-5

Die Mitteilungshefte ab der Nr. 134 (Jg. 2005) stehen als pdf-Datei über die Homepage des Instituts: www.iws.uni-stuttgart.de zur Verfügung.